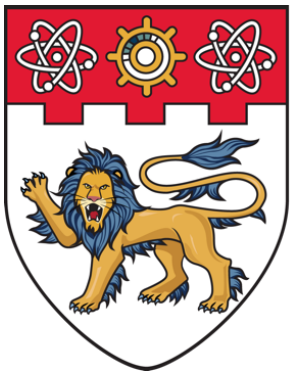

NANYANG TECHNOLOGICAL UNIVERSITY
SINGAPORE

Enantioconvergent Halogenophilic Nucleophilic Substitution (S_N2X) Reaction by Chiral Phase-Transfer Catalysis

ZHANG XIN

SCHOOL OF PHYSICAL AND MATHEMATICAL SCIENCES

2019

Enantioconvergent Halogenophilic Nucleophilic Substitution (S_N2X) Reaction by Chiral Phase-Transfer Catalysis

ZHANG XIN

SCHOOL OF PHYSICAL AND MATHEMATICAL SCIENCES

A thesis submitted to the Nanyang Technological University in partial fulfilment of the requirement for the degree of Doctor of Philosophy

2019

Statement of Originality

I hereby certify that the work embodied in this thesis is the result of original research done by me except where otherwise stated in this thesis. The thesis work has not been submitted for a degree or professional qualification to any other university or institution. I declare that this thesis is written by myself and is free of plagiarism and of sufficient grammatical clarity to be examined. I confirm that the investigations were conducted in accord with the ethics policies and integrity standards of Nanyang Technological University and that the research data are presented honestly and without prejudice.

Jan 10, 2019

. . . . . .
Date

. . . . . .
Zhang Xin

Supervisor Declaration Statement

I have reviewed the content and presentation style of this thesis and declare it of sufficient grammatical clarity to be examined. To the best of my knowledge, the thesis is free of plagiarism and the research and writing are those of the candidate's except as acknowledged in the Author Attribution Statement. I confirm that the investigations were conducted in accord with the ethics policies and integrity standards of Nanyang Technological University and that the research data are presented honestly and without prejudice.

Jan 10, 2019

. . . . . .

Date

. . . . . .

Tan Choon Hong

Authorship Attribution Statement

This thesis contains material from one paper published in the following peer-reviewed journal where I was the first author.

Chapter 2 and 3 are published as Xin Zhang, Jingyun Ren, Siu Min Tan, Davin Tan, Richmond Lee and Choon-Hong Tan. An Enantioconvergent Halogenophilic Nucleophilic Substitution (S_N2X) Reaction. *Science* **363**, 400–404 (2019). DOI:10.1126/science.aau7797.

The contributions of the co-authors are as follows:

- Prof Choon-Hong Tan provided the initial project direction.
- I and Jingyun prepared the manuscript drafts. The manuscript was revised by every author.
- I and Jingyun co-designed the study with Prof Choon-Hong Tan and performed the laboratory work at the School of Physical and Mathematical Sciences. I also analyzed the data.
- Dr Richmond Lee, Dr Davin Tan and Siu Min Tan conducted theory calculation.

Jan 10, 2019

. . . . . .

Date

. . . . . .

Zhang Xin

Abstract

Bimolecular nucleophilic substitution (S_N2) is a well-known textbook reaction and considered carbonophilic as the nucleophile (Nu) attacks the electrophile C-X bond from the 'backside' subsequently displacing X. Another form of substitution, that is less known, is the halogenophilic nucleophilic substitution (S_N2X) reaction. The S_N2X reaction occurs via attack of the 'front' X along the direction of the X-C bond, generating carbanion as a new nucleophile and Nu-X as a new electrophile. Their further reaction affords the product. Herein, we have achieved an enantioconvergent S_N2X process whereby substitution of tertiary bromide by thiocarboxylate generates tertiary thioester under phase-transfer conditions.

Chapter 1 introduces the development of phase-transfer catalysis and nucleophilic substitution reactions. We focus on the discussion of stereoselective S_N1, S_N2 and $S_{RN}1$ reactions with different approaches and their inherent deficiencies. Enantioconvergent S_N1 reactions through cation intermediates are achieved with chiral Lewis/ Brønsted acid catalysts, and $S_{RN}1$ reactions through radical intermediates are achieved with chiral transition metal catalysts. S_N2 reaction is not suitable for enantioconvergent transformation. Then less known S_N2X reaction is introduced and representative examples are discussed.

Chapter 2 discusses enantioconvergent S_N2X reactions under phase-transfer conditions utilizing tertiary electrophiles, which are still challenging with S_N1 and $S_{RN}1$ approaches. We find brominated cyanoesters and cyanophosphonates are excellent tertiary bromides for S_N2X reaction and the product tertiary thioesters were obtained with high enantioselectivities.

Chapter 3 discusses the reaction mechanism. Both experimental and computational studies support S_N2X mechanism. Computational modelling discloses the S···Br

intermolecular halogen bonding between tertiary bromide and thiocarboxylate, which is crucial for the efficient halogenophilic reaction.

Chapter 4 lists the experimental procedures and characterization data.

Acknowledgements

Frist and foremost, I would like to thank my supervisor, Professor Tan Choon Hong, with my sincere respect and gratitude. During the past four years, he has guided and encouraged me with his broad perspective and patience. He was always there whenever I was frustrated or tired with what I was working on. Without him, I could not keep my research on right track. Not only the guidance on the research, his thoughts about life and career have also inspired me.

Next, I want to show sincere thanks to all my lab mates in TCH lab for their generous help in research and life. They are Dr. Yuan Minjun, Dr. Wang Chao, Dr. Zong Lili, Dr. He Wei, Dr. Teng Bo, Dr. Chen Li, Dr. Chin Kek Foo, Dr. Cao Weidi, Dr. Valerie Wong, Dr. Ren Jingyun, Dr. Jackson Leow, Dr. Chua Zhijie, Mr. Xue Hansong, Dr. Jiang Huan, Dr. Wang Yang, Dr. Ge Yicen, Dr. Yao Zhen, Dr. Cui Xiyang, Dr. Ban Xu, Mr. Song Zhijian, Ms. Ye Xinyi, Mr. Chen Wenchao, Mr. Wang Tianxiang and Ms. Yang Ziqi.

I would also like to thank Professor Richard Webster and Dr. Gan Sher Li for their help in EPR and CV testing. And the calculation support from Dr. Richmond Lee and Dr. Davin Tan is much appreciated.

Additionally, I want to thank the CBC technical support staffs: Dr. Li Yongxin and Dr. Ganguly Rakesh (X-ray analysis), Ms. Goh Ee Ling, and Mr. Keith Leung (NMR analysis), Ms. Zhu Wenwei and Ms. Pui Pang Yi (ESI-MS), Ms. Seow Ai Hua (Teaching lab) for their assistance with common laboratory instruments. I would also like to thank Nanyang Technological University to award me generous research scholarship for financial support.

Last but not the least, I would like to thank all my family members for their love, encouragement and support during these years.

Table of Contents

Chapter 1

Introduction

1.1 Phase-transfer catalysis (PTC)

Phase-transfer catalysts can transfer ions from one phase to another and assist heterogeneous reactions (**Figure 1.1**). With the ion exchange process, they usually possess many advantages over homogeneous reactions. There are three most recognized aspects. First, rates of PTC reactions tend to be higher; Second, with water and more organic solvents to choose, they can be environmentally friendly; Third, for controlled amount of the reagents into the reaction phase, the reactions are more selective (fewer side products) and the products are easier to isolate. Because of these characteristics and potential large-scale synthesis, phase-transfer catalysis has attracted attention from both academia and industry[1-5].

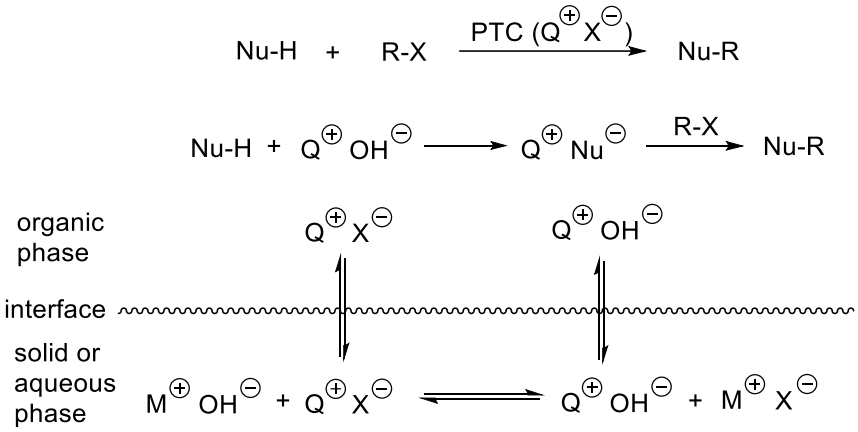

Figure 1.1 Representative mechanism of phase-transfer catalysis

Over the past thirty years, asymmetric phase-transfer catalysis has quickly developed, and many transformations have been achieved. In the meanwhile, these achievements have also encouraged the development of new chiral phase-transfer catalysts[6]. Representative examples are shown in **Figure 1.2**. Cinchona alkaloid derived ammounium was first used as phase-transfer catalyst in 1989. Since then several generations of this natural product derived phase-transfer catalysts have been developed and shown high efficiency and selectivity in various reaction. In 1999, Maruoka and co-workers developed a chiral spiro ammonium salts which is a very reliable phase-transfer

catalyst. This catalyst derived form from chiral binaphthol has a high rigid structure with axial chirality. Onium salts derived from TADDOL are also developed. Crown ethers are another representative type of phase-transfer catalysts. Neutral crown ethers can bind some cations strongly to generate a stable cationic complex. Ooi and co-workers developed the chiral 1,2,3-triazolium salts as new phase-transfer catalysts. Hii and co-workers designed chiral 2-oxopyrimidinium salts as phase-transfer catalysts. P-spiro chiral tetraaminophosphonium salts were also developed as phase-transfer catalysts and show high enantioselectivities[7]. These privileged catalysts are widely used in synthesis forming various chemical bonds under mild conditions.

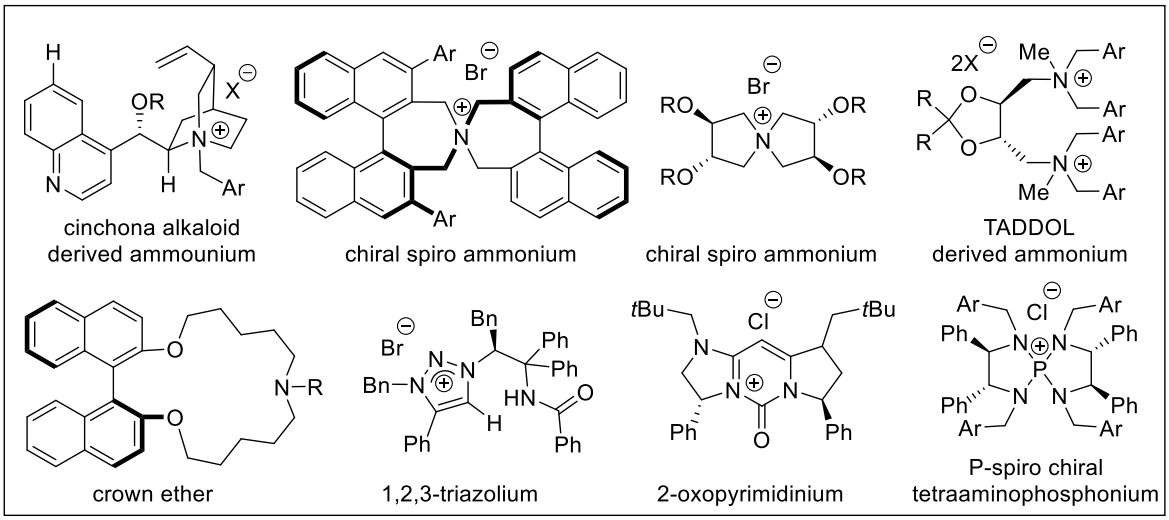

Figure 1.2 Representive phase-transfer catalysts

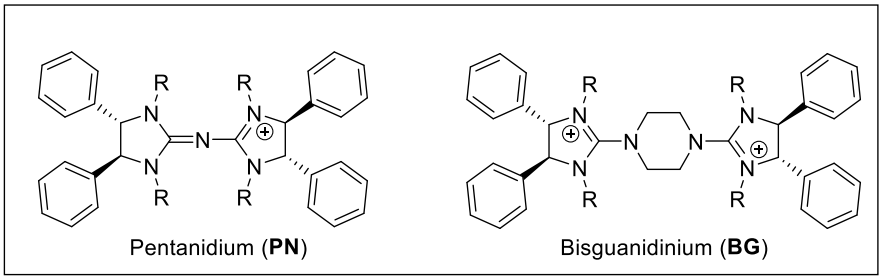

Figure 1.3 Pentanidium and bisguanidium developed in our group

Our group has developed a series of guanidine-based chiral pentanidium and bis-guanidinium salts as phase-transfer catalysts (**Figure 1.3**). They are widely utilized in

various asymmetric phase-transfer reactions and show high efficiency and selectivity[8, 9].

The pentanidium salt was first used as phase-transfer catalyst in 2010 (**Figure 1.4**). Asymmetric conjugation of glycine derived Schiff base to α,β-unsaturated carbonyl compound was achieved and the single diastereomer product was obtain in high yield and enantioselectivity. In the gram scale experiment, the catalyst loading is 0.05 mol% but the product yield and enantioselectivity were not significantly influenced[10].

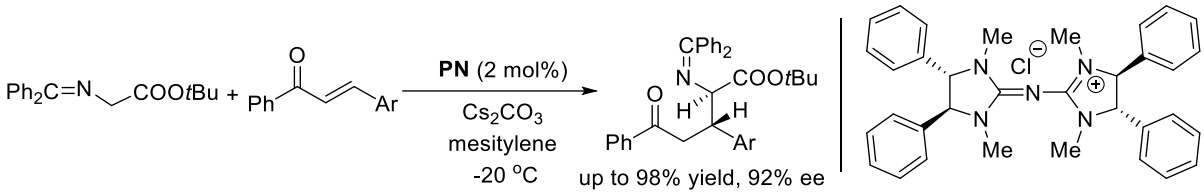

Figure 1.4 Pentanidium-catalyzed conjugate addition of Schiff base

Later, this catalyst was used in the asymmetric hydroxylation of oxindoles with dioxygen as oxidant (**Figure 1.5**). Mechanistic studies showed in the first step indole was oxidized to form enantioenriched hydroperoxide oxindole, which then formed hydroxylated oxindole by kinetic resolution via the reduction of enolates[11].

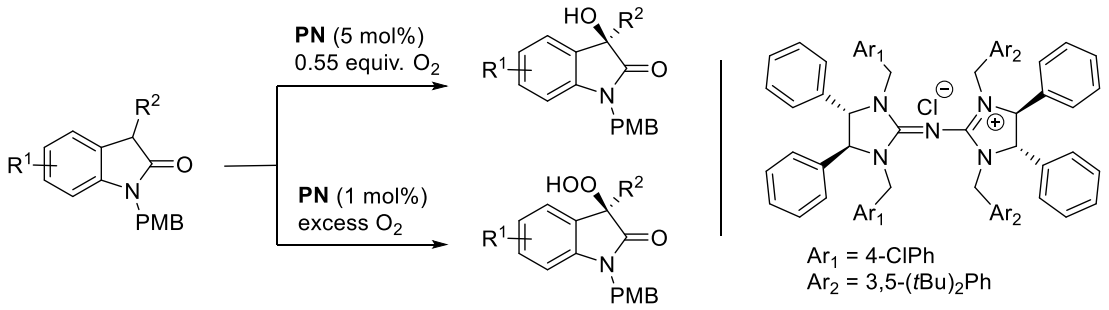

Figure 1.5 Pentanidium-catalyzed hydroxylation of oxindoles

In 2014, pentanidium was used in the enantioselective alkylation of the sulfonate anions (**Figure 1.6**). In this reaction, various sulfoxides were obtained in high yields and enantioselectivities utilizing the halogenated pentanidiums, and iodo-pentanidium was best. Calculation showed halogen bonding was important in the enantioselective bond

forming step. The Br-I halogen bonding between the leaving Br of benzyl bromide and the aryl iodide of pentanidium has stabilized the transition state accounting for the high enantioselectivity[12].

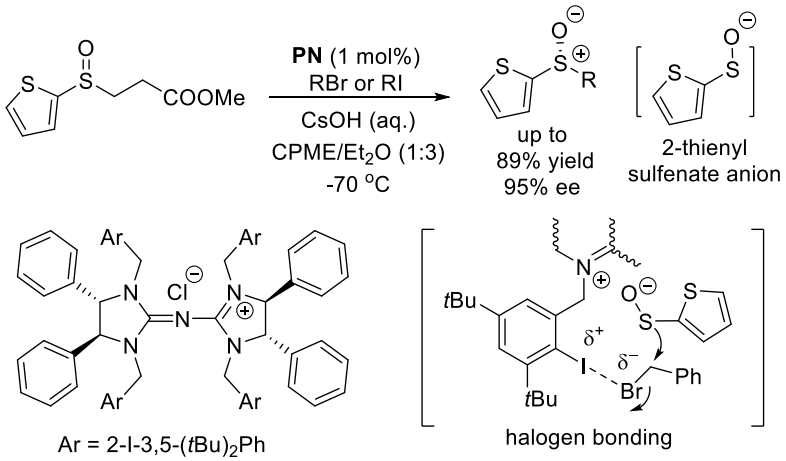

Figure 1.6 Pentanidium-catalyzed alkylation of the sulfonate anions

The asymmetric conjugate addition of substituted oxindoles to phenyl vinyl sulfone was also reported in high yields and ee values using pentanidium catalysts (**Figure 1.7**)[13].

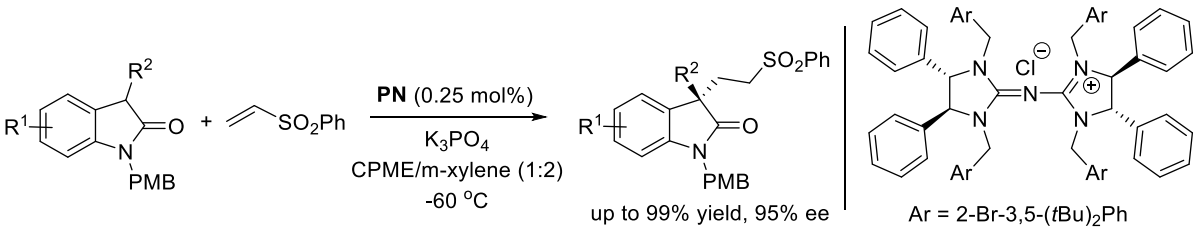

Figure 1.7 Pentanidium-catalyzed conjugate addition of oxindoles

In 2016, we developed a useful Brønsted probase strategy[14] and achieved the asymmetric alkylation of dihydrocoumarin, which is challenging under PTC condition, because the lactone will be decomposed using strong base like MOMe or MOH for their high nucleophilicity. Non-nucleophilic bases like K_3PO_4 or Cs_2CO_3 are not basic enough for the deprotonation of dihydrocoumarin. With this strategy, bis(trimethylsilyl)acetamide (BSA) combined with CsF were utilized to generate a

strong but non-nucleophilic base. Under this condition, various alkylated dihydrocoumarins were obtained in high yields and enantioselectivities (**Figure 1.8**).

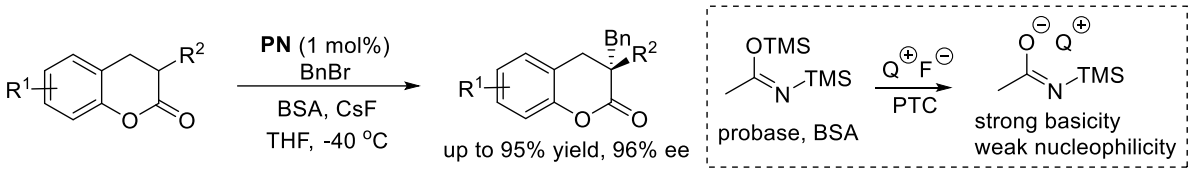

Figure 1.8 Pentanidium-catalyzed alkylation of dihydrocoumarin

Chiral dicationic bisguanidiniums were synthesized in 2015 and used as phase-transfer catalysts in the oxidation reaction of various alkenes with $KMnO_4$ as oxidant[15]. The enzyme-like mode of bisguanidinium, with active center deeply buried in a chiral pocket, accelerates oxidation reaction through the formation of intimate ion pair with enolate anion and chiral information is imparted through this interaction. The permanganate anion selectively coordinates to double bond from the *Si* face and generates the dihydroxylation and oxohydroxylation products with high enantioselectivities through the proposed transition state (**Figure 1.9**).

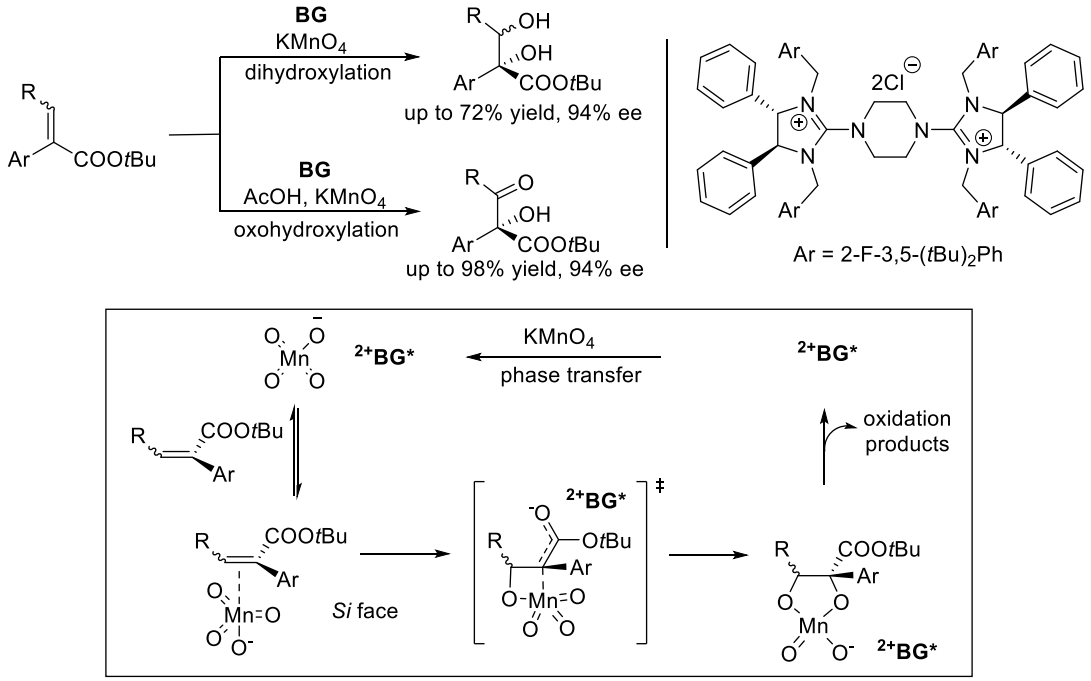

Figure 1.9 Bisguanidinium-catalyzed dihydroxylation and oxohydroxylation

1.2 Nucleophilic substitution reactions

Nucleophilic substitution reactions are important and useful approaches in organic synthesis. Nucleophilic substitution is known to happen at a sp^3, sp^2 or sp carbon atoms, and possible electrophiles can be aliphatic halide (nucleophilic aliphatic substitution), acyl halide (nucleophilic acyl substitution), aryl halide (nucleophilic aromatic substitution), haloalkene and haloalkyne. We will mainly discuss nucleophilic aliphatic substitution and related stereocontrol. The mechanism of nucleophilic aliphatic substitution was studied by C. K. Ingold in 1930s[16-18]. Typically, a nucleophile bearing an unshared electron pair will attack an aliphatic carbon atom to displace its leaving group. Depending on the reaction conditions and the nature of electrophiles and nucleophiles, several different reaction types have been proposed according to their mechanisms.

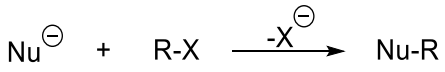

The S_N1 (unimolecular nucleophilic substitution)[19] and S_N2 (bimolecular nucleophilic substitution) reactions[20, 21] are are well-known fundamental, textbook reactions. They are widely used in synthesis to form carbon-carbon and carbon-heteroatom bonds, but their reaction scopes and stereoselectivities are limited because of their inherent deficiencies[22]. For S_N1 reaction, a dissociative mechanism is proposed (**Figure 1.10A**). Because of the carbocation intermediates, only substrates which can form stabilized carbocation intermediates are suitable. Furthermore, the carbocation intermediates will also undergo elimination and rearrangement reactions as side reactions making S_N1 reactions less efficient. In addition, because the S_N1 reactions usually need to be promoted by acids, the applicable nucleophiles are limited due to the possible protonation of nucleophiles. The stereocenters in S_N1 reaction will be racemized.

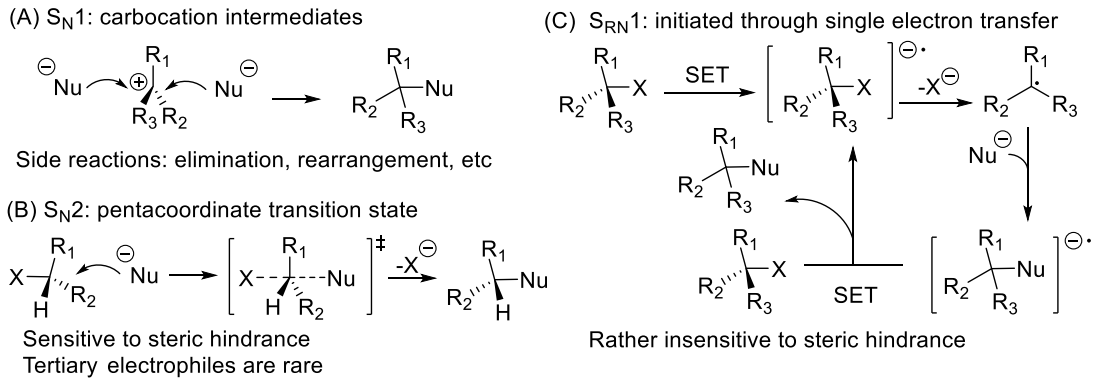

Figure 1.10 Different types of nucleophilic substitution reactions

For S_N2 reaction, a pentacoordinate transition state is proposed (**Figure 1.10B**). Usually, they are sensitive to steric hindrance and only successful when non-bulky primary and secondary electrophiles are utilized. Tertiary electrophiles are quite difficult for S_N2 reaction. The stereocenters in S_N2 reactions will be inverted.

Except for S_N1 and S_N2 reactions, other types of nucleophilic substitution reactions are also developed. The $S_{RN}1$ (unimolecular radical-nucleophilic substitution) reaction is known for its single electron transfer (SET) mechanism (**Figure 1.10C**)[23, 24]. This mechanism was first proposed in 1966 for the nucleophilic substitution of alkyl derivatives[25, 26], which bear electron withdrawing groups and leaving groups. The scope of this SET mechanism was extended to the nucleophilic substitution of unactivated aromatic halide substrates in 1970[27, 28]. $S_{RN}1$ reaction can be initiated by different methods and the most widely used are photochemical, electrochemical and thermal initiation. With radical intermediates, $S_{RN}1$ reaction is rather insensitive to steric hindrance and many inorganic and organic anionic nucleophiles are effective in such transformations to construct various chemical bonds.

1.2.1 Stereoselective S_N1-type reaction

The S_N1 reaction is discussed in every organic textbook. Nucleophiles are proposed to displace the leaving groups through carbocation intermediates. It is known that these

intermediates are highly unstable and active species, so the product yields and stereoselectivities usually are difficult to improve. To control the enantioselectivities, different strategies utilizing Lewis or Brønsted acid are developed.

In 2004, Braun reported the asymmetric substitution of alcohols, silyl ethers and acetals using chiral titanium (IV) complex as Lewis acid catalyst. Allyltrimethylsilane was used as nucleophile to form carbon-allylation product bearing a quaternary carbon center in high yields and enantioselectivities. Catalyzed by the strong Lewis acid, the silyl ether formed planar, achiral carbocation which form ion pair[29] with a chiral Ti anion. Then the carbocation was enantioselectively attacked by the allyltrimethylsilane[30] (**Figure 1.11**).

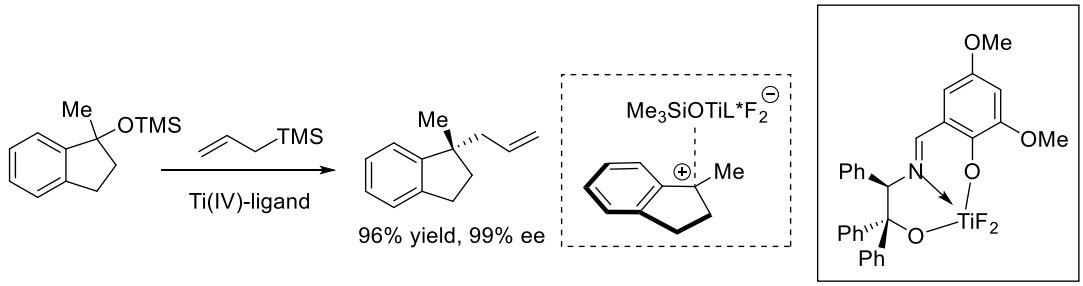

Figure 1.11 Chiral titanium complex catalyzed S_N1 reaction

In 2011, Nishibayashi reported cooperative catalytic reactions combining organocatalysts and Lewis acids[31]. Chiral amine was used to activate aldehyde to form chiral enamine. $InBr_3$ was used as Lewis acid to activate propargylic alcohol and form propargylic cation intermediate, which was trapped by chiral enamine to generate enantioenriched product bearing an internal alkyne with high enantioselectivities (**Figure 1.12**).

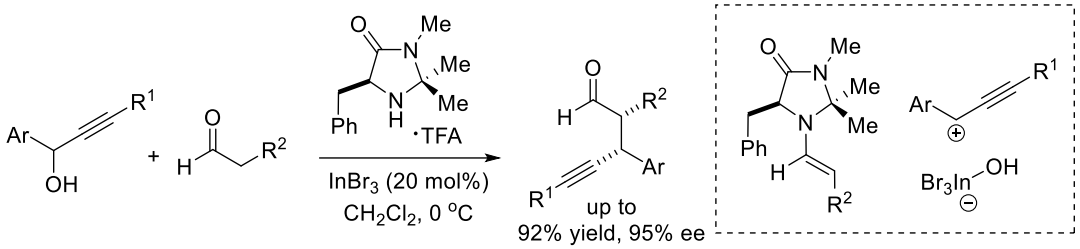

Figure 1.12 $InBr_3$ and chiral amine cocatalyzed S_N1 reaction

There are some examples using different chiral metal complexes as Lewis acids. In the meanwhile, metal-free method using chiral phosphoric acid (**CPA**) as Brønsted acid is also well developed[32]. To stabilize the intermediates, substrates that can form heteroatom-stabilized cations are chosen in most cases. Because of the introduction of a heteroatom, the carbocation will generate a rather stable form in which the positive charge is on the heteroatom. To suppress side reactions, like elimination reactions, the substituents of electrophile are usually limited to aryl or electron-withdrawing groups lacking β-hydrogen atoms.

In 2009, Gong reported the reaction between enamines and indolyl alcohols catalyzed by chiral phosphoric acids with high yields and excellent enantioselectivities (**Figure 1.13**)[33]. The chiral phosphoric acid was derived form H8-BINOL and protonated the oxygen atom of hydroxy group of the indolyl alcohol, followed by H_2O release to form the N-atom-stabilized cation. The cation formed a tight chiral ion pair with chiral phosphate. The phosphoryl oxygen is Lewis basic and can form hydrogen-bonding with the proton of enamide. With this interaction, the enamide was activated resulting the addition to the cation generating the product β-aryl 3-(3-indolyl)propanones in an enantioselective manner.

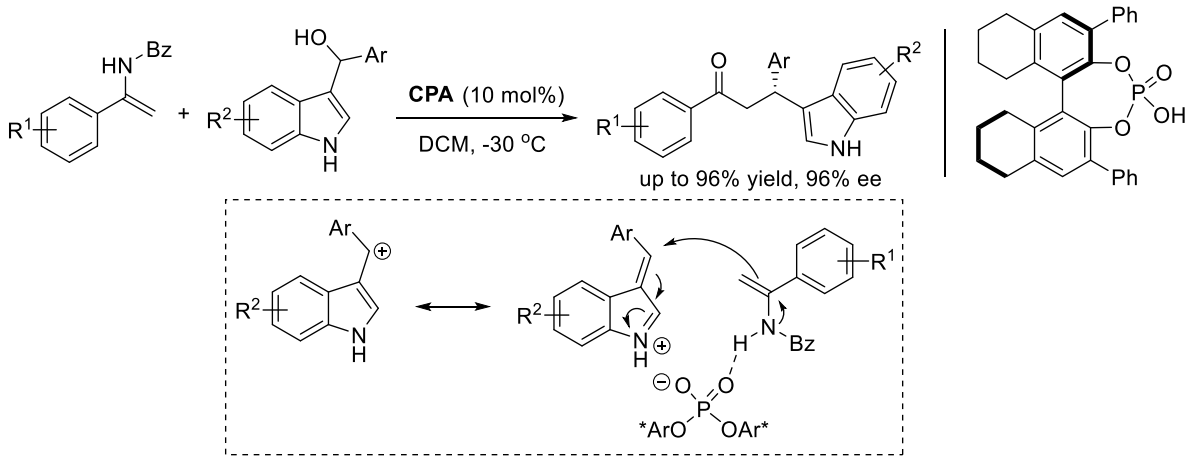

Figure 1.13 Chiral phosphoric acid catalyzed alkylation of enamines

In 2012, Peng reported the alkylation of unmodified ketones with an alcohol catalyzed by chiral phosphoric acids[34]. Chiral phosphoric acids were here used to promote the enol formation with the ketone (**Figure 1.14**). More importantly, the active carbocation intermediates were formed with the protonation of alcohols. The alcohol was activated with an electron-withdrawing amide group, which made the carbocation intermediates more electrophilic. The cation ion-paired with chiral phosphate reacted with ketones to generate 3-indolyloxindole, which was a novel type of indole and oxindole. Both cyclic and acyclic ketones could afford the products in high yields with high diastereoselectivities and enantioselectivities.

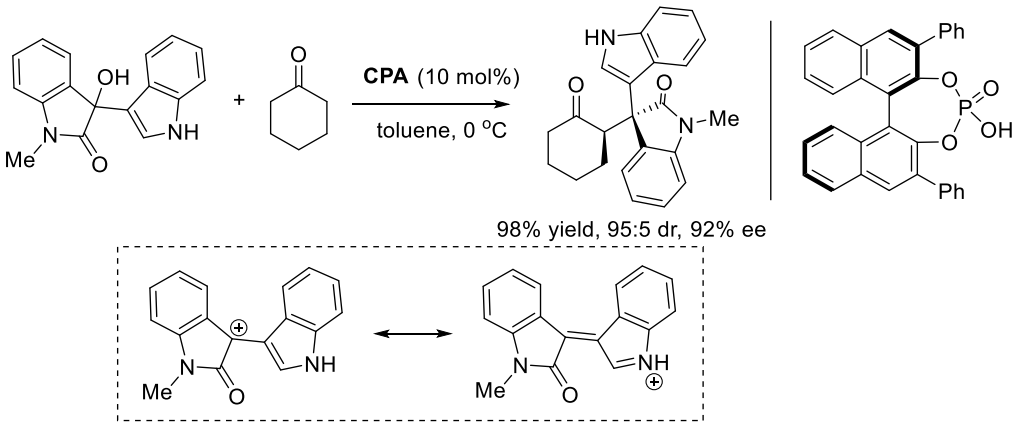

Figure 1.14 Chiral phosphoric acid catalyzed alkylation of ketones

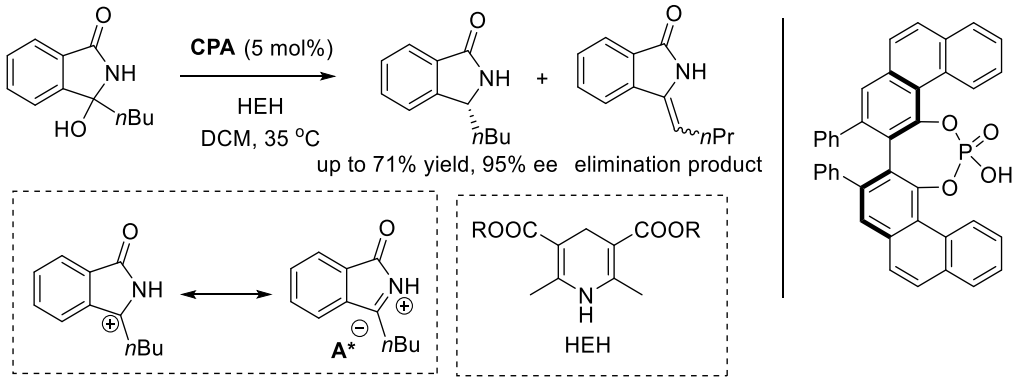

Figure 1.15 Chiral phosphoric acid catalyzed hydrogenolysis of tertiary alcohols

In 2012, Zhou reported the hydrogenolysis of tertiary alcohols catalyzed by chiral phosphoric acids[35]. The hydroxy group of racemic 3-hydroxysubstituted isoindolin-1-one was protonated then dehydrated to form the acyliminium ion, which formed ion pair with a chiral phosphate (**Figure 1.15**). The Hantzsch ester (HEH) was utilized as hydrogen scource to reduce the acyliminium ions and afforded the product 3-substituted isoindolin-1-ones with high enantioselectivities, albeit with moderate yields because of the side product alkenes from elimination of carbocation.

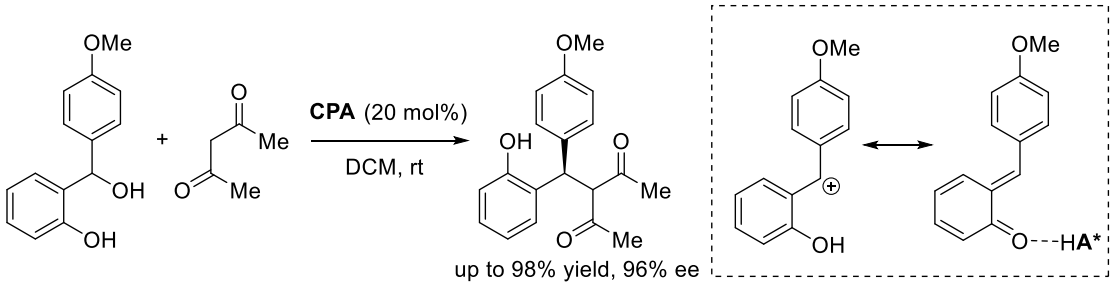

Figure 1.16 Chiral phosphoric acid catalyzed alkylation of β-diketones

In 2014, Schneider reported chiral phosphoric acid catalyzed reaction between ortho-hydroxy benzhydryl alcohol and β-diketone (**Figure 1.16**)[36]. Ortho-hydroxy benzhydryl alcohol could be converted to carbocation which would in situ form more stable resonance form, hydrogen bonded ortho-quinone methides, followed by addition of β-diketone. Product 4-aryl-4H-chromenes were generated in excellent yields and high enantioselectivities.

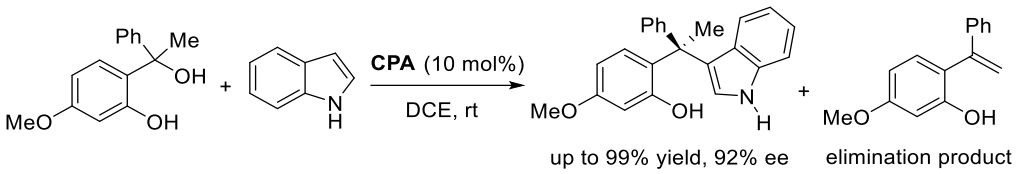

Figure 1.17 Chiral phosphoric acid catalyzed alkylation of indoles

In 2015, Sun improved this strategy and successfully utilized tertiary alkyl alcohol electrophiles to achieve the formation of all-carbon quaternary stereocenters (**Figure 1.17**)[37]. The nucleophile indole would react with the quinone methide which interacted with chiral phosphoric acid by hydrogen-bonding to afford the product containing indole and all-carbon quaternary stereocenters. Unfavorable steric hindrance of reaction center and the undersired elimination reaction were overcome in this reaction and useful indole products were obtained in high yields and enantioselectivities.

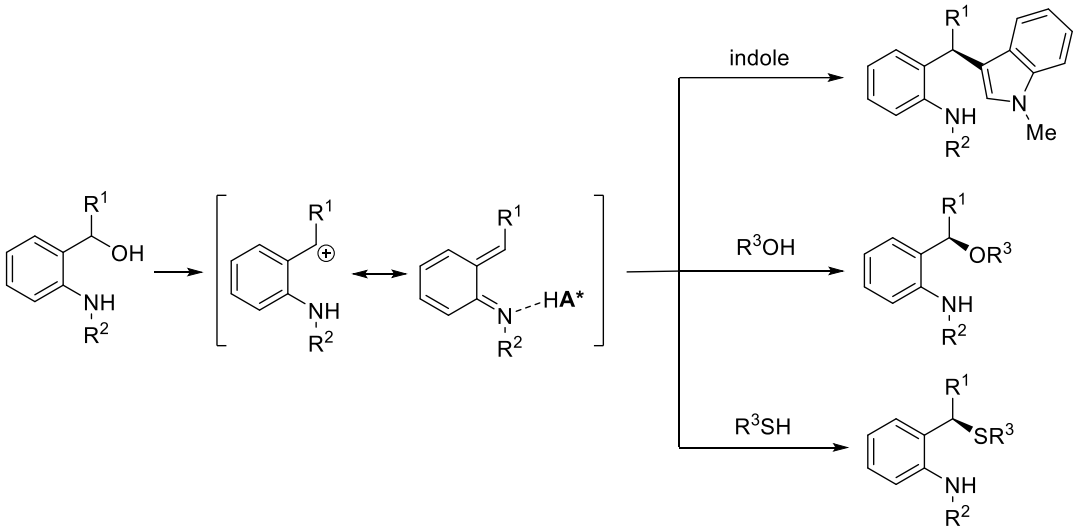

Figure 1.18 CPA catalyzed S_N1 reactions using ortho-amino benzyl alcohols

Rueping reported similar reactions using ortho-amino benzyl alcohol as electrophile (**Figure 1.18**)[38, 39]. Catalyzed by chiral phosphoric acids, various C-C, C-O and C-S bonding forming reactions were successfully developed with indoles, alcohols and thiols as nucleophiles. Different biologically active products were obtained with high yields and enantioselectivities.

In 2016, Gredicak reported the reaction between 3-hydroxy isoindolinones and thiols (**Figure 1.19**)[40]. This reaction was catalyzed by chiral phosphoric acids. N-acyl ketimines in situ generated from 3-hydroxy isoindolinones reacted with thiols to afford N(Acyl),S-acetals bearing a tetrasubstituted stereocenter. The reaction proceeds smoothly in high yields and enantioslectivities.

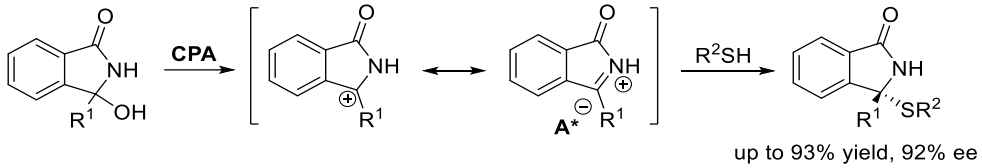

Figure 1.19 CPA **c**atalyzed S_N1 reactions using 3-hydroxy isoindolinones

In 2017, List reported the asymmetric synthesis of various chiral substituted oxygen-containing heterocycles (**Figure 1.20**)[41]. This reaction utilized lactol acetates as electrophiles and enolsilanes as nucleophiles catalyzed by a highly confined and active Brønsted acid, imidodiphosphorimidate (**IDPi**). The authors proposed a cyclic oxocarbenium ion intermediate which was paired with the confined chiral **IDPi** counteranion. The reaction between different lactol acetates and various nucleophiles afforded products in high yields and high enantioselectivities.

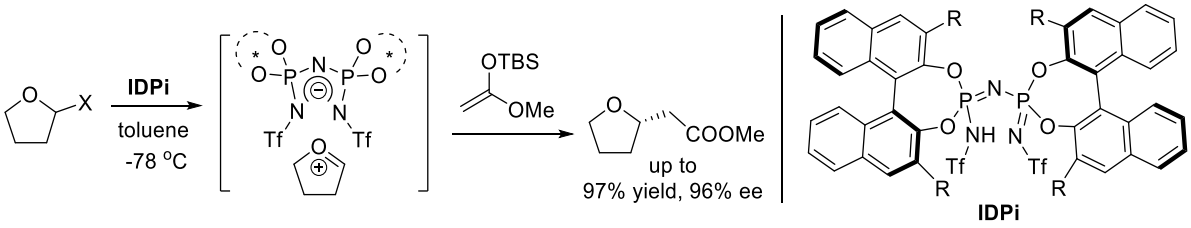

Figure 1.20 IDPi catalyzed S_N1 substitution of lactol acetates

In 2007, a chiral thiourea derivative as hydrogen-bond donor catalyst was reported by Jacobsen and applied in the enantioselective cyclization of hydroxylactams catalyzed via an S_N1-type mechanism (**Figure 1.21A**)[42]. With a chiral thiourea derivative as catalyst and chlorotrimethylsilane as additive, this cyclization reaction proceeded in

good-to-excellent yields and high enantioselectivities. As proposed by the authors, hydroxylactams and TMSCl reacted to form the corresponding chlorolactams. It is well established that ureas and thioureas have anion-binding properties. In the reaction, thiourea abstracted the chloride anion from the in situ generated chlorolactam, which formed an ion-paired N-acyliminium chloride-thiourea complex. The N-acyliminium ion would subsequently cyclize enantioselectively controlled by the anion-bounded thiourea. With the cationic intermediates, counterion interactions were proposed to induce the high levels of enantioselectivities. The anion-abstraction strategy was also used in the nucleophilic substitution of 1-chloroisochromans by silyl ketene acetals in 2008 (**Figure 1.21B**)[43]. Different isochromans were obtained efficiently with high enantioselectivities catalyzed by chiral thioureas.

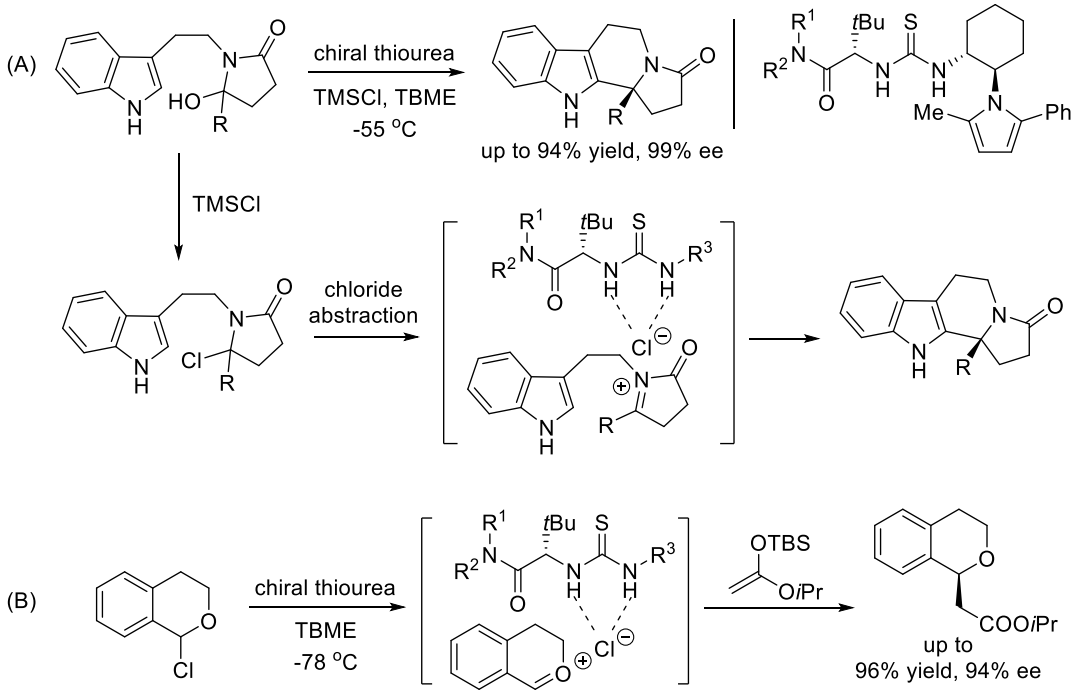

Figure 1.21 Chiral thiourea catalyzed S_N1-type cyclization

In 2018, Jacobsen reported the first example of stereoselective nucleophilic attack of non-heteroatom-stabilized carbocations generated from racemic tertiary electrophiles (**Figure 1.22**)[44]. The reactions between propargyl acetate tertiary electrophiles and

allyltrimethylsilanes afforded the products in moderate to high yields and enantioselectivities. After optimization, the authors found that using chiral squaramide as a hydrogen-bond-donor catalyst and TMSOTf as a Lewis-acid promoter could suppress elimination pathway and the product was obtained with the most satisfactory yields and enantioselectivities. This work has provided a foundation for enantioconvergently constructing other types of congested stereogenic centers.

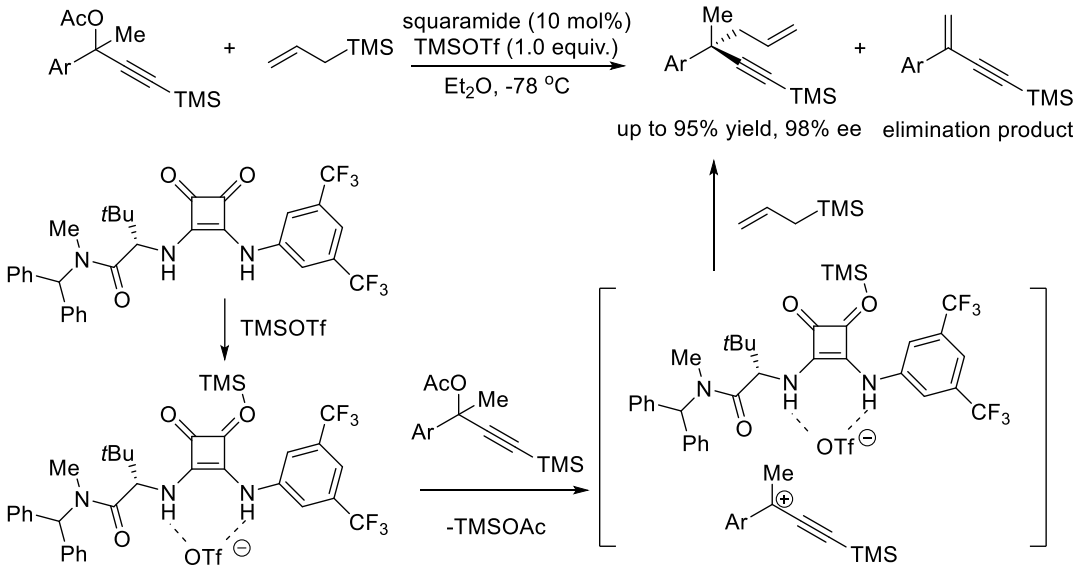

Figure 1.22 Nucleophilic reactions of non-heteroatom-stabilized tertiary carbocations

In the previous examples, racemic electrophiles are converted to products with high yields and high enantioselectivities in an enantioconvergent manner[45]. The prochiral cation intermediates and leaving groups are separated by solvents before they are captured by chiral anions, followed by enantioselective attack of nucleophiles. There are also some reports, in which the nascent cations can be trapped by nucleophiles in the contact ion-pair stage. Because the cations are still ion-paired with the leaving groups before they are separated by solvents, the stereocenters of chiral substrates will be inverted after nucleophilic substitution. However, such S_N1 reactions with high stereoinversion are still challenging and rarely reported, because of the competition between contact ion-pair attack and solvent separated ion attack.

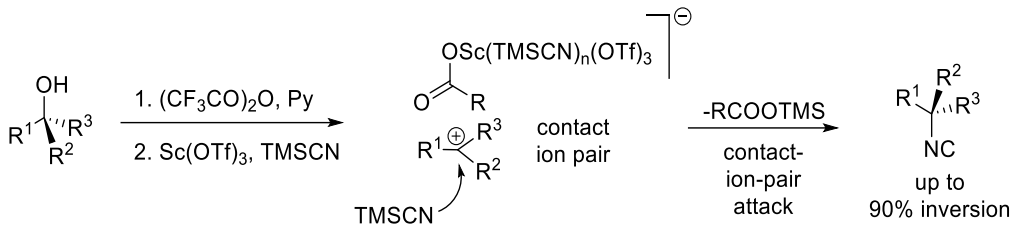

Figure 1.23 A rare S_N1 example with stereoinversion of tertiary alcohols

In 2013, Shenvi reported a successful S_N1 example with stereoinversion of tertiary alcohols (**Figure 1.23**)[46]. This reaction was initiated by scandium(III) triflate ($Sc(OTf)_3$) as Lewis acid catalyst and an excess amount of nucleophilic trimethylsilyl cyanide (TMSCN) was used as solvent. This Lewis-acid-catalyzed solvolysis generated stereochemically inverted tertiary alkyl isonitriles, complementing the limitation of stereospecific S_N2 reactions, which were not suitable for substitution of tertiary electrophiles.

1.2.2 Stereoselective S_N2-type reaction

The S_N2 reaction is also discussed in every organic textbook. It is widely used in organic synthesis to join two molecules together or to displace a functional group with another. In S_N2 reaction, the nucleophile attacks the electrophile carbon from the 'backside' displacing the leaving group through a pentacoordinate transition state, the stereocenter of the electrophile will be inverted. The S_N2 reaction is highly steric sensitive, so it has a significant limitation: only primary and secondary electrophiles are favored, whereas tertiary electrophiles usually fail to react. To obtain enantioenriched product via S_N2 reaction, the substrate usually needs to be chiral. For a stereoselective S_N2 reaction in a catalytic manner, only kinetic resolution of racemic substrates and desymmetrization of meso or prochiral compounds are plausible.

In 2007, Maruoka reported the alkylation of glycinate Schiff base under PTC conditions with a combination of chiral quaternary ammonium bromide and 18-crown-

6 (**Figure 1.24**)[47]. The alkylation products were obtained with high diastereoselectivities and enantioselectivities in this S_N2-type nucleophilic substitution reaction, when two equivalents of racemic secondary alkyl halides were used as electrophiles. Mechanistic studies showed the high stereoselectivities came from the kinetic resolution of racemic secondary alkyl bromides.

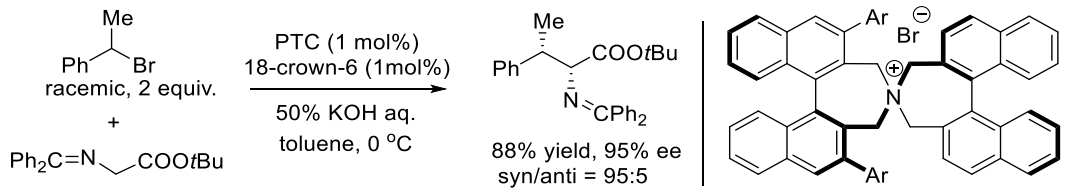

Figure 1.24 PTC catalyzed kinetic resolution of racemic secondary alkyl bromides

In 2012, List reported a kinetic resolution reaction via an asymmetric S_N2-type intramolecular O-alkylation catalyzed by a chiral phosphoric acid (**Figure 1.25**)[48]. As proposed by the author, both the nucleophile and the leaving group of the electrophile were simultaneously activated by the bifunctional chiral phosphoric acid. This was a rare example to use chiral phosphoric acid to catalyze the nucleophilic displacement at the sp^3-hybridized carbon center. The intramolecular transetherification reactions between racemic secondary benzylic ethers and alcohols were catalyzed to form 1,3-dihydroisobenzofuran via kinetic resolution and the selectivity factors range from 8 to 570.

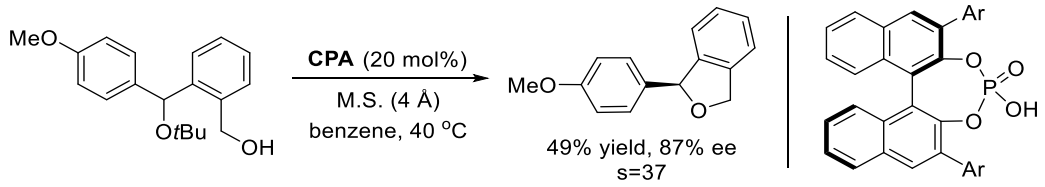

Figure 1.25 CPA catalyzed S_N2-type intramolecular O-alkylation via kinetic resolution

Except kinetic resolution, desymmetrization of meso or prochiral compounds can also achieve catalytic stereoselective S_N2-type reaction. Such reactions usually involve enantioselective ring opening of meso compounds, like epoxides, aziridine, cationic aziridinium, episulfonium and halonium ions.

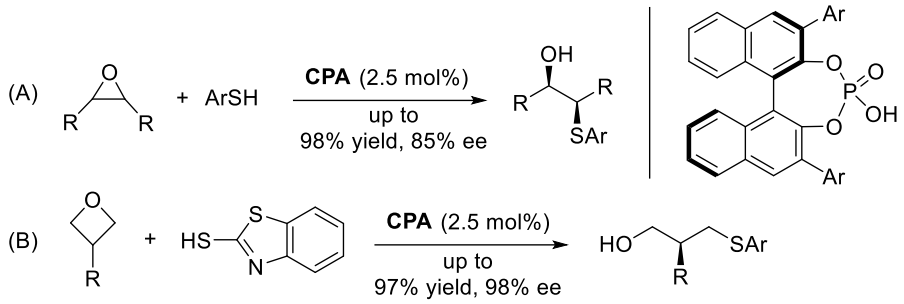

Figure 1.26 CPA catalyzed S_N2-type ring opening of meso-epoxides and phenyloxetane

In 2013, Sun reported the chiral phosphoric acid catalyzed asymmetric ring opening of meso-epoxides by nucleophilic attack of thiols (**Figure 1.26A**)[49]. 2-Mercaptobenzothiazole derivatives were utilized as nucleophiles to afford the desired product with good enantioselectivities. The authors believed that the bifunctional chiral phosphoric acid activated both the electrophile and nucleophile. The following work in this group achieved the ring opening of 3-phenyloxetane with the same catalyst and nucleophile (**Figure 1.26B**)[50] and the corresponding alcohols were generated.

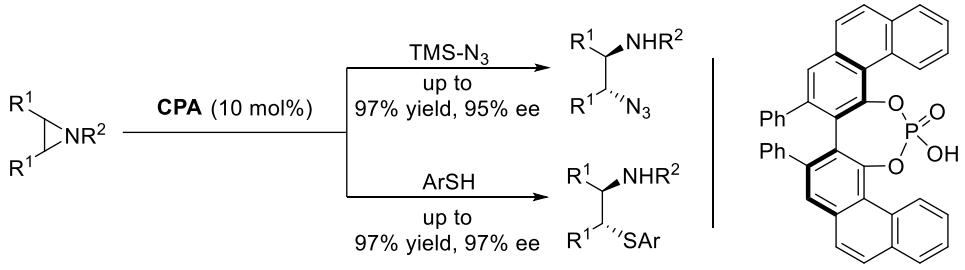

Figure 1.27 CPA catalyzed S_N2-type ring opening of meso-aziridines

This strategy using chiral phosphoric acid as catalyst is also developed in the asymmetric ring opening of meso-aziridines (**Figure 1.27**). Various nucleophiles, including $TMSN_3$[51], ArSH[52], etc., were reported.

Cationic meso-aziridinium and episulfonium ions were also used as electrophiles in desymmetrization S_N2 reactions. In 2008, Toste reported the aymmetric ring opening reactions of meso-aziridinium and episulfonium ions catalyzed by a chiral chiral phosphoric acid and Ag_2CO_3 (**Figure 1.28**)[53]. The in-situ generated silver phosphate salt was regarded as a chiral anion phase transfer catalyst.

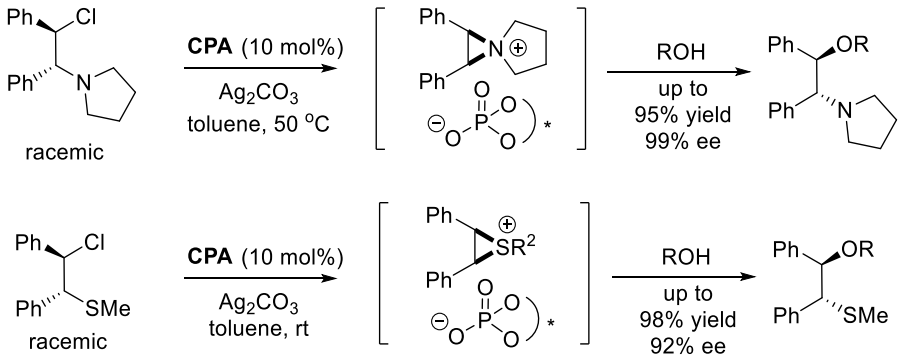

Figure 1.28 CPA catalyzed ring opening reactions of meso-aziridinium and episulfonium

In 2012, Jacobsen reported enantioselective ring-opening of episulfonium ion using a chiral thiourea catalyst together with sulfonic acid as cocatalyst (**Figure 1.29**)[54]. The episulfonium ions were in-situ generated from trichloroacetimidates type substrates and various indoles were utilized as nucleophiles. The products were obtained in high yields and ee values.

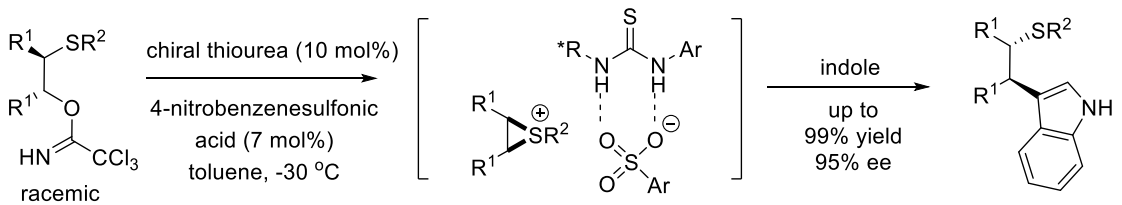

Figure 1.29 Chiral thiourea catalyst S_N2-type ring opening of episulfonium

Later in 2018, Gouverneur introduced hydrogen bonding phase-transfer catalysis. This approach was utilized in the enantioselective nucleophilic fluorination of episulfonium ion catalyzed with a chiral bis-urea catalyst (**Figure 1.30**)[55]. Metal fluoride was used as fluorine source for the ring opening of episulfonium ion, which is generated from the bromothioether.

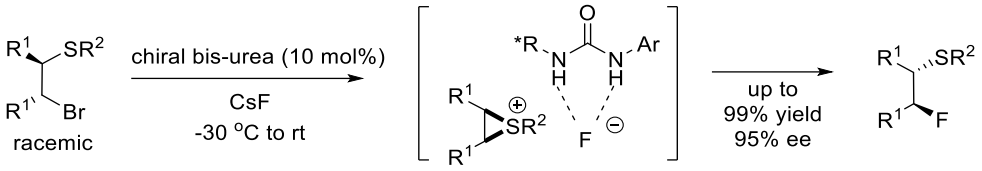

Figure 1.30 Chiral bis-urea catalyzed S_N2-type fluorination of episulfonium

In 2010, Frohlich reported the enantioselective intramolecular cyclization of meso-halonium ion catalyzed by a chiral phosphate anion (**Figure 1.31**)[56]. The meso-halonium ions were in-situ generated through reactions between symmetrical ene-diols and N-haloamides. Then the halonium ions ion-paired with a chiral anion cyclized affording enantioenriched haloetherification products.

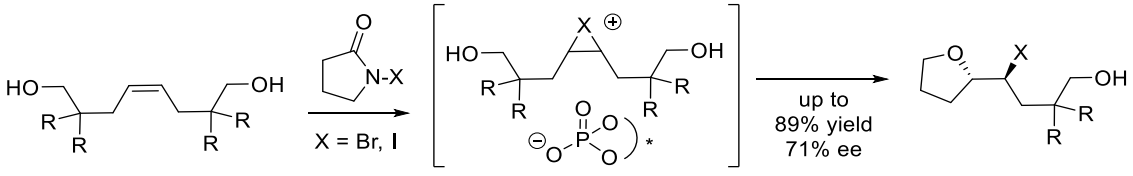

Figure 1.31 Chiral phosphate catalyzed intramolecular cyclization of meso-halonium ion

Although bulky tertiary electrophiles are regarded difficult in an S_N2-type reaction, there are several successful nucleophilic substitution examples of activated tertiary electrophiles in an S_N2 manner.

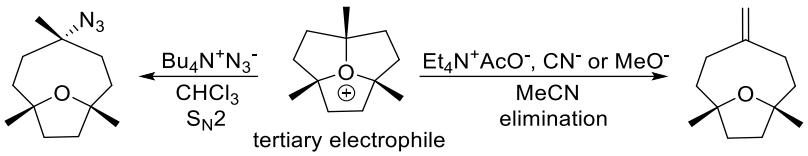

Figure 1.32 The 1,4,7-trimethyloxatriquinane as tertiary electrophile in S_N2 reaction

In 2010, Toney reported the nucleophilc substitution of 1,4,7-trimethyloxatriquinane at a tertiary carbon center (**Figure 1.32**)[57]. Alkyl oxonium salts are very reactive electrophiles and they are good alkylation agents. Investigated by the authors, 1,4,7-trimethyloxatriquinane was stable under the condition of S_N1 solvolysis reaction with alcohols (refluxing ethanol) and the substrate was recovered without any substitution or elimination in an S_N1 manner. When basic nucleophiles (like acetate, cyanide or methoxide) were introduced, the reaction generated the elimination product. When tetrabutylammonium azide was used as nucleophile, substitution reaction goes smoothly and affords the bicyclic azide efficiently. Mechanistic studies were in favor the S_N2 mechanism. This is the first example of S_N2 displacement that occurs on a tertiary carbon center.

In 2012, Iwasa reported the synthesis of the asymmetric chlorination of β-keto esters catalyzed by copper catalyst with the chiral pyridyl spirooxazoline ligand (**Figure 1.33**)[58]. Tertiary chlorides were generated in high yields and high enantioselectivities, which then subsequently substituted by sodium azides, alkylthiols and cesium fluorides. The corresponding tertiary azides, tertiary thioethers and tertiary fluoride were generated with inversion of stereochemistry determined by X-ray absolute configuration analysis, which indicated an S_N2 substitution. The tertiary chlorides might be activated by the two electron-withdrawing groups to undergo the challenging S_N2 displacement at a congested tertiary carbon center.

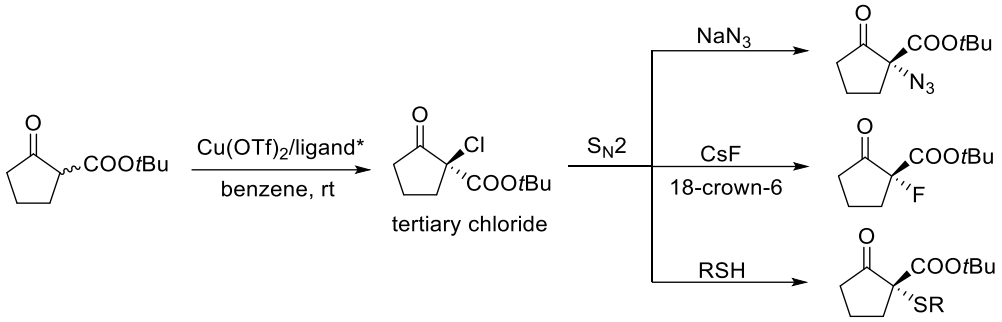

Figure 1.33 Chiral tertiary chloride as electrophile in S_N2 reaction

In 2017, Park reported the asymmetric phase-transfer catalyzed α-alkylation of a secondary bromide (diphenylmethyl *tert*-butyl α-bromomalonate) using a Maruoka catalyst (**Figure 1.34**)[59]. The tertiary bromides (α-bromo-α-alkylmalonates) were obtained with high yields and high enantioselectivities. Then nucleophiles sodium azides and phenolic alcohols were utilized to displace the bromide by S_N2 substitution, affording corresponding products α-azido-α-alkylmalonates and α-aryloxy-α-allylmalonates with inversion of stereochemistry.

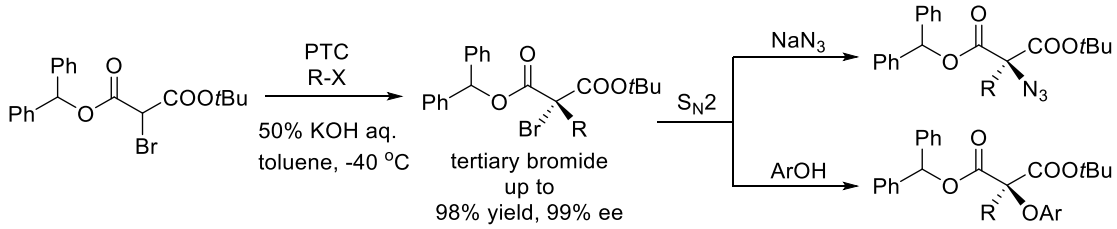

Figure 1.34 Chiral tertiary bromide as electrophile in S_N2 reaction

In 2017, Iwasa reported asymmetric decarboxylative chlorination of β-ketocarboxylic acids catalyzed by a 1,10-binaphthyl-based chiral amino ester (**Figure 1.35**)[60]. Both desired secondary chlorides and tertiary chlorides were obtained in high yields and enantioselectivities. Then the tertiary chloride α-chloroketone products were successfully substituted by sodium azides and sodium thiolates via S_N2 reaction.

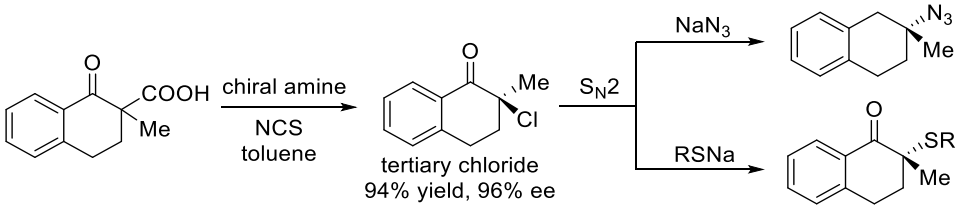

Figure 1.35 Chiral tertiary chloride as electrophile in S_N2 reaction

1.2.3 Stereoselective radical nucleophilic substitution reaction

Because of the inherent deficiencies of S_N1 and S_N2 reaction, there are many limitations in these reactions involving reaction efficiency, selectivity and scope. Radical nucleophilic substitution via SET process is potential to meet these challenges (**Figure 1.36**)[22].

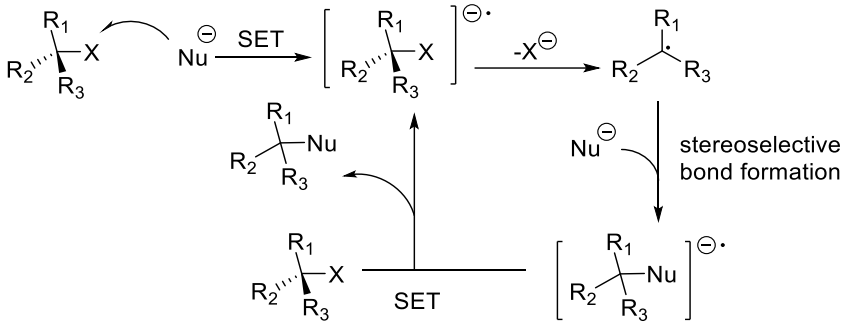

Figure 1.36 Mechanism of $S_{RN}1$ reaction

In $S_{RN}1$ reaction, activated alkyl halides with low-energy LUMO can get one electron from anionic nucleophile or initiated by other electron donors to generate radical intermediate and then react with another nucleophile to form new bond[23]. Many inorganic and organic anionic nucleophiles are effective in such transformations to construct different chemical bonds, like C-C, C-N, C-P, C-O, C-S, etc. bonds. Compared with S_N1 and S_N2 reaction, $S_{RN}1$ reaction involving radical intermediates is rather insensitive to steric hindrance and a wider substrates scope can be achieved. In addition, two enantiomers of racemic halides can be converted to the enantiopure product through the radical intermediate controlled by a chiral catalyst. Though many different $S_{RN}1$

reactions are well developed, asymmetric induction in $S_{RN}1$ reaction is still challenging because of the highly reactive radicals. There are limited examples controlling the stereoselectivities of the anionic nucleophiles using chiral auxiliaries or cinchona-derived phase-transfer catalysts.

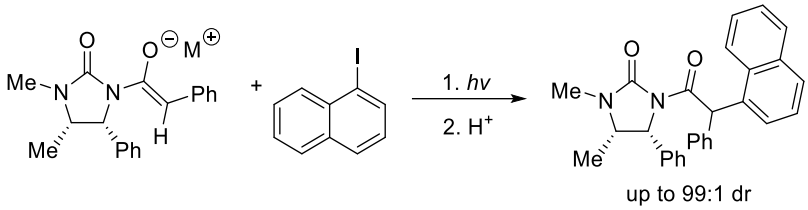

Figure 1.37 Chiral auxiliary assisted $S_{RN}1$ reaction

In 1994, Rossi reported a photo-initiated stereoselective $S_{RN}1$ reaction (**Figure 1.37**)[61]. Amide enolate attached to a chiral auxiliary reacted with 1-iodonaphthalene in liquid ammonia to afford chiral diarylacetic acid with moderate yield and high diastereoselectivity. The counter ions of the enolates had great influence on the diastereoselectivities. Lithium and titanium show best diastereoselectivities (the diastereomeric ratio > 99).

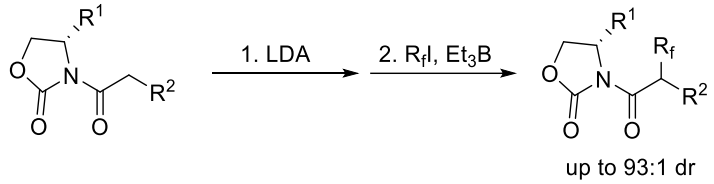

Figure 1.38 Chiral auxiliary assisted $S_{RN}1$ reaction

In 1995, Kobayashi reported a triethylborane (Et_3B) initiated $S_{RN}1$ reaction (**Figure 1.38**)[62]. Various N-acyloxazolidinones attached to chiral auxiliaries were deprotonated by LDA to form enolates in tetrahydrofuran. The perfluoroalkyl iodides were mediated by Et_3B to form perfluoroalkyl radicals, which were trapped by the chiral enolates to generate the α-perfluoroalkyl carboximides with high diastereoselectivities.

In 1999, Crozet reported the photo-initiated stereoselective alkylation of 2-nitropropionate anions assisted by chiral auxiliaries under $S_{RN}1$ reaction conditions

(**Figure 1.39**)[63]. The authors tried different chiral auxiliaries and found 8-phenylmenthol was best, but the yields and diastereoselectivities were still unsatisfactory.

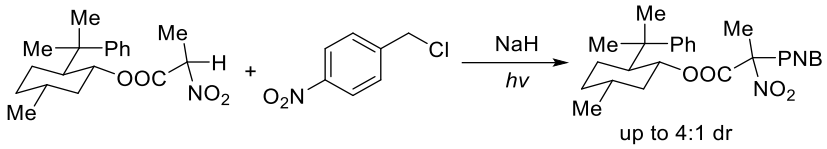

Figure 1.39 Chiral auxiliary assisted $S_{RN}1$ reaction

In 2015, Melchiorre reported a photo-initiated asymmetric perfluoroalkylation of ketoesters using cinchona-derived phase-transfer catalysts (**Figure 1.40**)[64]. Best results were obtained when a conbination of chlorobenzene and perfluorooctane was used as solvent. The authors proposed an interesting colored electron donor−acceptor (EDA) complex, generated from electron-deficient perfluoralkyl iodide and electron-rich enolate which was ion paired with a chiral cation. SET was induced by photo irradiation and a $S_{RN}1$ radical chain propagation pathway was proposed.

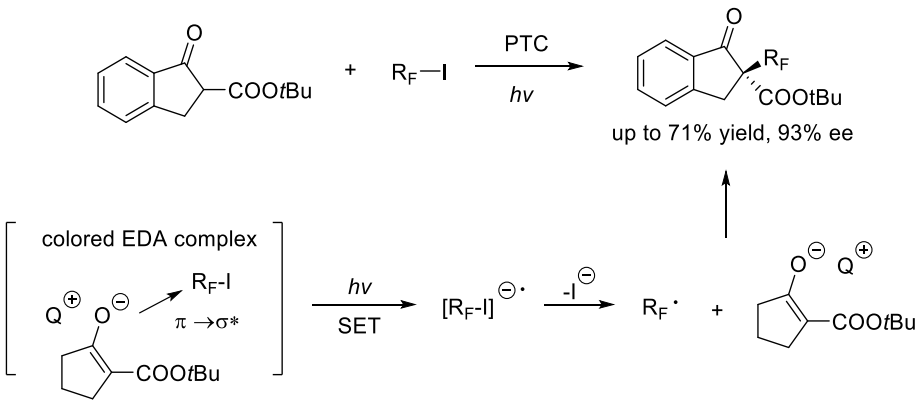

Figure 1.40 Photo-initiated asymmetric perfluoroalkylation of ketoesters by PTC

These are examples controlling the stereoselectivities of the anionic nucleophiles using chiral auxiliaries or cationic phase-transfer catalysts, but there is not any report about controlling the stereoselectivities of racemic electrophiles in metal-free radical nucleophilic substitution reactions to the best of our knowledge. In the meanwhile, such transformation known as enantioconvergent substitution of racemic electrophiles is well

developed in transition-metal catalysis. As reported, active alkyl radicals can be trapped by chiral transition metal species in a stereoselective manner (**Figure 1.41**).

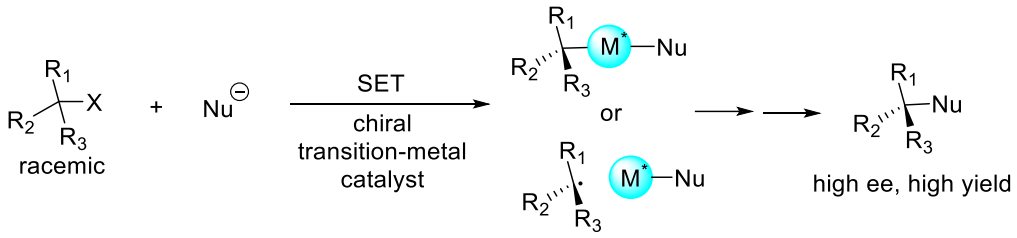

Figure 1.41 Radical nucleophilic substitution by chiral transition-metal catalysis

Fu has developed Ni-catalyzed enantioconvergent substitution of racemic electrophiles[22, 65]. They have done systematic studies for this important transformation, including reaction scope, mechanism study, reaction condition improvement, etc. For reaction scope, various activated/unactivated secondary/tertiary electrophiles and different atom-based nucleophiles including carbon, boron, silicon and nitrogen have been developed.

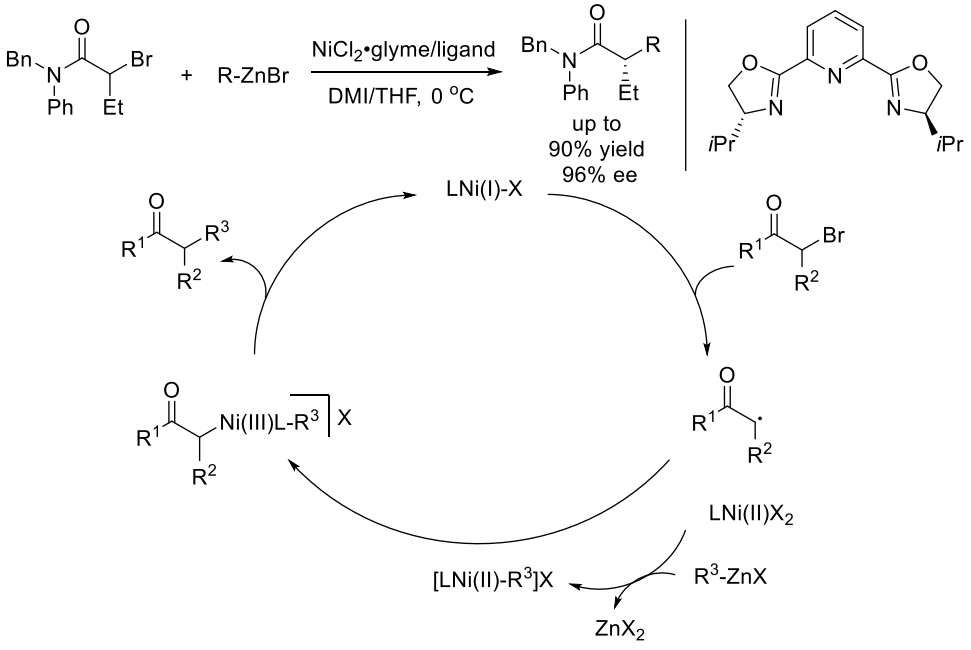

Figure 1.42 Chiral Ni-catalyzed Negishi cross-coupling reaction

In 2005, they reported the first catalytic enantioconvergent substitution of an activated secondary alkyl electrophile (**Figure 1.42**)[66]. In this Negishi cross-coupling

reaction, α-bromo amides were used as electrophiles to react with various unfunctionalized and functionalized organozinc reagents using Ni/(*i*-Pr)-Pybox catalysts. These enantioselective carbon-carbon bond forming reactions proceeded smoothly and the α-alkylated amides were obtained in high yields and enantioselectivities. Both enantiomers of the racemic secondary bromide are substituted to form the same enantiomer via radical intermediates. The following mechanism studies confirmed the enantioconvergent radical nucleophilic substitution mechanism[67].

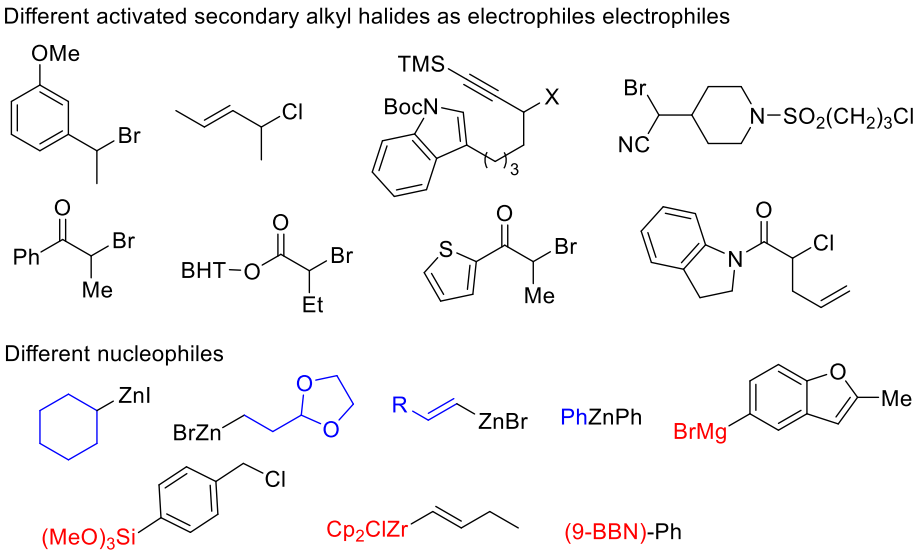

Figure 1.43 Electrophiles and nucleophiles in Ni-catalyzed radical nucleophilic substitutions

This asymmetric coupling of racemic activated secondary alkyl halides with organozinc reagents to form carbon-carbon bond is further developed (**Figure 1.43**). Various other activated secondary bromides can be utilized as electrophiles, like allylic[68], benzylic[69, 70], propargylic[71, 72] halides and α-halonitriles[73]. Various alkylzinc[69, 70], arylzinc[72, 74] and alkenylzinc[73] can be utilized as nucleophiles. In addition, the nucleophiles are not only limited to organozinc reagents. Organomagnesium[75], organozirconium[76], organoboron[77] and organosilicon[78]

reagents are also success nucleophiles in the coupling with various racemic α-halocarbonyl electrophiles.

Unactivated secondary alkyl halides that bearing two alkyl groups are also successful (**Figure 1.44**). However, to obtain products with high enantioselectivities, proper directing groups are necessary. An aromatic ring [79], aniline [80], sulfonamine [81] and carbonyl group [82] has been reported as effective directing groups in several reaction.

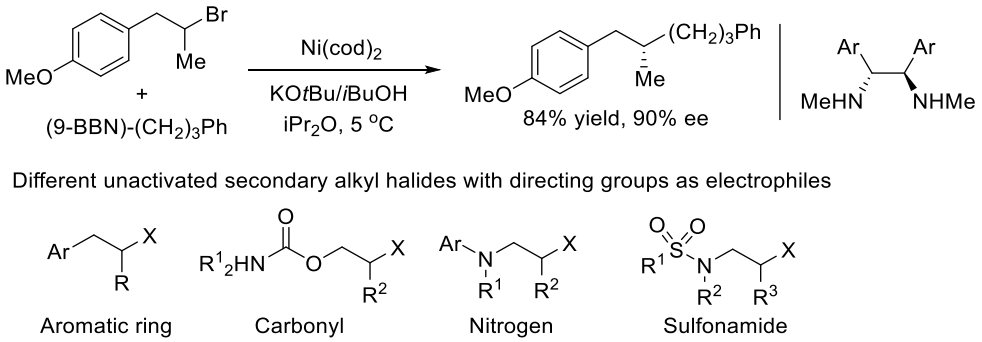

Figure 1.44 Unactivated secondary alkyl halides with directing groups as electrophiles

Other secondary halides bearing a perfluoroalkyl group[83] or boron substitution[84] also resulted in high yields and high enantioselectivities (**Figure 1.45**). Alkylboronate esters can be transformed to various organic compounds, so the enantioconvergent synthesis of alkylboronate esters is very useful and important.

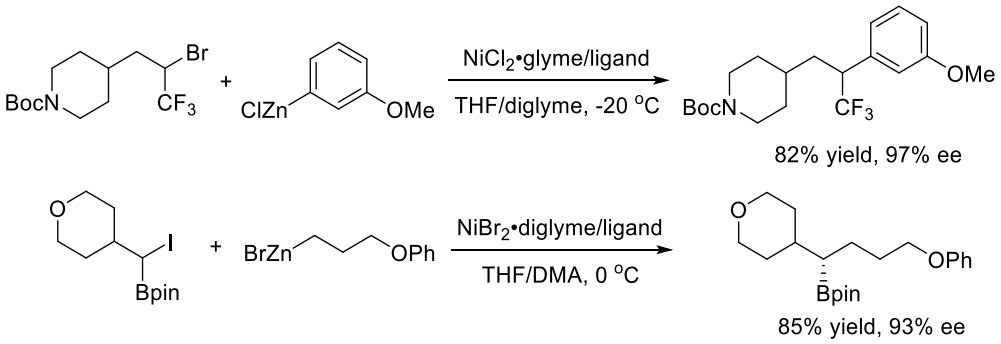

Figure 1.45 Unactivated secondary halides bearing a perfluoroalkyl group or boron

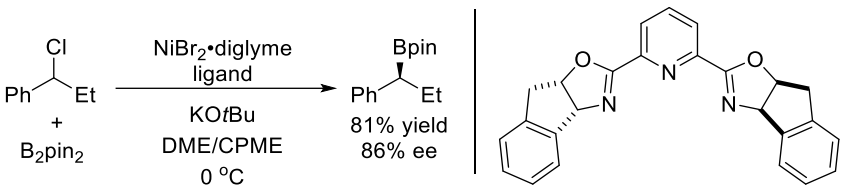

Figure 1.46 Enantioconvergent boration of secondary halides using B_2pin_2 as nucleophile

Utilizing boron and silicon-based nucleophiles to form C-B and C-Si bonds are also developed, but stereocontrol is still challenging in such reactions (**Figure 1.46**). The enantioconvergent substitution of racemic benzylic chlorides using B_2pin_2 as nucleophiles to form C-B bond is reported recently with moderate to good enantioselectivities[85].

Except for Nickle, other transition metals were also successful in such transformations (**Figure 1.47**). In 2014, Walsh reported the cobalt-bisoxazoline complex catalyzed cross-coupling of α-bromo esters and aryl Grignard reagents[86]. Various enantioenriched α-arylalkanoic esters were produced in high yields and enantioselecticities. In 2015, Nakamura reported the first iron-catalyzed example[87] and a chiral bisphosphine ligand was used. α-Chloro esters and aryl Grignard reagents were reacted to enantioselectively afford the desired products in good yields and enantioselecticities.

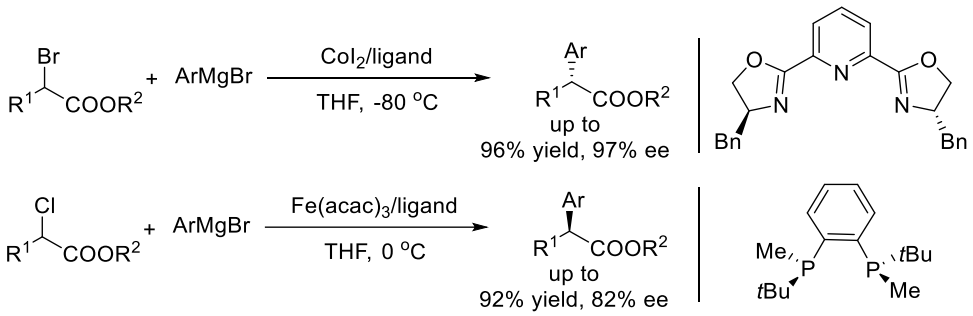

Figure 1.47 Chiral Co and Fe complex catalyzed radical nucleophilic substitution

Racemic secondary alkyl halides are well developed to be substituted by various nucleophiles in an enantiocovergent manner, but tertiary alkyl halides are still challenging and rarely reported in asymmetric metal-catalyzed radical nucleophilic substitution.

In 2016, Fu reported the asymmetric nucleophilic substitution of racemic tertiary alkyl halides using amines as nucleophiles (**Figure 1.48**)[88]. This C-N bond forming reaction was catalyzed by a chiral copper catalyst and induced by blue LED. Racemic tertiary chloride reacted with nitrogen nucleophile smoothly, affording the desired product bearing a tetrasubstituted stereocenter in high yield and enantioselectivity.

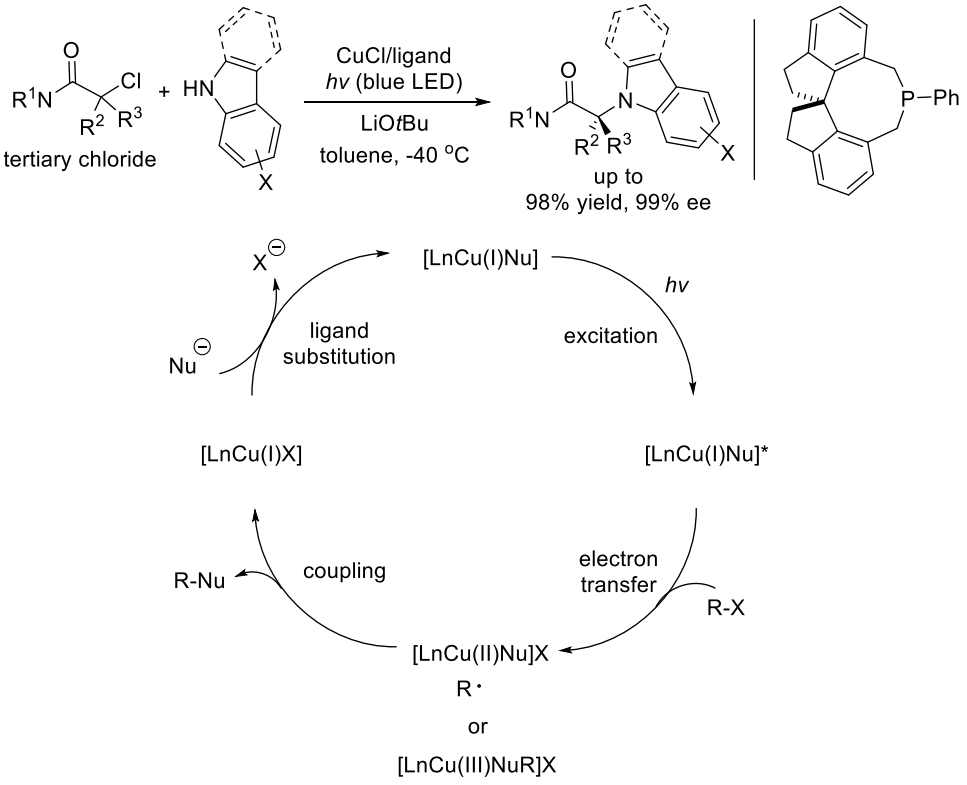

Figure 1.48 Radical nucleophilic substitution of tertiary halide electrophiles

1.2.4 Halogenophilic nucleophilic substitution (S_N2X) reaction

Traditionally, in S_N2 reaction, nucleophile approaches electrophile from the 'backside' of C-X bond and attack the carbon atom displacing the leaving group X, which can be considered as carbonophilic reactions. Whereas nucleophilic substitution usually occurs on a carbon atom displacing X, there are some reports about attack on the halogen atom by the nucleophile. In these reactions, nucleophile approaches electrophile from the 'front' of C-X bond and attack the X atom, while the carbon moiety becomes a leaving group to form carbanion. Such reactions can be considered as halogenophilic reactions[89, 90]. These reactions suggest that the C-X bond of an electrophile is ambident in nucleophilic attack. The role of halogen atom in such halogenophilic reaction has been discussed in some calculation studies[91, 92]. According to these studies, more stable halogen-bonded intermediates are the pre-reaction complexes and the halogenophilic pathway is promoted by halogen-bonding. In the meanwhile, C-X bonds are elongated and activated, followed by the bond cleavage and formation of carbanions.

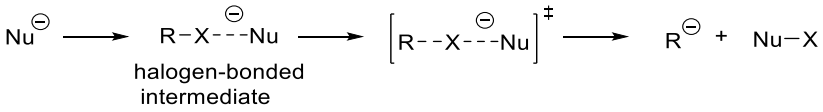

Figure 1.49 Halogen-bonding promoted halogenophilic reaction

Halogen bonding, which is well studied in crystal engineering, material science and also appears in biological systems, is the non-covalent interaction between the electrophilic site of halogen atom X and the nucleophilic site of another atom[93, 94]. Halogen atom is the electrophile center in halogen bond. Generally, the electronegativity of halogen atom is higher than carbon atom, so nucleophilic substitution usually occurs on a carbon atom. Confirmed by experimental and computational studies, when the halogen atom X is covalently bonded to other atoms, the electron density on the X atom is anisotropically distributed and the shape of the X atom becomes an ellipse (**Figure**

1.50). The region with higher electron density forms a belt around the center of X atom, and the electron density of the outermost region along the C-X bond is lower, which is called σ-hole[95]. The electron deficient σ-hole will be influenced by the size of the X atom and neighboring groups. The larger atom usually has better polarization, which makes the electronegative and electropositive region of the atom more distinct. The σ-hole on I atom is usually larger and more positive compared with Br and Cl atoms. The σ-hole is also enhanced when its neighboring groups are electron-withdrawing ones. Compound bearing a halogen atom is potential to be used as halogen-bonding donor.

There are increasing interests on studies about halogen bonding and their applications in catalysis and organic reactions have also attracted a lot of attention[12, 96, 97]. With the σ-hole acting as the electrophilic region, the X atom is possible to be the electrophile center of C-X bond not only in halogen bonding interactions but also in the reaction with nucleophiles. Such halogenophilic reactions are reported long ago, but still not known to many chemists [89, 90].

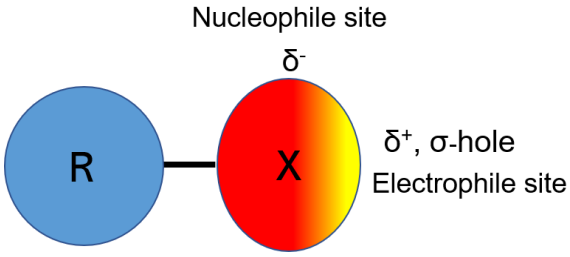

Figure 1.50 Anisotropically distributed electron density and σ-hole on a halogen atom

Generally, the structures of the halides and the inherent properties of the substrates determine the tendency of halogenophilic reactions. Such reaction is usually promoted when the nucleophilic substitution at the carbon atom is hampered making the competing carbonophilic reaction difficult to occur. The hampered carbon atoms can be sp-hybridized carbon, sp^2-hybridized carbon or steric-hindered sp^3-hybridized carbon atom.

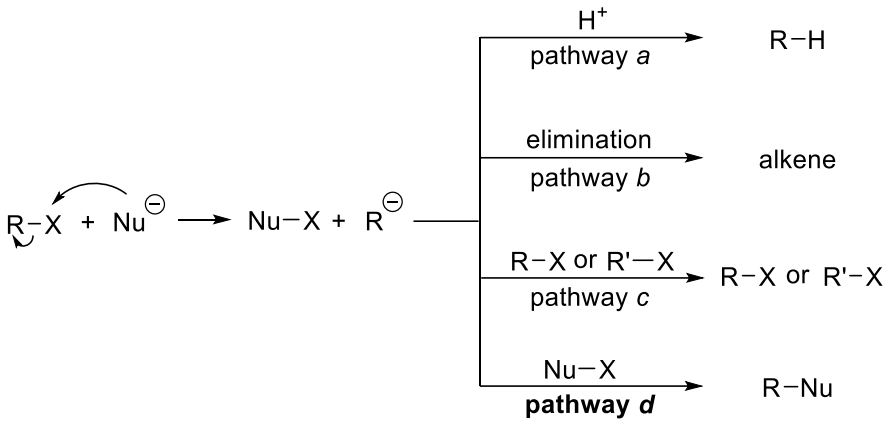

Figure 1.51 Possible reactions of carbanion generated in halogenophilic attack

Halogenophilic attack normally forms a pair of a carbanion intermediate and a new electrophilic intermediate (Nu-X) with reversed polarity. The further transformation of the carbanion intermediate can be useful in synthesis and has attracted some attention. Several pathways are summarized here (**Figure 1.51**). When there is proton source in the system, the carbanion can be quickly protonated to form protonated product, which is also called reduction of the C-X bond (pathway *a*). When there is an appropriate leaving group (like an adjacent halide) in the carbanion, elimination is possible to generate alkene specie product (pathway *b*). The carbanion can also react with the initial halide substrate R-X to form dimerization product R-R, which is usually obtained in a radical reaction. This pathway can be used as a synthetic alternative to some radical processes. If there are additional electrophilic agents, like another alkyl halide R'-X, the alkylation of carbanion with R'-X will afford product R-R' (pathway *c*). When the newly formed electrophile Nu-X is reactive enough, the reaction between carbanion and Nu-X is possible to occur affording R-Nu (pathway *d*). This pathway attracts our attention, because the product R-Nu is identical with the product formed in a common carbonophilic nucleophilic substitution. This type of reaction is what we care most and will be discussed in detail.

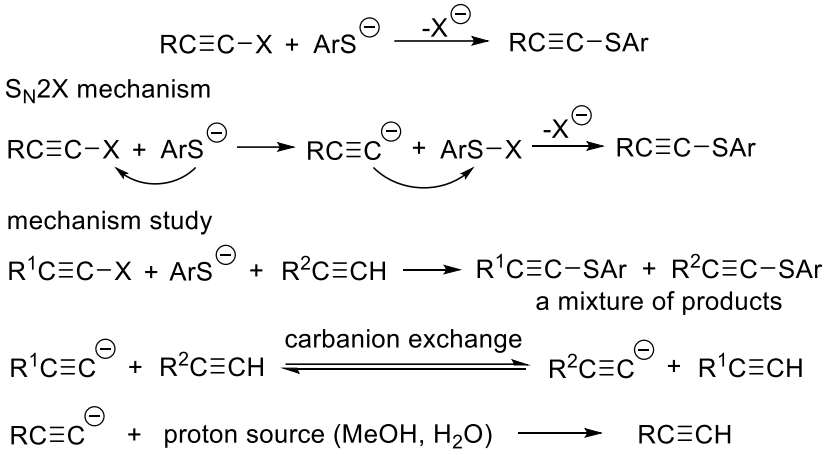

Figure 1.52 The S_N2X-type substitution of halo-alkynes

In 1971, Drenth reported the nucleophilic substitution of halo-alkynes using thiolates as nucleophiles (**Figure 1.52**)[98] . An S_N2X mechanism is proposed. The halogen atom bonded to a sp-hybridized carbon atom is attacked by a thiolate. The authors conducted a series of experimental studies to confirm the mechanism. Reaction between R^1 substituted bromo-alkyne and NaSEt was conducted with addition of R^2 substituted alkyne and afforded a mixture of substituted product alkynyl sulfides bearing R^1 or R^2 moiety. This result indicated the existence of acetylide anion intermediates and the resulting carbanion exchange. The acetylide anions were also confirmed by using methanol or water as solvents. In these protic solvents, these acetylide anions were quickly protonated before reacting with sulfenyl bromide (RS-Br) and generated acetylenes and disulfides as products.

In 1993, Scorrano reported the nucleophilic substitution of aryl halide which was activated by a nitro group (**Figure 1.53**)[99]. Thiolates were used as nucleophiles in solvent 2-PrOH generating o-nitrophenyl thioethers together with nitrobenzene. Mechanism studies supported an S_N2X pathway.

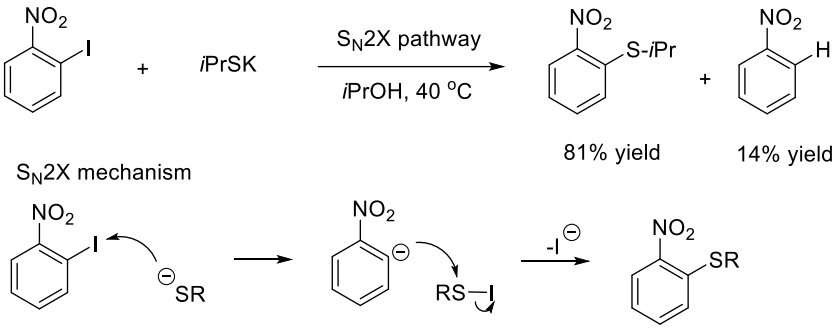

Figure 1.53 The S_N2X-type substitution of o-nitrophenyl thioethers

The S_N2X reaction using silyllithium compound as nucleophile is reported by Ito in 2017 (**Figure 1.54**)[100]. The reactions between dimethylphenylsilyllithium and different aryl bromides afforded various arylsilanes in good yields. Mechanistic studies excluded a radical pathway and agreed with a halogenophilic mechanism.

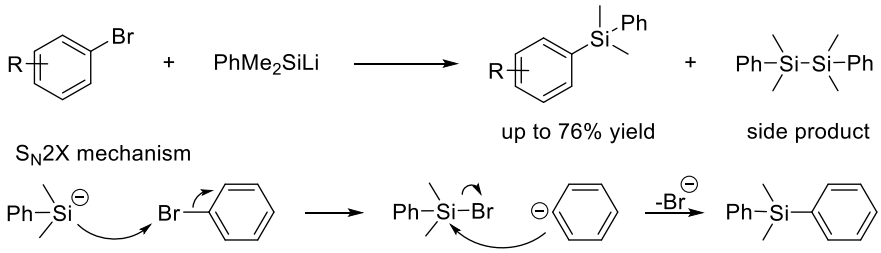

Figure 1.54 Arylation of dimethylphenylsilyllithium via S_N2X mechanism

In 2004, Strohmann reported the enantiodivergent alkylation of an enantioenriched silyllithium compound (**Figure 1.55**)[101]. The inversion and retention of the chiral Si stereocenter was controlled by changing the halogen atom of benzyl halide. When benzyl chloride was used, the chiral Si stereocenter remained. However, when benzyl bromide was used, the chiral Si stereocenter was inverted. The chiral silyllithium react with benzyl chloride in an S_N2 manner and carbon atom of C-Cl bond is attacked to retain the configuration. In the reaction with benzyl bromide, the bromide atom is attacked by silyllithium in an S_N2X manner to generate benzyllithium and enantiomerically pure bromosilane. The following nucleophilic attack on the silicon atom by benzyllithium afford the alkylated silicon with inverted configuration.

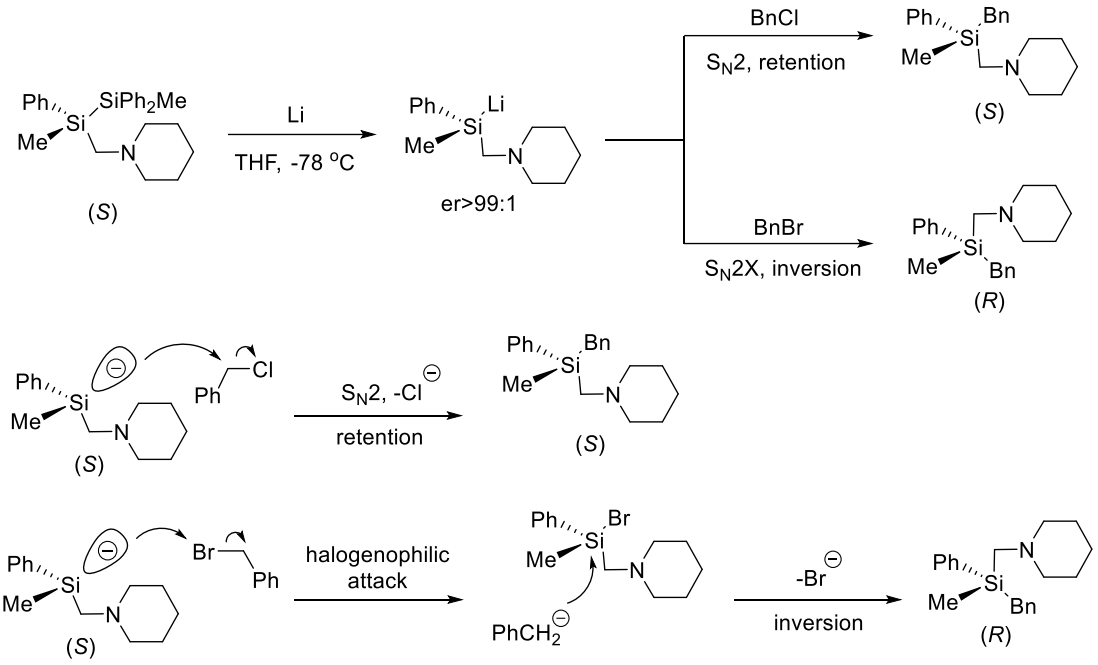

Figure 1.55 Enantiodivergent alkylation of an enantioenriched silyllithium compound

1.3 Summary and project design

The past several decades have witnessed the rapid development of phase-transfer catalysis. With regards to the chiral catalysts, many well-designed catalysts have been synthesized and shown strong power in asymmetric synthesis. Another aspect is the reaction scope. Many types of PTC reactions have been developed, like alkylation, conjugate addition, Mannich, Aldol, Darzens, epoxidation, aziridination, dihydroxylation, flurination, strecker, etc., reactions. These achievements are satisfying and also encouraging us to develop new catalysts and new reaction types.

Nucleophilic substitution reactions belong to the most significant organic chemistry concepts. They are so widely used in organic synthesis that controlling the stereoselectivity of these reactions has been attracting a lot of attention. According to different mechanisms, different strategies using various chiral catalysts are well developed. For S_N1-type reactions, chiral anionic catalysts are efficient. For S_N2-type reaction, kinetic resolution of racemic secondary electrophiles is reported under PTC condition or catalyzed by chiral phosphoric acids. Desymmetrization of meso or prochiral compounds via S_N2 attack are achieved with chiral Lewis or Brønsted acids. For radical nucleophilic substitution, chiral transition metal catalysis has developed and shown strong power. Many racemic halides and nucleophiles are successfully utilized in these approaches. On the other hand, these types of nucleophilic substitution reactions have their inherent limitations, not only about stereocontrol but also the substrate scope including nucleophiles and electrophiles.

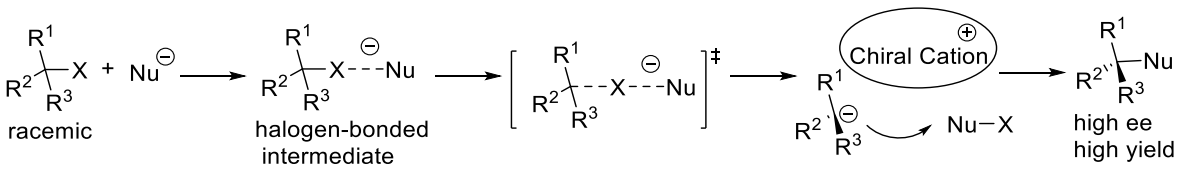

Figure 1.56 Project design: Phase-transfer catalyzed enantioconvergent S_N2X reaction

For the less known S_N2X reaction, successful stereocontrol has not been reported yet. The S_N2X reaction mechanism and scope also need further studies. Exploiting more nucleophiles and electrophiles are necessary in order to form various chemical bonds. We believe developing stereoselective S_N2X reactions will make a difference and complement other types of nucleophilic substitution reactions. Here, we have designed an enantioconvergent S_N2X reaction under PTC conditions. The carbanion intermediate can be controlled by our cationic pentanidium or bisguanidinium catalyst through ion-pairing, followed by stereoselective bond formation with Nu-X.

1.4 References

1. E. V. Dehmlow, Advances in Phase-Transfer Catalysis. *Angew Chem Int Edit* **16**, 493 (1977).
2. K. Maruoka, T. Ooi, Enantioselective amino acid synthesis by chiral phase-transfer catalysis. *Chem. Rev.* **103**, 3013 (2003).
3. T. Ooi, K. Maruoka, Recent advances in asymmetric phase-transfer catalysis. *Angew. Chem. Int. Ed.* **46**, 4222 (2007).
4. S. Shirakawa, K. Maruoka, Recent developments in asymmetric phase-transfer reactions. *Angew. Chem. Int. Ed.* **52**, 4312 (2013).
5. B. Lygo, B. I. Andrews, Asymmetric phase-transfer catalysis utilizing chiral quaternary ammonium salts: asymmetric alkylation of glycine imines. *Acc. Chem. Res.* **37**, 518 (2004).
6. S. Kaneko, Y. Kumatabara, S. Shirakawa, A new generation of chiral phase-transfer catalysts. *Org Biomol Chem*, (2016).
7. S. Liu, Y. Kumatabara, S. Shirakawa, Chiral quaternary phosphonium salts as phase-transfer catalysts for environmentally benign asymmetric transformations. *Green Chem.* **18**, 331 (2016).
8. L. Zong, C. H. Tan, Phase-Transfer and Ion-Pairing Catalysis of Pentanidiums and Bisguanidiniums. *Acc. Chem. Res.* **50**, 842 (2017).
9. N. Patel, R. Sood, P. V. Bharatam, $NL_2(+)$ Systems as New-Generation Phase-Transfer Catalysts. *Chem. Rev.* **118**, 8770 (2018).
10. T. Ma *et al.*, Pentanidium-Catalyzed Enantioselective Phase-Transfer Conjugate Addition Reactions. *J. Am. Chem. Soc.* **133**, 2828 (2011).
11. Y. Y. Yang *et al.*, Pentanidium-Catalyzed Enantioselective alpha-Hydroxylation of Oxindoles Using Molecular Oxygen. *Org. Lett.* **14**, 4762 (2012).

12. L. Zong, X. Ban, C. W. Kee, C. H. Tan, Catalytic Enantioselective Alkylation of Sulfenate Anions to Chiral Heterocyclic Sulfoxides Using Halogenated Pentanidium Salts. *Angew. Chem. Int. Ed.*, (2014).
13. L. Zong, S. Du, K. F. Chin, C. Wang, C. H. Tan, Enantioselective Synthesis of Quaternary Carbon Stereocenters: Addition of 3-Substituted Oxindoles to Vinyl Sulfone Catalyzed by Pentanidiums. *Angew. Chem. Int. Ed.* **54**, 9390 (2015).
14. B. Teng *et al.*, Pentanidium- and Bisguanidinium-Catalyzed Enantioselective Alkylations Using Silylamide as Bronsted Probase. *J. Am. Chem. Soc.* **138**, 9935 (2016).
15. C. Wang, L. Zong, C. H. Tan, Enantioselective Oxidation of Alkenes with Potassium Permanganate Catalyzed by Chiral Dicationic Bisguanidinium. *J. Am. Chem. Soc.* **137**, 10677 (2015).
16. E. D. Hughes, C. K. Ingold, A. D. Scott, 253. Reaction kinetics and the Walden inversion. Part II. Homogeneous hydrolysis, alcoholysis, and ammonolysis of α-phenylethyl halides. *J. Chem. Soc.* **0**, 1201 (1937).
17. T. P. Curran, A. J. Mostovoy, M. E. Curran, C. Berger, Introducing Aliphatic Substitution with a Discovery Experiment Using Competing Electrophiles. *J. Chem. Educ.* **93**, 757 (2016).
18. S. R. Hartshorn, *Aliphatic Nucleophilic Substitution*. (Cambridge University Press: London, 1973).
19. A. Streitwieser, Solvolytic Displacement Reactions At Saturated Carbon Atoms. *Chem. Rev.* **56**, 571 (1956).
20. E. D. Hughes, C. K. Ingold, R. J. L. Martin, D. F. Meigh, Walden Inversion and Reaction Mechanism - Walden Inversion in Unimolecular Reactions of Secondary and Tertiary Alkyl Halides. *Nature* **166**, 679 (1950).

21. C. A. Bunton, E. D. Hughes, C. K. Ingold, D. F. Meigh, Walden Inversion and Reaction Mechanism: Walden Inversion in the Acid Hydrolysis of Carboxylic Esters by Unimolecular Alkyl Fission. *Nature* **166**, 680 (1950).
22. G. C. Fu, Transition-Metal Catalysis of Nucleophilic Substitution Reactions: A Radical Alternative to S_N1 and S_N2 Processes. *ACS Cent. Sci.* **3**, 692 (2017).
23. R. A. Rossi, A. B. Pierini, A. B. Penenory, Nucleophilic substitution reactions by electron transfer. *Chem. Rev.* **103**, 71 (2003).
24. N. Kornblum, Substitution Reactions Which Proceed via Radical Anion Intermediates. *Angew. Chem. Int. Ed.* **14**, 734 (1975).
25. N. Kornblum, R. E. Michel, R. C. Kerber, Chain Reactions in Substitution Processes Which Proceed via Radical-Anion Intermediates. *J. Am. Chem. Soc.* **88**, 5662 (1966).
26. G. A. Russell, W. C. Danen, Coupling Reactions of the 2-Nitro-2-propyl Anion1. *J. Am. Chem. Soc.* **88**, 5663 (1966).
27. J. F. Bunnett, J. K. Kim, Alkali metal promoted aromatic "nucleophilic" substitution. *J. Am. Chem. Soc.* **92**, 7464 (1970).
28. J. F. Bunnett, J. K. Kim, Evidence for a radical mechanism of aromatic "nucleophilic" substitution. *J. Am. Chem. Soc.* **92**, 7463 (1970).
29. K. Brak, E. N. Jacobsen, Asymmetric ion-pairing catalysis. *Angew. Chem. Int. Ed.* **52**, 534 (2013).
30. M. Braun, W. Kotter, Titanium(IV)-catalyzed dynamic kinetic asymmetric transformation of alcohols, silyl ethers, and acetals under carbon allylation. *Angew. Chem. Int. Ed.* **43**, 514 (2004).
31. K. Motoyama, M. Ikeda, Y. Miyake, Y. Nishibayashi, Cooperative Catalytic Reactions Using Lewis Acids and Organocatalysts: Enantioselective Propargylic

Alkylation of Propargylic Alcohols Bearing an Internal Alkyne with Aldehydes. *Eur. J. Org. Chem.* **2011**, 2239 (2011).

32. M. Mahlau, B. List, Asymmetric counteranion-directed catalysis: concept, definition, and applications. *Angew. Chem. Int. Ed.* **52**, 518 (2013).
33. Q. X. Guo *et al.*, Highly Enantioselective Alkylation Reaction of Enamides by Bronsted-Acid Catalysis. *Org. Lett.* **11**, 4620 (2009).
34. L. Song, Q. X. Guo, X. C. Li, J. Tian, Y. G. Peng, The direct asymmetric alpha alkylation of ketones by Bronsted acid catalysis. *Angew. Chem. Int. Ed.* **51**, 1899 (2012).
35. M. W. Chen, Q. A. Chen, Y. Duan, Z. S. Ye, Y. G. Zhou, Asymmetric hydrogenolysis of racemic tertiary alcohols, 3-substituted 3-hydroxyisoindolin-1-ones. *Chem. Commun. (Camb)* **48**, 1698 (2012).
36. O. El-Sepelgy, S. Haseloff, S. K. Alamsetti, C. Schneider, Bronsted acid catalyzed, conjugate addition of beta-dicarbonyls to in situ generated ortho-quinone methides--enantioselective synthesis of 4-aryl-4H-chromenes. *Angew. Chem. Int. Ed.* **53**, 7923 (2014).
37. W. Zhao, Z. Wang, B. Chu, J. Sun, Enantioselective formation of all-carbon quaternary stereocenters from indoles and tertiary alcohols bearing a directing group. *Angew. Chem. Int. Ed.* **54**, 1910 (2015).
38. H. H. Liao, A. Chatupheeraphat, C. C. Hsiao, I. Atodiresei, M. Rueping, Asymmetric Bronsted Acid Catalyzed Synthesis of Triarylmethanes-Construction of Communesin and Spiroindoline Scaffolds. *Angew. Chem. Int. Ed.* **54**, 15540 (2015).

39. A. Chatupheeraphat *et al.*, Asymmetric Bronsted Acid Catalyzed Substitution of Diaryl Methanols with Thiols and Alcohols for the Synthesis of Chiral Thioethers and Ethers. *Angew. Chem. Int. Ed.* **55**, 4803 (2016).
40. J. Suc, I. Dokli, M. Gredicak, Chiral Bronsted acid-catalysed enantioselective synthesis of isoindolinone-derived N(acyl),S-acetals. *Chem. Commun. (Camb)* **52**, 2071 (2016).
41. S. Lee, P. S. Kaib, B. List, Asymmetric Catalysis via Cyclic, Aliphatic Oxocarbenium Ions. *J. Am. Chem. Soc.* **139**, 2156 (2017).
42. I. T. Raheem, P. S. Thiara, E. A. Peterson, E. N. Jacobsen, Enantioselective Pictet-Spengler-type cyclizations of hydroxylactams: H-bond donor catalysis by anion binding. *J. Am. Chem. Soc.* **129**, 13404 (2007).
43. S. E. Reisman, A. G. Doyle, E. N. Jacobsen, Enantioselective thiourea-catalyzed additions to oxocarbenium ions. *J. Am. Chem. Soc.* **130**, 7198 (2008).
44. A. E. Wendlandt, P. Vangal, E. N. Jacobsen, Quaternary stereocentres via an enantioconvergent catalytic SN1 reaction. *Nature* **556**, 447 (2018).
45. V. Bhat, E. R. Welin, X. Guo, B. M. Stoltz, Advances in Stereoconvergent Catalysis from 2005 to 2015: Transition-Metal-Mediated Stereoablative Reactions, Dynamic Kinetic Resolutions, and Dynamic Kinetic Asymmetric Transformations. *Chem. Rev.* **117**, 4528 (2017).
46. S. V. Pronin, C. A. Reiher, R. A. Shenvi, Stereoinversion of tertiary alcohols to tertiary-alkyl isonitriles and amines. *Nature* **501**, 195 (2013).
47. T. Ooi, D. Kato, K. Inamura, K. Ohmatsu, K. Maruoka, Practical stereoselective synthesis of beta-branched alpha-amino acids through efficient kinetic resolution in the phase-transfer-catalyzed asymmetric alkylations. *Org. Lett.* **9**, 3945 (2007).

48. I. Coric *et al.*, Bronsted acid catalyzed asymmetric SN2-type O-alkylations. *Angew. Chem. Int. Ed.* **52**, 3490 (2013).
49. Z. Wang, W. K. Law, J. Sun, Chiral phosphoric acid catalyzed enantioselective desymmetrization of meso-epoxides by thiols. *Org. Lett.* **15**, 5964 (2013).
50. Z. Wang, Z. Chen, J. Sun, Catalytic enantioselective intermolecular desymmetrization of 3-substituted oxetanes. *Angew. Chem. Int. Ed.* **52**, 6685 (2013).
51. E. B. Rowland, G. B. Rowland, E. Rivera-Otero, J. C. Antilla, Bronsted acid-catalyzed desymmetrization of meso-aziridines. *J. Am. Chem. Soc.* **129**, 12084 (2007).
52. G. Della Sala, A. Lattanzi, Highly enantioselective synthesis of beta-amidophenylthioethers by organocatalytic desymmetrization of meso-aziridines. *Org. Lett.* **11**, 3330 (2009).
53. G. L. Hamilton, T. Kanai, F. D. Toste, Chiral anion-mediated asymmetric ring opening of meso-aziridinium and episulfonium ions. *J. Am. Chem. Soc.* **130**, 14984 (2008).
54. S. Lin, E. N. Jacobsen, Thiourea-catalysed ring opening of episulfonium ions with indole derivatives by means of stabilizing non-covalent interactions. *Nat. Chem.* **4**, 817 (2012).
55. G. Pupo *et al.*, Asymmetric nucleophilic fluorination under hydrogen bonding phase-transfer catalysis. *Science* **360**, 638 (2018).
56. U. Hennecke, C. H. Muller, R. Frohlich, Enantioselective haloetherification by asymmetric opening of meso-halonium ions. *Org. Lett.* **13**, 860 (2011).
57. M. Mascal, N. Hafezi, M. D. Toney, 1,4,7-Trimethyloxatriquinane: S_N2 Reaction at Tertiary Carbon. *J. Am. Chem. Soc.* **132**, 10662 (2010).

58. K. Shibatomi, Y. Soga, A. Narayama, I. Fujisawa, S. Iwasa, Highly enantioselective chlorination of beta-keto esters and subsequent S_N2 displacement of tertiary chlorides: a flexible method for the construction of quaternary stereogenic centers. *J. Am. Chem. Soc.* **134**, 9836 (2012).
59. D. Kim *et al.*, Enantioselective Synthesis of Chiral alpha-Azido and alpha-Aryloxy Quaternary Stereogenic Centers via the Phase-Transfer-Catalyzed alpha-Alkylation of alpha-Bromomalonates, Followed by S_N2 Substitution. *J. Org. Chem.* **82**, 4936 (2017).
60. K. Shibatomi *et al.*, Enantioselective decarboxylative chlorination of beta-ketocarboxylic acids. *Nat Commun* **8**, 15600 (2017).
61. G. A. Lotz, S. M. Palacios, R. A. Rossi, Stereoselective reaction of a chiral assisted amide enolate ion with 1-iodonaphthalene by the $S_{RN}1$ mechanism. *Tetrahedron Lett.* **35**, 7711 (1994).
62. K. Iseki, M. Takahashi, D. Asada, T. Nagai, Y. Kobayashi, Diastereoselective Perfluoroalkylation of Chiral Imide Enolates with Perfluoroalkyl Iodides Mediated by Triethylborane. *J. Fluorine Chem.* **74**, 269 (1995).
63. R. Nouguier, V. Béraud, P. Vanelle, M. P. Crozet, Influence of the chiral auxiliary on the stereoselectivity of the SRN1 C-alkylation of 2-nitropropionate anions. *Tetrahedron Lett.* **40**, 5013 (1999).
64. L. Wozniak, J. J. Murphy, P. Melchiorre, Photo-organocatalytic Enantioselective Perfluoroalkylation of beta-Ketoesters. *J. Am. Chem. Soc.* **137**, 5678 (2015).
65. J. Choi, G. C. Fu, Transition metal-catalyzed alkyl-alkyl bond formation: Another dimension in cross-coupling chemistry. *Science* **356**, (2017).

66. C. Fischer, G. C. Fu, Asymmetric nickel-catalyzed negishi cross-couplings of secondary alpha-bromo amides with organozinc reagents. *J. Am. Chem. Soc.* **127**, 4594 (2005).

67. N. D. Schley, G. C. Fu, Nickel-Catalyzed Negishi Arylations of Propargylic Bromides: A Mechanistic Investigation. *J. Am. Chem. Soc.* **136**, 16588 (2014).

68. S. Son, G. C. Fu, Nickel-catalyzed asymmetric Negishi cross-couplings of secondary allylic chlorides with alkylzincs. *J. Am. Chem. Soc.* **130**, 2756 (2008).

69. J. T. Binder, C. J. Cordier, G. C. Fu, Catalytic Enantioselective Cross-Couplings of Secondary Alkyl Electrophiles with Secondary Alkylmetal Nucleophiles: Negishi Reactions of Racemic Benzylic Bromides with Achiral Alkylzinc Reagents. *J. Am. Chem. Soc.* **134**, 17003 (2012).

70. F. O. Arp, G. C. Fu, Catalytic enantioselective Negishi reactions of racemic secondary benzylic halides. *J. Am. Chem. Soc.* **127**, 10482 (2005).

71. A. J. Oelke, J. Sun, G. C. Fu, Nickel-Catalyzed Enantioselective Cross-Couplings of Racemic Secondary Electrophiles That Bear an Oxygen Leaving Group. *J. Am. Chem. Soc.* **134**, 2966 (2012).

72. S. W. Smith, G. C. Fu, Nickel-catalyzed asymmetric cross-couplings of racemic propargylic halides with arylzinc reagents. *J. Am. Chem. Soc.* **130**, 12645 (2008).

73. J. Choi, G. C. Fu, Catalytic Asymmetric Synthesis of Secondary Nitriles via Stereoconvergent Negishi Arylations and Alkenylations of Racemic alpha-Bromonitriles. *J. Am. Chem. Soc.* **134**, 9102 (2012).

74. H.-Q. Do, E. R. R. Chandrashekar, G. C. Fu, Nickel/Bis(oxazoline)-Catalyzed Asymmetric Negishi Arylations of Racemic Secondary Benzylic Electrophiles to Generate Enantioenriched 1,1-Diarylalkanes. *J. Am. Chem. Soc.* **135**, 16288 (2013).

75. S. Lou, G. C. Fu, Nickel/Bis(oxazoline)-Catalyzed Asymmetric Kumada Reactions of Alkyl Electrophiles: Cross-Couplings of Racemic alpha-Bromoketones. *J. Am. Chem. Soc.* **132**, 1264 (2010).

76. S. Lou, G. C. Fu, Enantioselective Alkenylation via Nickel-Catalyzed Cross-Coupling with Organozirconium Reagents. *J. Am. Chem. Soc.* **132**, 5010 (2010).

77. P. M. Lundin, G. C. Fu, Asymmetric Suzuki Cross-Couplings of Activated Secondary Alkyl Electrophiles: Arylations of Racemic alpha-Chloroamides. *J. Am. Chem. Soc.* **132**, 11027 (2010).

78. X. Dai, N. A. Strotman, G. C. Fu, Catalytic asymmetric Hiyama cross-couplings of racemic alpha-bromo esters. *J. Am. Chem. Soc.* **130**, 3302 (2008).

79. B. Saito, G. C. Fu, Enantioselective alkyl-alkyl suzuki cross-couplings of unactivated homobenzylic halides. *J. Am. Chem. Soc.* **130**, 6694 (2008).

80. Z. Lu, A. Wilsily, G. C. Fu, Stereoconvergent Amine-Directed Alkyl-Alkyl Suzuki Reactions of Unactivated Secondary Alkyl Chlorides. *J. Am. Chem. Soc.* **133**, 8154 (2011).

81. A. Wilsily, F. Tramutola, N. A. Owston, G. C. Fu, New Directing Groups for Metal-Catalyzed Asymmetric Carbon-Carbon Bond-Forming Processes: Stereoconvergent Alkyl-Alkyl Suzuki Cross-Couplings of Unactivated Electrophiles. *J. Am. Chem. Soc.* **134**, 5794 (2012).

82. N. A. Owston, G. C. Fu, Asymmetric Alkyl-Alkyl Cross-Couplings of Unactivated Secondary Alkyl Electrophiles: Stereoconvergent Suzuki Reactions of Racemic Acylated Halohydrins. *J. Am. Chem. Soc.* **132**, 11908 (2010).

83. Y. Liang, G. C. Fu, Catalytic Asymmetric Synthesis of Tertiary Alkyl Fluorides: Negishi Cross-Couplings of Racemic alpha,alpha-Dihaloketones. *J. Am. Chem. Soc.* **136**, 5520 (2014).

84. J. Schmidt, J. Choi, A. T. Liu, M. Slusarczyk, G. C. Fu, A general, modular method for the catalytic asymmetric synthesis of alkylboronate esters. *Science* **354**, 1265 (2016).

85. Z. Wang, S. Bachman, A. S. Dudnik, G. C. Fu, Nickel-Catalyzed Enantioconvergent Borylation of Racemic Secondary Benzylic Electrophiles. *Angew. Chem. Int. Ed.* **57**, 14529 (2018).

86. J. Mao *et al.*, Cobalt-bisoxazoline-catalyzed asymmetric Kumada cross-coupling of racemic alpha-bromo esters with aryl Grignard reagents. *J. Am. Chem. Soc.* **136**, 17662 (2014).

87. M. Jin, L. Adak, M. Nakamura, Iron-Catalyzed Enantioselective Cross-Coupling Reactions of alpha-Chloroesters with Aryl Grignard Reagents. *J. Am. Chem. Soc.* **137**, 7128 (2015).

88. Q. M. Kainz *et al.*, Asymmetric copper-catalyzed C-N cross-couplings induced by visible light. *Science* **351**, 681 (2016).

89. N. S. Zefirov, D. I. Makhon'kov, X-philic reactions. *Chem. Rev.* **82**, 615 (1982).

90. P. K. Sazonov, G. A. Artamkina, I. P. Beletskaya, Nucleophilic substitution at the halogen atom (halogenophilic reactions). *Russian Chem. Rev.* **81**, 317 (2012).

91. Y. Zhang, On the role of halogen bond in the halophilic reaction: A theoretical study. *Journal of Molecular Structure: THEOCHEM* **961**, 6 (2010).

92. C. A. Bayse, E. R. Rafferty, Is halogen bonding the basis for iodothyronine deiodinase activity? *Inorg. Chem.* **49**, 5365 (2010).

93. A. Mukherjee, S. Tothadi, G. R. Desiraju, Halogen bonds in crystal engineering: like hydrogen bonds yet different. *Acc. Chem. Res.* **47**, 2514 (2014).

94. G. Cavallo *et al.*, The Halogen Bond. *Chem. Rev.* **116**, 2478 (2016).

95. T. Clark, M. Hennemann, J. S. Murray, P. Politzer, Halogen bonding: the sigma-hole. Proceedings of "Modeling interactions in biomolecules II", Prague, September 5th-9th, 2005. *J. Mol. Model.* **13**, 291 (2007).

96. S. M. Walter, F. Kniep, E. Herdtweck, S. M. Huber, Halogen-bond-induced activation of a carbon-heteroatom bond. *Angew. Chem. Int. Ed.* **50**, 7187 (2011).

97. W. He, Y. C. Ge, C. H. Tan, Halogen-bonding-induced hydrogen transfer to C horizontal lineN bond with Hantzsch ester. *Org. Lett.* **16**, 3244 (2014).

98. M. C. Verploegh, L. Donk, H. J. T. Bos, W. Drenth, Nucleophilic displacements at halogen in 1-chloro-, 1-bromo- and 1-iodo-1-alkynes: I. Thiolates as nucleophiles. *Recl. Trav. Chim. Pays-Bas* **90**, 765 (1971).

99. S. Montanari, C. Paradisi, G. Scorrano, Thiol Anions in Nucleophilic Aromatic-Substitution Reactions with Activated Aryl Halides - Attack on Carbon Vs Attack on Halogen. *J. Org. Chem.* **58**, 5628 (1993).

100. E. Yamamoto, S. Ukigai, H. Ito, Formal Nucleophilic Silyl Substitution of Aryl Halides with Silyllithium Reagents via Halogenophilic Attack of Silyl Nucleophiles. *Synlett* **28**, 2460 (2017).

101. C. Strohmann, M. Bindl, V. C. Fraass, J. Hornig, Enantiodivergence in the reactions of a highly enantiomerically enriched silyllithium compound with benzyl halides: control of inversion and retention by selection of halide. *Angew. Chem. Int. Ed.* **43**, 1011 (2004).

Chapter 2

Enantioconvergent Nucleophilic Substitution of Tertiary Bromide by Thiocarboxylate

2.1 Introduction

In the first chapter, we have discussed the development of asymmetric phase-transfer catalysis. We have also discussed nucleophilic substitution reaction which is a fundamental concept in organic chemistry. Many important and interesting reactions have been developed in this area. According to our concerns, we focused on the enantioconvergent nucleophilic substitution of racemic aliphatic electrophiles through different approaches and mechanisms. There are many examples of secondary electrophiles, but tertiary electrophiles are more challenging and only limited examples are reported.

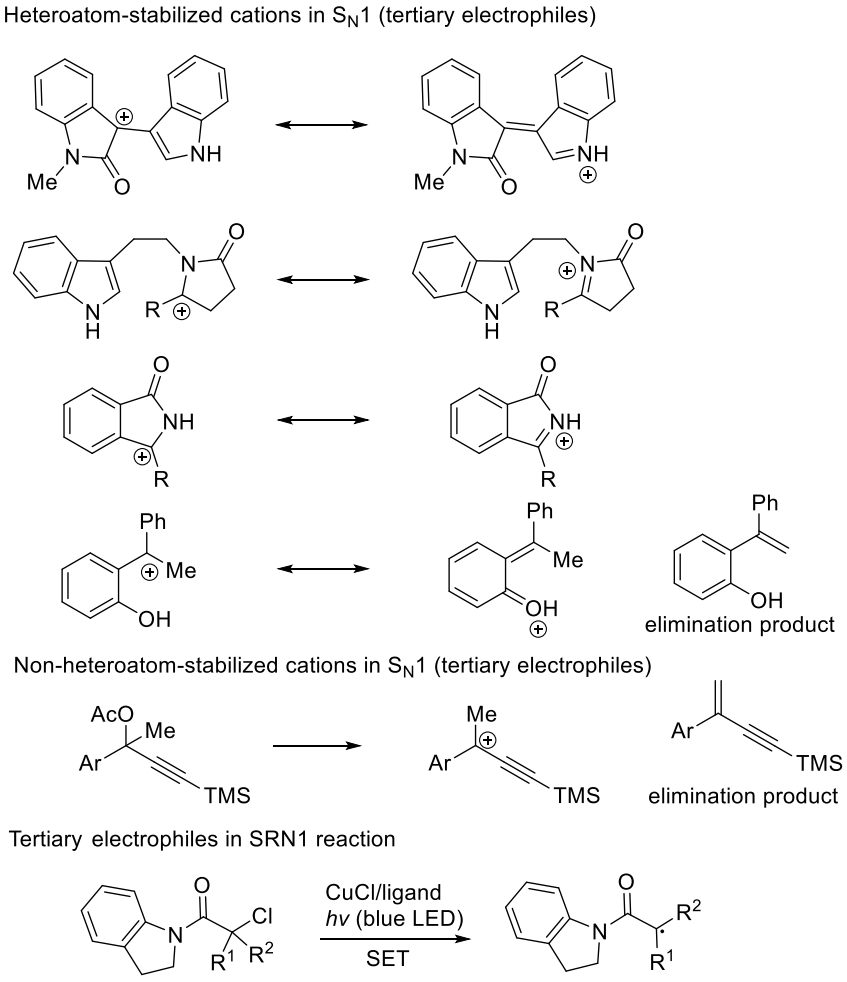

Figure 2.1 Tertiary electrophiles in stereoselective S_N1 and $S_{RN}1$ reactions

For S_N1 reactions, several racemic tertiary electrophiles were successful in some organocatalyzed substitution reactions. Because of the highly unstable and active carbocation intermediates in these reactions (**Figure 2.1**), electrophiles are limited to those that can formheteroatom-stabilized cations, and the substituents are limited to aryl or electron-withdrawing groups lacking β-hydrogen atoms to suppress elimination reactions. The first example of non-heteroatom-stabilized carbocations generated from propargyl acetate tertiary electrophiles was only reported recently in 2018 by Jacobsen[1]. Elimination reaction was partly suppressed, however, there were significant amounts of alkenes as side products in some cases.

Radical nucleophilic substitution reaction, which is still challenging for organocatalysis, has been well developed by chiral transition metal catalysis. But in most cases, only secondary electrophiles are successful. Racemic tertiary electrophiles (**Figure 2.1**) were reported only by Fu in 2016[2] in an asymmetric C-N bond forming reaction. α-Haloamides were reduced by the photo-excited copper complex to form a prochiral tertiary radical.

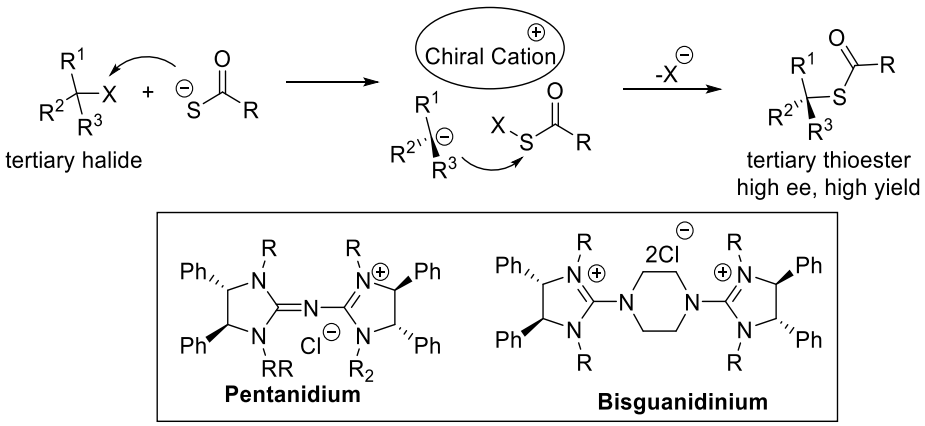

Figure 2.2 Tertiary radicals in stereoselective $S_{RN}1$ reactions

Compared with S_N1 reactions via carbocation intermediates and transition metal catalyzed radical nucleophilic substitution reactions, asymmetric S_N2X reaction via carbanion intermediates[3, 4] will have different reactivity and substrate scope to

complement the reported types. As we previously discussed, we need to hamper the carbon atom and making the competing carbonophilic reaction difficult in order to promote S_N2X reaction. Bulky tertiary halide is challenging in carbonophilic S_N2 reaction, which makes it an ideal electrophile for S_N2X reaction.

Considering the challenges in nucleophilic substitution of racemic tertiary electrophiles using S_N1 or radical nucleophilic substitution approaches, we will develop asymmetric phase-transfer catalyzed S_N2X reaction to improve the utility (**Figure 2.2**).

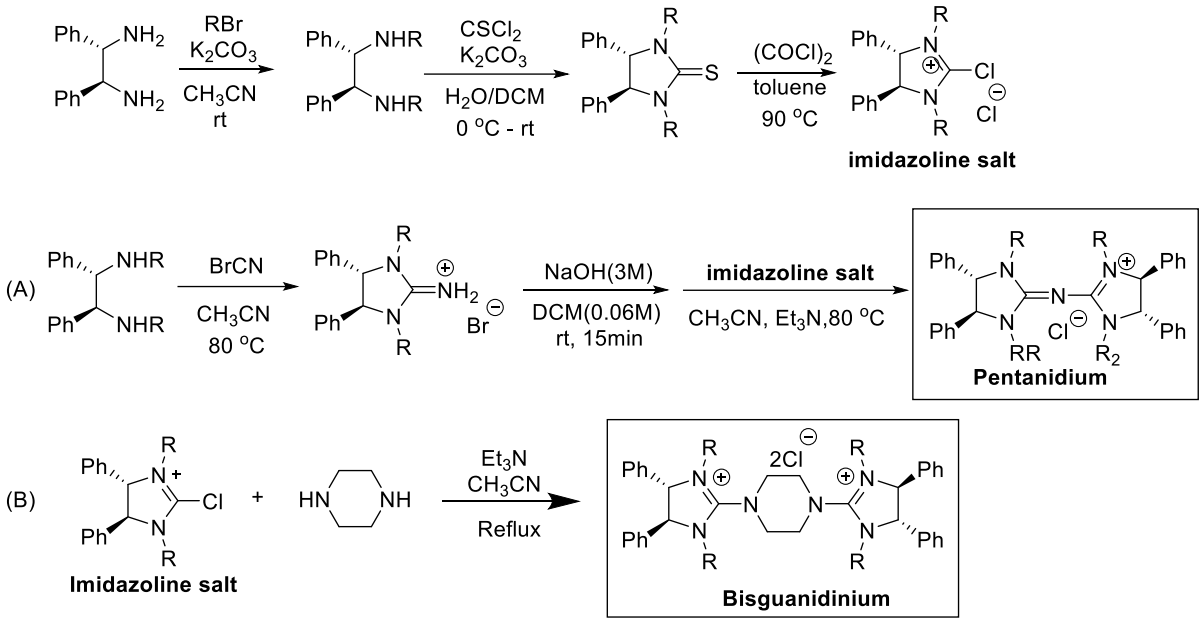

Figure 2.3 General methods for the synthesis of pentanidium and bisguanidinium

Our group has developed chiral cationic pentanidium and bisguanidinium as phase-transfer catalysts. These chiral catalysts can be easily synthesized in several steps from commercially available diphenyldiaminoethane and other commercially available and cheap reagents **(Figure 2.3)**[5-7]. After alkylation and reaction with thiophosgene, thiourea is obtained. Further reaction with oxalyl chloride generates imidazoline salt. Alkylated diphenyldiaminoethane reacts with bromine cyanide to form guanidinium salt and then the imidazoline salt reacts with this guanidinium salt to generate pentanidum (**Figure 2.3 A**). Bisguanidinium can be obtained from the reaction between two

equivalents of imidazoline salt and one equivalent of piperazine as linker (**Figure 2.3 B**).

For the nucleophiles, we will use thiocarboxylate salts to react with tertiary halides and generate tertiary thioesters. The tertiary thioesters are precursors to various organosulfur compounds, with potential utility in both chemistry and chemical biology[8-10].

2.2 Enantioconvergent nucleophilic substitution of brominated cyanoester by thiocarboxylate

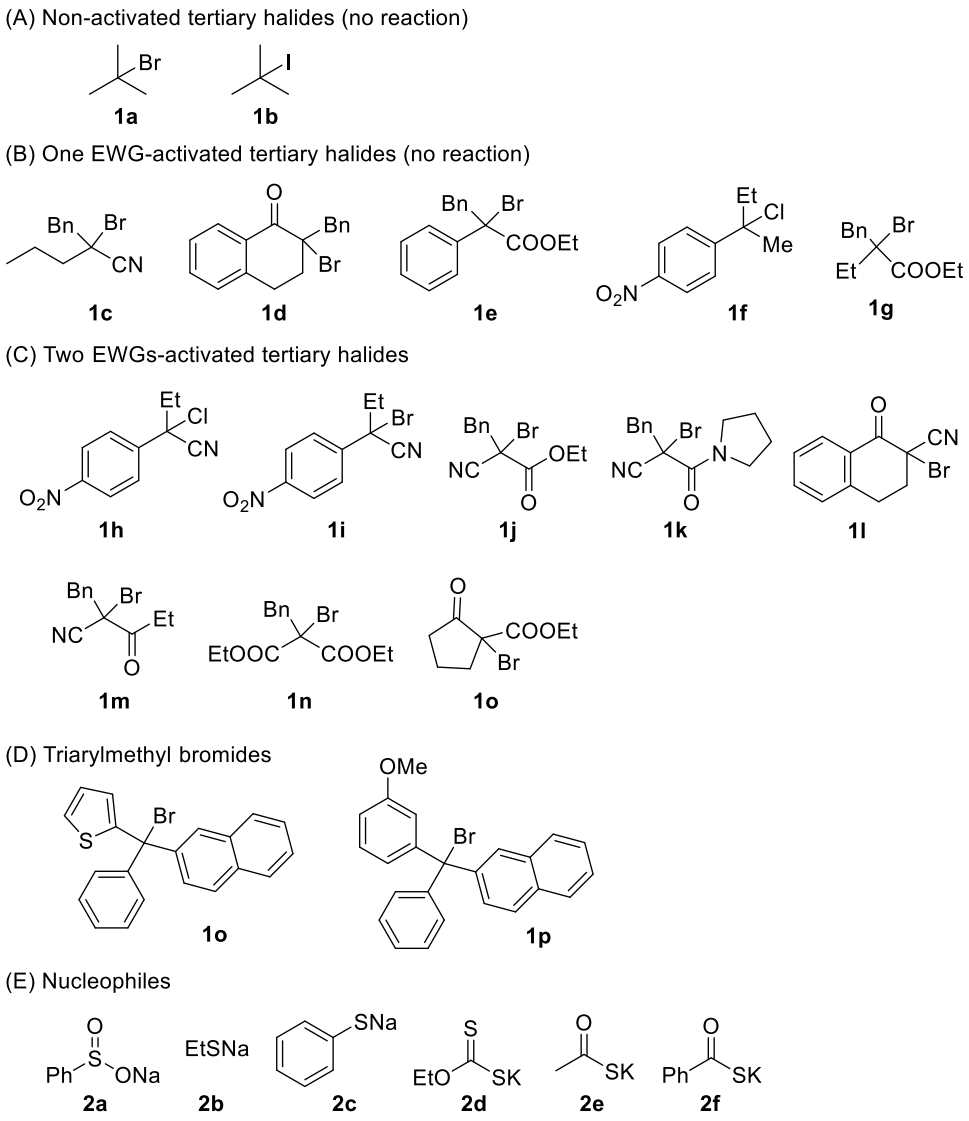

Figure 2.4 Initial investigation on different tertiary halides and nucleophiles

We started our investigations with a series of tertiary bromides and different sulfur centered nucleophiles using tetrabutylammonium bromide (TBAB) as phase-transfer catalyst. For non-activated tert-butyl bromide and tert-butyl iodide (**Figure 2.4A**), we couldn't detect any formation of new compounds. To enhance the σ-hole of the halide atom and promote the halogenophilic nucleophilic attack, we tried to synthesize activated tertiary halides with electron-withdrawing groups attached to the carbons. Several tertiary halides activated by one electron-withdrawing group (cyano, phenylacetyl, ester, nitrophenyl groups) were tried (**Figure 2.4B**), but the starting materials still remained without any product formation. To increase the activity, we tried to synthesize more reactive tertiary bromides activated by two electron-withdrawing

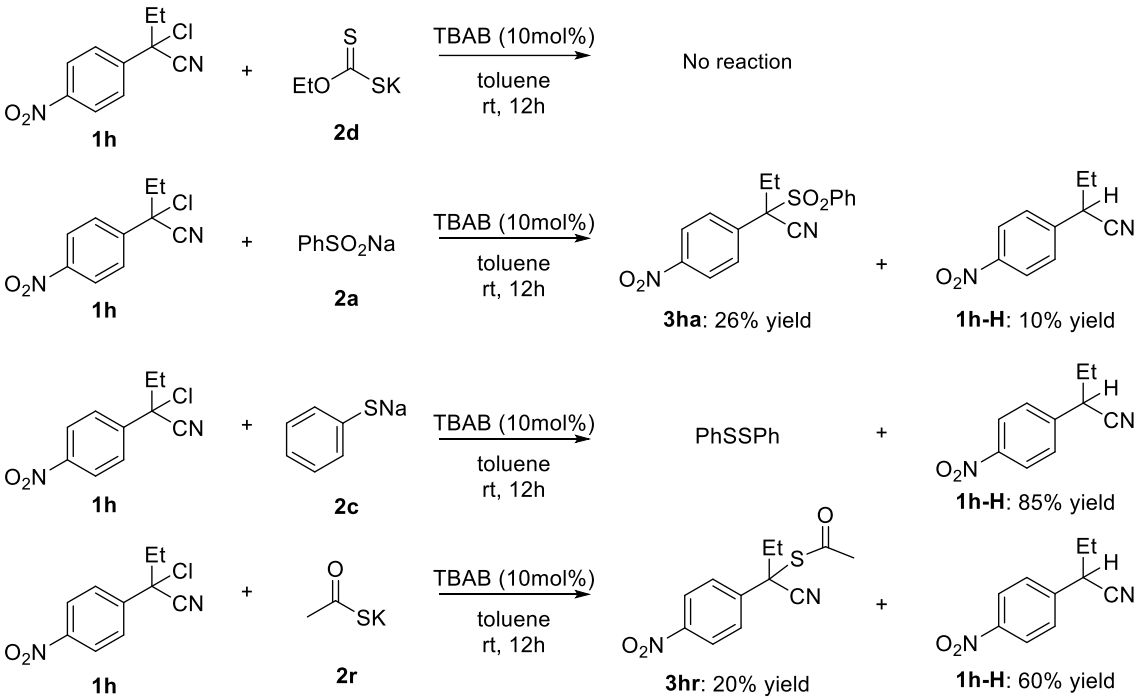

Figure 2.5 Results using tertiary bromide **1h** as electrophile

groups (**Figure 2.4C**). To our delight, most of these substrates are active enough to obtain some products with some ee values. We also tried triarylmethyl bromides and these substrates are quite good to generate products with excellent yields, but the

enantioselectivities of these substrates are always zero after a lot of catalysts and condition optimization (**Figure 2.4D**).

When the tertiary bromides activated by two electron-withdrawing groups were utilized, most reactions generated products together with some protonated products, indicating the existence of carbanion intermediates and the possible S_N2X mechanism. We discuss some representative results here. When tertiary chloride **1h** activated by cyano and nitrophenyl groups was used as electrophile, we tried different sulfur centered nucleophiles (**Figure 2.5**). When potassium ethyl xanthate **2d** was used, the substrates were recovered without any reaction. When sodium benzenesulfinate **2a** was used, the desired product **3ha** was obtained with 26% yield, protonated product **1h-H** was obtained with 10% yield and much substrates **1h** were recovered. When sodium thiophenolate **2c** was used, all substrates were consumed with formation of protonated product **1h-H** (85% yield) and disulfides, but the desired substitution product was not isolated. When potassium thioacetate **2r** was used, the substitution product **3hr** was isolated with 20% yield together with protonated product **1h-H** (60% yield).

When other tertiary halides were used, the side protonated product was also formed in large amount, which couldn't be avoided though we put a lot of efforts. The best type of substrate is **1j**, with a cyano and ester as electron-withdrawing groups (**Figure 2.6**). For this electrophile, when potassium thioacetate **2e** was used, the desired product **3je** was obtained in 45% yield and side product **1j-H** was in 46% yield at room temperature. To our delight, the amount of the side product was decreased and isolated in 20% yield at -20 ^{o}C with the desired product isolated in 69% yield. In the further optimization of this reaction using potassium benzothioate **2f** as nucleophile, the desired product was isolated with 90% yield and 36% ee value and only trace amount of side product was formed.

Because of the good results we have obtained using such activated tertiary bromides as electrophiles, we chose brominated alkyl cyanoacetate as model substrate in the following studies.

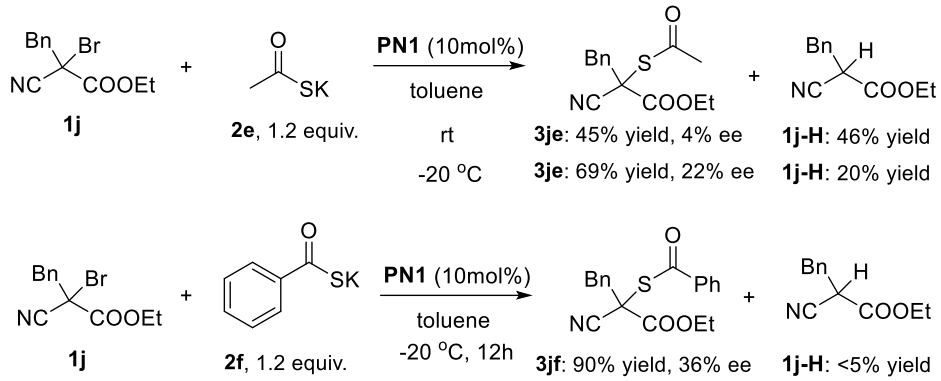

Figure 2.6 Results using tertiary bromide **1j** as electrophile

Then we started systematical optimization for the enantioconvergent nucleophilic substitution of brominated alkyl cyanoacetate by thiocarboxylate. To improve the enantioselectivity, we first tried different phase-transfer catalysts. Different chiral cationic pentanidium (**PN**) and dicationic bisguanidinium (**BG**) chlorides were synthesized and applied to the reaction (**Figure 2.7)**. When pentanidium **PN1** bearing 3,5-di-tert-butylbenzyl group was used, we isolated the product in 72% yield and 40% ee value. Later we modified the 3,5-di-tert-butylbenzyl group with halide atoms (**PN2-PN4**), but both the product yields and ee values decreased when these catalysts used. When the 3,5-di-tert-butylbenzyl group was modified with methoxy group (**PN5**), the product was obtained in 31% yield and 13% ee value. Then we tried different bisguanidinium chlorides. When **BG1** bearing 3,5-di-tert-butylbenzyl group was used, the product was isolated in 67% yield and 24% ee value. After the 3,5-di-tert-butylbenzyl group was modified with fluoro or chloro substitution, we got **BG2** and **BG3**, but the yields and ee values couldn't be increased. Then we changed half of the 3,5-di-tert-butylbenzyl group to 2,4-di-trifluoromethylbenzyl group and got **BG4**. This

reaction catalyzed by **BG4** proceeded well affording product in 74% yield and 53% ee value.

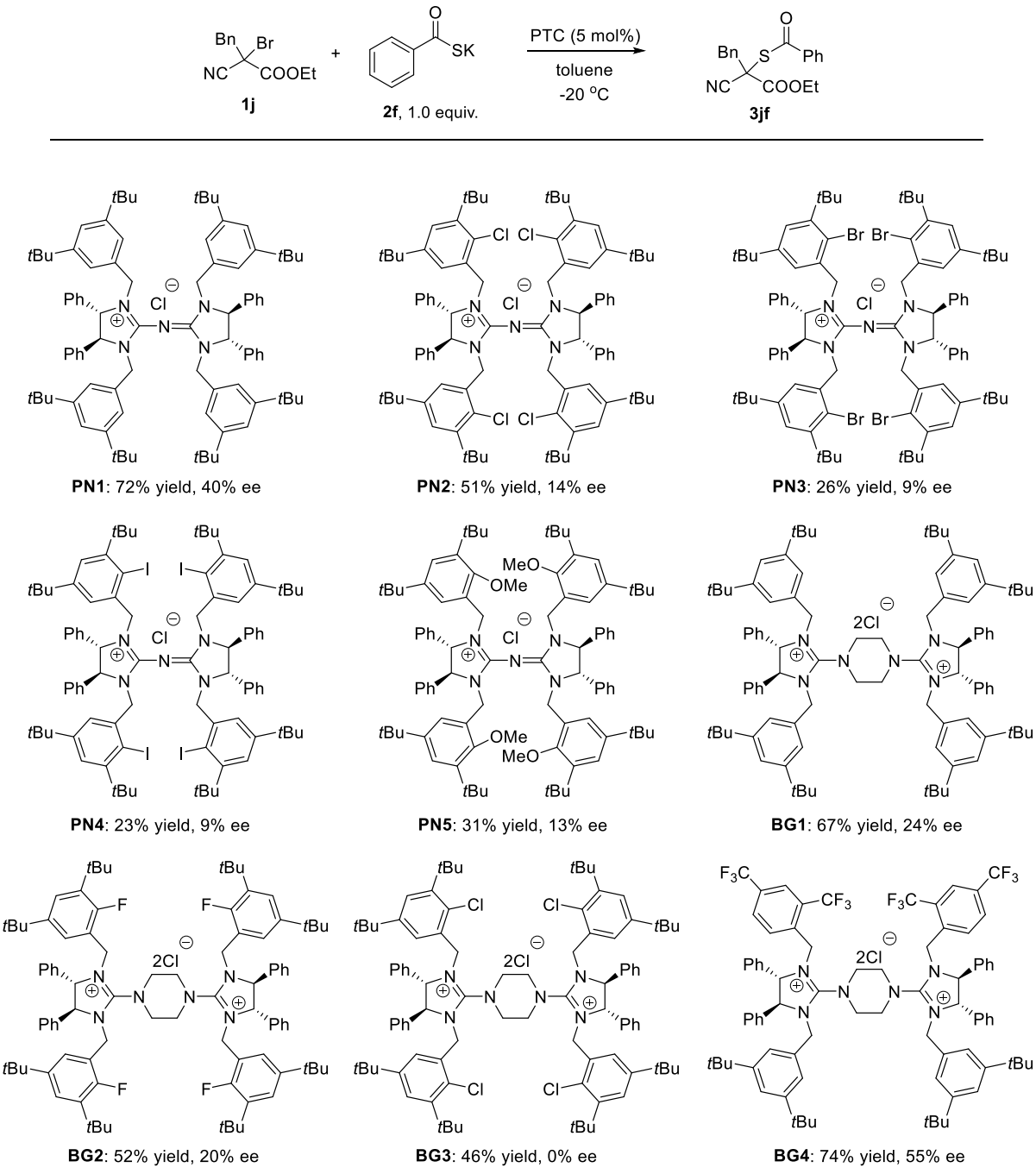

Figure 2.7 First investigation on phase-transfer catalysts

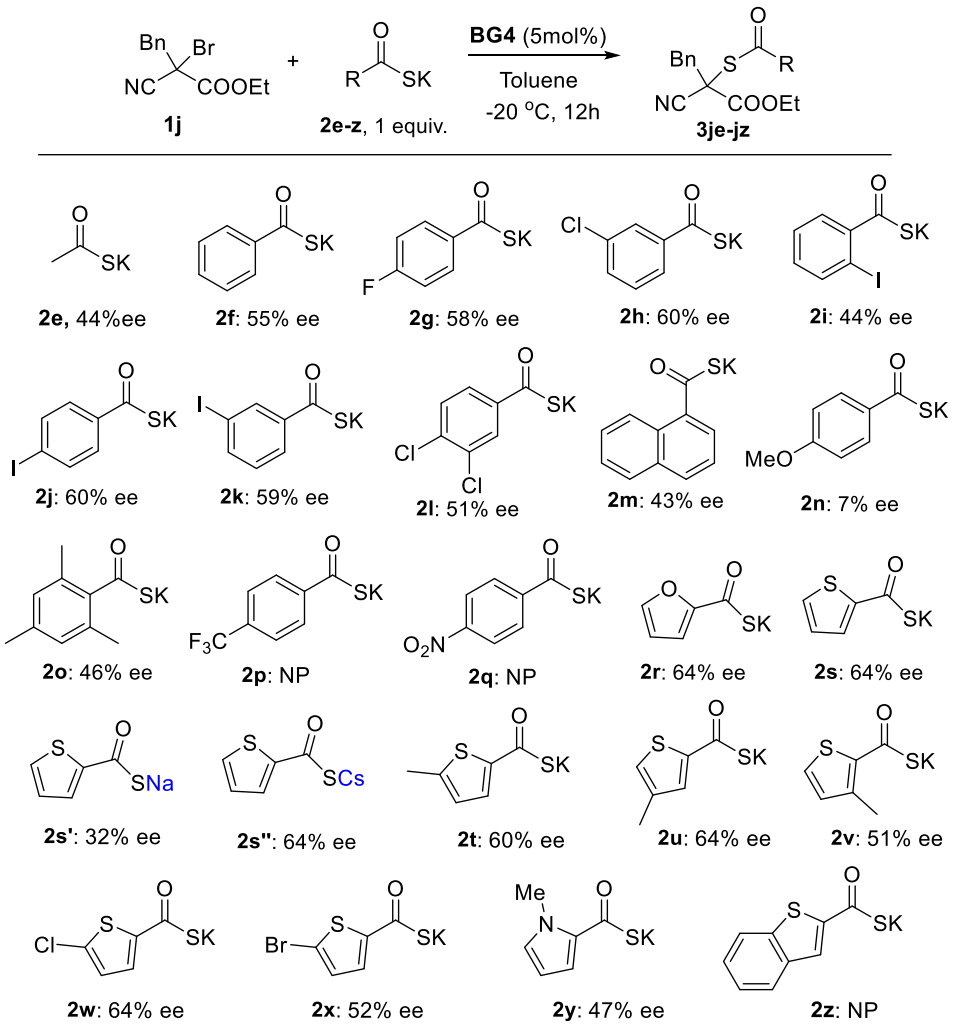

Figure 2.8 Optimization on the structure of thiocarboxylate

To further improve the enantioselectivity, we synthesized various thiocarboxylate salts (**Figure 2.8**, **2e-2z**) and utilized them in the reactions with tertiary bromide **1j** catalyzed by **BG4**. Various potassium benzothioates substituted by different halogen atoms (**2g-2l**) at different positions were synthesized, and the ee values of the isolated products ranged from 44% to 60%. Potassium benzothioates substituted by iodine at 2-position (**2i**) afforded product with lower 44% ee value. The product was isolated with 43% ee value in the reaction between potassium thiocarboxylate bearing naphthalene (**2m**). The potassium benzothioate (**2n**) substituted by methoxy group only afforded the product with 7% ee value. The electron-rich potassium 2,4,6-trimethylbenzothioate (**2o**) afforded the product with 46% ee value. The potassium benzothioates substituted by

strong electron-withdrawing group (**2p**, **2q**) couldn't react with **1j** to form substituted products under this condition. Best results with 64% ee values were obtained when furyl (**2r**) and thiophenyl (**2s**) thiocarboxylate potassium were applied to the reaction. When we changed the potassium counterion to sodium (**2s'**), the ee value of product decreased to 32%. When it was change to cesium (**2s''**), the ee value remained. We tried to further optimize the enantioselectivity by modifying the substituents on the thiophenyl thiocarboxylate with methyl group, chloride and bromide atom (**2t**-**2x**), but failed. The pyrrolyl thiocarboxylate salt (**2y**) was synthesized and product was isolated with 47% ee value. When benzothiophenyl thiocarboxylate potassium (**2z**) was used, we failed to isolate any product.

Table 2.1 Optimization on the reaction temperature

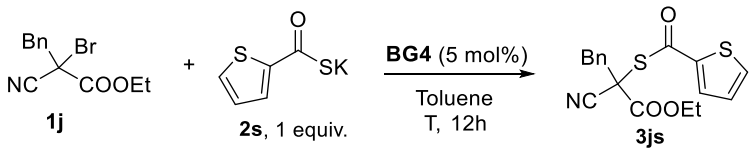

entry	T (^{o}C)	yield (%)	ee (%)
1	22	62	21
2	0	70	46
3	-20	78	64
4	-40	77	73
5	-60	78	79

The enantioselectivity of this substitution reaction could be further increased by lowering the reaction temperature (**Table 2.1**). This reaction was quite efficient and finished in 12h at -60 ^{o}C affording product with 78% yield and 79% ee.

Then we tried to modify the ester group to further improve the enantioselectivity (**Figure 2.9**). Various tertiary bromides bearing different ester groups were synthesized and reacted with thiophenyl thiocarboxylate **2s** catalyzed by **BG4**. As shown in **Figure 2.9**, for *p*-tolyl ester (**4a**) and trifluoroethyl (**4b**) ester substrates, the products obtained were racemic. For tertiary bromide bearing allyl ester (**4c**), the product was isolated with 49% ee value. When diphenylmethyl ester (**4d**) was used, the product was isolated with 46% ee value. Iso-propyl ester (**4e**) tertiary bromide achieved better results and product was isolated with 72% ee value. For butyl esters, when normal-butyl (**4f**) and iso-butyl (**4g**) esters were used in the reaction, products were isolated with similar ee values (69% and 65% respectively). But when bulky tert-butyl ester (**4h**) was used, the resulting product only had 9% ee value. These results suggested that except for electronic properties, the steric effects of the esters also influenced the enantioselectivities. A smaller ester may result in better enantioseletivity. This proposal also agreed with the bad enenatioselecticty (14% ee) using the tertiary bromide bearing bulky adamantanyl ester (**4i**). Trimethoxybenzyl ester substrate (**4j**) reacted to generate product with 35% ee. Better results were obtained when using tertiary bromides bearing ethyl (**1j**) or methyl ester groups (**6a**) (77% ee and 75% ee respectively). When we conducted the reactions with **PN1** as catalyst, some products were isolated with better ee value compared with those catalyzed by **BG4**. For Trimethoxybenzyl ester substrate (**4j**), the ee values of the products were 35% (with **BG4**) and 80% (with **PN1**). When methyl ester substrate (**6a**) was used with **PN1**, we isolated the product with best ee value (86%).

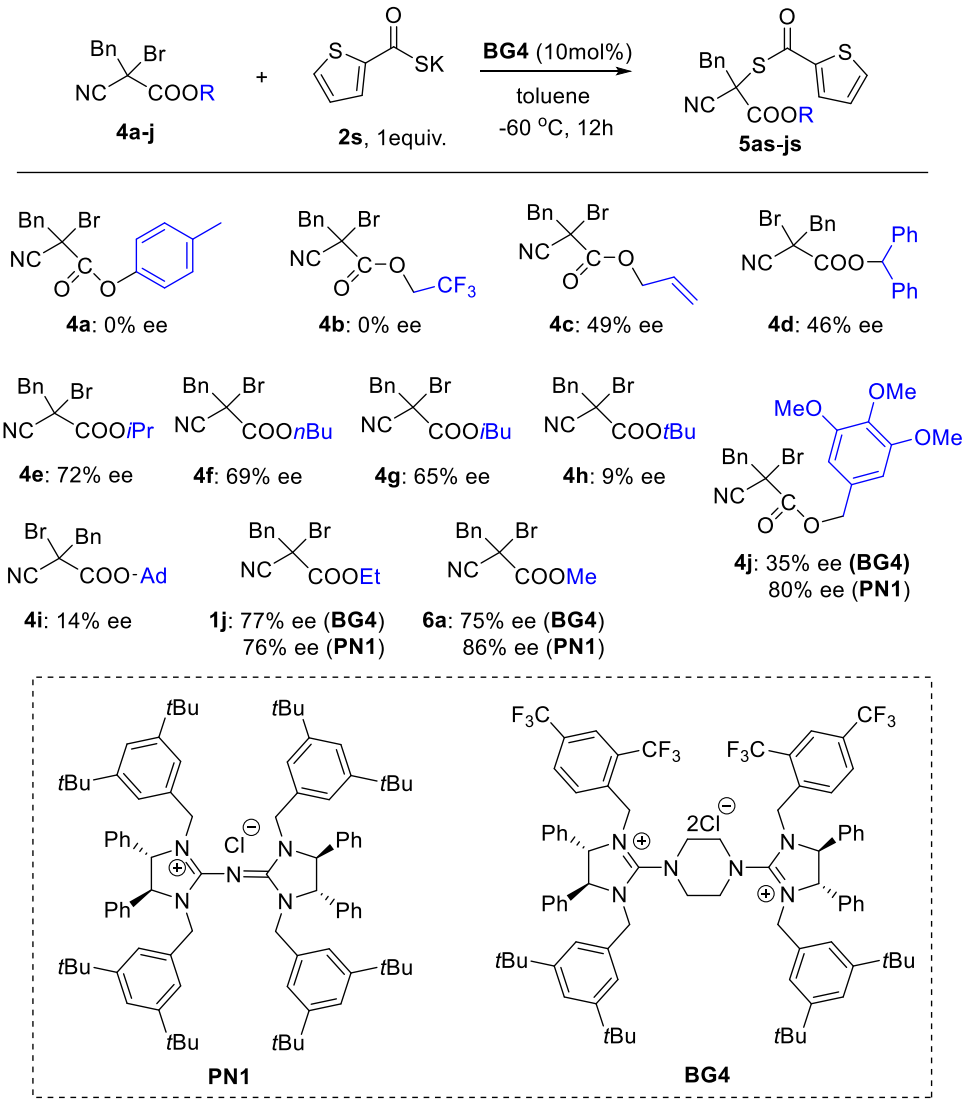

Figure 2.9 Optimization on the ester group of tertiary bromide

The enantioselectivity of this substitution reaction was significantly improved when we modified ester groups and the catalyst structures, which encouraged us to synthesize more catalysts for more efficient and selective reactions. We focused on the synthesis of CF_3 or F-containing benzyl group modified pentanidium or bisguanidinium catalysts (**Figure 2.10**). We first prepared pentanidiums bearing di-trifluoromethylbenzyl groups. Compared with **PN1**, when half of the 3,5-di-tert-butylbenzyl groups were changed to 3,5-di-trifluoromethylbenzyl groups, we got **PN6**. This pentanidium efficiently catalyzed the reaction to generate product in

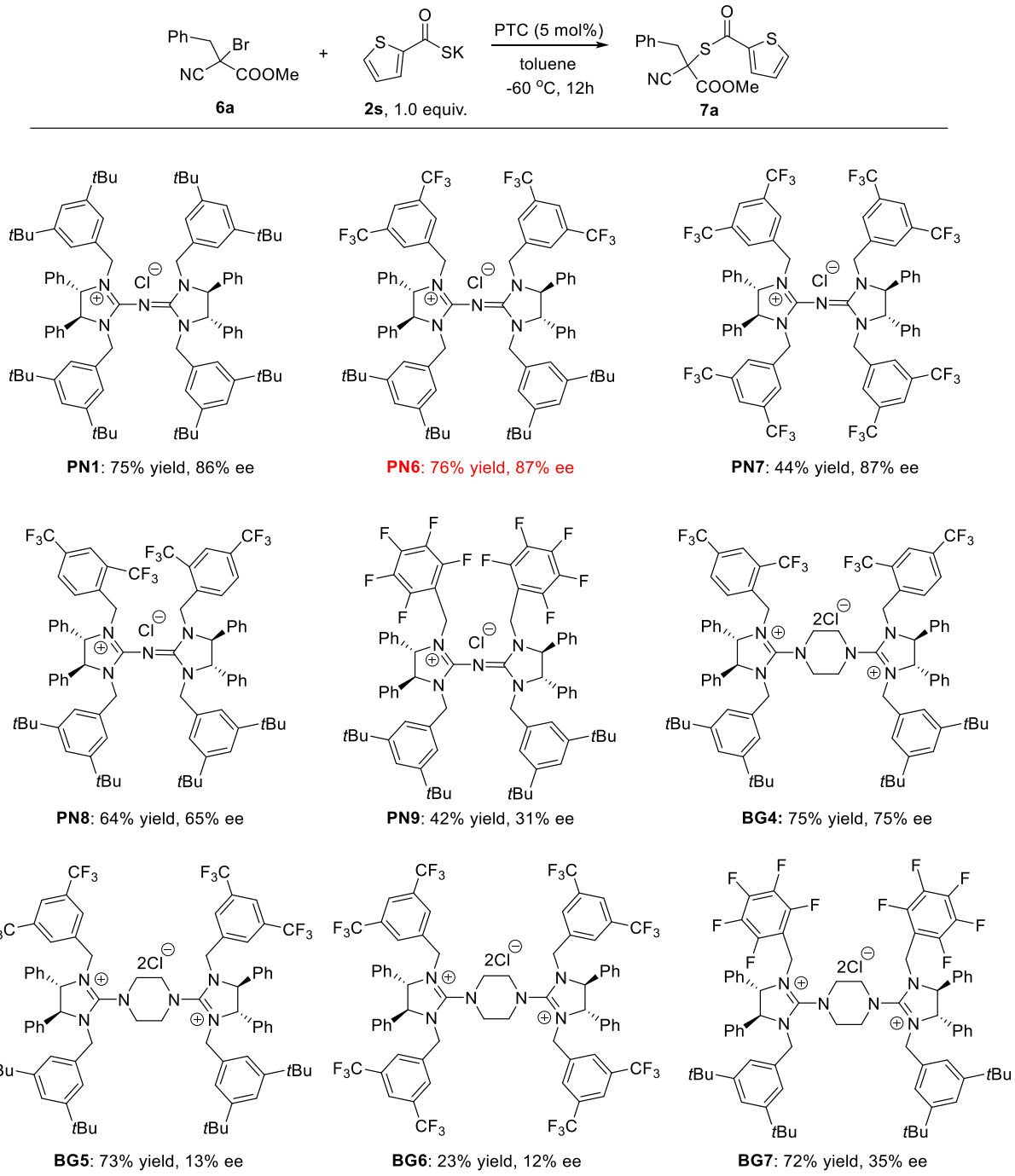

Figure 2.10 Second investigation on phase-transfer catalysts

76% yield and 87% ee value. When all the 3,5-di-tert-butylbenzyl groups were changed to 3,5-di-trifluoromethylbenzyl groups, this pentanidium **PN7** catalyzed the reaction to generate product with the same 87% ee value, but only in 44% yield. The possible reason might be the lower solubility of **PN7** in toluene compared with **PN6**. In pentanidium

Table 2.2 Optimization on the solvent and equivalent of thiocarboxylate[a]

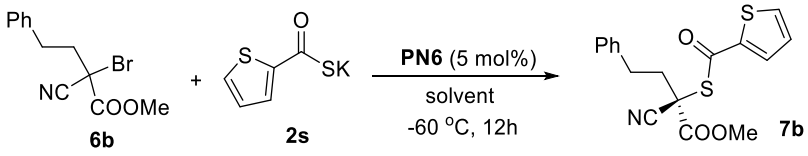

entry	solvent	equiv. of **2s**	yield (%)[b]	ee (%)[c]
1	toluene	1.1	85	87
2[d]	mesitylene	1.1	81	91
3	cumene	1.1	81	64
4[d]	m-xylene	1.1	85	69
5[d]	*t*-butyltoluene	1.1	86	83
6[d]	chlorobenzene	1.1	45	58
7	4-fluorotoluene	1.1	26	68
8	Bu_2O	1.1	80	82
9	MTBE	1.1	82	54
10	iPr_2O	1.1	76	53
11	*t*BuOEt	1.1	79	80
12	Et_2O	1.1	69	56
13	CH_2Cl_2	1.1	35	47
14	$CHCl_3$	1.1	42	54
15[d]	**mesitylene**	**1.3**	**93**	**91**
16[d]	mesitylene	1.5	93	86
17[e]	mesitylene	1.3	64	60

[a]The reaction was conducted on 0.1 mmol scale in 1 ml solvent. [b]Isolated yields. [c]Determined by chiral HPLC. [d]Reaction was conducted at -50 °C for solvent froze at -60 °C. [e]Tertiary chloride was used and this reaction was conducted at -20 °C.

PN8, half of the 3,5-di-tert-butylbenzyl groups were changed to 2,4-di-trifluoromethylbenzyl groups. The isolated product was in 64% yield and 65% ee value catalyzed by **PN8**. When pentafluorobenzyl group was introduced into the structure of pentanidium, we got **PN9**. The enantioselectivity using this catalyst for the reaction was not good (31% ee). Later, we also modified the bisguanidinium catalysts with these substituents and got **BG5**, **BG6** and **BG7**. Those bisguanidinium catalysts bearing 3,5-di-trifluoromethylbenzyl groups or pentafluorobenzyl groups were not as good as the bisguanidinium bearing 2,4-di-trifluoromethylbenzyl groups (**BG4**). With these efforts, we found pentanidium **PN6** was the best catalyst for the enantioconvergent nucleophilic substitution reaction.

Then we optimized the solvents and equivalent of thiocarboxylate **2s** using racemic tertiary bromide **6b** as the model substrate (**Table 2.2**). Different solvents were then tested. For aromatic solvents, eletron-rich aromatic solvents (entry 1-5) usually afforded products in good

yields, but electron-deficient aromatic solvents (entry 6-7) usually resulted in low yields. The ee values of product obtained in armoatic solvents ranged from 58% to 91% and best enantioselectivity was obtain using mesitylene as solvent (entry 2). For ether solvents (entry 8-12), most product yields were good ranging from 69% to 82% and ee values ranged from 53% to 82%. Dibutyl ether was the best ether solvent affording product in 80% yield and 82% ee value (entry 8). Haloalkane solvents were not good solvents for this reaction resulting in low yields and enantioselectivities (entry 13-14). The present solvent with best enantioselectivity was mesitylene (entry 2) affording product in 81% yield and 91% ee value. The equivalent of thiocarboxylate **2s** used was 1.1 equiv. Then we increased the equivalent to improve the yields. The best amount of **2s** was 1.3 equiv. affording product in 93% yield and 91% ee value (entry 15). More

amounts of **2s** (1.5 equiv.) afforded product in 93% yield but the ee value decreased to 86% (entry 16). Tertiary chloride was also synthesized and utilized in the reaction. Because of the lower reactivity, the reaction was conducted at -20 ^{o}C affording product with 64% yield and 60% ee value (entry 17). We failed to obtain pure tertiary iodide because it's unstable.

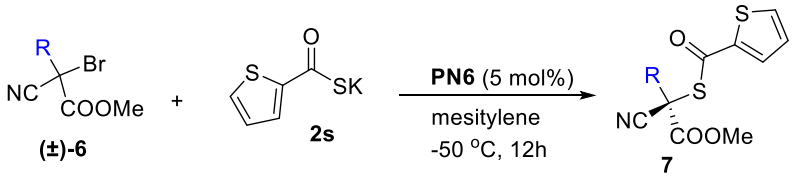

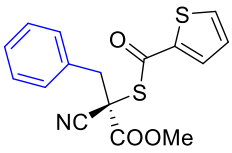
7a: 87% yield, 90% ee

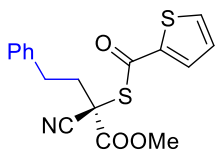
7b: 93% yield, 91% ee

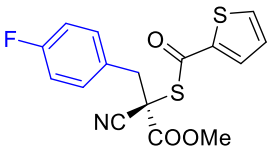
7c: 89% yield, 88% ee

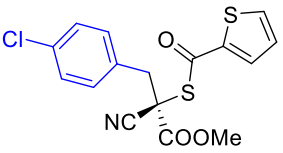
7d: 87% yield, 88% ee

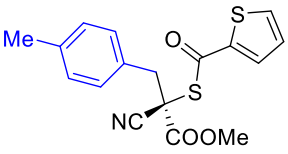
7e: 90% yield, 88% ee

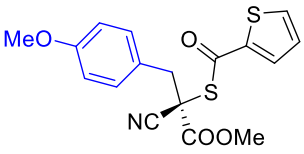
7f: 91% yield, 88% ee

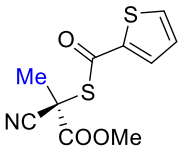
7g: 88% yield, 90% ee

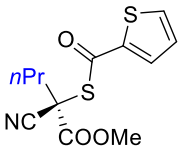
7h: 93% yield, 92% ee

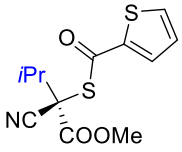
7i: 88% yield, 91% ee

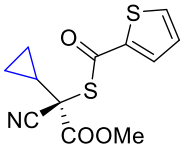
7j: 93% yield, **90**% ee

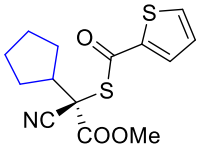
7k: 98% yield, 93% ee

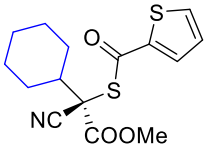
7l: 96% yield, 93% ee

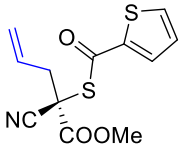
7m: 85% yield, 90% ee

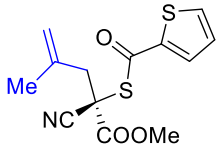
7n: 80% yield, 88% ee

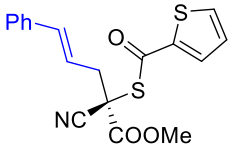
7o: 90% yield, 87% ee

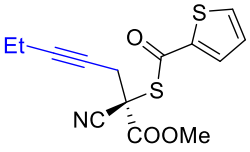
7p: 86% yield, 87% ee

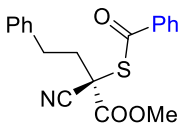
7q: 87% yield, 86% ee

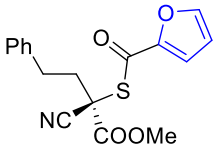
7r: 96% yield, 90% ee

Figure 2.11 Substrate scope for substitution reaction.

With the optimized reaction condition in hand, we started the investigation of the substrate scope (**Figure 2.11**). Different brominated alkyl cyanoesters were prepared and provided good results. These racemic tertiary bromides were substituted to afford products in high yields and enantioselectivities, indicating this was an enantioconvergent reaction. Benzyl group-substituted substrate afforded product (**7a**) in 87% yield and 90% ee value. Tertiary bromide bearing phenylethyl group was transformed to product (**7b**) in 93% yield and 91% ee value. Then we synthesized substrates bearing different substituted benzyl groups. Both electron-withdrawing (**7c**-**7d**) and electron-donating (**7e**-**7f**) groups were tolerated. Next, more alkyl groups were tested. Methyl (**7g**) and normal-propyl (**7h**) substituted tertiary bromides afforded their respective products in good yields and enantiomeric excess. For bulkier secondary alkyl-substituted substrates, this reaction was also effective. Iso-propyl (**7i**), cyclopropyl (**7j**), cyclopentyl (**7k**) and cyclohexyl (**7l**) substituted tertiary bromides efficiently afforded their respective products. Then we synthesized substrates bearing different allylic substituents (**7m**-**7o**) and the respective products were isolated in high yields and enantioselectivities. Propargylic group substituted substrates also reacted smoothly and provided products in 86% yield and 87% ee value.

2.3 Enantioconvergent nucleophilic substitution of brominated cyanophosphonate by thiocarboxylate

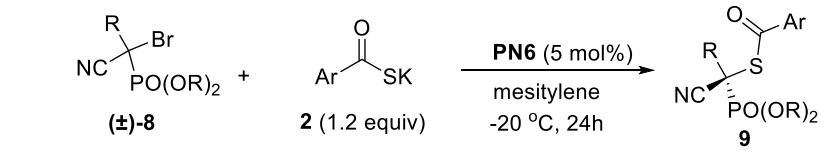

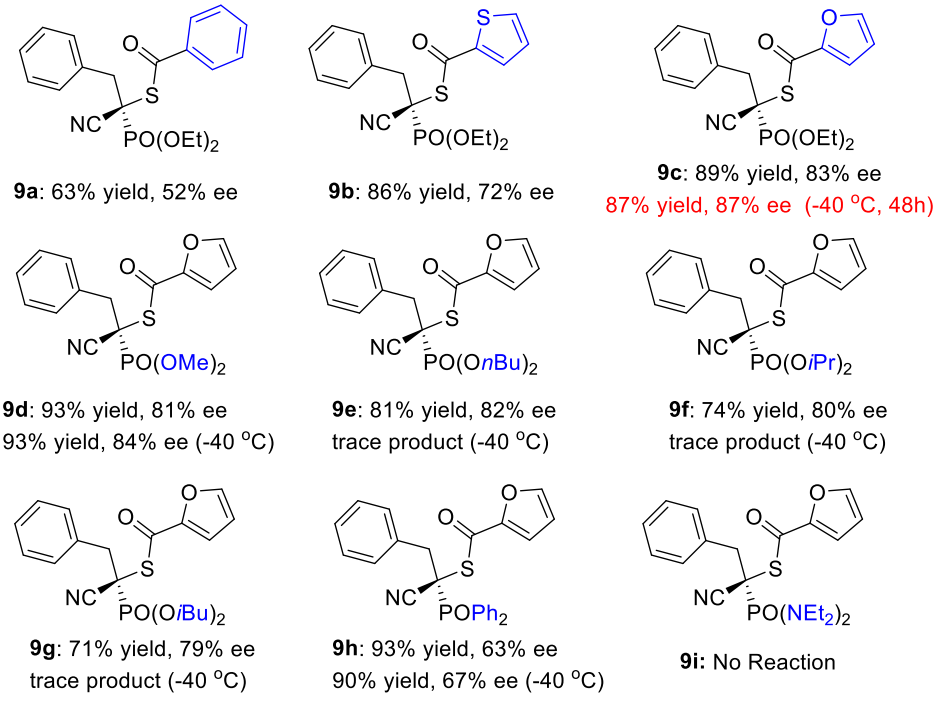

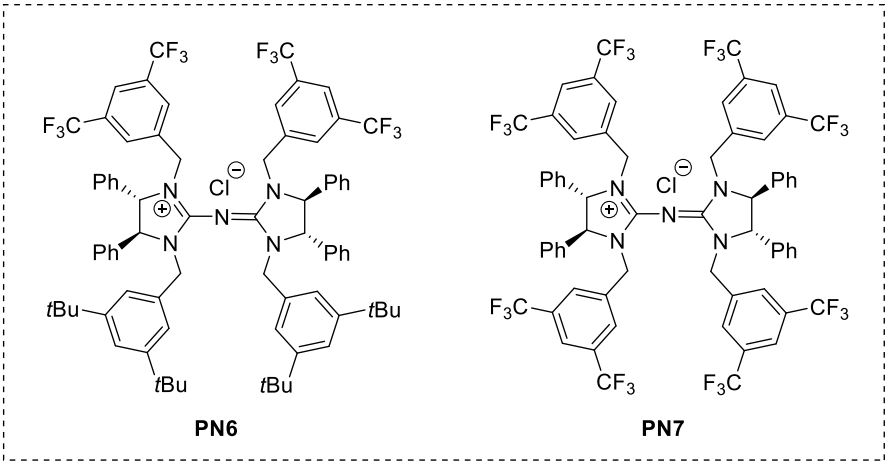

Figure 2.12 Optimization on the structure of thiocarboxylate and cyanophosphonate

Encouraged by the good results obtained when brominated cyanoesters were utilized as electrophiles, we would like to exploit another tertiary bromide, brominated alkyl cyanophosphonate in the enantioconvergent nucleophilic substitution reaction by

thiocarboxylate. We first tried different potassium thiocarboxylates and different cyanophosphonate esters to improve the enantioselectivity (**Figure 2.12**). Phenyl (**2r**), furyl (**2r**) and thiophenyl (**2s**) thiocarboxylate potassiums were tried, and furyl thiocarboxylate potassium afforded the product (**9c**) most efficiently with highest enantioselectivity. Then we tried different cyanophosphonate esters for this reaction. Different from the results we obtained when we optimized the structure of the brominated cyanoesters, when we changed diethyl phosphate group to other phosphate ester groups, the enantioselectivity of this reaction was not significantly influenced (**9c-9g**). However, the reactivity of this reaction was influenced a lot. When we tried to improve the enantioselectivity by decreasing the temperature to -40 ^{o}C, dimethyl phosphate (**9d**) substrate showed highest reaction rate and the product was isolated in 93% yield and 84% ee value. The result of diethyl phosphate substrate (**9c**) with longer reaction time was also good, and the product was isolated in 87% yield and 87% ee value. When dibutyl phosphate (**9e**), diisopropyl (**9f**) and diisobutyl phosphate (**9g**) substrates were used, only trace product was isolated at -40 ^{o}C. We also tried diphenylphosphoryl substrates and the reactivity was good, but only moderate ee value was achieved (**9h**). For phosphonic amide substrate (**9i**), we failed to observe any product and the substrate was recovered for the worse reactivity.

Then we tried to optimize the solvent with the model reaction between tertiary bromide **8a** and thiocarboxylate **2r** catalyzed by **PN6**. Various aromatic solvents and ether solvents were tested (**Table 2.3**). Compared with mesitylene (entry 2), reaction in toluene (entry 1) afforded product in higher yield but lower ee value. Other aromatic solvents resulted in worse enantioselectivities (entry 3-5). Ether solvents also failed to improve the enantioselecticity (entry 6-9). Adjustment of the equivalent of thiocarboxylate **2r** showed that 1.2 equivalent of **2r** afforded the product with best

enantioselectivity (entry 10, 11). More optimization was conducted, we found when the catalyst was change to **PN7** with longer reaction time (entry 12), the ee value can be improved to 89% in 86% yield.

Table 2.3 Optimization on the solvent and equivalents of thiocarboxylate

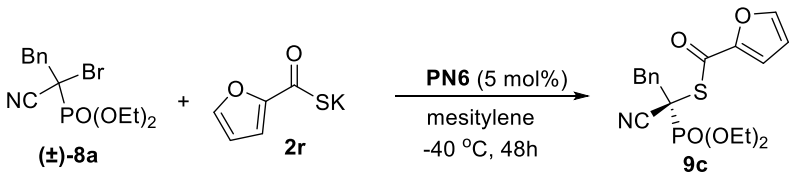

entry	solvent	equiv. of **2r**	yield (%)[b]	ee (%)[c]
1	toluene	1.2	91	82
2	mesitylene	1.2	87	87
3	cumene	1.2	85	54
4	m-xylene	1.2	88	51
5	*t*-butyltoluene	1.2	82	77
6	Bu_2O	1.2	71	81
7	iPr_2O	1.2	65	43
8	*t*BuOEt	1.2	61	72
9	Et_2O	1.2	81	41
10	mesitylene	1.0	67	87
11	mesitylene	1.4	91	84
12[d]	mesitylene	1.2	86	89

[a]The reaction was conducted on 0.1 mmol scale in 1 ml solvent. [b]Isolated yields. [c]Determined by chiral HPLC. [d]Reaction was conducted at -30 °C for 72h catalyzed **PN7**.

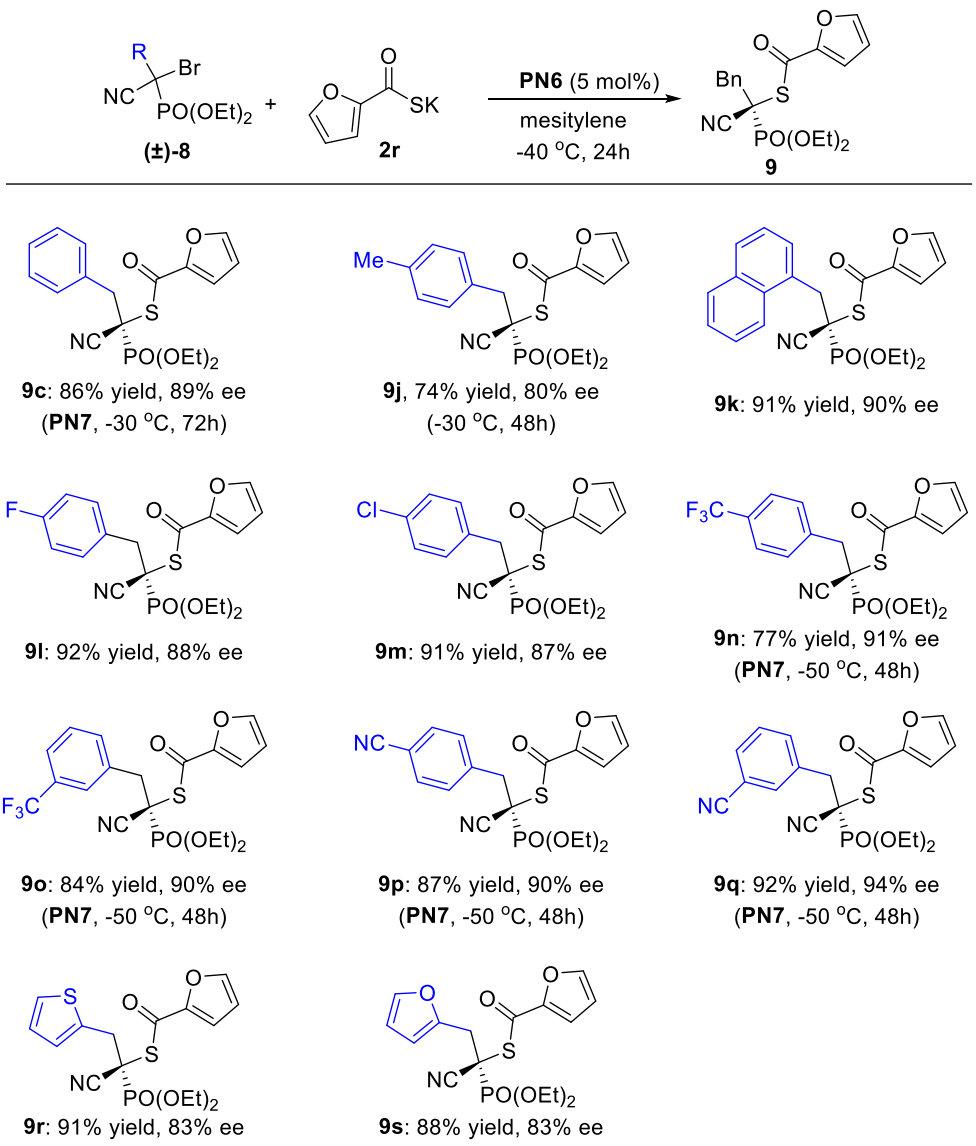

Figure 2.13 Substrate scope for substitution of brominated cyanophosphonate by thiocarboxylate

Then we synthesized various substituted brominated cyanophosphonate to investigate the substrate scope (**Figure 2.13**). We found this reaction was efficient for different benzyl groups substituted substrate and the best condition for each substrate usually needed to be adjusted because the reactivity and selectivity were significantly influenced by the benzyl groups. In the following investigations, we used a general condition (**PN6** as catalyst, in mesitylene, -20 °C for 24h) for these different substrates

in initial attempt. Then we adjusted the conditions for each substrate to achieve the best yield and enantioselectivity as shown in **Figure 2.13**. The 4-methylbenzyl group substituted substrate was less active and the reaction was conducted in -30 ^{o}C for 48 h affording product in 74% yield and 80% ee value (**9j**). Substrate bearing naphthyl group afforded product in 91% yield and 90% ee value (**9k**). For the substrates bearing fluorinated (**9i**) and chlorinated (**9m**) benzyl groups, they were also transformed to product in high yields and enantioselectivities. When the benzyl groups were substituted by strong electron-withdrawing groups, the reactions could be conducted at -50 ^{o}C affording products in excellent ee values (**9n**-**9q**). Cyanophosphonates bearing 3-(methyl)furan (**9r)** and 3-(methyl)thiophene (**9s)** groups also gave good results, albeit with slightly lower enantioselectivities.

2.4 Absolute configuration determination by X-ray crystallography

The absolute configurations of **7a**, **7l** and **9s** are determined by X-ray crystallography. For other products, the absolute configurations are determined by analogy.

The supplementary crystallographic data can be obtained free of charge from the Cambridge Crystallographic Data Centre via www.ccdc.cam.ac.uk/data_request/cif.

(A) Single-crystal structure of **7a**

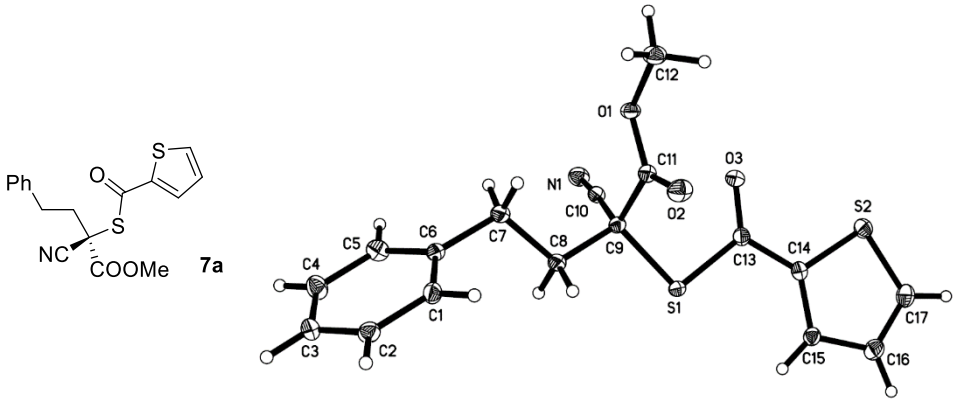

Figure 2.14 Single-crystal structure of **7a** (CCDC 1845292)

(B) Single-crystal structure of **7l**

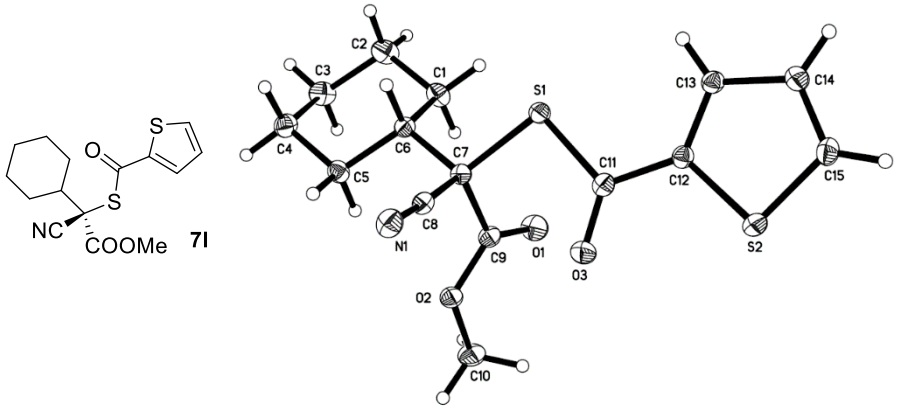

Figure 2.15 Single-crystal structure of **7l** (CCDC 1845290)

(C) Single-crystal structure of **9s**

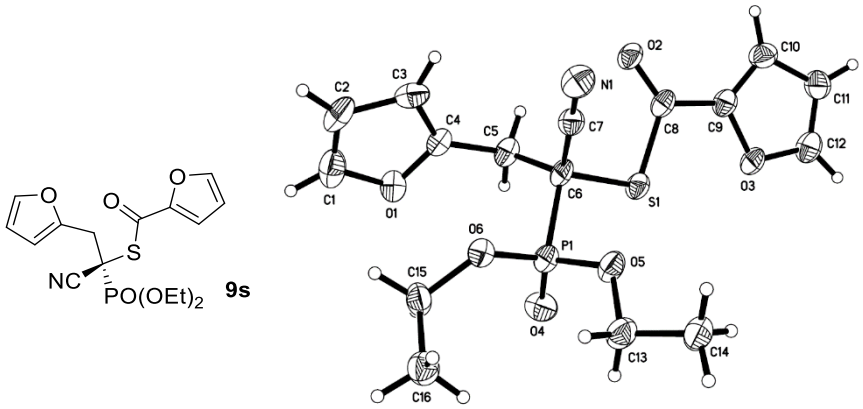

Figure 2.16 Single-crystal structure of **9s** (CCDC 1845291)

2.5 Summary

In summary, we have achieved the enantioconvergent nucleophilic substitution of tertiary bromides by thiocarboxylates under phase-transfer conditions. Activated tertiary bromides including brominate cyanoesters and brominated cyanophosphonates were utilized as electrophiles. We modified the structures of the tertiary bromides, thiocarboxylate salts and the catalysts to improve the reactivity and enantioselectivity. With further optimization on solvents and reaction temperature, the enantioenriched tertiary thioesters were obtained in high yields and enantioselectivities. The reaction condition was simple and mild. Different brominated cyanoesters bearing various alkyl groups were suitable. The alkyl groups could be primary alkyl, secondary alkyl, benzylic, allylic and propargylic groups. For brominated cyanophosphonate substrates, different benzylic substituents showed good results.

Compared with the enantioconvergent substitution of tertiary bromides through chiral Lewis/Brønsted acid catalyzed S_N1 reactions or transition-metal catalyzed $S_{RN}1$ reactions, our approach can achieve different substrate scope without any metal catalysts. Alkyl substituents usually result in significant elimination product in S_N1 reactions, but they are well tolerated in our reactions. In the meanwhile, our approach also needs further improvement. The tertiary bromides now are limited to those activated by two electron-withdrawing groups. More tertiary bromide species should be exploited, and more nucleophiles should be tried to generate various chemical bonds. For these purposes, a better understanding of the reaction mechanism is necessary, which will be discussed in the next chapter.

2.6 References

1. A. E. Wendlandt, P. Vangal, E. N. Jacobsen, Quaternary stereocentres via an enantioconvergent catalytic SN1 reaction. *Nature* **556**, 447 (2018).
2. Q. M. Kainz *et al.*, Asymmetric copper-catalyzed C-N cross-couplings induced by visible light. *Science* **351**, 681 (2016).
3. N. S. Zefirov, D. I. Makhon'kov, X-philic reactions. *Chem. Rev.* **82**, 615 (1982).
4. P. K. Sazonov, G. A. Artamkina, I. P. Beletskaya, Nucleophilic substitution at the halogen atom (halogenophilic reactions). *Russian Chem. Rev.* **81**, 317 (2012).
5. L. Zong, X. Ban, C. W. Kee, C. H. Tan, Catalytic Enantioselective Alkylation of Sulfenate Anions to Chiral Heterocyclic Sulfoxides Using Halogenated Pentanidium Salts. *Angew. Chem. Int. Ed.*, (2014).
6. B. Teng *et al.*, Pentanidium- and Bisguanidinium-Catalyzed Enantioselective Alkylations Using Silylamide as Bronsted Probase. *J. Am. Chem. Soc.* **138**, 9935 (2016).
7. C. Wang, L. Zong, C. H. Tan, Enantioselective Oxidation of Alkenes with Potassium Permanganate Catalyzed by Chiral Dicationic Bisguanidinium. *J. Am. Chem. Soc.* **137**, 10677 (2015).
8. A. Peschiulli, B. Procuranti, O. C. CJ, S. J. Connon, Synergistic organocatalysis in the kinetic resolution of secondary thiols with concomitant desymmetrization of an anhydride. *Nat. Chem.* **2**, 380 (2010).
9. J. Clayden, P. Maclellan, Asymmetric synthesis of tertiary thiols and thioethers. *Beilstein J. Org. Chem.* **7**, 582 (2011).
10. P. Chauhan, S. Mahajan, D. Enders, Organocatalytic carbon-sulfur bond-forming reactions. *Chem. Rev.* **114**, 8807 (2014).

Chapter 3

Mechanistic Studies

3.1 Introduction

After we achieved the enantioconvergent nucleophilic substitution of racemic activated tertiary bromide under phase-transfer conditions, we started to consider the mechanism of our reactions. We first excluded the carbonophilic S_N2 mechanism, because of its stereospecific transformation with inverted stereocenter.

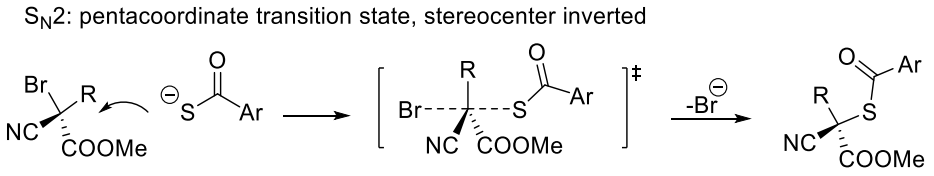

Figure 3.1 The S_N2 mechanism

For S_N1 reaction via prochiral carbocation intermediate, it is possible for enantioconvergent substitution by phase-transfer catalysis. However, in our reaction the tertiary bromide is highly electron-deficient with two electron-withdrawing groups resulting in a highly unstable carbocation, which makes S_N1 mechanism impossible.

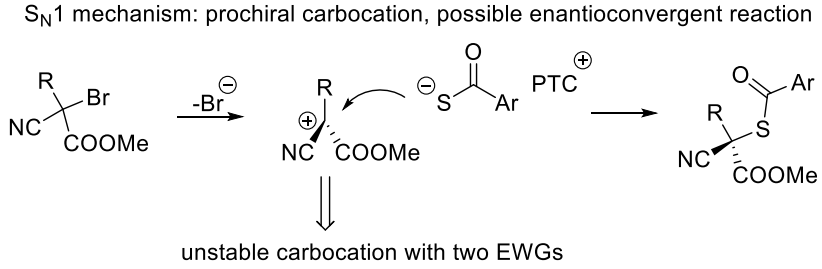

Figure 3.2 The S_N1 mechanism

Then we considered radical-based $S_{RN}1$ mechanism[1, 2]. In this mechanism, thiocarboxylate salt is transferred into organic phase by our chiral PTC before initial SET. In the initiation step, one electron of thiocarboxylate anion is transferred to the tertiary bromide, forming the thiol radical and radical anion intermediate. The thiol radical will go through homocoupling and form the disulfide. In the propagation chain, radical anion intermediate will release bromide anion and form tertiary radical specie. The prochiral radical enantioselectively reacts with another thiocarboxylate anion,

which is ion-paired with chiral cationic PTC. Then the enantioenriched radical anion intermediate is formed. This intermediate will go on to form substituted product by transferring one electron to next tertiary bromide, and at the same time a new radical anion intermediate is also generated for next cycle. This is possible mechanism, because the disulfides, which usually indicate a radical mechanism, are isolated as side product in our reaction. Because of the prochiral radical intermediate, it is possible for enantioconvergent transformation.

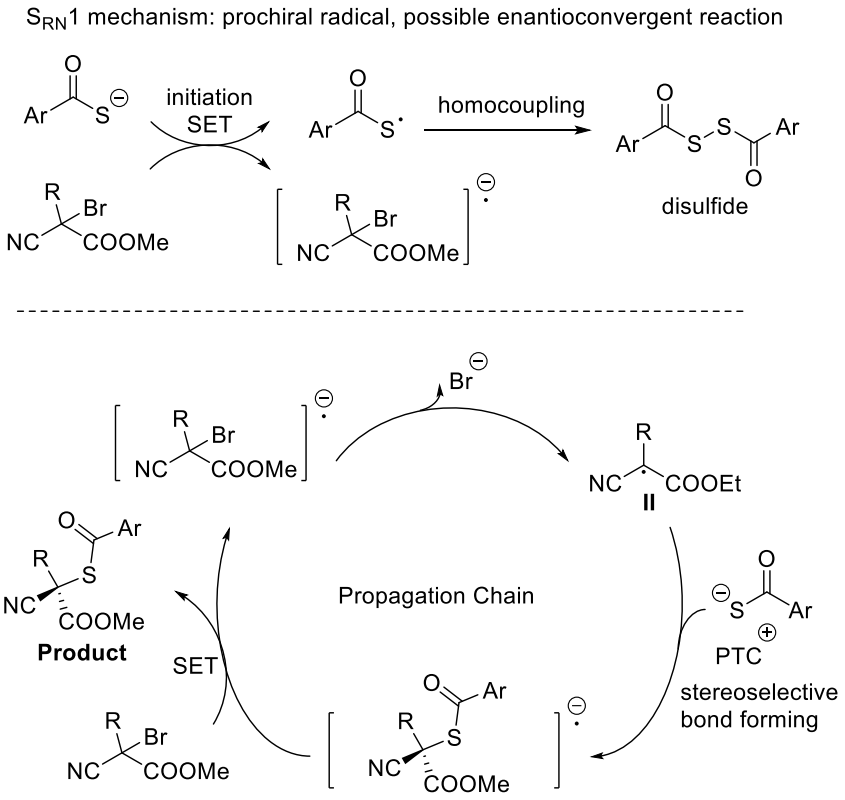

Figure 3.3 Possible $S_{RN}1$ mechanism

Another mechanism is the less-known halogenophilic nucleophilic substitution (S_N2X) mechanism[3, 4], and we prefer this mechanism. In this mechanism, the bromide atom of tertiary bromide is attacked by thiocarboxylate to generate a carbanion intermediate and a new electrophilic intermediate (sulfenyl bromide) with reversed polarity. The carbanion ion-paired with chiral PTC reacts with the sulfenyl bromide to generate the enantioenriched product. This mechanism also explains the isolated

disulfide, which is formed in the side reaction between sulfenyl bromide and thiocarboxylate. When proton source is added in the reaction, the carbanion can be quickly protonated to form protonated product.

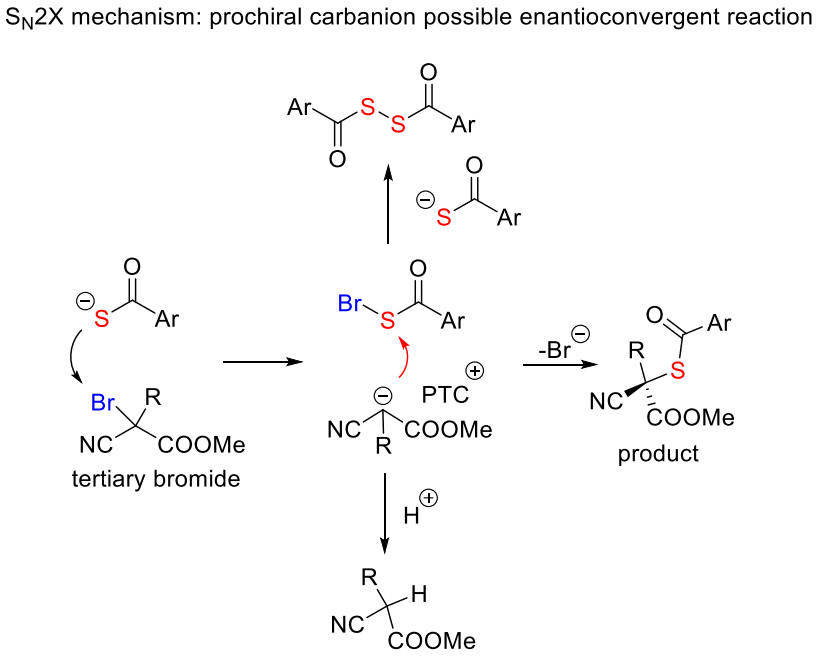

Figure 3.4 Possible S_N2X mechanism

Based on these discussions, we have proposed the two possible mechanisms: radical-based $S_{RN}1$ mechanism and anionic S_N2X mechanism. These two mechanisms have similar profiles: The products can be generated in high yields and enantioselectivities and the disulfide as side product can be generated via both mechanisms. Further mechanistic studies need to be conducted.

One method to distinguish these two mechanisms was conducted by Scorrano in 1993[5]. When they were investigating the nucleophilic substitution of *o*-iodonitrobenzene, they found the mechanism changed depending on the nucleophiles (**Figure 3.5**). When potassium 2-propanolate was used as nucleophile, this reaction proceeded through $S_{RN}1$ mechanism. In contrast, when potassium isopropanethiolate was used, the mechanism was changed to S_N2X instead of SET pathway. Both reactions generated the substitution product together with some protonated product nitrobenzene.

The authors used D-labelling experiment to investigate the mechanism. When the substitution reaction with *i*PrOK was conducted in *i*PrOD solvent, the nitrobenzene was formed without D-incorporation, suggesting the hydrogen was from isopropyl group of *i*PrOD and radical was involved. When the substitution reaction with *i*PrSK was conducted in *i*PrOD solvent, the nitrobenzene formed was deuterated, suggesting the hydrogen was from hydroxy group of *i*PrOD and carbanion intermediate was involved. These results helped distinguished the radical and anionic mechanisms, because radical would abstract hydrogen atom from C-H bond whose homolytic bond dissociation energy was lower than O-H bond. However, carbanion would abstract proton from more acidic O-H group[6]. Then we designed several experiments to investigate our reaction mechanism.

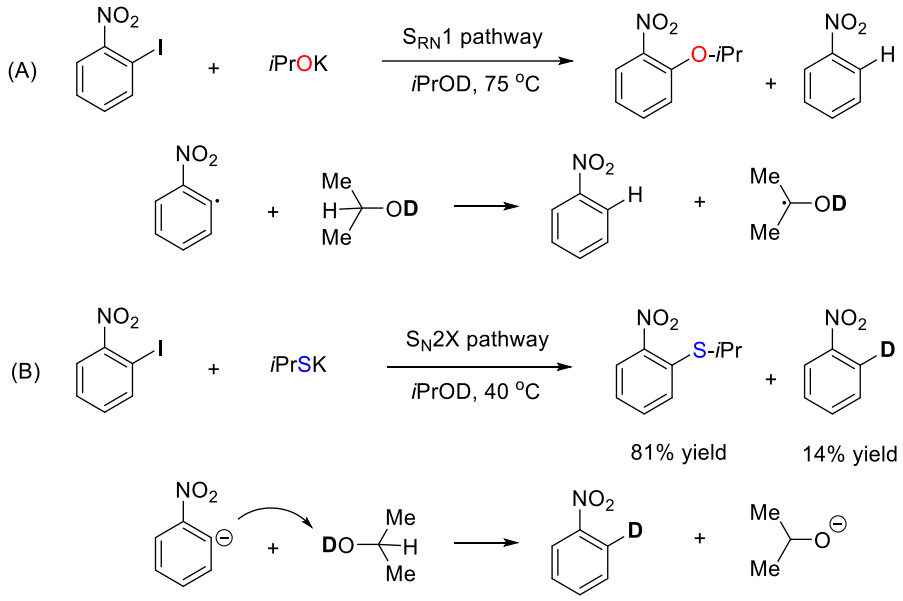

Figure 3.5 Mechanistic studies on nucleophilic substitution of *o*-iodonitrobenzene

3.2 Mechanistic investigations into the radical-based $S_{RN}1$ mechanism

Because we isolated disulfide as side product in our reaction, which usually suggested a SET mechanism, radical pathway was possible for our reaction. To confirm the formation of disulfide was through the reaction with tertiary bromide, we conducted the control experiment without bromide and we didn't observe any formation of disulfide (**Figure 3.6**). This suggested that the reaction between thiocarboxylate and tertiary bromide resulted in the formation of disulfides. Catalyst **PN6** or oxygen didn't interact with or oxidize thiocarboxylate **2s** to form disulfide under the experimental conditions.

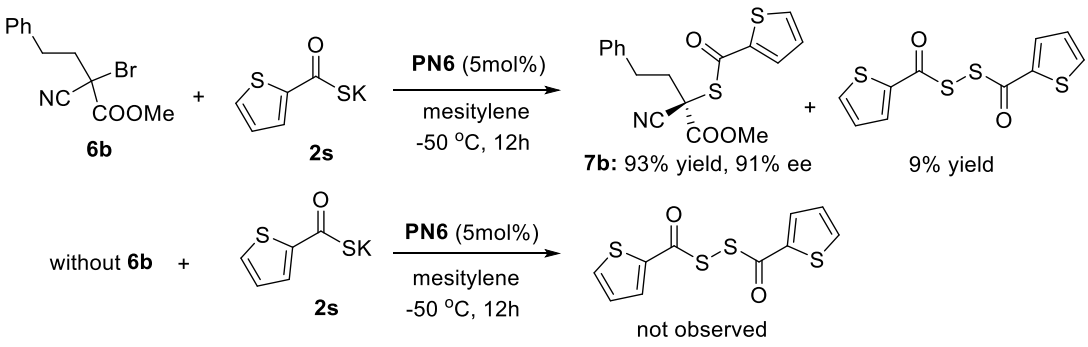

Figure 3.7 The control experiment without bromide

Then we tried to add the radical trap TEMPO and redox trap *m*-dinitrobenzene (*m*-DNB), *p*-dinitrobenzene (*p*-DNB) to our reactions (**Table 3.1**), but the reactions were not significantly influenced and products were isolated in high yields and enantioselectivities.

To further distinguish the radical or anionic mechanism, we tried to add some hydrogen-donors in our reaction. Two types of hydrogen-donors were chosen (**Table 3.2**). One type was hydrogen-atom donors (1,4-dicyclohexene, fluorene, xanthene and triethylsilane), and they were widely used in radical reactions as hydrogen-atom source. Another type was proton donors (water, methanol and phenol), and they were widely used in anionic reactions as proton source. When hydrogen-atom donors were added

(entry 1-4), the substitution products **7b** were isolated in high yields without formation of protonated product **6b-H**. When proton donors were added, the yields of the substitution product **7b** decreased sharply and a lot of protonated product **6b-H** were isolated. These results also agreed with an anionic mechanism rather than a radical mechanism.

Table 3.1 Radical inhibitor experiment

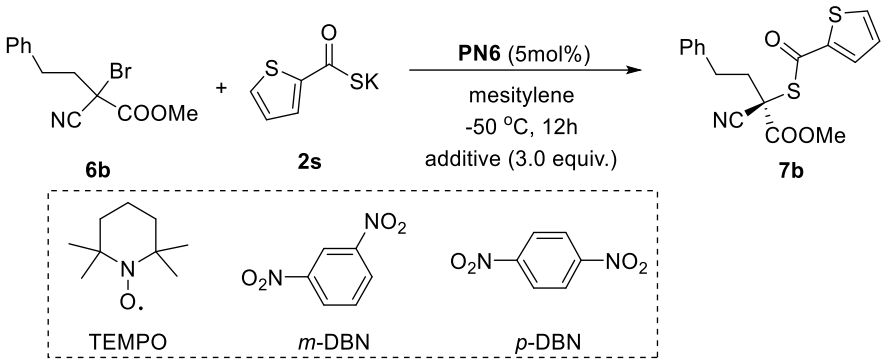

entry	additive	**7b**, yield (%)	ee (%)
1	TEMPO	81	87
2	*m*-DNB	79	86
3	*p*-DNB	78	87

Table 3.2 Effects of hydrogen-atom donors and proton donors

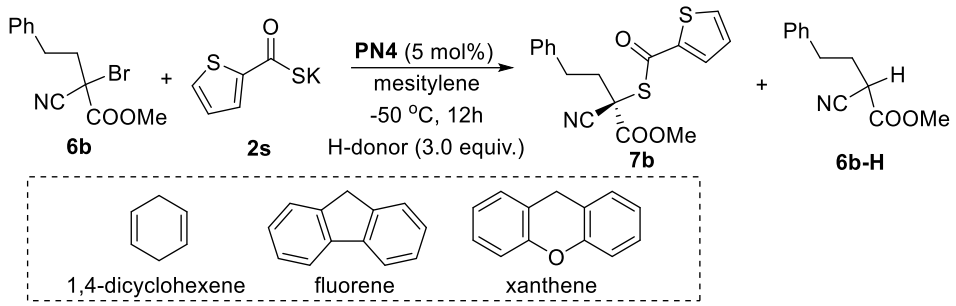

entry	H-donor	**7b**, yield (%)	**6b-H**, yield (%)
1	1,4-dicyclohexene	89	0
2	fluorene	88	0
3	xanthene	86	0
4	Et_3SiH	86	0
5	MeOH	13	55
6	PhOH	22	54
7	H_2O	66	22

3.3 Mechanistic investigations into the halogenophilic S_N2X mechanism

Later, we designed several experiments to support the halogenophilic S_N2X mechanism. We conducted Hammett analysis through competition experiments with *p*-substituted benzyl substrates **6c**–**6f** and benzyl substrate **6a** using a limiting amount of thiocarboxylate **2s**[7, 8].

Table 3.3 Hammett analysis through competition experiments

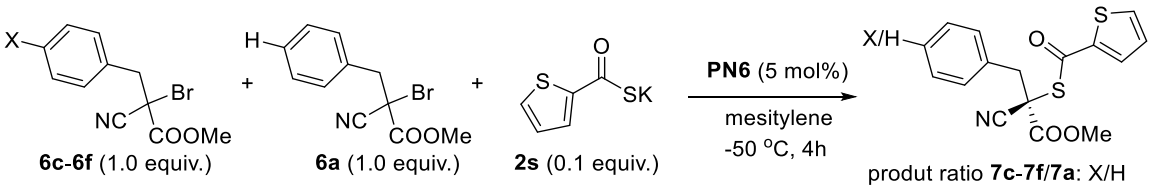

X	σ	Product Ratio	$\log(k_{Ar}/k_{Ph})$
OMe (**6f**)	-0.27	0.27/1	-0.57
Me (**6e**)	-0.17	0.55/1	-0.26
H (**6a**)	0	-	0
F (**6c**)	0.06	2.40/1	0.38
Cl (**6d**)	0.23	4.86/1	0.72

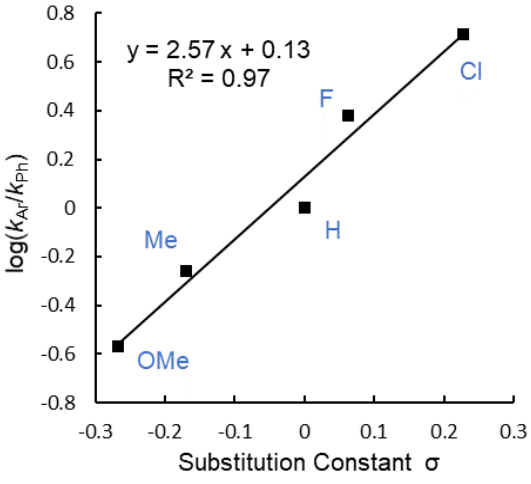

Figure 3.8 Hammett plot versus σ

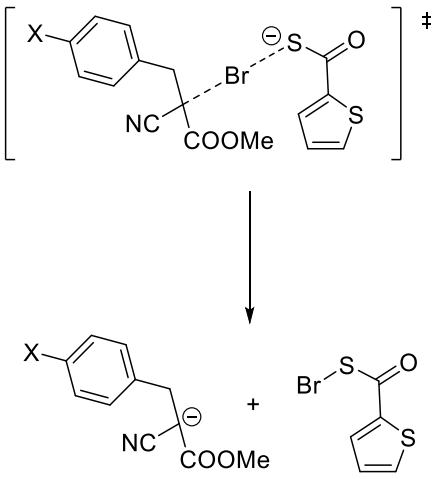

Figure 3.9 Accumulation of negative charge

A plot of log(k_{Ar}/k_{Ph}) obtained in the formation of **6c**–**6f** versus the corresponding substituent constant σ values[9] resulted in the Hammett plot (**Figure 3.8**). A linear correlation with a positive slope (ρ = +2.57) was obtained through this Hammett plot. This suggested that there was an accumulation of negative charge in the rate-determining transition state, which was stabilized by electron-withdrawing groups. These results agreed with an S_N2X mechanism (**Figure 3.9)**.

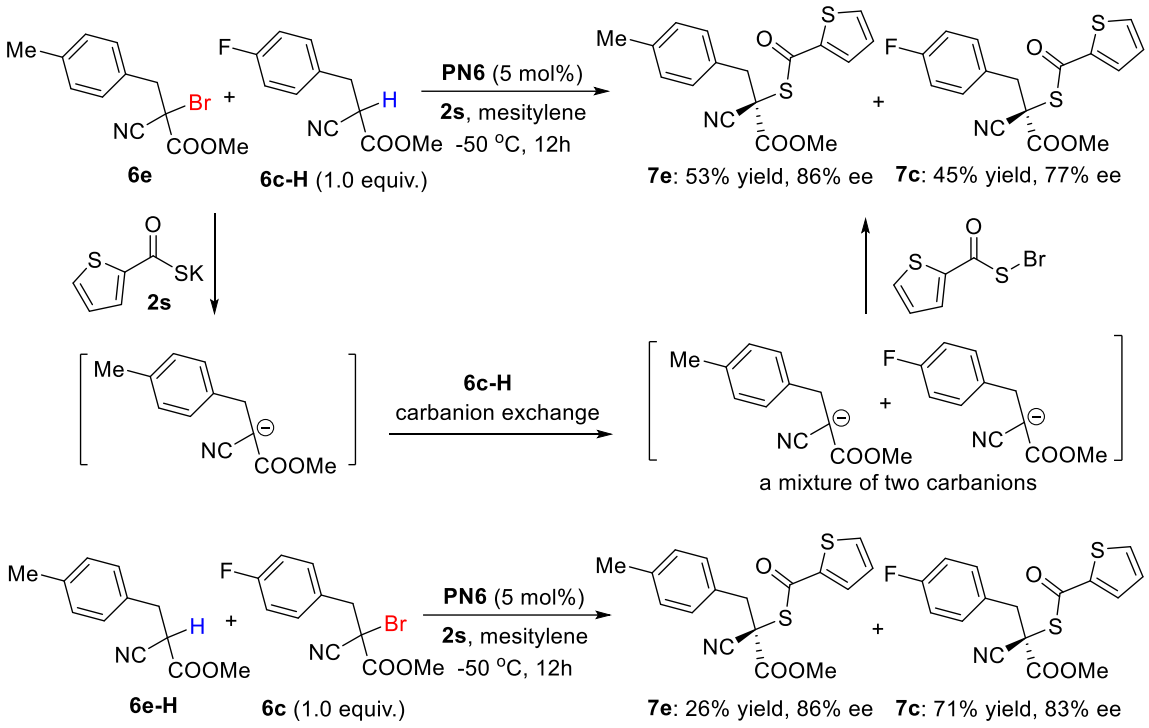

Figure 3.10 Carbanion exchange experiments

Carbanion exchange experiments (**Figure 3.10**) were conducted to provide experimental evidence of the proposed carbanion intermediate[10]. When a mixture of tertiary bromide **6e** (bearing a 4-methylbenzyl group) and methyl cyanoacetate **6c-H** (bearing a 4-fluorobenzyl group) was subjected to the standard reaction conditions, a mixture of tertiary thioester **7e** (53% yield, 86% ee) and tertiary thioester **7c** (45% yield, 77% ee) was obtained. This result suggested that the initial carbanion generated from **6e** abstracted a proton from **6c-H** to generate the corresponding carbanion. Both carbanions

reacted with the sulfenyl bromide to generate the mixture of tertiary thioesters **7e** and **7c**. In the meanwhile, we conducted the reaction with a mixture of tertiary bromide **6c** (bearing a 4-fluorobenzyl group) and methyl cyanoacetate **6e-H** (bearing a 4-methybenzyl group) and also obtained a mixture of tertiary thioester **7e** (26% yield, 86% ee) and tertiary thioester **7c** (71% yield, 83% ee).

At this moment, these results indicated carbanion intermediates and favored an S_N2X pathway. Another key feature of S_N2X reactions is the generation of a new electrophilic intermediate (Nu-X) from the attack of the nucleophile (Nu) on the halogen (X) atom. In order to prove this (**Figure 3.11**), benzoylsulfenyl bromide **10a**, the proposed new electrophilic intermediate, was prepared[11, 12] and reacted with carbanion **6b-A**, derived from **6b-H**, in the presence of pentanidium **PN6**. This afforded a mixture of the tertiary bromide **6b** (12% yield, 0% ee) and tertiary thioester **7q** (66% yield, 82% ee *c.f.* **7q** in **Figure 3.11**). These experiments indicated that benzoylsulfenyl bromide **10a** is plausible intermediate in these reactions and **10a** is an ambident electrophile. It is interesting to note that while the tertiary thioesters were obtained in high ee values, the tertiary bromides were obtained as racemate. This suggested that our catalyst couldn't induce asymmetry in the C-Br bonding forming step.

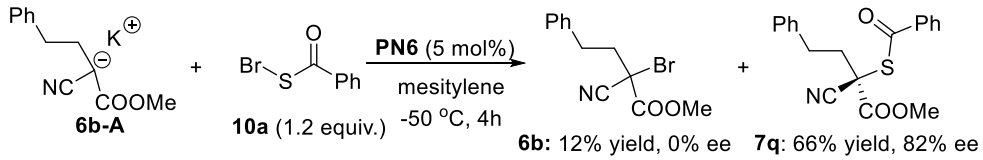

Figure 3.11 Reactions using the proposed S_N2X intermediates, benzoylsulfenyl bromide **10a**

Next, we separated the two enantiomers of tertiary bromide **6o** using preparative HPLC and subjected them to enantioconvergent thiocarboxylate substitution separately (**Figure 3.12**). It was found that both enantiomers were transformed to the same

enantiomer of thioester, (+)-**3k** (87% ee) and the recovered **6o** was racemized. From these results, we propose that the sulfenyl bromides are generated through the S_N2X mechanism and they are ambident electrophiles. Essentially, the C-Br bond cleavage step is reversible which can explain the racemization of enantioenriched tertiary bromide **6o**.

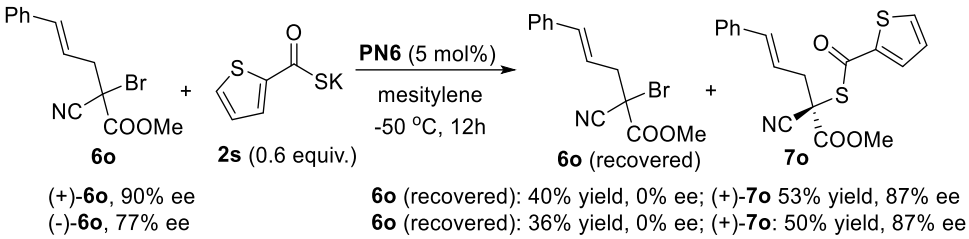

Figure 3.12 Reactions with enantioenriched tertiary bromides

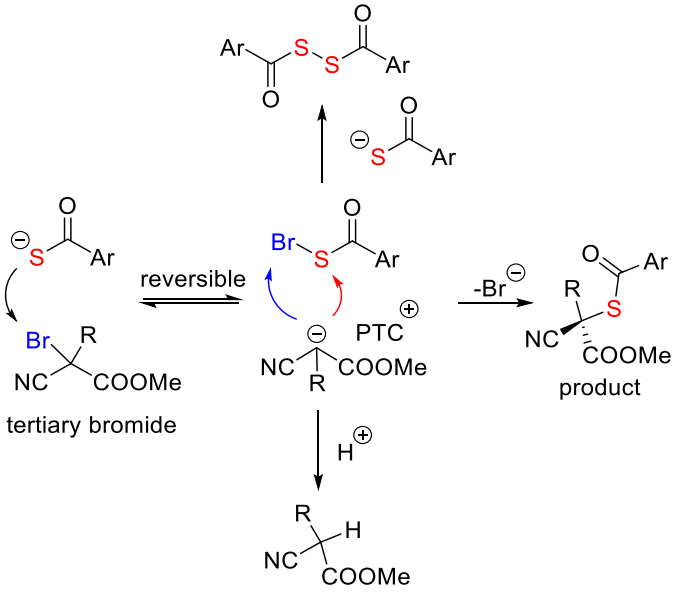

Figure 3.13 Proposed S_N2X mechanism

According these results, we have proposed the S_N2X mechanism (**Figure 3.13**). The bromine atom is attacked by the thiocarboxylate and the carbanion is generated together with a new electrophile, sulfenyl bromide. The sulfenyl bromide is an ambident electrophile. Carbanion can attack the bromine atom of sulfenyl bromide to form the starting tertiary bromide and thiocarboxylate, making the C-Br cleavage step reversible.

When the carbanion attacks the sulfur atom of sulfenyl bromide, the product tertiary thioester is generated enantioselectively. This mechanism also explains the formation of disulfides as side product and the formation of protonated product in the presence of proton sources.

3.4 Computational Studies of the halogenophilic S_N2X mechanism

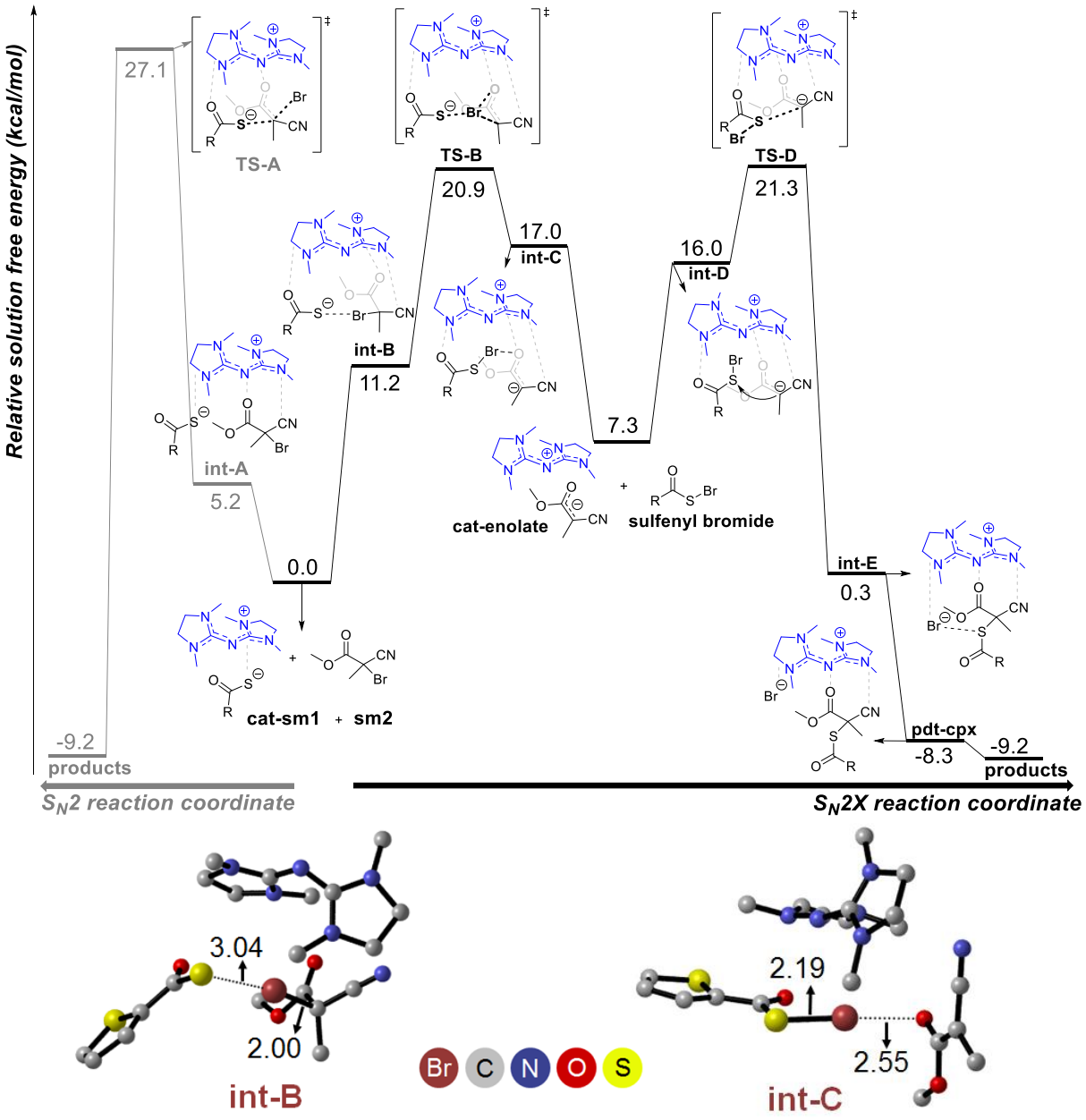

Figure 3.14 DFT calculation

Density functional theory calculations were performed using a simplified molecular model for the pentanidium catalyst, in which the benzyl groups were truncated into either H or methyl groups, to cut down on computational costs. Two possible pathways to achieve the observed product formation via a conventional S_N2 route and our proposed halogenophilic S_N2X pathway are considered (**Figure 3.14**).

In the S_N2 pathway, coordination of the tertiary bromide starting material with the catalyst and thiocarboxylate forms intermediate **int-A**, ΔG_{sol} = 5.2 kcal/mol relative to starting materials **cat-sm1** and **sm2.** Here, geometrical optimizations revealed that the tertiary bromide is able to form cation-dipole interactions via the cyanide and carbonyl functional groups with the pentanidium moiety. Conventional S_N2 'backside' attack from the thiocarboxylate S atom to the quaternary C atom of tertiary bromide via **TS-A** requires overcoming a relative free energy barrier of 27.1 kcal/mol. This results in the crucial S-C bond formation and Br displacement, leading to the formation of the observed product and pentanidium bromide species (ΔG_{sol} = -9.2 kcal/mol).

In our proposed S_N2X pathway (**Figure 3.14**), apart from the cation-dipole interaction, we envisioned that the tertiary bromide could interact via intermolecular halogen bonding[13] with the S atom of the thiocarboxylate, forming **int-B**, ΔG_{sol} = 11.2 kcal/mol. The Br possesses a σ-hole[14] through which intermolecular halogen bonding occurs, and is enhanced by the two covalently bonded electron withdrawing functional groups, the cyanide and ester moieties. This intermediate is thus primed for C-Br bond cleavage due to the halogen bonding. The calculated S···Br atomic distance in **int-B** is 3.04 Å, which is well within the reported range for halogen bonds and the C-Br bond of tertiary bromide is slightly elongated to 2.00 Å.

The formed **int-B** could proceed via **TS-B** ($\Delta G^{\ddagger}_{sol}$ = 20.9 kcal/mol), a transition state we calculated to be lower than **TS-A**. The process through **TS-B** results in the simultaneous formation of the S-Br bond and breakage of the Br-C bond leading to the sulfenyl bromide/enolate complex **int-C** (ΔG_{sol} = 17.0 kcal/mol), which is held by halogen-bonding (Br···O atomic distance of 2.55 Å). The formed sulfenyl bromide dissociated out of the catalyst pocket (ΔG_{sol} = 7.3 kcal/mol) and then interacted with carbanion to form **int-D** (ΔG_{sol} = 16.0 kcal/mol). Subsequently, C-S bond formation

via **TS-D** ($\Delta G^{\ddagger}_{sol}$ = 21.3 kcal/mol) lead to the formation of pre-product **int-E** (ΔG_{sol} = 0.3 kcal/mol) and then product complex **cat-pdt** (ΔG_{sol} = -8.3 kcal/mol). The activation barriers **TS-B** and **TS-D** relative to **cat-enolate/sulfenyl bromide** are nearly isoenergetic, consistent with experimental evidence, suggesting that sulfenyl bromide is an ambident electrophile.

Overall, the relative energy barrier for the S_N2X pathway is 21.3 kcal/mol (**TS-D**) which is kinetically more favored than that of the S_N2 route ($\Delta G^{\ddagger}_{sol}$ = 27.1 kcal/mol, **TS-A**). In addition, the proposed S_N2X mechanism which takes into account the formation of halogen-bonding interaction is intriguing and corroborates our experimental observations.

Computational modelling with NCIplot mapping non-covalent interaction surface (**Figure 3.15**)[15, 16] for **int-B** showed strong positive interaction between the σ-hole of the Br atom in the tertiary bromide and the nucleophilic S anion of thiocarboxylate. For intermediate **int-C**, it was observed from NCIplot that the negatively charged enolate O interacts favorably with Br of bromo-thiocarboxylate via halogen bonding interactions similar to **int-B**.

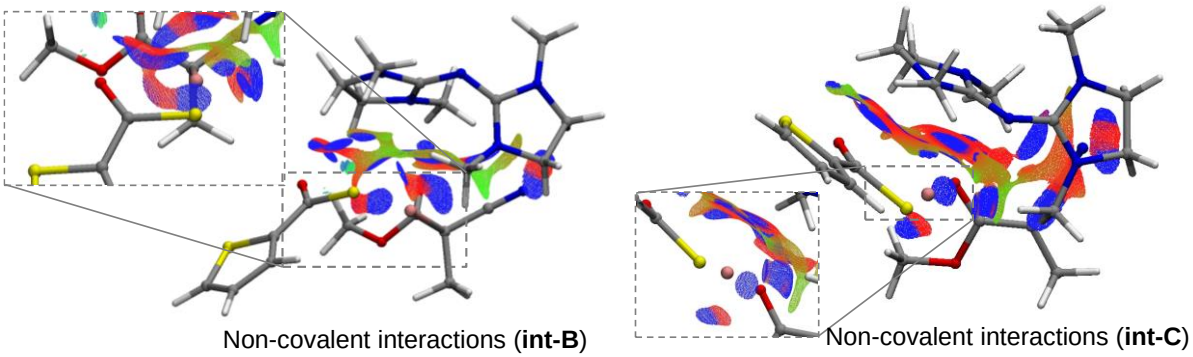

Figure 3.15 Non-covalent interaction (NCI) surface mapping for **int-B** and **int-C**, with zoomed-in view of the intermolecular halogen-bonding interactions between Br and S for the former and Br and O for the latter structures. The 3D mesh-grid surfaces are BGR color-coded to represent NCI with repulsive (red), van der Waals (green) and attractive (blue) regions. Atoms are stick-figures and color-coded: C (gray), H (white), S (yellow), O (red), N (blue) and Br (pink)

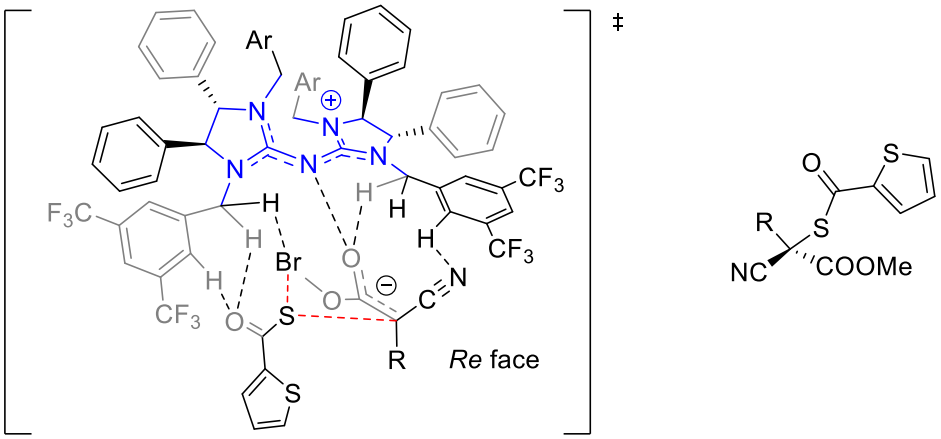

Figure 3.16 Proposed transition state structure for stereoinduction

According to previous calculations, pentanidium is known to provide hydrogen bonding as noncovalent interaction in catalysis[17]. Based on the absolute configuration determined by X-ray crystallography and the enantioselective bond-forming step, we have proposed the possible transition state structure (**Figure 3.16**). The cationic pentanidium traps the anionic enolate in the chiral pocket through the formation of a tight ion pair and hydrogen bonds. The sulfenyl bromide approaches the enolate from the *Re* face, which is directed by the hydrogen bonds formed with pentanidium. The formation of ion pair and multiple hydrogen bonds stabilize the substrates in the TS and account for the high enantioselectivity.

3.5 Summary

In summary, we have conducted a series of mechanistic studies for this enantioconvergent nucleophilic substitution of tertiary bromides by thiocarboxylate. Radical inhibitor and radical clock experiments failed to prove any radical specie in our reactions. By comparing the effects of H-atom donors and proton donors to our reactions, we have found carbanions are reasonable intermediates rather than radicals, which is further confirmed by Hammett analysis and carbanion exchange experiments. We also synthesized the key intermediate, sulfenyl bromide, and conducted its reaction between carbanion catalyzed by **PN6**, which afforded the product tertiary ester with high enantioselectivity proving sulfenyl bromide was the reaction intermediate. In the meanwhile, some racemic tertiary bromides were also isolated, suggesting the sulfenyl bromide was an ambident electrophile and the C-Br bond cleavage step was reversible. We also conducted reactions using enantioenriched tertiary bromide with limited amount of thiocarboxylate. Each enantiomer of the tertiary bromide resulted in the product with the same configuration, and the recovered tertiary bromide was racemized because of the reversible C-Br bond cleavage step.

DFT calculations were also conducted for our reaction. The results were consistent with our experimental studies and support S_N2X mechanism. Computational modelling also disclosed the S···Br intermolecular halogen bonding between tertiary bromide and thiocarboxylate, which was crucial for the efficient halogenophilic reaction. While halogen bonding has been well-exploited in the field of supramolecular chemistry and crystal engineering, their role in reaction development and catalysis is still in its infancy and requires more exploration.

3.6 Calculation archive files

(A) Computational methods

Density functional theory studies were carried out with Gaussian 16 computational chemistry suite. Geometries of gas phase minimum and transition state electronic structures were optimised using the Minnesota functional M11[18] with Pople's basis set 6-31G(d,p)[19]. Frequency calculations were carried out at that level to ensure convergence (all positive eigenvalues for minima and single negative for saddle points). Thermochemical corrections and zero point vibrational energies, as well as the infrared, were determined at the gas phase M11/6-31G(d,p) level using the unscaled frequencies. Solvation energies were considered with single point calculations with the SMD model[20] (toluene parameters) on gas phase optimized structures carried out with same functional M11 and Wiegend and Aldrich's triple zeta def2-TZVP [21, 22] basis set. The M11/def2-TZVP energies together with thermal and vibrational corrections based on gas-phase vibrations constitute the solution free energy, ΔG_{sol}, reported here and in the manuscript. Interatomic distances and bond lengths are in units of angstroms (Å). Relative energies are corrected for the enthalpy and entropy factors at 298K and are listed in kcal/mol.

(B) 3D rendered molecular images

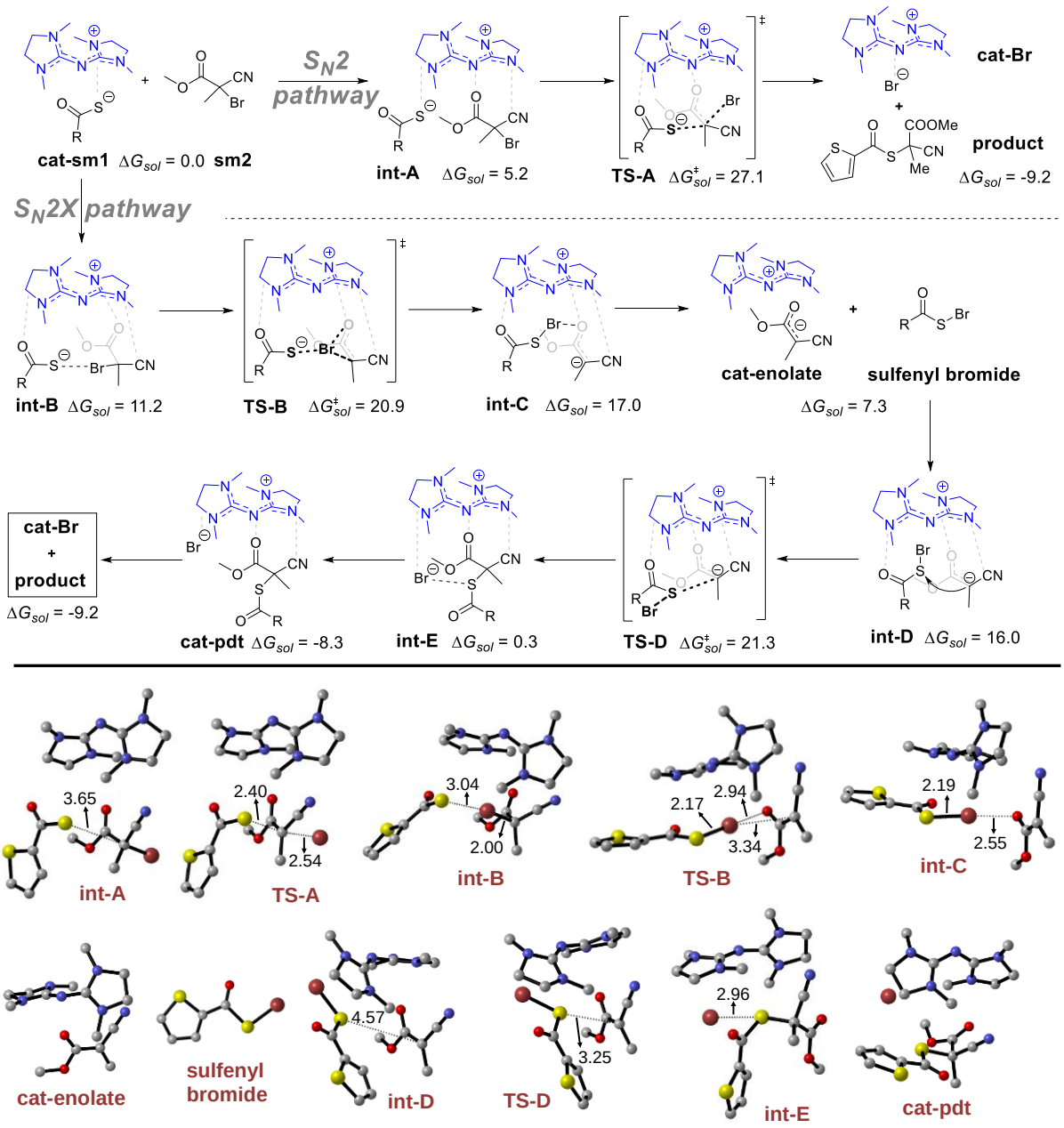

Figure 3.17 DFT calculated relative free energies and 3D rendered molecular images of the various minima and transition structures of the S_N2 and S_N2X pathways. C-H hydrogen atoms were omitted for visual clarity. Atoms are color coded in the 3D rendered molecular images to represent different elements: gray (carbon), red (oxygen), yellow (sulfur), blue (nitrogen) and brown (bromine). Selected bond distances (Å) are shown.

(C) PES plots

To gain a deeper understanding of the mechanistic pathways, each transition state was used as the starting structure and perturbed in both the forward and backward directions to generate a potential energy scan (PES) plot. In all cases, these plots linked the transition state structures to our proposed minima structures of the corresponding starting material(s) and the product(s).

The PES plot generated using **TS-B** and structures from four key points along the PES are shown in **Figure 3.18**. As the C-Br bond of the organic bromide breaks and the S-Br bond forms in thiocarboxylate, the initial low energy intermediate (structure A which optimizes to **int-B**) forms structure B, in which the bromine atom of the organic bromide has completely migrated to the sulfur atom of thiocarboxylate. As the complex undergoes rotation of the thiocarboxylate, which brings the bromide closer to the enolate O atom, an energy maximum (structure C, **TS-B**) is reached before structure D (optimizes to **int-C**) is formed.

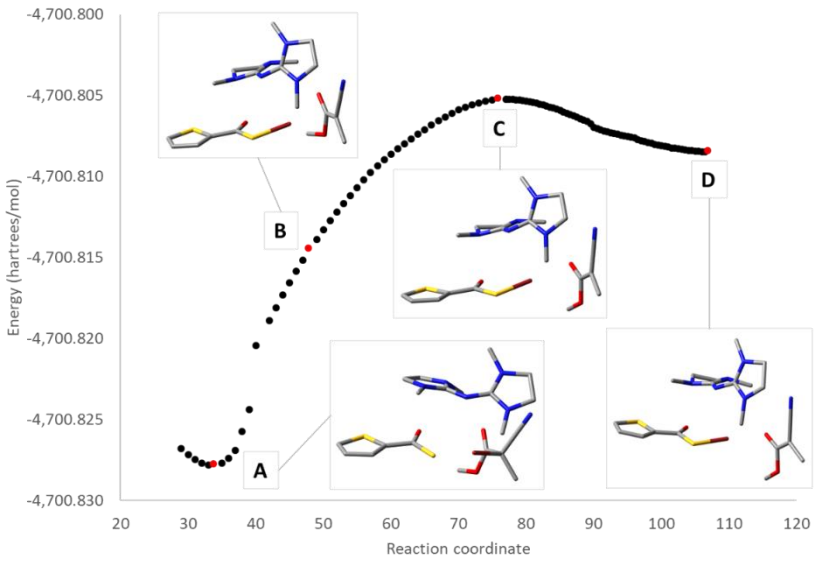

Figure 3.18 Plot of potential energy scan when **TS-B** (structure **C**) is perturbed and structures from four key points along the scan

The PES plot generated using **TS-D** and structures from four key points along the PES are shown in **Figure 3.19**. Structure A, which optimizes to **int-D**, undergoes rotation of the bromo-thiocarboxylate, which brings the S-Br atoms of the bromo-thiocarboxylate in the correct orientation to undergo a nucleophilic substitution with the carbanion. An energy maximum (structure B, **TS-E**) is reached before complete dissociation of bromine (structure C, optimizes to **int-E**) and formation of the S-C bond in the product (structure D which optimizes to **cat-pdt**).

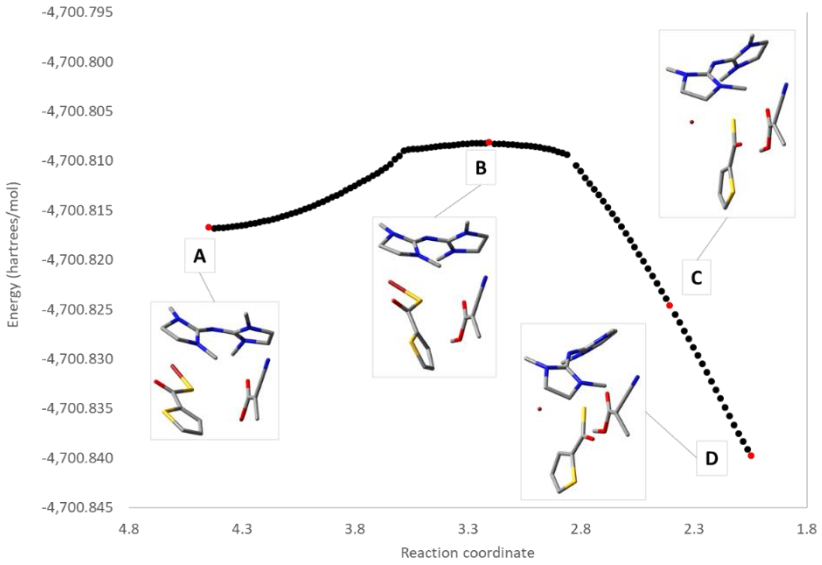

Figure 3.19 Plot of potential energy scan when **TS-D** (structure **B**) is perturbed and structures from four key points along the scan

Table 3.4 Summary of energies of optimized electronic structures

Structure	$E_{M11/def2-TZVP+SMD}$	G_{corr}	H_{corr}	ZPE	G_{sol}
cat-sm1	-1730.695324	0.325773	0.408003	0.382487	-1085806.89
sm2	-2973.170781	0.070646	0.11886	0.107699	-1865620.33
int-A	-4703.883036	0.421646	0.529059	0.492017	-2951422.02
TS-A	-4703.847262	0.420781	0.52776	0.490769	-2951400.12
int-B	-4703.871248	0.419378	0.529119	0.491597	-2951416.05
TS-B	-4703.859398	0.423031	0.52738	0.491265	-2951406.32
int-C	-4703.862011	0.419465	0.52832	0.490973	-2951410.20
cat-enolate	-1066.074756	0.363078	0.446998	0.419824	-668734.08
sulfenyl bromide	-3637.778333	0.032035	0.079095	0.069307	-2282685.80
int-D	-4703.869195	0.42498	0.529065	0.492558	-2951411.24
TS-D	-4703.861207	0.425426	0.527763	0.491826	-2951405.95
int-E	-4703.892272	0.423137	0.529408	0.492519	-2951426.88
cat-pdt	-4703.905784	0.422819	0.529569	0.492593	-2951435.56
cat-Br	-3240.659353	0.267643	0.33309	0.314073	-2033345.80
product	-1463.223268	0.130583	0.194144	0.176703	-918090.66

*All energy values are in hartrees

XYZ Coordinates

cat-sm1

46

C	-3.07705	-0.02738	0.41258
N	-2.68175	-1.27983	0.71147
C	-3.82732	-2.12577	1.01558
C	-4.92276	-1.09383	1.31619
N	-4.43058	0.07197	0.59984
H	-4.08118	-2.75600	0.14650
H	-3.60609	-2.78132	1.86759
H	-4.99708	-0.88116	2.39784
H	-5.91149	-1.39915	0.95060
C	-1.28142	1.17669	-0.65924
N	-0.43441	2.19850	-0.42766
C	0.68639	2.17362	-1.36413
C	0.30464	1.04125	-2.33996
N	-0.93772	0.52051	-1.77130
H	0.78636	3.14780	-1.86409
H	1.61128	1.94141	-0.81909
H	1.05130	0.23521	-2.37766
H	0.10974	1.41319	-3.35796
N	-2.38068	1.02988	0.07808
C	-1.62328	-0.57510	-2.41458
H	-1.83778	-0.31404	-3.46206
H	-2.57352	-0.77716	-1.90755
H	-0.97902	-1.46694	-2.38110
C	-0.24711	2.75914	0.89417
H	0.54405	2.19997	1.41833
H	-1.19009	2.67885	1.44494
H	0.03255	3.81739	0.80857
C	-1.34989	-1.84115	0.57201
H	-0.59839	-1.05103	0.43958
H	-1.29237	-2.52632	-0.28469
H	-1.10034	-2.40009	1.48449
C	-5.10583	1.34499	0.70392
H	-5.16765	1.68238	1.75256
H	-6.12245	1.26015	0.29803
H	-4.54148	2.08355	0.12680
C	5.42410	0.46379	1.30446
S	3.73502	0.79750	1.35351
C	3.39577	-0.54519	0.30415
C	4.53998	-1.20331	-0.04811
C	5.70910	-0.62436	0.52858
H	6.12414	1.08554	1.85592
H	4.51270	-2.07173	-0.70366
H	6.71841	-1.00127	0.37195
C	1.97033	-0.79413	-0.07613
S	1.63257	-2.09250	-1.14697
O	1.13864	0.00475	0.40742

sm2

15

C	0.28284	0.59119	0.39159
H	0.20519	1.86184	2.12513
C	0.81064	1.02642	1.75136
H	0.72008	0.18645	2.44737
H	1.85689	1.33702	1.66658
C	0.35476	1.66294	-0.60595
N	0.41096	2.54400	-1.35009
C	-1.14970	0.03838	0.50172
O	-1.66877	-0.22417	1.55592
O	-1.70659	-0.11755	-0.69182
C	-3.03487	-0.66397	-0.67225
H	-3.01813	-1.66178	-0.21738
H	-3.35248	-0.71400	-1.71638
H	-3.69703	-0.01250	-0.08948
Br	1.36656	-0.91432	-0.28219

int-A

61

C	-2.99616	-1.86910	-0.66585
N	-2.54733	-3.12599	-0.49428
C	-1.09466	-3.15711	-0.72731
C	-0.85952	-1.88045	-1.54440
N	-2.07738	-1.10930	-1.26372
H	-0.55604	-3.09038	0.23120
H	-0.78864	-4.06834	-1.25318
H	-0.79241	-2.06899	-2.62769
H	0.02938	-1.34423	-1.19970
C	-4.44963	-0.34246	0.27143
N	-5.64827	0.30474	0.21386
C	-5.50473	1.63371	0.79747
C	-4.28136	1.45663	1.70678
N	-3.60015	0.32464	1.07986
H	-5.31041	2.37683	0.00339
H	-6.40800	1.93186	1.34475
H	-4.57791	1.18868	2.73471
H	-3.62168	2.33078	1.73042
N	-4.24067	-1.48462	-0.34435
C	-2.42133	-0.28062	1.68795
H	-1.53447	-0.21383	1.04527
H	-2.61148	-1.34105	1.91931
H	-2.20367	0.25218	2.62044
C	-6.57550	0.07270	-0.87171
H	-6.36824	0.73817	-1.72810
H	-7.60208	0.25003	-0.52669
H	-6.47542	-0.96850	-1.19459
C	-3.16441	-4.04453	0.43633
H	-4.22633	-3.79322	0.52884
H	-2.68228	-3.98203	1.42679
H	-3.06402	-5.07156	0.06303
C	-2.28310	0.23809	-1.75338

H	-1.97580	0.98625	-1.00843
H	-3.34361	0.37557	-2.00962
H	-1.66757	0.37753	-2.64946
C	1.30689	2.40992	0.33368
Br	1.68549	4.13434	-0.57297
H	2.00127	3.11572	2.24897
C	2.20295	2.28899	1.55888
H	3.24663	2.32423	1.22955
H	1.99870	1.31999	2.03534
C	-0.11961	2.43823	0.67609
N	-1.23254	2.49345	0.97960
C	1.54414	1.35786	-0.76617
O	0.67656	0.97688	-1.51464
O	2.82050	1.03017	-0.82233
C	3.17617	0.10828	-1.87027
H	2.56928	-0.80261	-1.78885
H	4.23393	-0.12067	-1.71078
H	3.01075	0.58738	-2.84375
H	7.00407	-2.38098	0.11169
C	6.00232	-2.07302	0.39924
C	5.65712	-1.09788	1.29329
C	4.24376	-0.97642	1.44112
C	3.55219	-1.85590	0.65607
S	4.62417	-2.85311	-0.27620
H	6.38364	-0.49147	1.83149
H	3.73284	-0.27379	2.09623
C	2.08152	-2.01737	0.42472
O	1.75608	-2.79805	-0.48067
S	0.99486	-1.07159	1.39082

TS-A

61

C	-2.93258	-1.80098	-0.72673
N	-2.46450	-3.06368	-0.81151
C	-1.06093	-3.03254	-1.23425
C	-0.96451	-1.66214	-1.90450
N	-2.04746	-0.92690	-1.23478
H	-0.39617	-3.07790	-0.35454
H	-0.82978	-3.86432	-1.91054
H	-1.18504	-1.71869	-2.98412
H	0.00480	-1.18507	-1.74386
C	-4.37978	-0.43536	0.45095
N	-5.49425	0.33121	0.32307
C	-5.32650	1.54958	1.11397
C	-4.24705	1.14249	2.13005
N	-3.61490	0.01312	1.45509
H	-4.97002	2.36783	0.46354
H	-6.26896	1.85597	1.58464
H	-4.68713	0.81276	3.08536
H	-3.50619	1.93061	2.30755
N	-4.15203	-1.51101	-0.28031
C	-2.53769	-0.75557	2.05344
H	-1.71787	-0.90590	1.33967
H	-2.91048	-1.72688	2.41720
H	-2.13417	-0.17775	2.89139
C	-6.24721	0.35800	-0.91292
H	-5.85062	1.12193	-1.60408
H	-7.30044	0.58187	-0.70208
H	-6.17223	-0.62739	-1.38424
C	-2.98837	-4.13826	0.00107
H	-4.03485	-3.91820	0.23760
H	-2.41475	-4.24094	0.93786
H	-2.93210	-5.08446	-0.55203
C	-2.39749	0.42326	-1.65217
H	-2.76431	1.00995	-0.80151
H	-3.15138	0.40062	-2.45722
H	-1.47881	0.90851	-1.99819
C	1.22612	1.51770	0.52524
Br	1.26920	3.84352	-0.50514
H	2.38666	2.90774	1.69646
C	2.25934	1.82748	1.59985
H	3.20851	1.37001	1.30130
H	1.93485	1.39623	2.55253
C	-0.18105	1.73755	0.81029
N	-1.28595	1.86097	1.13194
C	1.56948	1.13526	-0.89396
O	0.75871	0.88538	-1.75708
O	2.88748	1.02937	-1.04214
C	3.30828	0.70930	-2.37487
H	2.91396	-0.27534	-2.65702
H	4.40136	0.70044	-2.34672
H	2.93716	1.47830	-3.06399
H	7.11149	-2.02968	0.80559
C	6.05493	-1.82974	0.96235
C	5.45170	-1.40283	2.11383
C	4.04735	-1.23787	1.95571
C	3.62280	-1.54533	0.68952
S	4.93601	-2.04702	-0.32286
H	5.99045	-1.21151	3.03951
H	3.35653	-0.90873	2.73027
C	2.26555	-1.50391	0.10485
O	2.07696	-1.92909	-1.02581
S	0.96471	-0.80053	1.10378

int-B

61

C	1.81350	-1.99754	1.11942
N	0.93763	-2.95582	1.45107
C	-0.20713	-2.39769	2.17673
C	0.17513	-0.91349	2.34768
N	1.41883	-0.80230	1.57994
H	-1.11491	-2.49246	1.56549
H	-0.34064	-2.92112	3.13414
H	0.37077	-0.65080	3.39871
H	-0.60324	-0.26262	1.92758
C	3.51412	-1.41302	-0.35546
N	4.82650	-1.08450	-0.35394
C	5.07709	-0.03126	-1.33453
C	3.86778	-0.17300	-2.26634
N	2.88446	-0.82559	-1.40334

H	5.07254	0.95438	-0.83886	H	-2.69598	-0.77926	2.32735
H	6.03689	-0.17976	-1.84539	H	-1.96690	-2.35524	2.80155
H	4.08769	-0.82239	-3.13139	H	-0.25256	-0.87512	3.70226
H	3.49783	0.79686	-2.61982	H	-0.57981	0.37448	2.44733
N	2.98304	-2.23757	0.52352	C	1.63322	-2.40789	-0.65933
C	1.69866	-1.40582	-2.01284	N	2.33684	-3.32014	0.03704
H	1.14839	-0.62619	-2.55061	C	3.76052	-3.22868	-0.30097
H	1.02121	-1.79687	-1.24649	C	3.73400	-2.43394	-1.62073
H	1.98176	-2.21021	-2.71201	N	2.38533	-1.86788	-1.61795
C	5.64742	-1.20945	0.83054	H	4.30040	-2.65495	0.46808
H	5.66492	-0.26404	1.39884	H	4.19200	-4.23217	-0.41119
H	6.67453	-1.47213	0.54676	H	3.87120	-3.07002	-2.50951
H	5.22687	-2.00281	1.45702	H	4.47646	-1.62785	-1.59931
C	0.84442	-4.22522	0.76382	N	0.33126	-2.13935	-0.50642
H	1.77808	-4.39142	0.21475	C	2.00090	-0.72610	-2.42263
H	-0.00643	-4.20482	0.06396	H	2.42824	0.20021	-2.00694
H	0.70281	-5.03861	1.48838	H	0.90728	-0.66126	-2.42348
C	2.28840	0.34697	1.71376	H	2.36005	-0.87411	-3.44957
H	1.68817	1.20287	2.04296	C	1.82453	-4.11637	1.12492
H	2.73391	0.62357	0.75034	H	1.99453	-3.64309	2.10485
H	3.08664	0.16128	2.45248	H	2.31556	-5.09826	1.11113
C	0.50798	2.89006	-0.58996	H	0.74638	-4.26109	0.98281
Br	-0.18205	1.01144	-0.64409	C	-2.41805	-2.50726	0.01789
H	-1.20075	3.62928	-1.64969	H	-2.13334	-2.38402	-1.03407
C	-0.11152	3.67131	-1.74540	H	-3.44531	-2.14756	0.15927
H	0.18420	3.21638	-2.69707	H	-2.37450	-3.57911	0.27776
H	0.21838	4.71869	-1.72438	C	1.82522	-0.77666	1.72316
C	1.96381	2.79535	-0.69593	H	1.86536	0.18459	2.25097
N	3.10579	2.68601	-0.84050	H	2.13532	-0.55731	0.69694
C	0.09456	3.36732	0.79796	H	2.55101	-1.47542	2.16369
O	0.80705	3.33853	1.77422	C	3.50587	2.06817	-0.29052
O	-1.17525	3.75460	0.79798	Br	0.22858	1.41351	-0.21478
C	-1.73424	4.00665	2.09666	H	2.78066	2.83695	-2.18070
H	-1.73744	3.07538	2.67635	C	3.73660	2.68931	-1.64856
H	-2.75547	4.35265	1.92022	H	4.37663	2.04414	-2.26633
H	-1.14121	4.76567	2.62029	H	4.21822	3.67616	-1.58111
H	-7.70056	-0.51799	-0.45264	C	4.08803	0.84005	0.03889
C	-6.65617	-0.76432	-0.62441	N	4.56245	-0.20800	0.26946
C	-6.12408	-1.43180	-1.69248	C	2.66730	2.69051	0.65763
C	-4.71028	-1.57918	-1.58823	O	2.25091	2.25286	1.74541
C	-4.20531	-1.02162	-0.44657	O	2.21530	3.91501	0.21559
S	-5.45578	-0.30638	0.51968	C	1.27199	4.53747	1.07346
H	-6.71873	-1.80535	-2.52431	H	0.35722	3.93024	1.14962
H	-4.06428	-2.07080	-2.31316	H	1.04208	5.50974	0.62273
C	-2.80274	-0.94968	0.05791	H	1.68222	4.66884	2.08338
O	-2.61825	-0.37391	1.13420	H	-7.46212	-0.45546	-0.29079
S	-1.56114	-1.67923	-0.92417	C	-6.43364	-0.23309	-0.56178
				C	-5.83738	-0.41118	-1.78094
TS-B				C	-4.47525	-0.00498	-1.77596
61				C	-4.08118	0.47641	-0.55336
C	-0.17676	-1.75238	0.64236	S	-5.36539	0.43280	0.60438
N	-1.52343	-1.71647	0.83453	H	-6.35117	-0.81787	-2.64900
C	-1.81024	-1.42036	2.23358	H	-3.81116	-0.07581	-2.63722
C	-0.52161	-0.70746	2.65312	C	-2.75834	0.93901	-0.09899
N	0.46552	-1.30976	1.74914	O	-2.52839	1.26468	1.04084

S	-1.51903	0.94908	-1.40915

int-C

61

C	0.41704	1.71152	0.58478
N	1.76346	1.62307	0.74795
C	2.07431	1.40680	2.15596
C	0.76234	0.79427	2.65505
N	-0.21763	1.38525	1.73597
H	2.92601	0.72447	2.27116
H	2.29630	2.36771	2.65443
H	0.53275	1.04638	3.69682
H	0.76504	-0.30037	2.52004
C	-1.37436	2.42610	-0.72296
N	-1.95905	3.45537	-0.08280
C	-3.37486	3.55616	-0.44727
C	-3.46645	2.63492	-1.68155
N	-2.19577	1.91286	-1.63895
H	-4.00702	3.16654	0.36343
H	-3.63249	4.59982	-0.67349
H	-3.54807	3.19279	-2.62756
H	-4.29886	1.93017	-1.57589
N	-0.10475	2.03654	-0.57544
C	-1.97390	0.65077	-2.31736
H	-2.48990	-0.17091	-1.79321
H	-0.89590	0.45533	-2.33501
H	-2.34985	0.72707	-3.34591
C	-1.33668	4.26955	0.93127
H	-1.52931	3.88903	1.94686
H	-1.72259	5.29449	0.85357
H	-0.25288	4.28940	0.75962
C	2.67316	2.30214	-0.14894
H	2.36619	2.09639	-1.18161
H	3.68803	1.91578	0.00951
H	2.67444	3.39381	0.01472
C	-1.60611	0.93411	1.77222
H	-1.68836	0.04017	2.40063
H	-1.94251	0.61998	0.77873
H	-2.28501	1.71589	2.14166
C	-4.20671	-1.69965	-0.14363
Br	-0.19877	-1.50437	-0.06063
H	-4.69416	-2.97388	-1.82062
C	-5.20515	-2.36711	-1.05997
H	-5.81848	-1.61743	-1.57689
H	-5.88805	-3.04008	-0.51779
C	-4.34225	-0.35000	0.21157
N	-4.45473	0.78440	0.48134
C	-3.16954	-2.40898	0.47581
O	-2.31335	-1.97312	1.28419
O	-3.12740	-3.72947	0.10941
C	-2.11232	-4.49613	0.74190
H	-1.11158	-4.14558	0.45268
H	-2.25909	-5.53003	0.40960
H	-2.19601	-4.43078	1.83507
H	7.58234	0.04731	-0.36891
C	6.54337	-0.15195	-0.61679
C	5.94323	-0.03685	-1.84123
C	4.56576	-0.38781	-1.79901
C	4.16340	-0.76541	-0.54385
S	5.45953	-0.69264	0.59984
H	6.46468	0.28647	-2.73937
H	3.89574	-0.35337	-2.65770
C	2.82505	-1.13743	-0.04473
O	2.61259	-1.38173	1.12118
S	1.56446	-1.15746	-1.32078

cat-enolate

49

C	-0.94621	-1.59911	0.02670
N	-0.63255	-2.84259	0.47094
C	-0.14585	-3.67952	-0.60639
C	0.25314	-2.62093	-1.63569
N	-0.62645	-1.50339	-1.29869
H	0.70327	-4.29450	-0.27862
H	-0.94260	-4.34725	-0.98135
H	0.10560	-2.94204	-2.67445
H	1.29623	-2.29382	-1.48540
C	-1.82513	0.52986	0.62194
N	-2.81940	0.97855	-0.17753
C	-2.81498	2.44104	-0.21857
C	-1.95567	2.80167	1.00860
N	-1.30299	1.53425	1.31955
H	-2.32567	2.79073	-1.14114
H	-3.83950	2.83172	-0.15773
H	-2.55792	3.13467	1.86908
H	-1.19691	3.55029	0.75216
N	-1.50854	-0.74612	0.83796
C	-0.15474	1.43930	2.19447
H	0.65066	2.07769	1.80300
H	0.19906	0.40430	2.18569
H	-0.42909	1.75736	3.21116
C	-3.51733	0.17652	-1.15094
H	-3.12064	0.33848	-2.16639
H	-4.58633	0.43028	-1.14335
H	-3.40008	-0.88076	-0.88800
C	-1.05883	-3.37224	1.74036
H	-1.29417	-2.52996	2.39866
H	-0.24906	-3.96702	2.18485
H	-1.95243	-4.01077	1.63772
C	-0.34713	-0.26522	-2.00971
H	0.73734	-0.08746	-2.04261
H	-0.78156	0.60347	-1.51161
H	-0.74791	-0.33887	-3.03109
C	2.46420	1.68972	-0.44726
H	4.32659	2.54233	0.28516
C	3.76997	2.42070	-0.65659
H	3.58763	3.41995	-1.07163
H	4.43335	1.88312	-1.35110
C	1.23943	2.29170	-0.76354
N	0.21285	2.79349	-1.02526

C	2.41654	0.38390	0.06989
O	1.41982	-0.33875	0.27643
O	3.67042	-0.11040	0.36574
C	3.67797	-1.41914	0.90143
H	3.05892	-1.48309	1.80729
H	4.72284	-1.65186	1.13729
H	3.28785	-2.15248	0.17807

sulfenyl bromide

12

Br	2.91988	-0.09700	-0.00004
H	-5.01607	-0.25285	-0.00005
C	-3.96935	0.03873	-0.00009
C	-3.46039	1.30981	-0.00013
C	-2.04042	1.31643	-0.00013
C	-1.51517	0.04830	0.00015
S	-2.74785	-1.16327	0.00009
H	-4.07620	2.20614	-0.00017
H	-1.43553	2.22303	-0.00001
C	-0.11086	-0.39031	0.00002
O	0.24537	-1.53759	-0.00014
S	1.05699	1.01212	0.00015

int-D

61

C	-0.96349	3.34153	-0.35752
C	-0.08159	3.39903	-1.45621
N	0.64924	3.43666	-2.36763
C	-2.31192	4.01325	-0.44443
H	-2.22837	5.09679	-0.62138
H	-2.84878	3.87471	0.50226
H	-2.93057	3.59823	-1.25598
C	-0.43302	2.75623	0.79514
O	-1.30658	2.74711	1.88169
C	-0.69942	2.46966	3.13363
H	-0.33688	1.43356	3.19088
H	-1.47200	2.63228	3.89387
H	0.15125	3.14279	3.31304
Br	0.47450	-2.56462	1.78245
O	0.69288	2.23399	0.94177
S	-0.78893	-0.81332	1.52559
C	-2.02149	-1.56503	0.41844
O	-1.93721	-2.70629	0.03001
C	-3.09587	-0.64742	0.03188
C	-3.28979	0.67568	0.34808
C	-4.46141	1.19668	-0.26569
H	-2.62753	1.27087	0.98405
C	-5.11151	0.26562	-1.02937
H	-4.79884	2.22361	-0.14695
H	-6.02451	0.40255	-1.60257
S	-4.32840	-1.25993	-1.02271
C	2.83196	0.47702	-0.24290
N	2.94259	1.37240	-1.23331
N	3.22752	1.00778	0.92730
N	2.52850	-0.81603	-0.32918
C	3.51790	2.43188	0.78902
H	2.75661	3.00116	1.33643
H	4.52029	2.65887	1.18015
C	3.40206	2.66708	-0.73082
H	2.66775	3.43966	-0.99167
H	4.37229	2.91035	-1.19255
C	2.94045	1.11127	-2.65584
H	3.96283	1.20017	-3.05805
H	2.28453	1.84364	-3.14664
H	2.57609	0.09667	-2.85211
C	2.81688	0.47199	2.20686
H	3.64942	0.52414	2.92184
H	2.51735	-0.57261	2.06985
H	1.95802	1.05503	2.57487
C	1.66074	-1.44605	-1.08341
N	0.49048	-1.02523	-1.60758
C	-0.11312	-2.07491	-2.42199
C	0.58274	-3.32654	-1.87736
N	1.83487	-2.76869	-1.37944
H	-1.20112	-2.09856	-2.27737
H	0.10680	-1.90708	-3.49010
H	0.76275	-4.08851	-2.64588
H	0.00616	-3.76337	-1.04312
C	2.77253	-3.60413	-0.66651
H	3.26516	-4.30002	-1.35879
H	2.25735	-4.18768	0.11563
H	3.52160	-2.95884	-0.19672
C	-0.01360	0.33557	-1.61201
H	0.38894	0.88835	-0.75370
H	-1.10795	0.30771	-1.51772
H	0.24218	0.87225	-2.53629

TS-D

61

C	-1.85429	2.28389	-0.76821
C	-0.70220	2.38175	-1.56885
N	0.22251	2.44805	-2.28278
C	-3.19586	2.23605	-1.46449
H	-3.31782	3.07498	-2.16749
H	-3.99758	2.31034	-0.72061
H	-3.34623	1.30488	-2.03307
C	-1.66793	2.63061	0.58922
O	-2.83134	2.58643	1.33705
C	-2.64686	2.86722	2.71796
H	-2.00375	2.10885	3.18813
H	-3.64442	2.85090	3.17122
H	-2.17794	3.84974	2.85793
Br	0.63388	-1.49665	2.17371
O	-0.60111	2.91308	1.15308
S	-0.68134	-0.21176	0.94696
C	-1.53450	-1.60692	0.12432
O	-0.99128	-2.66896	-0.07537
C	-2.91124	-1.31742	-0.27542
C	-3.76084	-0.33696	0.17156
C	-5.05927	-0.46245	-0.39304

H	-3.46032	0.45932	0.85564
C	-5.15899	-1.52952	-1.24324
H	-5.88013	0.21967	-0.18254
H	-6.03151	-1.84356	-1.80988
S	-3.69413	-2.41396	-1.36887
C	2.74994	1.17010	-0.31713
N	3.06232	1.77698	-1.47568
N	2.37269	2.07078	0.59140
N	2.94755	-0.10874	0.00749
C	2.30666	3.41653	0.02694
H	1.25582	3.73483	0.00273
H	2.89125	4.10913	0.64986
C	2.91682	3.22829	-1.37766
H	2.23930	3.58297	-2.16310
H	3.90526	3.70447	-1.48208
C	3.40073	1.14595	-2.72412
H	4.33920	1.56661	-3.11491
H	2.59368	1.31451	-3.45400
H	3.54014	0.06949	-2.56694
C	2.11715	1.81385	1.99230
H	2.86635	2.33840	2.60619
H	2.18956	0.73688	2.16714
H	1.10892	2.16826	2.24125
C	2.54490	-1.25156	-0.47053
N	1.57994	-1.55876	-1.36899
C	1.55089	-2.99469	-1.62430
C	2.24679	-3.53926	-0.37811
N	3.10466	-2.41815	-0.01406
H	0.51644	-3.34358	-1.71656
H	2.10906	-3.22872	-2.54776
H	2.83318	-4.44680	-0.56848
H	1.50899	-3.72656	0.42253
C	3.87051	-2.46784	1.20970
H	4.68372	-3.19986	1.11535
H	3.23151	-2.75208	2.06336
H	4.29039	-1.47470	1.39738
C	0.81302	-0.65746	-2.19561
H	0.89706	0.37627	-1.84833
H	-0.25032	-0.93759	-2.15342
H	1.14137	-0.70935	-3.24637

int-E

61

C	0.88227	2.10730	0.98628
C	-0.42049	2.59286	1.45357
N	-1.45326	2.92026	1.85915
C	1.87566	2.02872	2.15166
H	2.02194	3.02873	2.57998
H	2.84050	1.65833	1.78756
H	1.49750	1.35287	2.92633
C	1.35333	2.97160	-0.17424
O	2.67138	2.87573	-0.33994
C	3.17267	3.44777	-1.55455
H	2.67657	2.97937	-2.41454
H	4.24577	3.23861	-1.56284
H	2.97980	4.52722	-1.57304
Br	0.39634	-2.16931	-1.25353
O	0.61738	3.58655	-0.91411
S	0.51984	0.47509	0.06594
C	1.75710	-0.57551	0.94689
O	1.52117	-1.00278	2.05317
C	3.06288	-0.71326	0.29313
C	3.44009	-0.36437	-0.97721
C	4.80922	-0.64499	-1.22671
H	2.72451	0.02268	-1.70113
C	5.43234	-1.19909	-0.14005
H	5.30974	-0.45842	-2.17446
H	6.47159	-1.50596	-0.05892
S	4.37193	-1.40097	1.19352
C	-3.00285	0.67016	-0.51152
N	-3.81523	1.44528	0.24022
N	-2.30330	1.43691	-1.36351
N	-3.00815	-0.64602	-0.56084
C	-2.67194	2.84604	-1.25887
H	-1.79126	3.44421	-0.98691
H	-3.06019	3.20322	-2.22486
C	-3.75915	2.84623	-0.15857
H	-3.47866	3.47391	0.69638
H	-4.74227	3.16729	-0.53803
C	-4.66162	0.97851	1.30713
H	-5.70216	1.29182	1.13500
H	-4.32115	1.38080	2.27448
H	-4.62208	-0.11723	1.33506
C	-1.47671	0.93351	-2.44326
H	-2.03490	0.94952	-3.39322
H	-1.14631	-0.09031	-2.21603
H	-0.59037	1.57642	-2.53308
C	-2.54065	-1.63254	0.16097
N	-1.91506	-1.60531	1.35395
C	-1.34972	-2.90816	1.68562
C	-1.87726	-3.81771	0.55750
N	-2.68578	-2.91492	-0.25614
H	-0.25160	-2.84254	1.67230
H	-1.69002	-3.22389	2.68373
H	-2.48599	-4.65510	0.92934
H	-1.04165	-4.19430	-0.05010
C	-2.91679	-3.24024	-1.64872
H	-3.44017	-4.20360	-1.71351
H	-1.95235	-3.28742	-2.18004
H	-3.54260	-2.45958	-2.09268
C	-1.77913	-0.49751	2.26671
H	-2.05086	0.44165	1.77674
H	-0.73096	-0.42197	2.58940
H	-2.42232	-0.64193	3.15195

cat-pdt

61

C	-0.75154	2.83652	-0.52149
C	0.13328	2.41553	-1.61965
N	0.86935	2.08524	-2.44725

C	-1.67901	3.99069	-0.93540
H	-1.08330	4.84606	-1.27949
H	-2.27707	4.28371	-0.06486
H	-2.33370	3.65350	-1.74571
C	0.16483	3.25397	0.65676
O	-0.53993	3.31677	1.77234
C	0.17481	3.28457	3.03016
H	0.22625	2.22681	3.33003
H	-0.42785	3.85954	3.73854
H	1.16598	3.73253	2.90215
Br	-0.52939	-0.42494	2.91657
O	1.34843	3.46792	0.54304
S	-1.68799	1.40204	0.16476
C	-2.48268	0.79158	-1.31109
O	-2.34688	1.27258	-2.41711
C	-3.30283	-0.39813	-1.02077
C	-3.53349	-1.01317	0.18736
C	-4.35902	-2.16219	0.04592
H	-3.08504	-0.69654	1.13636
C	-4.72519	-2.38557	-1.25447
H	-4.66522	-2.79485	0.87608
H	-5.35219	-3.18665	-1.63665
S	-4.08465	-1.21286	-2.33168
C	3.29963	-0.80734	-0.72650
N	4.32053	-0.55975	-1.59339
N	2.78132	0.35038	-0.28063
N	2.96435	-2.02621	-0.35343
C	3.57720	1.48077	-0.76004
H	2.93850	2.33002	-1.02147
H	4.28935	1.78643	0.02500
C	4.28712	0.85449	-1.96381
H	3.68615	0.99193	-2.88096
H	5.29714	1.25017	-2.12706
C	4.76214	-1.56190	-2.53795
H	5.82383	-1.41084	-2.77108
H	4.18293	-1.51312	-3.47688
H	4.62751	-2.54857	-2.08268
C	1.92273	0.43615	0.88811
H	2.07944	-0.41695	1.55911
H	0.85513	0.44216	0.62616
H	2.15938	1.35368	1.43885
C	1.71736	-2.33821	0.01465
N	0.61127	-2.09927	-0.70943
C	-0.58551	-2.44730	0.05718
C	-0.01831	-3.33188	1.17883
N	1.41739	-3.04911	1.11053
H	-1.01411	-1.53605	0.49951
H	-1.32191	-2.95382	-0.58306
H	-0.19991	-4.40603	1.02078
H	-0.41134	-3.00227	2.15093
C	2.24595	-3.09241	2.29834
H	2.28939	-4.11510	2.69601
H	1.81012	-2.41383	3.05136
H	3.25760	-2.76914	2.02828
C	0.54459	-1.32512	-1.92734
H	0.41551	-0.25053	-1.72973
H	-0.30415	-1.68127	-2.52686
H	1.46770	-1.46824	-2.50574

cat-Br

36

C	1.74261	0.01278	0.36401
N	2.70870	-0.81875	-0.12275
C	3.98713	-0.11548	-0.14408
C	3.53987	1.35746	-0.15491
N	2.19814	1.27410	0.40288
H	4.57038	-0.35367	0.76230
H	4.57950	-0.38976	-1.02605
H	3.49695	1.76662	-1.17835
H	4.18786	2.00246	0.45235
C	-0.42143	-1.00094	0.32080
N	-0.58415	-1.36174	-0.98447
C	-1.99651	-1.72148	-1.19245
C	-2.57967	-1.78736	0.23356
N	-1.43992	-1.44368	1.08081
H	-2.48268	-0.90879	-1.75180
H	-2.07060	-2.67223	-1.73781
H	-2.97255	-2.77946	0.49684
H	-3.35459	-1.01561	0.35674
N	0.57714	-0.33523	0.85072
C	-1.69497	-0.82997	2.37354
H	-2.10708	0.17864	2.20037
H	-0.75622	-0.75896	2.93206
H	-2.40305	-1.45512	2.93121
C	0.03320	-0.57256	-2.04665
H	-0.31804	0.47103	-1.96159
H	-0.28811	-0.99390	-3.00650
H	1.12667	-0.63959	-2.00304
C	2.63068	-2.25591	0.04168
H	1.62698	-2.59882	-0.23799
H	2.84603	-2.56378	1.07787
H	3.35674	-2.72751	-0.63155
C	1.33299	2.43374	0.56585
H	1.50068	3.12358	-0.27370
H	1.55741	2.95280	1.50744
H	0.27866	2.11423	0.54134
Br	-2.17251	1.51209	-0.29168

product

25

C	-1.75229	0.58076	0.18049
H	-2.75442	1.73057	1.72136
C	-1.89019	1.05823	1.63975
H	-2.04222	0.18374	2.28207
H	-0.98579	1.59634	1.93589
C	-1.57060	1.71047	-0.74304
N	-1.43819	2.60528	-1.45958
C	-3.04565	-0.15764	-0.22079
O	-3.85582	0.24932	-1.00944
S	-0.38655	-0.64961	-0.01853

C	1.02941	0.44098	0.22641	H	4.43905	-2.64373	-0.92382
O	0.91849	1.59244	0.57682	H	5.82172	-0.55430	-0.11609
C	2.32608	-0.21132	-0.01082	O	-3.16534	-1.29434	0.47156
C	2.60504	-1.46745	-0.48874	C	-4.36095	-2.04005	0.19305
C	4.00123	-1.71337	-0.56959	H	-4.39677	-2.30272	-0.87100
C	4.73893	-0.63703	-0.15416	H	-4.30834	-2.93562	0.81720
S	3.76364	0.68395	0.33625	H	-5.24255	-1.43724	0.44234
H	1.83850	-2.18425	-0.78127				

3.7 References

1. N. Kornblum, Substitution Reactions Which Proceed via Radical Anion Intermediates. *Angew. Chem. Int. Ed.* **14**, 734 (1975).
2. R. A. Rossi, A. B. Pierini, A. B. Penenory, Nucleophilic substitution reactions by electron transfer. *Chem. Rev.* **103**, 71 (2003).
3. N. S. Zefirov, D. I. Makhon'kov, X-philic reactions. *Chem. Rev.* **82**, 615 (1982).
4. P. K. Sazonov, G. A. Artamkina, I. P. Beletskaya, Nucleophilic substitution at the halogen atom (halogenophilic reactions). *Russian Chem. Rev.* **81**, 317 (2012).
5. S. Montanari, C. Paradisi, G. Scorrano, Thiol Anions in Nucleophilic Aromatic-Substitution Reactions with Activated Aryl Halides - Attack on Carbon Vs Attack on Halogen. *J. Org. Chem.* **58**, 5628 (1993).
6. J. F. Bunnett, Base-catalyzed halogen dance, and other reactions of aryl halides. *Acc. Chem. Res.* **5**, 139 (1972).
7. D. R. Edwards, Y. B. Hleba, C. J. Lata, L. A. Calhoun, C. M. Crudden, Regioselectivity of the Rhodium-Catalyzed Hydroboration of Vinyl Arenes: Electronic Twists and Mechanistic Shifts. *Angew. Chem.* **119**, 7945 (2007).
8. K. W. Fiori, J. Du Bois, Catalytic intermolecular amination of C-H bonds: method development and mechanistic insights. *J. Am. Chem. Soc.* **129**, 562 (2007).
9. C. Hansch, A. Leo, R. W. Taft, A survey of Hammett substituent constants and resonance and field parameters. *Chem. Rev.* **91**, 165 (1991).
10. M. C. Verploegh, L. Donk, H. J. T. Bos, W. Drenth, Nucleophilic displacements at halogen in 1-chloro-, 1-bromo- and 1-iodo-1-alkynes: I. Thiolates as nucleophiles. *Recl. Trav. Chim. Pays-Bas* **90**, 765 (1971).

11. S. Kato, K. Miyagawa, S. Kawabata, M. Ishida, A Convenient Preparation of Acylsulfenyl Bromides: a New Class of Electrophilic Thiocarboxylating Agents. *Synthesis*, 1013 (1982).
12. T. Murai, S. Oida, S. Min, S. Kato, Thiophilic Halogenation of Thiocarboxylic Acid O-Silyl Esters - a Facile Preparation of Acylsulfenyl Halides. *Tetrahedron Lett.* **27**, 4593 (1986).
13. G. Cavallo *et al.*, The Halogen Bond. *Chem. Rev.* **116**, 2478 (2016).
14. T. Clark, M. Hennemann, J. S. Murray, P. Politzer, Halogen bonding: the sigma-hole. Proceedings of "Modeling interactions in biomolecules II", Prague, September 5th-9th, 2005. *J. Mol. Model.* **13**, 291 (2007).
15. J. Contreras-Garcia *et al.*, NCIPLOT: A Program for Plotting Noncovalent Interaction Regions. *J Chem. Theory Comput.* **7**, 625 (2011).
16. E. R. Johnson *et al.*, Revealing noncovalent interactions. *J. Am. Chem. Soc.* **132**, 6498 (2010).
17. L. Zong, X. Ban, C. W. Kee, C. H. Tan, Catalytic Enantioselective Alkylation of Sulfenate Anions to Chiral Heterocyclic Sulfoxides Using Halogenated Pentanidium Salts. *Angew. Chem. Int. Ed.*, (2014).
18. R. Peverati, D. G. Truhlar, Improving the Accuracy of Hybrid Meta-GGA Density Functionals by Range Separation. *The Journal of Physical Chemistry Letters* **2**, 2810 (2011).
19. R. Ditchfield, W. J. Hehre, J. A. Pople, Self-Consistent Molecular-Orbital Methods. IX. An Extended Gaussian-Type Basis for Molecular-Orbital Studies of Organic Molecules. *The Journal of Chemical Physics* **54**, 724 (1971).

20. A. V. Marenich, C. J. Cramer, D. G. Truhlar, Universal solvation model based on solute electron density and on a continuum model of the solvent defined by the bulk dielectric constant and atomic surface tensions. *J. Phys. Chem. B* **113**, 6378 (2009).
21. F. Weigend, R. Ahlrichs, Balanced basis sets of split valence, triple zeta valence and quadruple zeta valence quality for H to Rn: Design and assessment of accuracy. *Phys. Chem. Chem. Phys.* **7**, 3297 (2005).
22. F. Weigend, Accurate Coulomb-fitting basis sets for H to Rn. *Phys. Chem. Chem. Phys.* **8**, 1057 (2006).

Chapter 4

Experimental Procedures

4.1 General remarks

THF were distilled over sodium/benzophenone under N_2 atmosphere. Toluene, Acetonitrile and Dichloromethane were distilled over CaH_2 under N_2 atmosphere. Commercially available materials and other solvents purchased from commercial suppliers were used as received. ^{1}H and ^{13}C NMR spectra were recorded on Bruker AV-300 (300 MHz), Bruker Avance III 400 (400MHz) (100 MHz) spectrometer. Chemical shifts are recorded as δ in units of parts per million (ppm). ^{19}F and ^{31}P NMR was performed on a Bruker Avance III 400 (400MHz) spectrometer. High resolution mass spectra (HRMS) were obtained on the Q-Tof Premier mass spectrometer (Waters Corporation). HRMS were reported in units of mass of charge ratio (*m/z*). Enantiomeric excess values were determined by HPLC analysis on Shimadzu LC-20AT and LC-2010CHT HPLC workstations. Optical rotations were measured in CH_2Cl_2 using a 1 mL cell with a 1 cm path length on a Jasco P-1030 polarimeter with a sodium lamp of wavelength 589 nm and reported as follows: $[\alpha]^{T}_{D}$ (*c* g/100 mL, solvent). X-ray crystallography analysis was performed on Bruker X8 APEX X-ray diffractionmeter. Flash chromatography separations were performed on Merck 60 (0.040 - 0.063mm) mesh silica gel. Analytical thin-layer chromatography (TLC) was performed on Merck 60 F254 silica gel plates. Visualization was performed using a UV lamp or potassium permanganate stain. Procedures involving air- or moisture-sensitive materials were conducted with degassed solvents under an inert atmosphere of N_2 or argon using standard Schlenk techniques.

4.2 Experiment procedures for substrates synthesis

4.2.1 Synthesis of tertiary bromides

Method A

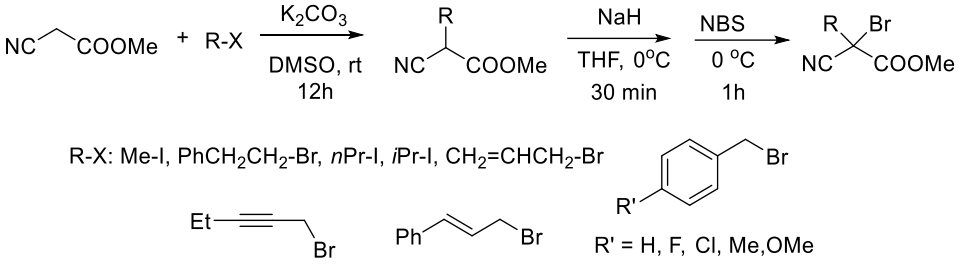

Figure 4.1 Synthesis of tertiary bromide (Method A)

Potassium carbonate (15 mmol) was added to a solution of cyanoester (15 mmol) in DMSO (10 mL). After stirring for 30 min, R-X (10 mmol) was added. The mixture was stirred at rt for 12 h. Then the mixture was added water (20 mL) and then extracted with DCM. The combined organic phase was washed with brine, dried over anhydrous Na_2SO_4, filtered and concentrated. The residue was purified by flash chromatography (hexane: ethyl acetate = 5:1 as the eluent) to get the alkylated cyanoester.

The alkylated cyanoester was dissolved in anhydrous THF (15 mL) under N_2 atmosphere at 0 ℃, and then NaH (1.0 equiv.) was added slowly. After stirring for 30 min, NBS (1.1 equiv) was added. The mixture was stirred for 1 h. Then the mixture was added water (10 mL) and then extracted with DCM. The combined organic phase was washed with brine, dried over anhydrous Na_2SO_4, filtered, and concentrated. The residue was purified by flash chromatography (hexane: ethyl acetate = 10:1 as the eluent) to get the brominated cyanoester.

Method B

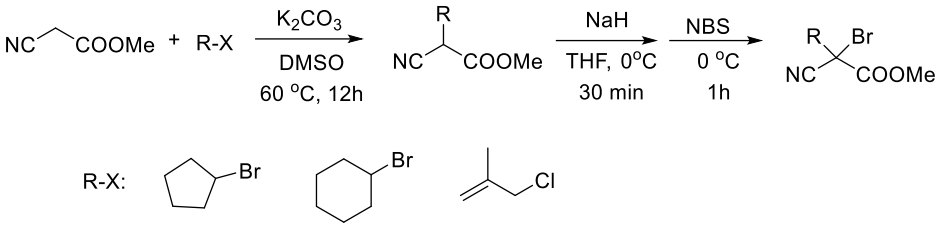

Figure 4.2 Synthesis of tertiary bromide (Method B)

Potassium carbonate (15 mmol) was added to a solution of cyanoester (10 mmol) in DMSO (10 mL). After stirring for 30 min, R-X (10 mmol) was added at 60 ℃. The mixture was stirred at 60 ℃ for 12 h. Then the mixture was cooled and added water (20 mL) and then extracted with DCM. The combined organic phase was washed with brine, dried over anhydrous Na_2SO_4, filtered and concentrated. The residue was purified by flash chromatography (hexane: ethyl acetate = 5:1 as the eluent) to get the alkylated cyanoester.

The alkylated cynaoester was converted to the corresponding brominated cyanoester as described in method A.

Method C

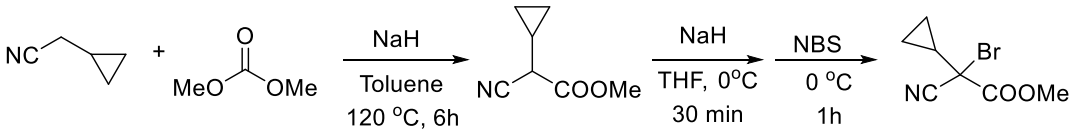

Figure 4.3 Synthesis of tertiary bromide (Method C)

The cyclopropylacetonitrile (10 mmol) and dimethyl carbonate (20 mmol) were dissolved in anhydrous toluene under N_2 atomasphere, and then NaH (20 mmol) was added slowly. The mixture was brought to reflux for 6 h and cooled to rt. The reaction was quenched with acetic acid (1 mL) and then water (10 mL) was added. Separate the

organic phase and extract aqueous phase with DCM. The combined organic phase was washed with brine, dried over anhydrous Na_2SO_4, filtered, and concentrated. The residue was purified by flash chromatography (hexane: ethyl acetate = 5:1 as the eluent) to get the alkylated cyanoester.

The alkylated cyanoester was converted to the corresponding brominated cyanoester as described in method A.

Method D

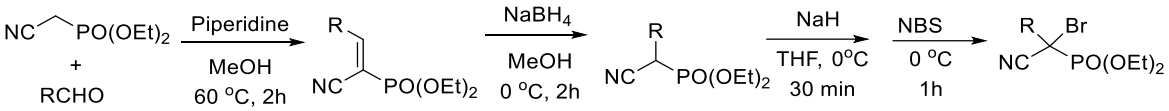

Figure 4.4 Synthesis of tertiary bromide (Method D)

Diethyl cyanomethylphosphonate (10 mmol) and aldehyde (12 mmol) were dissolved in MeOH (15 mL) under N_2 atmosphere, and then piperidine (1 mmol) was added. After stirring for 2h at 60 ℃ (monitored by TLC), all diethyl cyanomethylphosphonate were consumed. The mixture was cooled down and the solvents are removed under reduced pressure. Then the residue was dissolved in MeOH (15 mL). $NaBH_4$ (10 mmol) was then added slowly at 0 ℃. After stirring for 30 min at 0 ℃, the mixture was quenched with saturated NH_4Cl solution and then extracted with DCM. The combined organic phase was washed with brine, dried over anhydrous Na_2SO_4, filtered, and concentrated. The residue was purified by flash chromatography (hexane: ethyl acetate = 2:1 as the eluent) to get the alkylated diethyl cyanomethylphosphonate.

The alkylated diethyl cyanomethylphosphonate was dissolved in anhydrous THF (15 mL) under N_2 atmosphere at 0 ℃, and then NaH (1.0 equiv.) was added slowly. After stirring for 30 min, NBS (1.1 equiv) was added. The mixture was stirred for 1 h. Then

the mixture was added water (10 mL) and then extracted with DCM. The combined organic phase was washed with brine, dried over anhydrous Na_2SO_4, filtered, and concentrated. The residue was purified by flash chromatography (hexane: ethyl acetate = 4:1 as the eluent) to get the brominated diethyl cyanomethylphosphonate.

4.2.2 Synthesis of thiocarboxylate salts

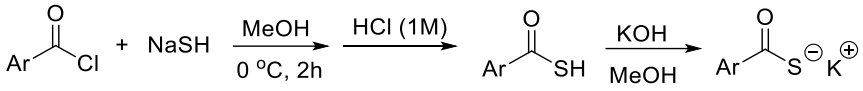

Figure 4.5 Synthesis of thiocarboxylate salts

NaSH (60 mmol) was suspended in MeOH (60 mL) and cooled to 0 ℃. Acyl chloride (20 mmol) was added slowly. After stirring at this temperature for 2 h, the mixture was quenched with HCl (1M) and extracted with DCM. The combined organic phase was washed with brine, dried over anhydrous Na_2SO_4, filtered and concentrated to get the thiocarboxylic acid. Then the thiocarboxylic acid was dissolved in MeOH (20 mL). A solution of KOH (16 mmol) in MeOH (10 mL) was added to the thiocarboxylic acid solution. After shaking, the solvent was removed using rotary evaporator. The resulting solid was washed with DCM (20 mL) and collected by filtration. The solid was then recrystallized from MeOH/toluene for further purification.

4.3 Enantioconvergent nucleophilic substitution of tertiary bromide by thiocarboxylate

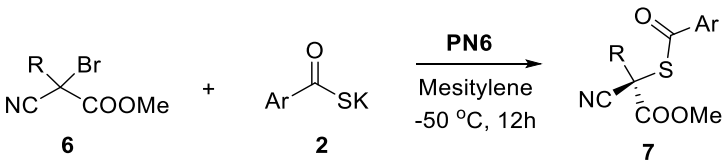

Figure 4.6 Nucleophilic substitution of tertiary bromide by thiocarboxylate

The amount of thiocarboxylate salts **2** is adjusted according to different substrates.

For synthesis of **7b, 7g-7l, 7n, 7q:** A solution of substrate **1** (0.1 mmol) and **PN6** (5 mol%) in mesitylene (1 mL) was cooled to -50 ^{o}C, and then thiocarboxylate salts **2** (0.13 mmol) was added in one portion. The mixture was stirred at this temperature for 12 h and then purified by flash chromatography (hexane: ethyl acetate = 5:1 as the eluent).

For synthesis of **7m, 7o, 7e, 7f, 7r:** The amount of thiocarboxylate salts **2b** is 0.12 mmol.

For synthesis of **7a, 7c, 7d, 7p:** The amount of thiocarboxylate salts **2b** is 0.10 mmol.

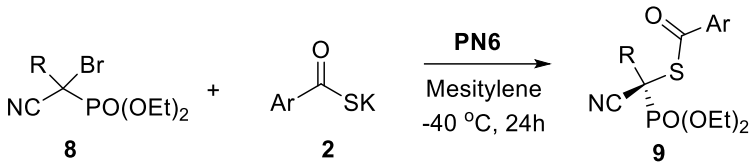

Figure 4.7 Nucleophilic substitution of tertiary bromide by thiocarboxylate

For synthesis of **9k-9m, 9r** and **9s:** A solution of substrate **4** (0.1 mmol) and **PN6** (5 mol%) in mesitylene (1 mL) was cooled to -40 ^{o}C, and then thiocarboxylate salts **2** (0.12 mmol) was added in one portion. The mixture was stirred at this temperature for 24 h and then purified by flash chromatography (hexane: ethyl acetate = 2:1 as the eluent).

For synthesis of **9c:** Reaction was conducted at -30 ^{o}C for 72h using **PN7** (5 mol%) as catalyst.

For synthesis of **9c:** Reaction was conducted at -30 ^{o}C for 48h using **PN6** (5 mol%) as catalyst.

For synthesis of **9n-9q:** Reaction was conducted at -50 ^{o}C for 48h using **PN7** (5 mol%) as catalyst.

4.4 Experiment procedures for mechanism studies

4.4.1 Experiments to prove radical-based $S_{RN}1$ mechansim

(A) Addition of radical inhibitor in reactions

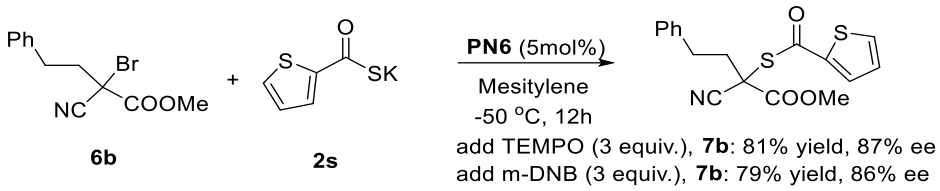

Figure 4.8 Radical inhibitor experiments

A solution of substrate **6b** (0.1 mmol) and **PN6** (5 mol%) in mesitylene (1 mL) was cooled to -50 °C, and then 0.3 mmol radical inhibitor (TEMPO or m-DBN) and thiocarboxylate salt **2s** (0.13 mmol) was added in one portion. The mixture was stirred at this temperature for 12 h and then purified by flash chromatography (hexane: ethyl acetate = 5:1 as the eluent). When TEMPO was added, **7b** was isolated with 81% yield and 87% ee. When m-DNB was added, **7b** was isolated with 79% yield and 86% ee.

(B) Addition of H-donors in reactions

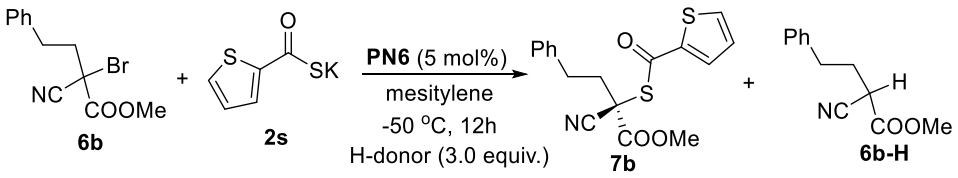

H-donor	1,4-dicyclohexene	fluorene	xanthene	Et_3SiH	MeOH	H_2O^*	PhOH
7b, yield(%)	89%	88%	86%	86%	13%	66%	22%
6a-H, yield(%)	0%	0%	0%	0%	55%	22%	54%

* Reaction was conducted at 0 °C

Figure 4.9 Effects of H-atom donor and proton donor

A solution of substrate **6b** (0.1 mmol) and **PN6** (5 mol%) in mesitylene (1 mL) was cooled to -50 °C, and then 0.3 mmol H-donor and thiocarboxylate salt **2s** (0.13 mmol) was added in one portion. The mixture was stirred at this temperature for 12 h and then purified by flash chromatography (hexane: ethyl acetate = 5:1 as the eluent).

4.4.2 Experiments to prove S_N2X mechanism

(A) Hammett analysis through competition experiments with *p*-substituted benzyl substrates

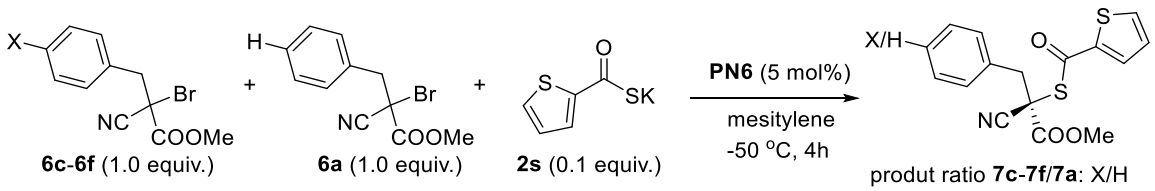

Figure 4.10 Hammett analysis through competition experiments

The typical experiment procedure: A solution of substrate **6c** (0.2 mmol), **6a** (0.2 mmol) and **PN6** (5 mol%) in mesitylene (2 mL) was cooled to -50 °C, and then thiocarboxylate salt **2s** (0.02 mmol) was added in one portion. The mixture was stirred at this temperature for 4 h and then purified by flash chromatography to afford a mixture of product **7c** and **7a** (X=H). The ratio **7c**/**7a** was determined by NMR. Similar procedure is used to determine ratios **7d**/**7a**, **7e**/**7a**, **7d**/**7a**. A plot of log(k_{Ar}/k_{Ph}) obtained versus the corresponding σ or σ⁻values resulted in two Hammett plots.

(B) Carbanion exchange experiments

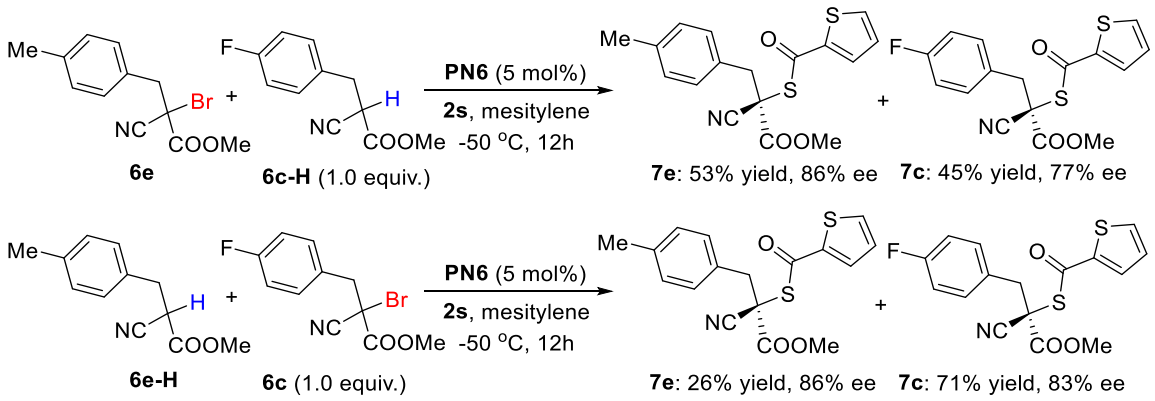

Figure 4.11 Carbanion exchange experiments

A solution of substrate **6e** (0.1 mmol), **6c-H** (0.1 mmol) and **PN6** (5 mol%) in mesitylene (1 mL) was cooled to -50 °C, and then and thiocarboxylate salt **2s** (0.12 mmol) was added in one portion. The mixture was stirred at this temperature for 12 h and then

purified by flash chromatography. A mixture of products **7e** (53% yield, 86% ee) and **7c** (45% yield, 77% ee) were isolated. Procedure was the same when **6c** and **6e-H** was used. The mixture of products **7e** (26% yield, 86% ee) and **7c** (71% yield, 83% ee) was isolated. The carbanion exchange experiments indicated the anionic intermediates.

(C) Synthesis of reaction intermediates and their use in reactions

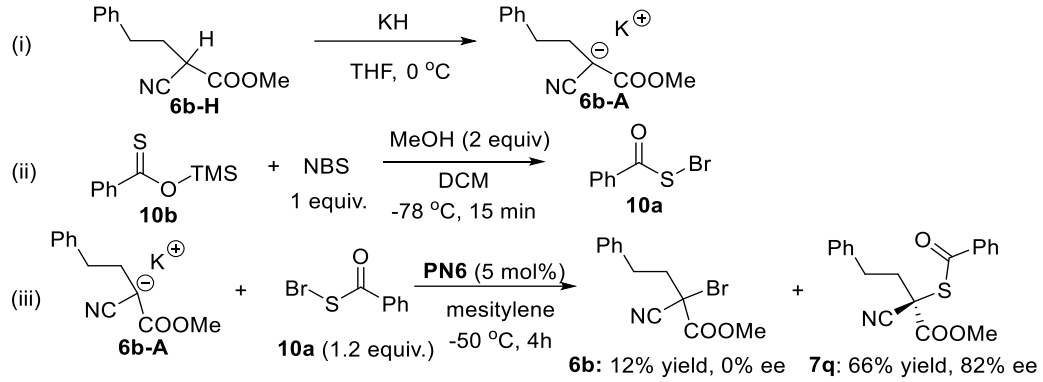

Figure 4.12 Synthesis of reaction intermediates and their use in reactions

(i) KH (30 wt % dispersion in mineral oil) was washed with THF to remove oil before use. KH (1 mmol) was suspended in THF (5mL) and cooled to 0 °C under an N_2 atmosphere, and then **6b-H** (1.1 mmol) was added slowly. After stirring for 1 h at room temperature, the solvent was dried in vacuum. The resulting white solid **6b-A** was washed with toluene, filtered and dried in vacuum (95% yield).

(ii) Benzoylsulfenyl bromide **10a** was synthesized according to reported method (28) and protected from light using aluminum foil. Trimethylsilyl ester **10b** (1 mmol) was dissolved in DCM (3 mL) and cooled to -78 °C under an N_2 atmosphere. Then MeOH (2 mmol) and NBS (1 mmol) was added. After stirring at this temperature for 15 min, the solvent was dried in vacuum. Then hexane (10 ml) was added to dissolve the product. After removal of the insoluble white solid by filtration, the filtrate was dried in vacuum. The resulting benzoylsulfenyl bromide **10a** was dissolved in hexane and cooled at -78

°C for half hour. The product **10a** precipitated out as a white solid, which was collected by filtration and dried in vacuum (65% yield).

(iii) A suspension of salt **6b-A** (0.1 mmol), **PN6** (5 mol%) and mesitylene (1.0 mL) were cooled to -50 °C. Then benzoylsulfenyl bromide **10a** (1.2 equiv) was added to the previous suspension. The mixture was stirred at this temperature for 4h and then purified by flash chromatography (hexane: ethyl acetate = 5:1 as the eluent). A mixture of the tertiary bromide **6b** (12% yield, 0% ee) and the thioester **7b** (66% yield, 82% ee) were isolated.

(D) Reactions with enantioenriched tertiary bromides

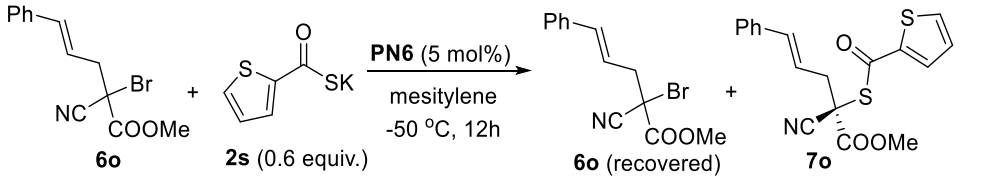

The enantiomers of **6o** were separated by preparative HPLC on a Phenomenex Lux® 5μm i-Amylose-1 column, size: 250×10 mm (Hex/IPA = 99/1, 2.5 mL/min, 22°C).

HPLC analysis: Chiralcel IE (Hex/IPA = 95/5, 1.0 mL/min, 254 nm, 22°C), 6.6 min (major), 7.3 min, 90% *ee*; $[\alpha]^{22}_{D}$= +20.88 (*c* 0.8, CH_2Cl_2); HPLC analysis: Chiralcel IE (Hex/IPA = 95/5, 1.0 mL/min, 254 nm, 22°C), 6.7 min, 7.4 (major) min, -77% *ee*; $[\alpha]^{22}_{D}$= -17.42 (*c* 1.6, CH_2Cl_2).

A solution of substrate **6o** (0.05 mmol), and **PN6** (5 mol%) in mesitylene (1 mL) was cooled to -50 °C, and then thiocarboxylate salt **2s** (0.03 mmol) was added in one portion. The mixture was stirred at this temperature for 12 h and then purified by flash chromatography to collect unreacted **6o** and product **7o**. Both enantiomers were transformed to the same enantiomer of product (+)-**7o** (87% ee) and the recovered **6o** were racemized.

4.5 Analytical data

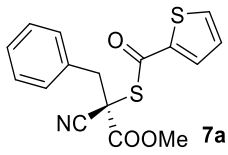

7a

methyl (R)-2-cyano-3-phenyl-2-((thiophene-2-carbonyl)thio)propanoate (7a): White solid, 87% yield; ^{1}H NMR (400 MHz, Chloroform-*d*) δ 7.77 (d, *J* = 3.6 Hz, 1H), 7.72 (d, *J* = 4.9 Hz, 1H), 7.41 – 7.30 (m, 5H), 7.14 (dd, *J* = 4.9, 3.6 Hz, 1H), 3.78 (s, 3H), 3.51 – 3.35 (m, 2H). ^{13}C NMR (101 MHz, Chloroform-*d*) δ 179.8, 166.6, 139.5, 135.0, 132.9, 132.2, 130.2, 128.9, 128.8, 128.4, 116.7, 54.5, 51.9, 41.7; HRMS (ESI) calcd for $C_{12}H_{13}NO_3S_2Na$ *m/z* $[M+Na]^+$: 354.0235; found: 354.0227; $[\alpha]^{22}_D$= +80.07 (*c* 2.8, CH_2Cl_2); HPLC analysis: Chiralcel IA-3 (Hex/IPA = 80/20, 1.0 mL/min, 254 nm, 22°C), 10.2 min, 12.3 min (major), 90% *ee.*

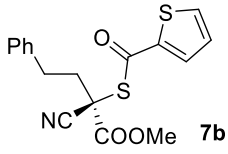

7b

methyl (R)-2-cyano-4-phenyl-2-((thiophene-2-carbonyl)thio)butanoate (7b): white solid, 93% yield; ^{1}H NMR (400 MHz, Chloroform-*d*) δ 7.80 (dd, *J* = 3.9, 1.1 Hz, 1H), 7.76 (dd, *J* = 4.9, 1.1 Hz, 1H), 7.35 (m, 2H), 7.30 – 7.20 (m, 3H), 7.17 (dd, *J* = 4.9, 4.0 Hz, 1H), 3.92 (s, 3H), 3.03 (td, *J* = 12.6, 11.6, 5.3 Hz, 1H), 2.90 (td, *J* = 13.6, 12.6, 5.5 Hz, 1H), 2.63 – 2.30 (m, 2H); ^{13}C NMR (101 MHz, Chloroform-*d*) δ 179.8, 166.7, 139.2, 138.5, 135.1, 132.8, 128.8, 128.4, 126.9, 116.7, 54.6, 50.3, 37.5, 31.8; HRMS (ESI) calcd for $C_{17}H_{15}NO_3S_2Na$ *m/z* $[M+Na]^+$: 368.0391; found: 368.0392; $[\alpha]^{22}_D$= +106.3 (*c* 2.5, CH_2Cl_2): HPLC analysis: Chiralcel IA-3 (Hex/IPA = 80/20, 1.0 mL/min, 254 nm, 22°C), 8.3 min, 9.1 min (major), 91% *ee*.

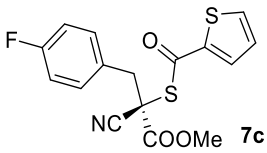

7c

methyl (R)-2-cyano-3-(4-fluorophenyl)-2-((thiophene-2-carbonyl)thio)propanoate (3c): White solid, 89% yield; ^{1}H NMR (400 MHz, Chloroform-*d*) δ 7.77 (dd, *J* = 3.9, 1.1 Hz, 1H), 7.73 (dd, *J* = 4.9, 1.1 Hz, 1H), 7.36 – 7.28 (m, 2H), 7.15 (dd, *J* = 4.9, 3.9 Hz, 1H), 7.11 – 7.00 (m, 2H), 3.79 (s, 3H), 3.48 – 3.34 (m, 2H); ^{13}C NMR (101 MHz, Chloroform-*d*) δ 179.7, 166.5, 163.1 (d, J_{CF}= 248.1 Hz), 139.4, 135.1, 133.0, 131.9 (d, J_{CF} = 8.3 Hz), 128.5, 128.0 (d, J_{CF}= 3.4 Hz), 116.6, 116.0 (d, J_{CF} = 21.6 Hz), 54.6, 51.8, 40.9; HRMS (ESI) calcd for $C_{16}H_{12}NO_3S_2FNa$ *m/z* $[M+Na]^+$: 372.0140; found: 372.0146; $[\alpha]^{22}_D$= +74.60 (*c* 2.9, CH_2Cl_2); HPLC analysis: Chiralcel IA-3 (Hex/IPA = 80/20, 1.0 mL/min, 254 nm, 22°C), 9.9 min, 11.0 min (major), 88% *ee.*

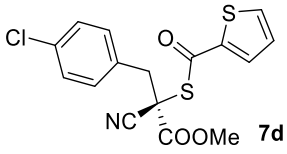

7d

methyl (R)-3-(4-chlorophenyl)-2-cyano-2-((thiophene-2-carbonyl)thio)propanoate (7d): White solid, 87% yield; ^{1}H NMR (400 MHz, Chloroform-*d*) δ 7.78 – 7.75 (m, 1H), 7.73 (dd, *J* = 4.9, 0.9 Hz, 1H), 7.38 – 7.24 (m, 4H), 7.16 – 7.12 (m, 1H), 3.80 (s, 3H), 3.49 – 3.34 (m, 2H); ^{13}C NMR (101 MHz, Chloroform-*d*) δ 179.6, 166.5, 139.3, 135.2, 135.0, 133.0, 131.5, 130.7, 129.2, 128.5, 116.5, 54.7, 51.6, 41.0; HRMS (ESI) calcd for $C_{16}H_{13}NO_3ClS_2$ *m/z* $[M+H]^+$: 366.0025; found: 366.0023; $[\alpha]^{22}_D$= +54.01 (*c* 1.8, CH_2Cl_2); HPLC analysis: Chiralcel IA-3 (Hex/IPA = 80/20, 1.0 mL/min, 254 nm, 22°C), 12.3 min, 13.5 min (major), 88% *ee.*

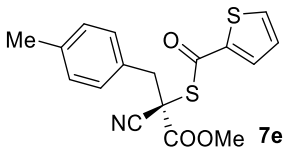

7e

methyl (R)-2-cyano-2-((thiophene-2-carbonyl)thio)-3-(p-tolyl)propanoate (7e): white solid, 90% yield; ^{1}H NMR (400 MHz, Chloroform-*d*) δ 7.77 (dd, *J* = 3.9, 1.1 Hz, 1H), 7.72 (dd, *J* = 5.0, 1.1 Hz, 1H), 7.20 (m, 4H), 7.23 – 7.17 (dd, *J* = 4.9, 3.9 Hz, 1H), 3.80 (s, 3H), 3.45 – 3.35 (m, 2H), 2.36 (s, 3H); ^{13}C NMR (101 MHz, Chloroform-*d*) δ 179.9, 166.7, 139.5, 138.7, 135.0, 132.9, 130.1, 129.6, 129.1, 128.4, 116.8, 54.5, 52.0, 41.4, 21.3; HRMS (ESI) calcd for $C_{17}H_{15}NO_3S_2Na$ *m/z* $[M+Na]^+$: 368.0391; found: 368.0390; $[\alpha]^{22}_D$= +72.35 (*c* 2.8, CH_2Cl_2); HPLC analysis: Chiralcel IA-3 (Hex/IPA = 80/20, 1.0 mL/min, 254 nm, 22°C), 8.6 min, 10.0 min (major), 88% *ee.*

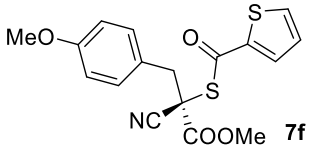

7f

methyl (R)-2-cyano-3-(4-methoxyphenyl)-2-((thiophene-2-carbonyl)thio)propanoate (7f): White solid, 91% yield; ^{1}H NMR (400 MHz, Chloroform-*d*) δ 7.77 (d, *J* = 3.8 Hz, 1H), 7.72 (d, *J* = 4.8 Hz, 1H), 7.25 (d, *J* = 8.3 Hz, 2H), 7.14 (t, *J* = 4.4 Hz, 1H), 6.90 (d, *J* = 8.6 Hz, 2H), 3.81 (s, 3H), 3.80 (s, 3H), 3.38 (q, *J* = 13.6 Hz, 2H); ^{13}C NMR (101 MHz, Chloroform-*d*) δ 179.9, 166.7 , 159.9, 139.5, 135.0, 132.9, 131.3, 128.4, 124.1, 116.9, 114.3, 55.4, 54.5, 52.1, 41.1; HRMS (ESI) calcd for $C_{17}H_{16}NO_4S_2$ *m/z* $[M+H]^+$: 362.0521; found: 362.0521; $[\alpha]^{22}_D$= +64.35 (*c* 1.9, CH_2Cl_2); HPLC analysis: Chiralcel IA-3 (Hex/IPA = 80/20, 1.0 mL/min, 254 nm, 22°C), 12.8 min, 15.3 min (major), 88% *ee.*

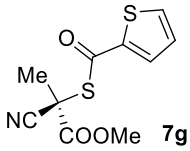

7g

methyl (R)-2-cyano-2-((thiophene-2-carbonyl)thio)propanoate (7g): white solid; 88% yield; ^{1}H NMR (400 MHz, Chloroform-*d*) δ 7.78 (dd, *J* = 3.9, 1.1 Hz, 1H), 7.74 (dd, *J* = 4.9, 1.1 Hz, 1H), 7.15 (dd, *J* = 4.9, 3.9 Hz, 1H), 3.94 (s, 3H), 1.97 (s, 3H); ^{13}C NMR (101 MHz, Chloroform-*d*) δ 180.0, 167.3, 139.4, 135.0, 132.8, 128.5, 117.7, 54.9, 45.4, 22.9; HRMS (ESI) calcd for $C_{10}H_{10}NO_4S$ *m/z* $[M+H]^+$: 240.0331; found: 240.0325; $[\alpha]^{22}_D$= +100.48 (*c* 2.1, CH_2Cl_2); HPLC analysis: Chiralcel IA-3 (Hex/IPA = 80/20, 1.0 mL/min, 254 nm, 22°C), 6.9 min, 7.5 min (major), 90% *ee.*

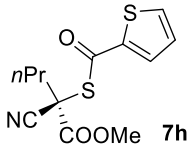

7h

methyl (R)-2-cyano-2-((thiophene-2-carbonyl)thio)pentanoate (7h): colorless oil, 93% yield; ^{1}H NMR (400 MHz, Chloroform-*d*) δ 7.77 (dd, *J* = 3.9, 1.1 Hz, 1H), 7.72 (dd, *J* = 4.9, 1.1 Hz, 1H), 7.14 (dd, *J* = 4.9, 3.9 Hz, 1H), 3.93 (s, 3H), 2.27 – 2.00 (m, 2H), 1.80 – 1.54 (m, 2H), 1.02 (t, *J* = 7.3 Hz, 3H); ^{13}C NMR (101 MHz, Chloroform-*d*) δ 180.2, 167.1, 139.6, 134.9, 132.8, 128.4, 117.1, 54.7, 50.7, 38.1, 19.3, 13.7; HRMS (ESI) calcd for $C_{12}H_{14}NO_3S_2$ *m/z* $[M+H]^+$: 284.0415; found: 284.0411; $[\alpha]^{22}_D$= +106.71 (*c* 2.4, CH_2Cl_2); HPLC analysis: Chiralcel IA-3 (Hex/IPA = 80/20, 1.0 mL/min, 254 nm, 22°C), 6.8 min, 7.4 min (major), 92% *ee.*

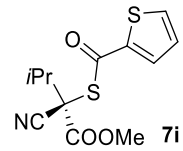

7i

methyl (R)-2-cyano-3-methyl-2-((thiophene-2-carbonyl)thio)butanoate (7i): white solid, 88% yield; ^{1}H NMR (400 MHz, Chloroform-*d*) δ 7.78 (dd, *J* = 3.9, 1.1 Hz, 1H),

7.72 (dd, *J* = 4.9, 1.1 Hz, 1H), 7.14 (dd, *J* = 4.9, 3.9 Hz, 1H), 3.93 (s, 3H), 2.46 (m, *J* = 6.8 Hz, 1H), 1.29 (d, *J* = 6.8 Hz, 3H), 1.19 (d, *J* = 6.7 Hz, 3H); ^{13}C NMR (101 MHz, Chloroform-*d*) δ 180.3, 167.1, 139.7, 134.8, 132.7, 128.4, 116.1, 56.8, 54.4, 35.7, 19.5, 19.0; HRMS (ESI) calcd for $C_{12}H_{13}NO_3S_2Na$ *m/z* $[M+Na]^+$: 306.0235; found: 306.0232; $[\alpha]^{22}_D$= +91.6 (*c* 2.3, CH_2Cl_2); HPLC analysis: Chiralcel IA-3 (Hex/IPA = 80/20, 1.0 mL/min, 254 nm, 22°C), 6.6 min, 6.9 min (major), 91% *ee*.

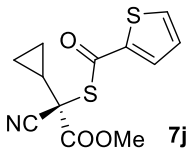

7j

methyl (R)-2-cyano-2-cyclopropyl-2-((thiophene-2-carbonyl)thio)acetate (7j): White solid, 93% yield; ^{1}H NMR (400 MHz, Chloroform-*d*) δ 7.80 (dd, *J* = 3.9, 1.1 Hz, 1H), 7.75 (dd, *J* = 4.9, 1.1 Hz, 1H), 7.17 (dd, *J* = 4.9, 3.9 Hz, 1H), 3.97 (s, 3H), 1.53 – 1.42 (m, 1H), 1.07 – 0.97 (m, 1H), 0.95 – 0.74 (m, 3H); ^{13}C NMR (101 MHz, Chloroform-*d*) δ 180.7, 166.8, 139.5, 134.9, 132.7, 128.4, 114.7, 54.8, 53.9, 14.5, 4.1, 3.9; HRMS (ESI) calcd for $C_{12}H_{11}NO_3S_2Na$ *m/z* $[M+Na]^+$: 304.0078; found: 304.0074; $[\alpha]^{22}_D$= +116.03 (*c* 2.2, CH_2Cl_2); HPLC analysis: Chiralcel IA-3 (Hex/IPA = 90/10, 1.0 mL/min, 254 nm, 22°C), 9.6 min, 10.0 min (major), 90% *ee*.

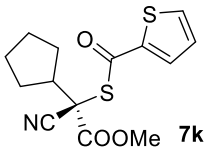

7k

Methyl (R)-2-cyano-2-cyclopentyl-2-((thiophene-2-carbonyl)thio)acetate (7k): White solid, 98% yield; ^{1}H NMR (400 MHz, Chloroform-*d*) δ 7.77 (dd, *J* = 4.0, 1.2 Hz, 1H), 7.71 (dd, *J* = 4.9, 1.2 Hz, 1H), 7.14 (dd, *J* = 5.0, 3.9 Hz, 1H), 3.92 (s, 3H), 2.52 (m, 1H), 1.97 (m, 1H), 1.79 (m, 4H), 1.66 (m, 4H); ^{13}C NMR (101 MHz, Chloroform-*d*) δ 180.4, 167.3, 139.6, 134.8, 132.7, 128.4, 116.4, 55.1, 54.5, 45.4, 29.8, 29.2, 25.4, 25.2; HRMS (ESI) calcd for $C_{14}H_{15}NO_3S_2Na$ *m/z* $[M+Na]^+$: 332.0391; found: 332.0398;

$[\alpha]^{22}_D$= +84.15 (*c* 2.4, CH_2Cl_2); HPLC analysis: Chiralcel IC (Hex/IPA = 50/50, 1.0 mL/min, 254 nm, 22°C), 8.7 min (major), 18.1 min, 93% *ee*.

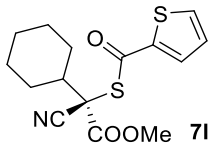

7l

methyl (R)-2-cyano-2-cyclohexyl-2-((thiophene-2-carbonyl)thio)acetate (7l): White solid, 96% yield; ^{1}H NMR (400 MHz, Chloroform-*d*) δ 7.77 (dd, *J* = 3.9, 1.1 Hz, 1H), 7.71 (dd, *J* = 5.0, 1.2 Hz, 1H), 7.13 (dd, *J* = 5.0, 3.9 Hz, 1H), 3.92 (s, 3H), 2.11 (m, 1H), 2.06 – 1.65 (m, 5H), 1.50 – 1.14 (m, 6H). ^{13}C NMR (101 MHz, Chloroform-*d*) δ 180.4, 167.0, 139.8, 134.7, 132.6, 128.4, 116.3, 56.5, 54.4, 44.3, 29.7, 29.1, 26.0, 25.9, 25.5; HRMS (ESI) calcd for $C_{15}H_{17}NO_3S_2Na$ *m/z* $[M+Na]^+$: 346.0548; found: 346.0546; $[\alpha]^{22}_D$= +71.14 (*c* 2.5, CH_2Cl_2); HPLC analysis: Chiralcel IA-3 (Hex/IPA = 80/20, 1.0 mL/min, 254 nm, 22°C), 6.9 min, 7.6 min (major), 93% *ee*.

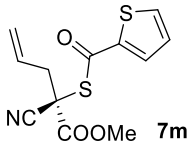

7m

methyl (R)-2-cyano-2-((thiophene-2-carbonyl)thio)pent-4-enoate (7m): White solid, 85% yield; ^{1}H NMR (400 MHz, Chloroform-*d*) δ 7.78 (dd, *J* = 3.9, 1.2 Hz, 1H), 7.73 (dd, *J* = 4.9, 1.2 Hz, 1H), 7.15 (dd, *J* = 5.0, 3.9 Hz, 1H), 5.89 (m, 1H), 5.36 (s, 1H), 5.33 (dd, *J* = 7.9, 1.3 Hz, 1H), 3.91 (s, 3H), 2.91 (m, 2H); ^{13}C NMR (101 MHz, Chloroform-*d*) δ 179.9, 166.5, 139.5, 135.0, 132.9, 128.9, 128.4, 122.5, 116.6, 54.6, 50.4, 40.3; HRMS (ESI) calcd for $C_{12}H_{12}NO_3S_2$ *m/z* $[M+H]^+$: 282.0259; found: 282.0264; $[\alpha]^{22}_D$= +88.39 (*c* 2.4, CH_2Cl_2); HPLC analysis: Chiralcel IA-3 (Hex/IPA = 80/20, 1.0 mL/min, 254 nm, 22°C), 6.9 min, 7.3 min (major), 90% *ee*.

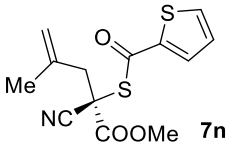

7n

methyl (R)-2-cyano-4-methyl-2-((thiophene-2-carbonyl)thio)pent-4-enoate (7n): white solid, 80% yield; ^{1}H NMR (400 MHz, Chloroform-*d*) δ 7.78 (dd, *J* = 3.9, 1.1 Hz, 1H), 7.73 (dd, *J* = 4.9, 1.1 Hz, 1H), 7.15 (dd, *J* = 4.9, 3.9 Hz, 1H), 5.12 – 5.06 (m, 1H), 5.00 (s, 1H), 3.91 (s, 3H), 2.97 – 2.74 (m, 2H), 1.94 (s, 3H); ^{13}C NMR (101 MHz, Chloroform-*d*) δ 180.0, 166.8, 139.5, 137.7, 134.9, 132.8, 128.4, 118.9, 117.3, 54.6, 49.9, 43.7, 23.0; HRMS (ESI) calcd for $C_{13}H_{13}NO_3S_2Na$ *m/z* $[M+Na]^+$: 318.0235; found: 318.0233; $[\alpha]^{22}_D$= +84.02 (*c* 2.4, CH_2Cl_2); HPLC analysis: Chiralcel IA-3 (Hex/IPA = 80/20, 1.0 mL/min, 254 nm, 22°C), 6.7 min, 7.4 min (major), 88% *ee.*

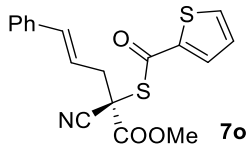

7o

methyl (R,E)-2-cyano-5-phenyl-2-((thiophene-2-carbonyl)thio)pent-4-enoate (7o): White solid, 90% yield, ^{1}H NMR (400 MHz, Chloroform-*d*) δ 7.78 (dd, *J* = 3.9, 1.1 Hz, 1H), 7.73 (dd, *J* = 4.9, 1.1 Hz, 1H), 7.40 (m, 2H), 7.38 – 7.19 (m, 3H), 7.14 (dd, *J* = 4.9, 3.9 Hz, 1H), 6.64 (d, *J* = 15.7 Hz, 1H), 6.32 – 6.13 (m, 1H), 3.91 (s, 3H), 3.25 – 2.75 (m, 2H); ^{13}C NMR (101 MHz, Chloroform-*d*) δ 180.0, 166.6, 139.5, 137.0, 136.0, 135.0, 132.9, 128.8, 128.5, 128.4, 126.8, 119.8, 116.8, 54.7, 50.8, 39.8; HRMS (ESI) calcd for $C_{18}H_{15}NO_3S_2Na$ *m/z* $[M+Na]^+$: 380.0391; found: 380.0392; $[\alpha]^{22}_D$= +61.63 (*c* 2.9, CH_2Cl_2); HPLC analysis: Chiralcel IA-3 (Hex/IPA = 80/20, 1.0 mL/min, 254 nm, 22°C), 9.0 min, 10.2 min (major), 87% *ee.*

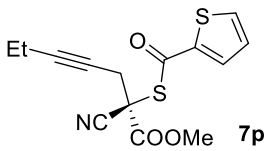

7p

methyl (R)-2-cyano-2-((thiophene-2-carbonyl)thio)hept-4-ynoate (7p): white solid, 86% yield; ^{1}H NMR (300 MHz, Chloroform-*d*) δ 7.79 (dd, *J* = 3.9, 1.1 Hz, 1H), 7.73

(dd, *J* = 4.9, 1.1 Hz, 1H), 7.15 (dd, *J* = 4.9, 3.9 Hz, 1H), 3.95 (s, 3H), 3.18 – 2.96 (m, 2H), 2.34 – 2.03 (m, 2H), 1.15 (t, *J* = 7.5 Hz, 3H); ^{13}C NMR (75 MHz, Chloroform-*d*) δ 179.8, 166.0, 139.5, 135.0, 132.9, 128.4, 116.3, 89.3, 70.3, 54.9, 50.5, 27.8, 13.8, 12.6; HRMS (ESI) calcd for $C_{14}H_{14}NO_3S_2$ *m/z* $[M+H]^+$: 308.0415; found: 308.0421; each; HPLC analysis: Chiralcel IA-3 (Hex/IPA = 80/20, 1.0 mL/min, 254 nm, 22°C), 7.1 min, 9.8 min (major), 87% *ee*.

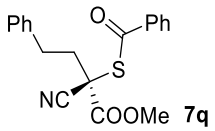

7q

methyl (R)-2-(benzoylthio)-2-cyano-4-phenylbutanoate (7q): white solid, 87% yield; ^{1}H NMR (400 MHz, Chloroform-*d*) δ 7.90 (dd, *J* = 8.4, 1.2 Hz, 2H), 7.69 – 7.60 (m, 1H), 7.55 – 7.40 (m, 2H), 7.36 – 7.27 (m, 2H), 7.27 – 7.17 (m, 3H), 3.91 (s, 3H), 3.02 (td, *J* = 12.6, 11.7, 5.3 Hz, 1H), 2.88 (td, *J* = 13.5, 12.7, 5.4 Hz, 1H), 2.48 (ddd, *J* = 18.9, 11.7, 5.3 Hz, 2H); ^{13}C NMR (101 MHz, Chloroform-*d*) δ 188.3, 167.1, 138.7, 135.0, 134.9, 129.1, 128.9, 128.6, 127.8, 127.0, 117.0, 54.7, 50.3, 37.7, 32.1; HRMS (ESI) calcd for $C_{19}H_{18}NO_3S$ *m/z* $[M+H]^+$: 340.1007; found: 340.1014; $[\alpha]^{22}_D$= +56.9 (*c* 2.7, CH_2Cl_2); HPLC analysis: Chiralcel IA-3 (Hex/IPA = 80/20, 1.0 mL/min, 254 nm, 22°C), 7.8 min, 8.6 min (major), 86% *ee*.

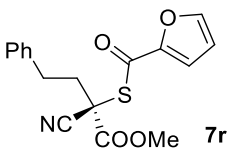

7r

methyl (R)-2-cyano-2-((furan-2-carbonyl)thio)-4-phenylbutanoate (7r): white solid; 96% yield; ^{1}H NMR (400 MHz, Chloroform-*d*) δ 7.65 (dd, *J* = 1.7, 0.7 Hz, 1H), 7.38 – 7.31 (m, 2H), 7.29 (dd, *J* = 3.7, 0.7 Hz, 1H), 7.28 – 7.21 (m, 3H), 6.63 (dd, *J* = 3.7, 1.7

Hz, 1H), 3.92 (s, 3H), 3.03 (td, *J* = 12.6, 11.7, 5.2 Hz, 1H), 2.90 (td, *J* = 13.6, 12.7, 5.4 Hz, 1H), 2.59 – 2.34 (m, 2H); ^{13}C NMR (101 MHz, Chloroform-*d*) δ 176.5, 166.9, 149.1, 147.5, 138.7, 128.9, 128.5, 127.0, 117.7, 116.8, 113.2, 54.7, 49.8, 37.7, 32.0; HRMS (ESI) calcd for $C_{17}H_{15}NO_4SNa$ *m/z* $[M+Na]^+$: 352.0619; found: 352.0620; $[\alpha]^{22}_D$= +71.15 (*c* 2.6, CH_2Cl_2); HPLC analysis: Chiralcel IA-3 (Hex/IPA = 80/20, 1.0 mL/min, 254 nm, 22°C), 6.5 min, 7.1 min (major), 90% *ee.*

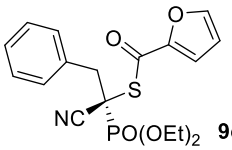

9c

(R)-S-(1-cyano-1-(diethoxyphosphoryl)-2-phenylethyl) furan-2-carbothioate (9c): colorless oil, 86% yield; ^{1}H NMR (400 MHz, Chloroform-*d*) δ 7.61 (d, *J* = 1.5 Hz, 1H), 7.53 – 7.46 (m, 2H), 7.39 – 7.27 (m, 4H), 6.59 (dd, *J* = 3.6, 1.7 Hz, 1H), 4.36 – 4.08 (m, 4H), 3.76 – 3.55 (m, 2H), 1.33 – 1.20 (m, 6H); ^{13}C NMR (101 MHz, Chloroform-*d*) δ 175.2 (d, J_{CP} = 7.8 Hz), 149.3 (d, J_{CP} = 2.0 Hz), 147.3, 133.8 (d, J_{CP} = 4.8 Hz), 131.3, 128.2, 128.1, 117.4, 115.4 (d, J_{CP} = 7.8 Hz), 112.9, 65.8 (dd, J_{CP} = 7.5, 5.8 Hz), 44.6 (d, J_{CP} = 143.3 Hz), 40.3 (d, J_{CP} = 3.7 Hz), 16.3 (d, J_{CP} = 6.0 Hz), 16.2 (d, J_{CP} = 6.1 Hz); ^{31}P NMR (162 MHz, Chloroform-*d*) δ 12.7; HRMS (ESI) calcd for $C_{18}H_{21}NO_5PS$ *m/z* $[M+H]^+$: 394.0878; found: 394.0887; $[\alpha]^{22}_D$= -47.85 (*c* 1.5, CH_2Cl_2); HPLC analysis: Chiralcel IA-3 (Hex/IPA = 80/20, 1.0 mL/min, 254 nm, 22°C), 10.5 min (major), 12.0 min, 89% *ee.*

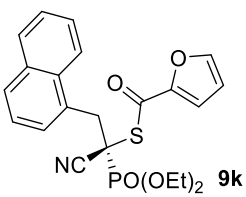

9k

(R)-S-(1-cyano-1-(diethoxyphosphoryl)-2-(naphthalen-1-yl)ethyl) furan-2-carbothioate (9k): colorless oil, 91% yield; ^{1}H NMR (400 MHz, Chloroform-*d*) δ 8.47 (d, *J* = 8.6 Hz, 1H), 7.96 – 7.73 (m, 3H), 7.63 – 7.40 (m, 4H), 7.25 (s, 1H), 6.58 (dd, *J* = 3.6, 1.7 Hz, 1H), 4.41 – 3.90 (m, 6H), 1.25 (t, *J* = 7.1 Hz, 3H), 1.02 (t, *J* = 7.1 Hz, 3H); ^{13}C NMR (101 MHz, Chloroform-*d*) δ 175.3 (d, J_{CP} = 8.5 Hz), 149.3 (d, J_{CP} = 2.0 Hz), 147.3, 133.9, 132.8, 130.5 (d, J_{CP} = 4.4 Hz), 130.3, 128.9, 128.6, 126.1, 125.8, 125.1, 124.9, 117.5, 115.6 (d, J_{CP} = 8.5 Hz), 112.9, 66.1 (d, J_{CP} = 7.5 Hz), 65.6 (d, J_{CP} = 7.9 Hz), 45.0 (d, J_{CP} = 142.3 Hz), 36.5 (d, J_{CP} = 3.6 Hz), 16.3 (d, J_{CP} = 5.8 Hz), 15.9 (d, J_{CP} = 6.4 Hz); ^{31}P NMR (162 MHz, Chloroform-*d*) δ 12.6; HRMS (ESI) calcd for $C_{22}H_{23}NO_5PS$ *m/z* $[M+H]^+$: 444.1035; found: 444.1035; $[\alpha]^{22}_D$= -85.29 (*c* 4.1, CH_2Cl_2); HPLC analysis: Chiralcel IA-3 (Hex/IPA = 80/20, 1.0 mL/min, 254 nm, 22°C), 14.9 min, 17.4 min (major), 90% *ee.*

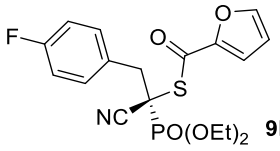

9l

(R)-S-(1-cyano-1-(diethoxyphosphoryl)-2-(4-fluorophenyl)ethyl) furan-2-carbothioate (9l): colorless oil, 92% yield, ^{1}H NMR (400 MHz, Chloroform-*d*) δ 7.62 (dd, *J* = 1.6, 0.6 Hz, 1H), 7.47 (dd, *J* = 8.7, 5.4 Hz, 2H), 7.30 – 7.26 (m, 1H), 7.01 (t, *J* = 8.7 Hz, 2H), 6.60 (dd, *J* = 3.6, 1.7 Hz, 1H), 4.38 – 4.12 (m, 4H), 3.73 – 3.52 (m, 2H), 1.38 – 1.22 (m, 6H); ^{13}C NMR (101 MHz, Chloroform-*d*) δ 175.2 (d, J_{CP} = 8.0 Hz), 162.8 (d, J_{CF} = 246.8 Hz), 149.3 (d, J_{CP} = 1.9 Hz), 147.4, 133.0 (d, J_{CF} = 8.2 Hz), 129.7 (dd, J_{CP} = 4.4 Hz, J_{CF} = 3.4 Hz), 117.5, 115.3 (d, J_{CP} = 8.2 Hz), 115.1 (d, J_{CF} = 21.4 Hz), 113.0, 66.0, 65.9, 44.7 (d, J_{CP} = 142.9 Hz), 39.6 (d, J_{CP} = 3.7 Hz),16.4 (d, J_{CP} = 6.1 Hz), 16.3 (d, J_{CP} = 6.2 Hz); ^{31}P NMR (162 MHz, Chloroform-*d*) δ 12.6; HRMS (ESI) calcd for $C_{18}H_{20}NO_5PSF$ *m/z* $[M+H]^+$: 412.0784; found: 412.0783; $[\alpha]^{22}_D$= -64.13 (*c* 1.5,

CH_2Cl_2); HPLC analysis: Chiralcel IA-3 (Hex/IPA = 80/20, 1.0 mL/min, 254 nm, 22°C), 11.6 min (major), 12.8 min, 88% *ee*.

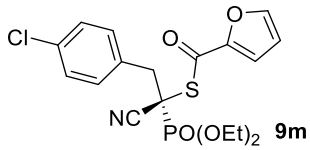

9m

(R)-S-(2-(4-chlorophenyl)-1-cyano-1-(diethoxyphosphoryl)ethyl) furan-2-carbothioate (9m): colorless oil, 91% yield; ^{1}H NMR (400 MHz, Chloroform-*d*) δ 7.64 (s, 1H), 7.47 (s, 1H), 7.45 (s, 1H), 7.36 – 7.26 (m, 3H), 6.62 (dd, *J* = 3.5, 1.5 Hz, 1H), 4.40 – 4.17 (m, 4H), 3.77 – 3.54 (m, 2H), 1.38 – 1.24 (m, 6H); ^{13}C NMR (101 MHz, Chloroform-*d*) δ 175.2 (d, J_{CP} = 7.9 Hz), 149.3 (d, J_{CP} = 1.9 Hz), 147.4, 134.2, 132.6, 132.4 (d, J_{CP} = 4.4 Hz), 128.4, 117.5, 115.3 (d, J_{CP} = 8.1 Hz), 113.0, 66.0, 65.9, 44.5 (d, J_{CP} = 142.9 Hz), 39.6 (d, J_{CP} = 3.7 Hz), 16.4 (d, J_{CP} = 5.9 Hz), 16.3 (d, J_{CP} = 6.1 Hz); ^{31}P NMR (162 MHz, Chloroform-*d*) δ 12.5; HRMS (ESI) calcd for $C_{18}H_{20}NO_5PSCl$ *m/z* $[M+H]^+$: 428.0488; found: 428.0486; $[\alpha]^{22}_D$= -68.80 (*c* 2.9, CH_2Cl_2); HPLC analysis: Chiralcel IA-3 (Hex/IPA = 80/20, 1.0 mL/min, 254 nm, 22°C), 13.5 min (major), 14.6 min, 87% *ee*.

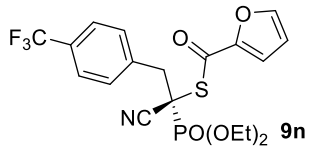

9n

(R)-S-(1-cyano-1-(diethoxyphosphoryl)-2-(4-(trifluoromethyl)phenyl)ethyl) furan-2-carbothioate (9n): colorless oil, 77% yield; ^{1}H NMR (400 MHz, Chloroform-*d*) δ 7.72 – 7.47 (m, 5H), 7.28 (d, *J* = 3.6 Hz, 1H), 6.61 (dd, *J* = 3.5, 1.4 Hz, 1H), 4.39 – 4.01 (m, 4H), 3.98 – 3.36 (m, 2H), 1.39 – 1.11 (m, 6H); ^{13}C NMR (101 MHz, Chloroform-*d*) δ 175.1 (d, J_{CP} = 8.2 Hz), 149.2 (d, J_{CP} = 2.0 Hz), 147.5, 138.0 (d, J_{CP} = 4.1 Hz), 131.7, 130.3 (q, J_{CF} = 32.5 Hz), 125.1 (q, J_{CF} = 3.8 Hz), 124.2 (q, J_{CF} = 272.2 Hz), 117.6, 115.2 (d, J_{CP} = 8.5 Hz), 113.1, 66.1 (d, J_{CP} = 7.5 Hz), 66.0 (d, J_{CP} = 7.7 Hz), 44.4 (d, J_{CP} =

143.1 Hz), 40.0 (d, J_{CP} = 3.7 Hz), 16.3 (d, J_{CP} = 5.9 Hz), 16.2 (d, J_{CP} = 6.1 Hz); ^{31}P NMR (162 MHz, Chloroform-*d*) δ 12.3; ^{19}F NMR (282 MHz, Chloroform-*d*) δ -62.7; HRMS (ESI) calcd for $C_{19}H_{20}NO_5PSF_3$ *m/z* $[M+H]^+$: 462.0752; found: 462.0759; $[\alpha]^{22}_D$= -65.22 (*c* 3.2, CH_2Cl_2); HPLC analysis: Chiralcel IG-3 (Hex/IPA = 80/20, 1.0 mL/min, 254 nm, 22°C), 23.0 min (major), 31.4 min, 91% *ee*.

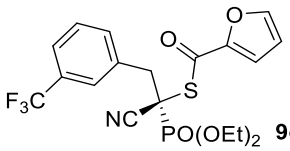

9o

(R)-S-(1-cyano-1-(diethoxyphosphoryl)-2-(3-(trifluoromethyl)phenyl)ethyl) furan-2-carbothioate (9o): colorless oil, 84% yield; ^{1}H NMR (400 MHz, Chloroform-*d*) δ 7.75 (d, *J* = 7.7 Hz, 1H), 7.71 (s, 1H), 7.62 (s, 1H), 7.57 (d, *J* = 7.9 Hz, 1H), 7.47 (t, *J* = 7.7 Hz, 1H), 7.28 (d, *J* = 3.6 Hz, 1H), 6.60 (dd, *J* = 3.5, 1.5 Hz, 1H), 4.38 – 4.11 (m, 4H), 3.82 – 3.58 (m, 2H), 1.27 (q, *J* = 6.7 Hz, 6H); ^{13}C NMR (75 MHz, Chloroform-*d*) δ 175.2 (d, J_{CP} = 8.6 Hz), 149.2 (d, J_{CP} = 2.2 Hz), 147.5, 135.0 (d, J_{CP} = 4.0 Hz), 134.7, 130.5 (q, J_{CF} = 32.3 Hz), 128.8, 128.1 (q, J_{CF} = 3.9 Hz) 124.9 (q, J_{CF} = 3.8 Hz), 124.1 (d, J_{CF} = 272.4 Hz), 117.7, 115.1 (d, J_{CP} = 8.7 Hz), 113.0, 66.1 (d, J_{CP} = 7.4 Hz), 66.0 (d, J_{CP} = 7.7 Hz), 44.5 (d, J_{CP} = 142.3 Hz), 40.1 (d, J_{CP} = 3.8 Hz), 16.3 (d, J_{CP} = 5.9 Hz), 16.2 (d, J_{CP} = 6.1 Hz); ^{31}P NMR (162 MHz, Chloroform-*d*) δ 12.4; ^{19}F NMR (282 MHz, Chloroform-*d*) δ -62.7; HRMS (ESI) calcd for $C_{19}H_{20}NO_5PSF_3$ *m/z* $[M+H]^+$: 462.0752; found: 462.0753; $[\alpha]^{22}_D$= -58.88 (*c* 3.5, CH_2Cl_2); HPLC analysis: Chiralcel IA-3 (Hex/IPA = 80/20, 1.0 mL/min, 254 nm, 22°C), 10.1 min (major), 10.7 min, 91% *ee*.

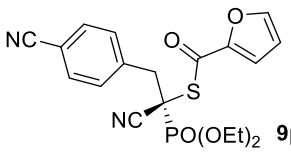

9p

(R)-S-(1-cyano-2-(4-cyanophenyl)-1-(diethoxyphosphoryl)ethyl) furan-2-carbothioate (9p): colorless oil, 87% yield; ^{1}H NMR (400 MHz, Chloroform-*d*) δ 7.62

(s, 5H), 7.28 (d, *J* = 3.6 Hz, 1H), 6.61 (dd, *J* = 3.5, 1.5 Hz, 1H), 4.38 – 4.13 (m, 4H), 3.84 – 3.55 (m, 2H), 1.29 (dt, *J* = 14.1, 7.1 Hz, 6H); ^{13}C NMR (101 MHz, Chloroform-*d*) δ 175.0 (d, J_{CP} = 8.4 Hz), 149.1 (d, J_{CP} = 2.0 Hz), 147.6, 139.4 (d, J_{CP} = 4.4 Hz), 132.1, 131.9, 118.7, 117.7, 115.0 (d, J_{CP} = 8.6 Hz), 113.1, 112.0, 66.2 (d, J_{CP} = 7.7 Hz), 66.1 (d, J_{CP} = 7.3 Hz), 44.2 (d, J_{CP} = 142.3 Hz), 40.2 (d, J_{CP} = 3.7 Hz), 16.4 (d, J_{CP} = 5.8 Hz), 16.3 (d, J_{CP} = 5.9 Hz); ^{31}P NMR (162 MHz, Chloroform-*d*) δ 12.2; HRMS (ESI) calcd for $C_{19}H_{20}N_2O_5PS$ *m/z* $[M+H]^+$: 419.0831; found: 419.0826; $[\alpha]^{22}_D$= -73.50 (*c* 3.6, CH_2Cl_2); HPLC analysis: Chiralcel IA-3 (Hex/IPA = 80/20, 1.0 mL/min, 254 nm, 22°C), 25.8 min (major), 27.5 min, 90% *ee*.

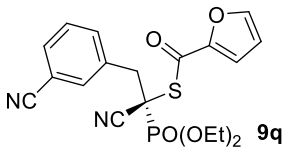

9q

(R)-S-(1-cyano-2-(3-cyanophenyl)-1-(diethoxyphosphoryl)ethyl) furan-2-carbothioate (9q): colorless oil, 92% yield; ^{1}H NMR (400 MHz, Chloroform-*d*) δ 7.79 (d, *J* = 7.9 Hz, 1H), 7.75 (s, 1H), 7.63 (dd, *J* = 1.6, 0.7 Hz, 1H), 7.60 (d, *J* = 7.8 Hz, 1H), 7.47 (d, *J* = 7.8 Hz, 1H), 7.33 – 7.27 (m, 1H), 6.61 (dd, *J* = 3.6, 1.7 Hz, 1H), 4.36 – 4.16 (m, 4H), 3.75 – 3.59 (m, 2H), 1.36 – 1.26 (m, 6H); ^{13}C NMR (101 MHz, Chloroform-*d*) δ 175.1 (d, J_{CP} = 8.6 Hz), 149.1 (d, J_{CP} = 2.1 Hz), 147.6, 135.8, 135.5 (d, J_{CP} = 4.2 Hz), 134.8, 131.8, 129.1, 118.6, 117.8, 115.0 (d, J_{CP} = 8.6 Hz), 113.1, 112.3, 66.2 (d, J_{CP} = 7.7 Hz), 66.1 (d, J_{CP} = 7.3 Hz), 44.3 (d, J_{CP} = 142.2 Hz), 39.8 (d, J_{CP} = 3.8 Hz), 16.4 (d, J_{CP} = 5.4 Hz), 16.3 (d, J_{CP} = 5.6 Hz); ^{31}P NMR (162 MHz, Chloroform-*d*) δ 12.3; HRMS (ESI) calcd for $C_{19}H_{20}N_2O_5PS$ *m/z* $[M+H]^+$: 419.0831; found: 419.0831; $[\alpha]^{22}_D$= -68.57 (*c* 3.5, CH_2Cl_2); HPLC analysis: Chiralcel IA-3 (Hex/IPA = 80/20, 1.0 mL/min, 254 nm, 22°C), 20.3 min (major), 22.2 min, 94% *ee*.

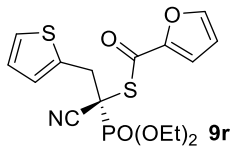

9r

(R)-S-(1-cyano-1-(diethoxyphosphoryl)-2-(thiophen-2-yl)ethyl) furan-2-carbothioate (9r): colorless oil, 91% yield; ^{1}H NMR (400 MHz, Chloroform-*d*) δ 7.61(d, *J* = 0.8 Hz, 1H), 7.27 (d, *J* = 3.6 Hz, 1H), 7.24 (dd, *J* = 5.1, 1.0 Hz, 1H), 7.18 (d, *J* = 3.1 Hz, 1H), 6.97 (dd, *J* = 5.1, 3.6 Hz, 1H), 6.59 (dd, *J* = 3.6, 1.7 Hz, 1H), 4.34 – 4.16 (m, 4H), 3.91 (d, *J* = 14.5 Hz, 2H), 1.37 – 1.27 (m, 6H); ^{13}C NMR (101 MHz, Chloroform-*d*) δ 175.2 (d, J_{CP} = 7.6 Hz), 149.3 (d, J_{CP} = 1.8 Hz), 147.4, 134.9 (d, J_{CP} = 5.7 Hz), 129.6, 126.8, 126.2, 117.5, 115.4 (d, J_{CP} = 7.8 Hz), 113.0, 65.8 (d, J_{CP} = 7.6 Hz), 65.7 (d, J_{CP} = 7.5 Hz), 44.7 (d, J_{CP} = 143.1 Hz), 34.7 (d, J_{CP} = 3.7 Hz), 16.3 (d, J_{CP} = 5.9 Hz); ^{31}P NMR (162 MHz, Chloroform-*d*) δ 12.6; HRMS (ESI) calcd for $C_{16}H_{19}NO_5PS_2$ *m/z* $[M+H]^+$: 400.0442; found: 400.0442; $[\alpha]^{22}_D$= -55.40 (*c* 3.7, CH_2Cl_2); HPLC analysis: Chiralcel IA-3 (Hex/IPA = 80/20, 1.0 mL/min, 254 nm, 22°C), 11.7 min (major), 13.0 min, 83% *ee*.

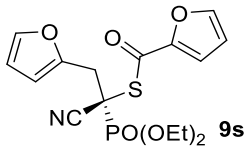

9s

(R)-S-(1-cyano-1-(diethoxyphosphoryl)-2-(furan-2-yl)ethyl) furan-2-carbothioate (9s): white solid, 88% yield; ^{1}H NMR (400 MHz, Chloroform-*d*) δ 7.60 (s, 1H), 7.38 (s, 1H), 7.27 (s, 1H), 6.59 (dd, *J* = 3.3, 1.3 Hz, 1H), 6.40 (d, *J* = 3.1 Hz, 1H), 6.33 (s, 1H), 4.36 – 4.21 (m, 4H), 3.75 (d, *J* = 14.2 Hz, 2H), 1.35 (q, *J* = 6.7 Hz, 6H); ^{13}C NMR (101 MHz, Chloroform-*d*) δ 175.2 (d, J_{CP} = 8.1 Hz), 149.3 (d, J_{CP} = 2.0 Hz), 147.9 (d, J_{CP} = 5.8 Hz), 147.3, 142.7, 117.4, 115.3 (d, J_{CP} = 8.1 Hz), 112.9, 110.8, 110.7, 66.0 (d, J_{CP} = 7.4 Hz), 65.9 (d, J_{CP} = 7.5 Hz), 43.4 (d, J_{CP} = 143.0 Hz), 33.3 (d, J_{CP} = 3.9 Hz), 16.4 (d,

J_{CP} = 6.0 Hz); ^{31}P NMR (162 MHz, Chloroform-*d*) δ 12.4; HRMS (ESI) calcd for $C_{16}H_{19}NO_6PS$ *m/z* $[M+H]^+$: 384.0671; found: 384.0676; $[\alpha]^{22}_D$= -31.30 (*c* 2.4, CH_2Cl_2); HPLC analysis: Chiralcel IA-3 (Hex/IPA = 80/20, 1.0 mL/min, 254 nm, 22°C), 12.1 min (major), 12.8 min, 83% *ee.*

Appendix (NMR and HPLC spectra)

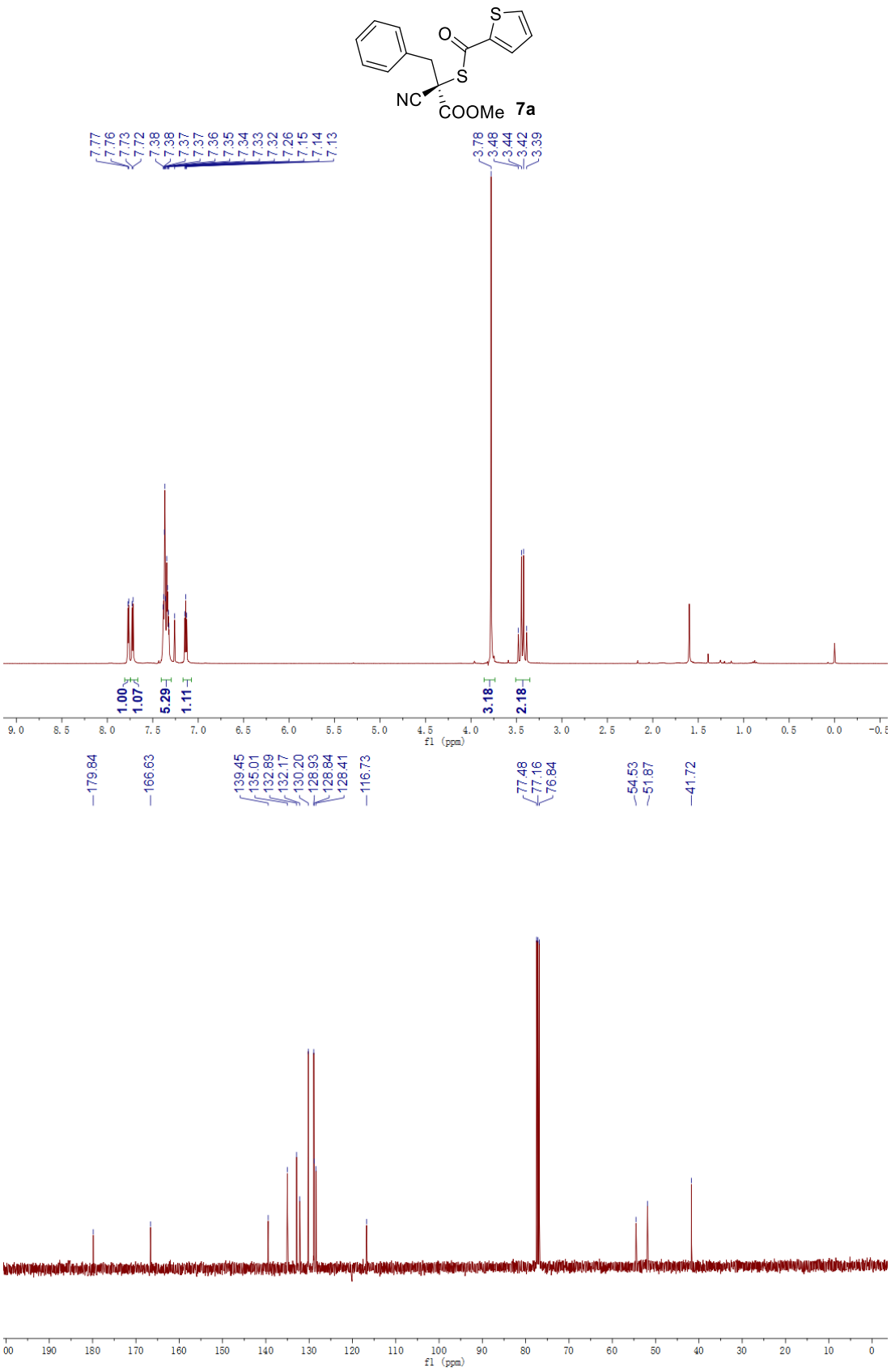

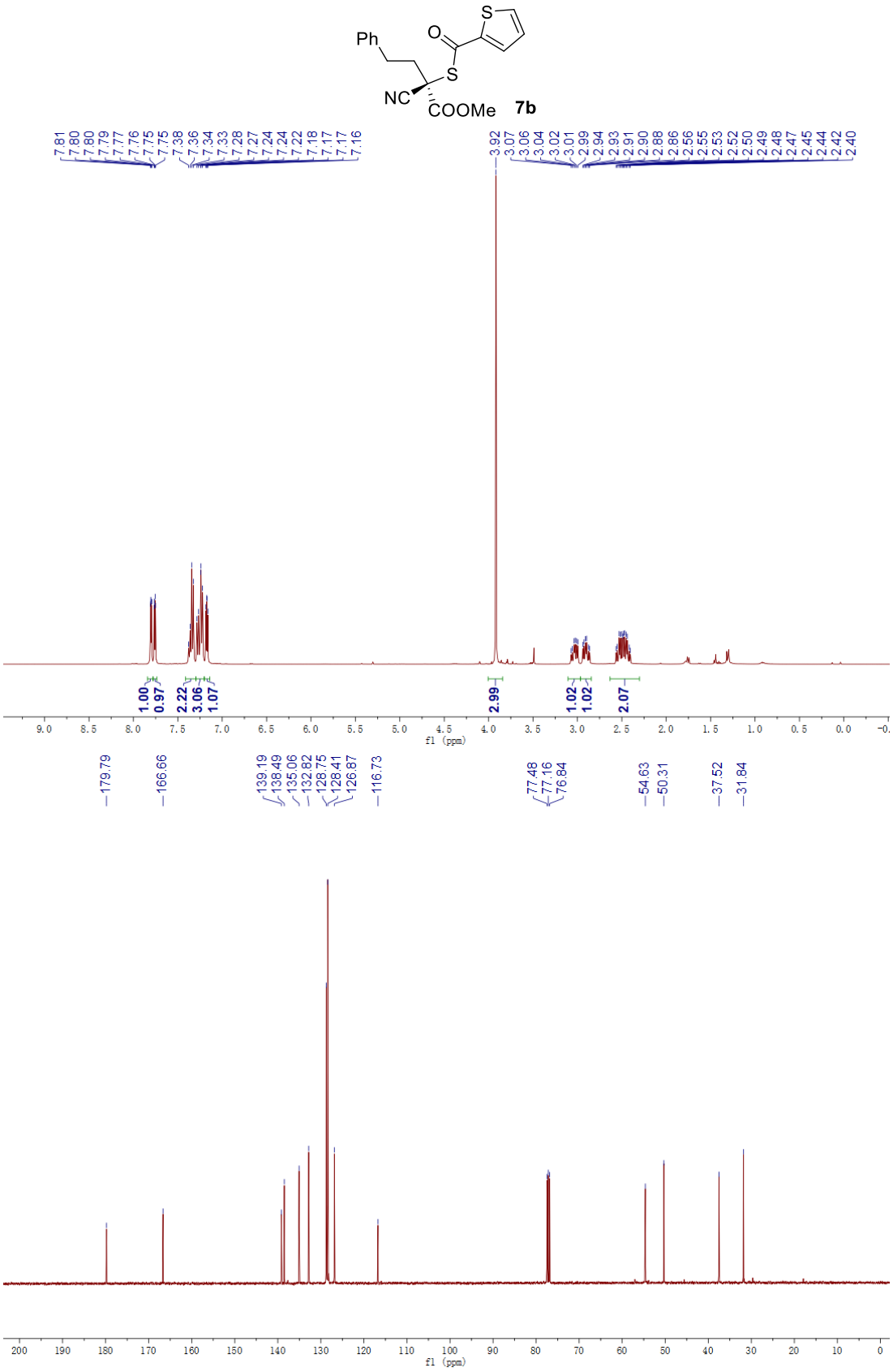
Ph
O
S
S
NC
COOMe
7b
7.81
7.80
7.80
7.79
7.77
7.76
7.75
7.75
7.38
7.36
7.34
7.33
7.28
7.27
7.24
7.24
7.22
7.18
7.17
7.16
3.92
3.07
3.06
3.04
3.02
3.01
2.99
2.94
2.93
2.91
2.90
2.88
2.86
2.56
2.55
2.53
2.52
2.50
2.49
2.48
2.47
2.45
2.44
2.42
2.40
1.00
0.97
2.22
3.06
1.07
2.99
1.02
1.02
2.07
f1 (ppm)
179.79
166.66
139.19
138.49
135.06
132.82
128.75
128.41
126.87
116.73
77.48
77.16
76.84
54.63
50.31
37.52
31.84
f1 (ppm)

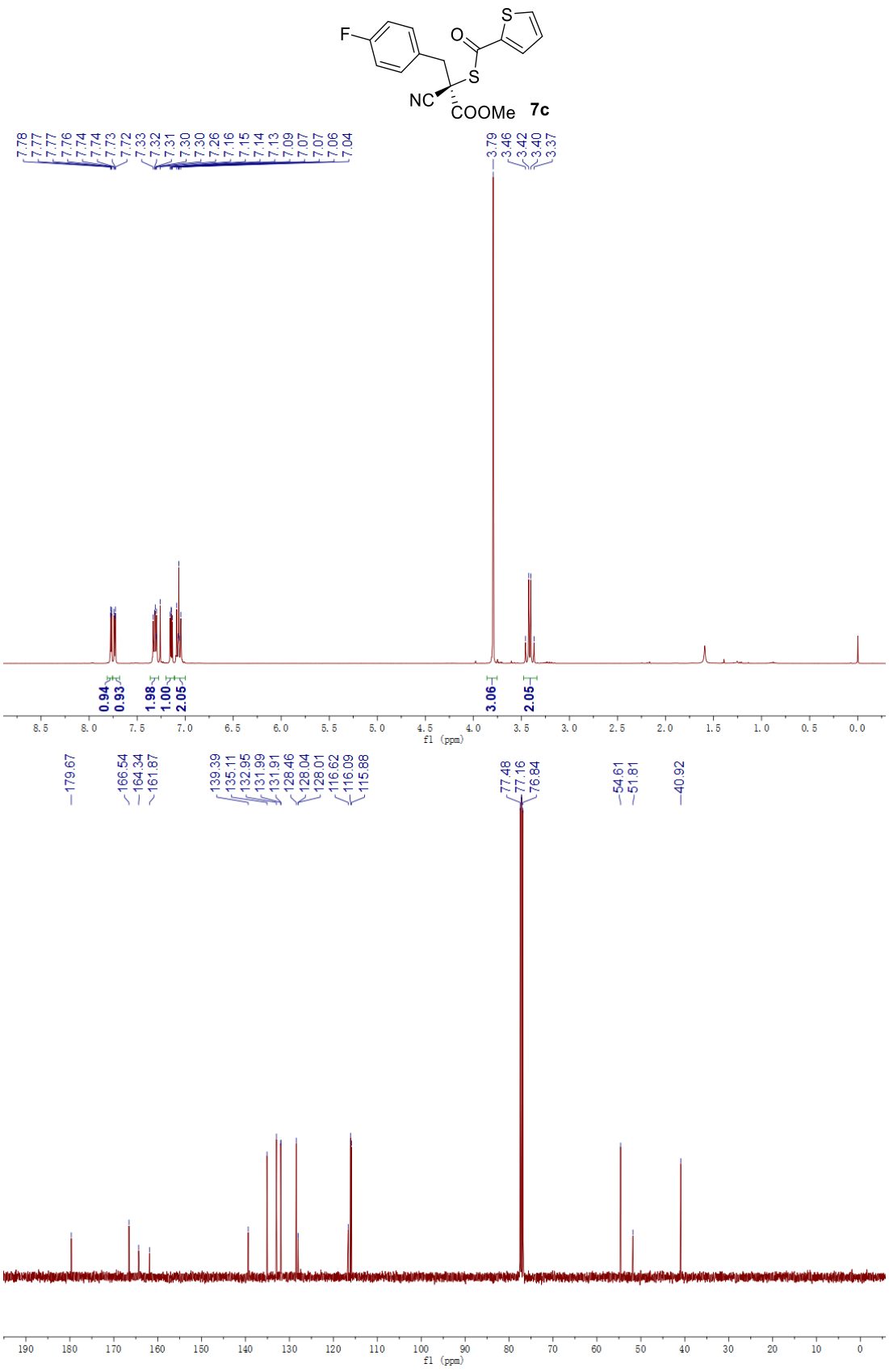
F
O
S
S
NC
COOMe
7c
7.78
7.77
7.77
7.76
7.74
7.74
7.73
7.72
7.33
7.32
7.31
7.30
7.30
7.26
7.16
7.15
7.14
7.13
7.09
7.07
7.07
7.06
7.04
3.79
3.46
3.42
3.40
3.37
0.94
0.93
1.98
1.00
2.05
3.06
2.05
f1 (ppm)
179.67
166.54
164.34
161.87
139.39
135.11
132.95
131.99
131.91
128.46
128.04
128.01
116.62
116.09
115.88
77.48
77.16
76.84
54.61
51.81
40.92
f1 (ppm)

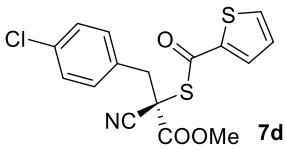
Cl
O
S
S
NC
COOMe

7d

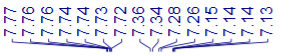
7.77
7.76
7.76
7.74
7.74
7.73
7.72
7.36
7.34
7.28
7.26
7.15
7.14
7.14
7.13

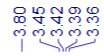
3.80
3.45
3.42
3.39
3.36

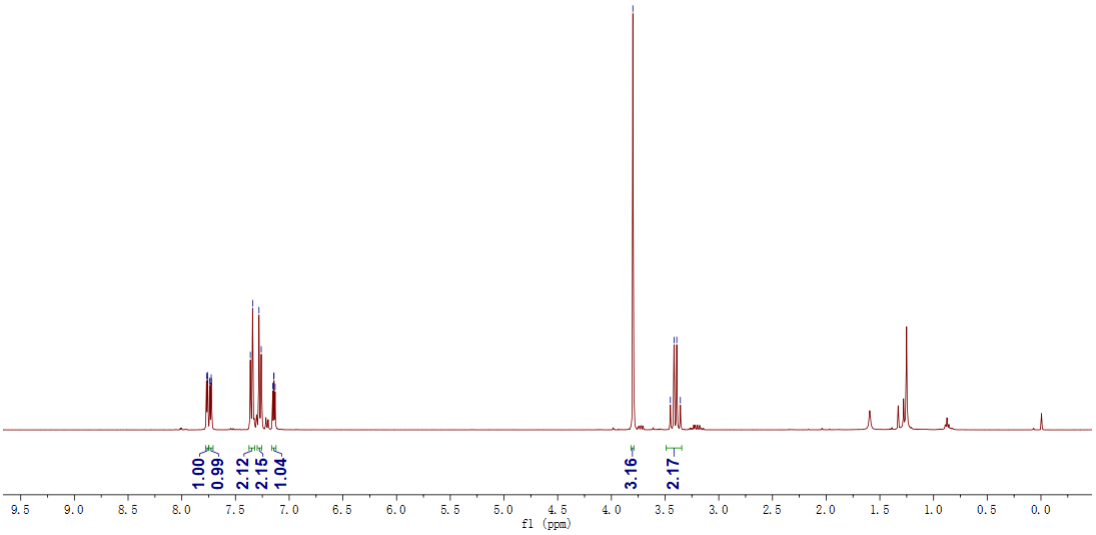
1.00
0.99
2.12
2.15
1.04
3.16
2.17
f1 (ppm)


179.61
166.47
139.33
135.17
135.03
132.98
131.54
130.67
129.19
128.47
116.53
77.48
77.16
76.84
54.67
51.63
40.99
29.82

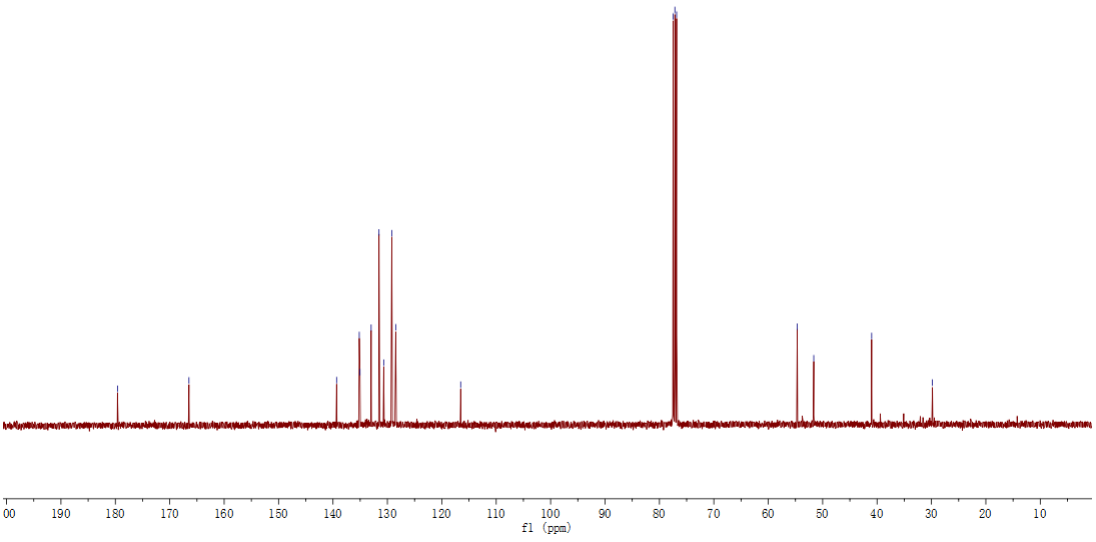
f1 (ppm)

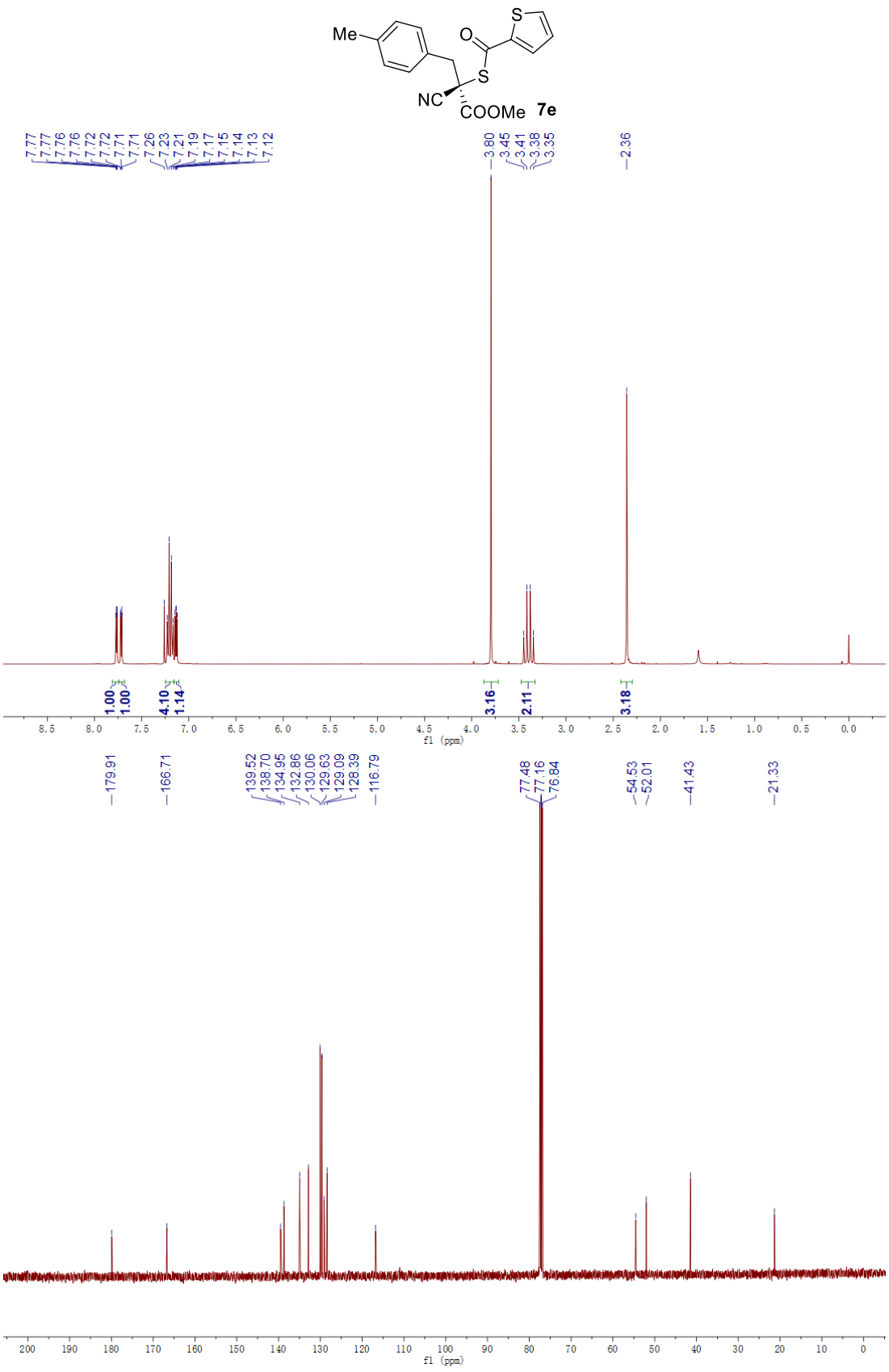
Me
O
S
S
NC
COOMe
7e
7.77
7.77
7.76
7.76
7.72
7.72
7.71
7.71
7.26
7.23
7.21
7.19
7.17
7.15
7.14
7.13
7.12
3.80
3.45
3.41
3.38
3.35
2.36
1.00
1.00
4.10
1.14
3.16
2.11
3.18
f1 (ppm)
179.91
166.71
139.52
138.70
134.95
132.86
130.06
129.63
129.09
128.39
116.79
77.48
77.16
76.84
54.53
52.01
41.43
21.33
f1 (ppm)

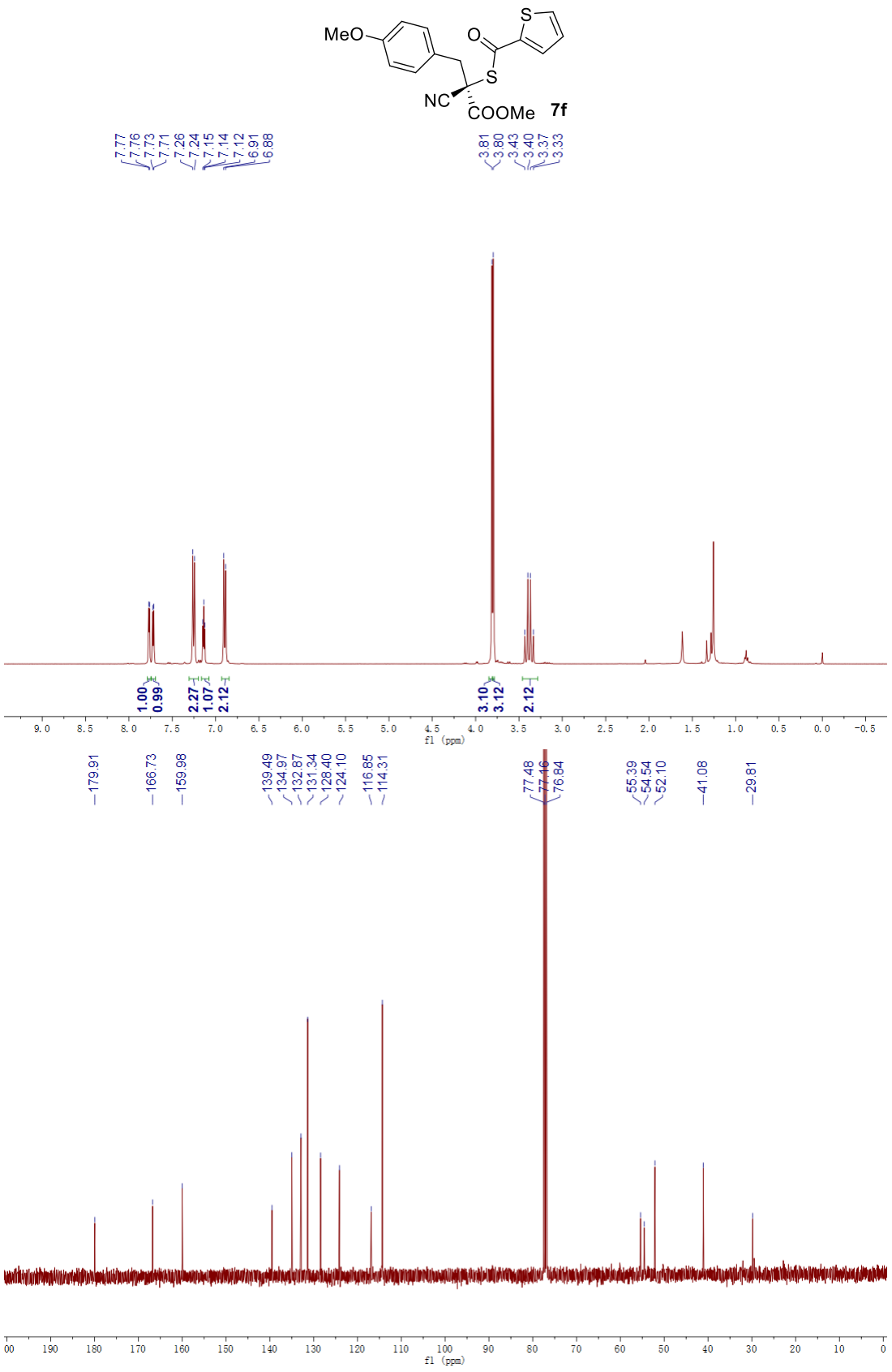
MeO
O
S
S
NC
COOMe
7f
7.77
7.76
7.73
7.71
7.26
7.24
7.15
7.14
7.12
6.91
6.88
3.81
3.80
3.43
3.40
3.37
3.33
1.00
0.99
2.27
1.07
2.12
3.10
3.12
2.12
f1 (ppm)
179.91
166.73
159.98
139.49
134.97
132.87
131.34
128.40
124.10
116.85
114.31
77.48
77.16
76.84
55.39
54.54
52.10
41.08
29.81
f1 (ppm)

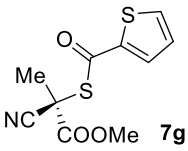
S
O
Me
S
NC
COOMe

7g

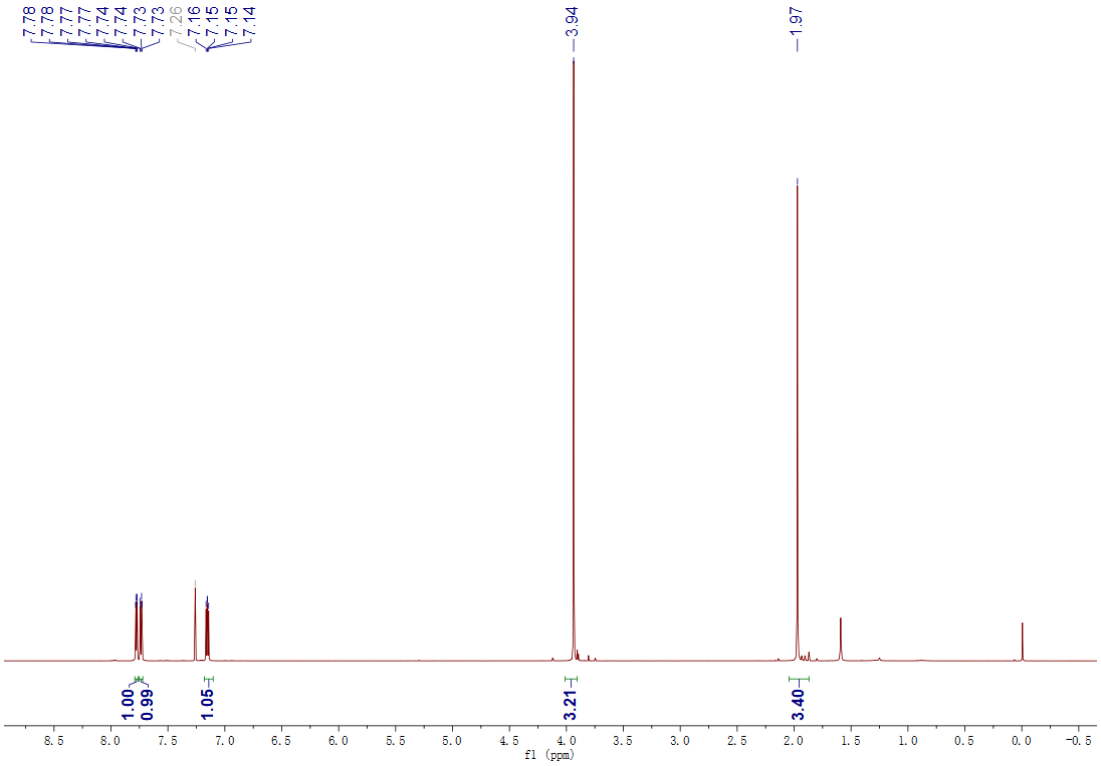
7.78
7.78
7.77
7.77
7.74
7.74
7.73
7.73
7.26
7.16
7.15
7.14
3.94
1.97
1.00
0.99
1.05
3.21
3.40
f1 (ppm)

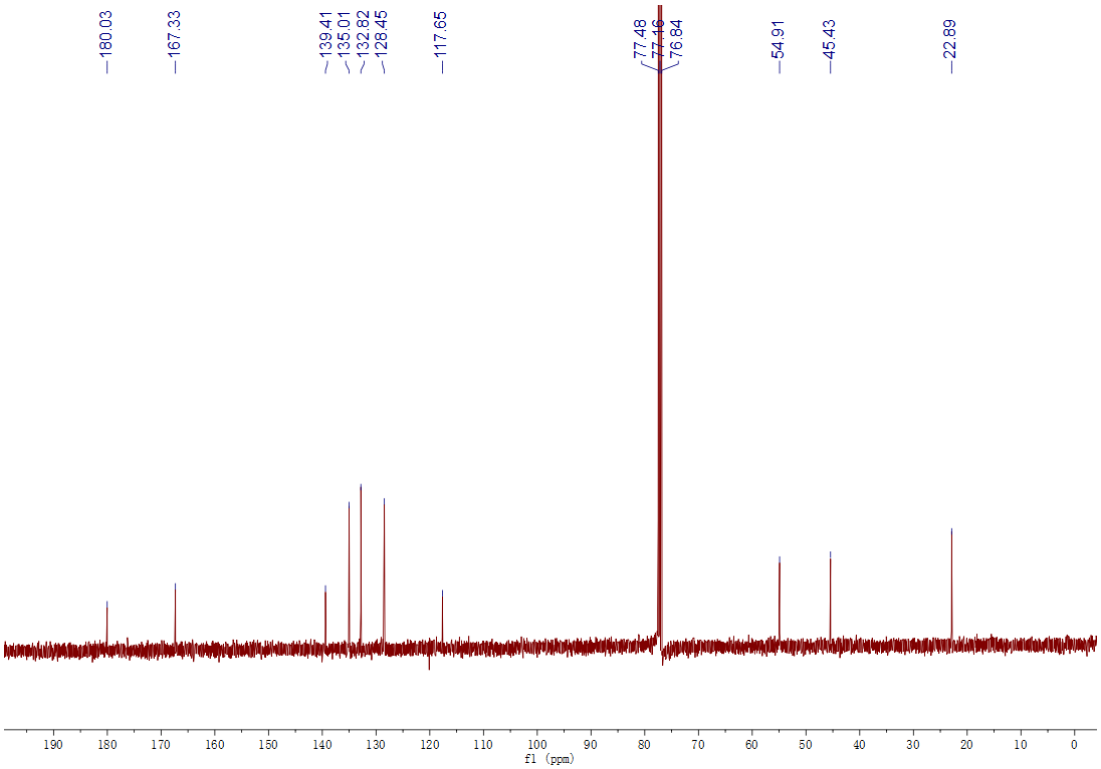
180.03
167.33
139.41
135.01
132.82
128.45
117.65
77.48
77.16
76.84
54.91
45.43
22.89
f1 (ppm)

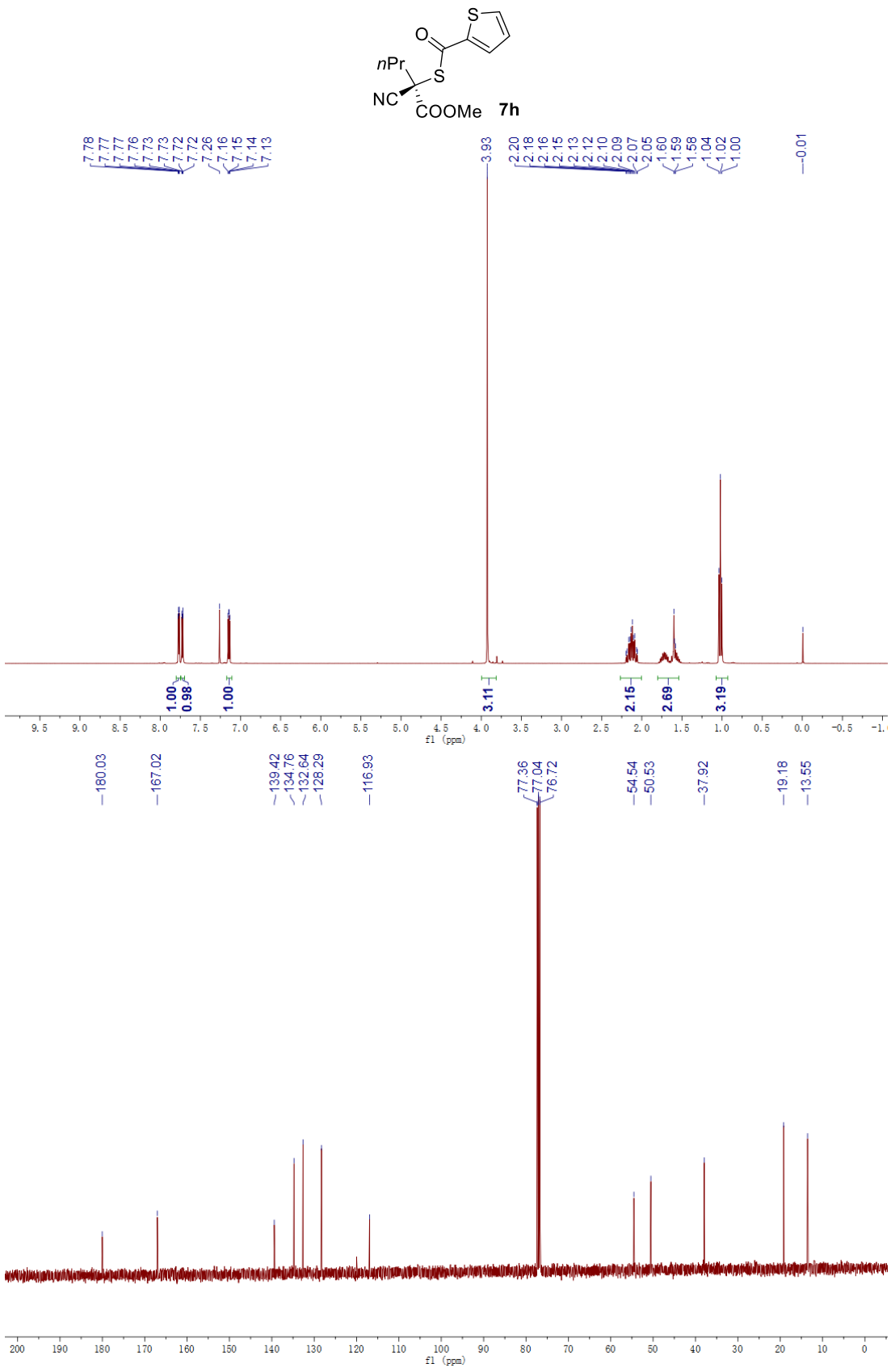
S
O
nPr
S
NC
COOMe
7h
7.78
7.77
7.77
7.76
7.73
7.73
7.72
7.72
7.26
7.16
7.15
7.14
7.13
3.93
2.20
2.18
2.16
2.15
2.13
2.12
2.10
2.09
2.07
2.05
1.60
1.59
1.58
1.04
1.02
1.00
-0.01
1.00
0.98
1.00
3.11
2.15
2.69
3.19
f1 (ppm)
180.03
167.02
139.42
134.76
132.64
128.29
116.93
77.36
77.04
76.72
54.54
50.53
37.92
19.18
13.55
f1 (ppm)

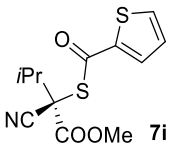
S
O
iPr
S
NC
COOMe

7i

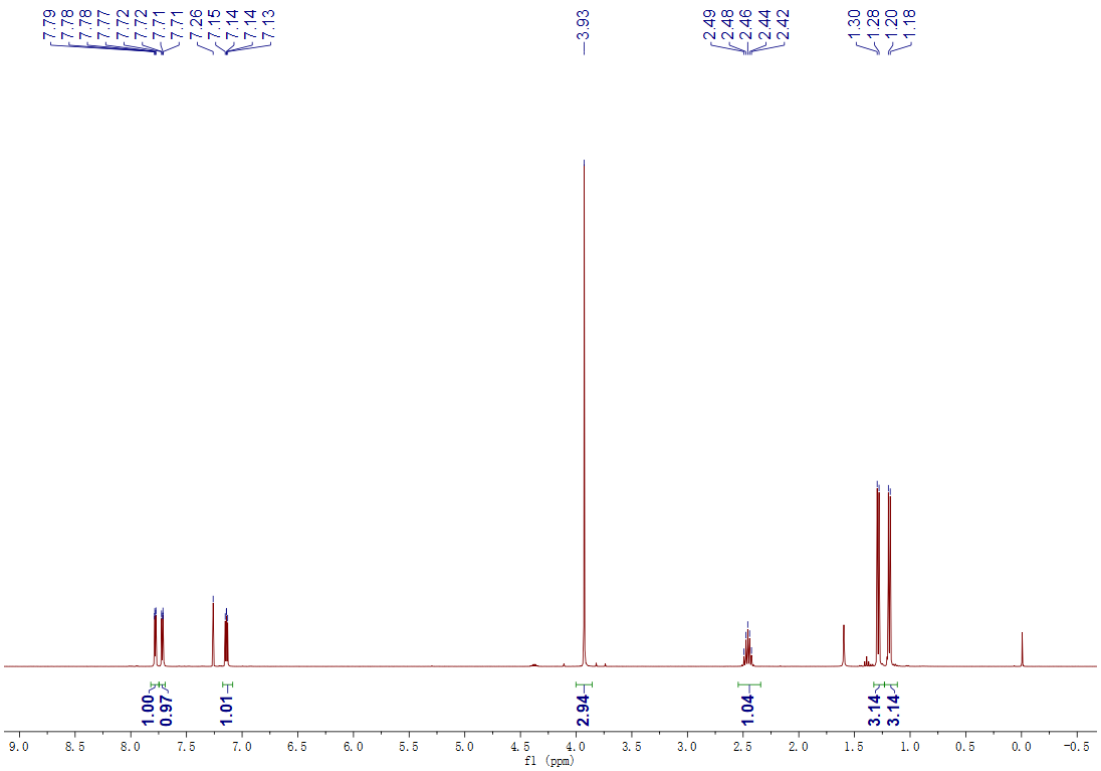
7.79
7.78
7.78
7.77
7.72
7.72
7.71
7.71
7.26
7.15
7.14
7.14
7.13
3.93
2.49
2.48
2.46
2.44
2.42
1.30
1.28
1.20
1.18
1.00
0.97
1.01
2.94
1.04
3.14
3.14
f1 (ppm)

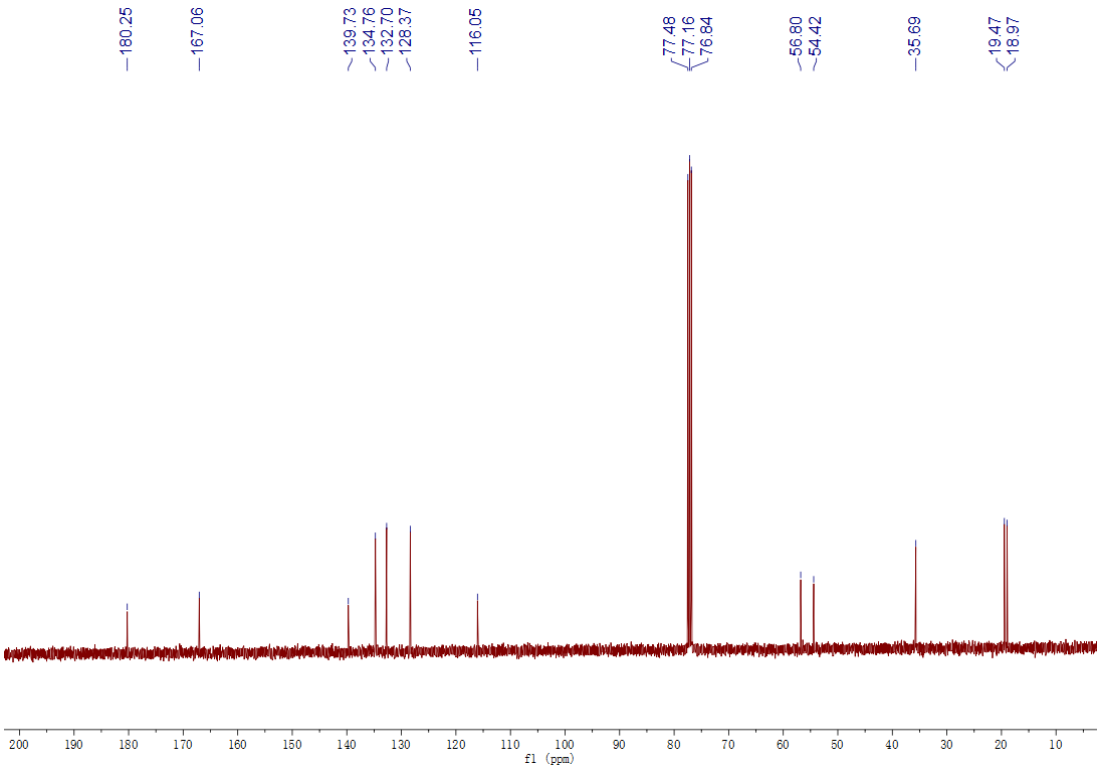
180.25
167.06
139.73
134.76
132.70
128.37
116.05
77.48
77.16
76.84
56.80
54.42
35.69
19.47
18.97
f1 (ppm)

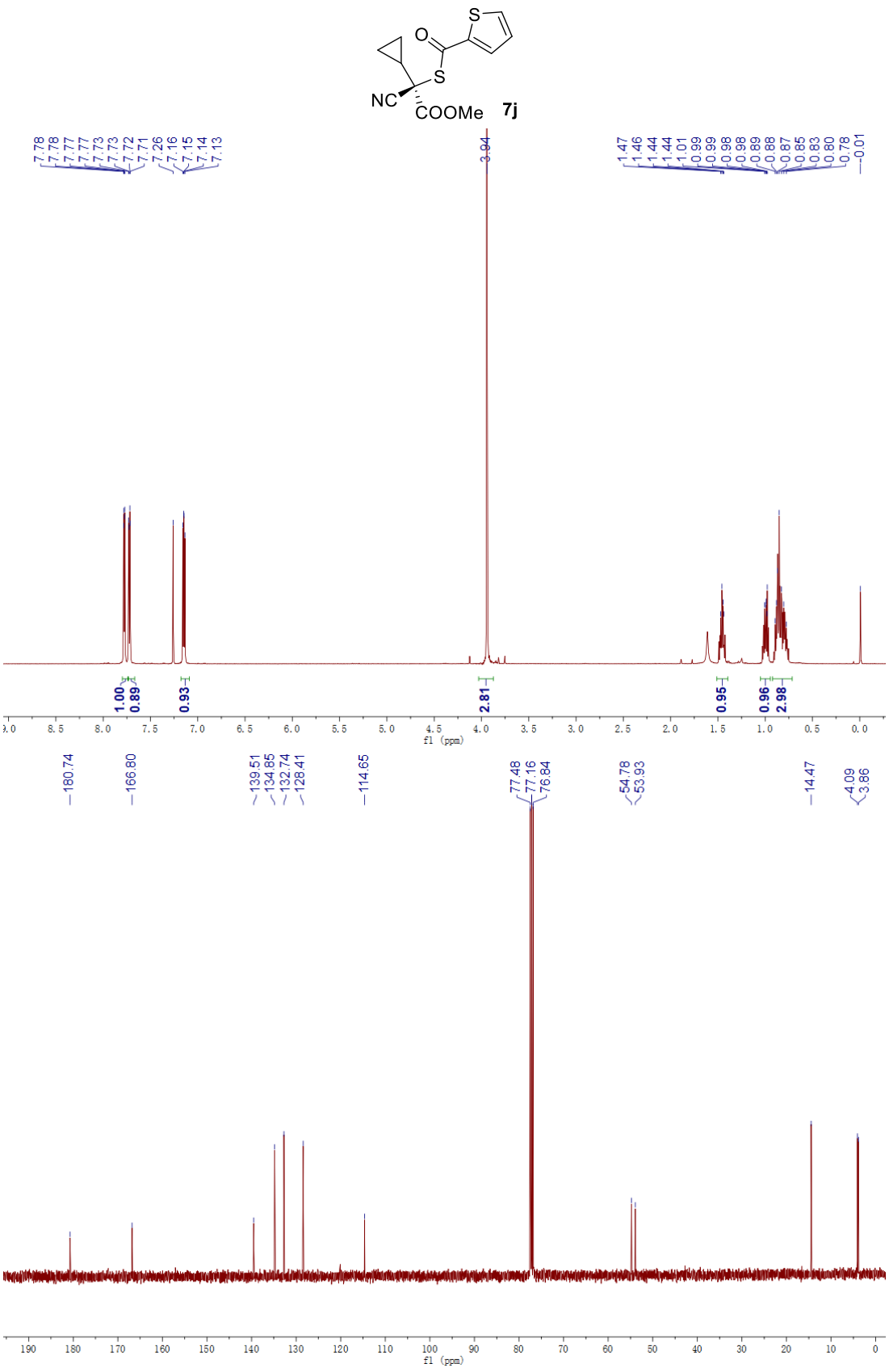
S
O
S
NC
COOMe
7j
7.78
7.78
7.77
7.77
7.73
7.73
7.72
7.71
7.26
7.16
7.15
7.14
7.13
3.94
1.47
1.46
1.44
1.44
1.01
0.99
0.99
0.98
0.98
0.89
0.88
0.87
0.85
0.83
0.80
0.78
0.01
1.00
0.89
0.93
2.81
0.95
0.96
2.98
f1 (ppm)
180.74
166.80
139.51
134.85
132.74
128.41
114.65
77.48
77.16
76.84
54.78
53.93
14.47
4.09
3.86
f1 (ppm)

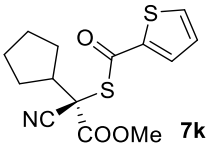
S
O
S
NC
COOMe

7k

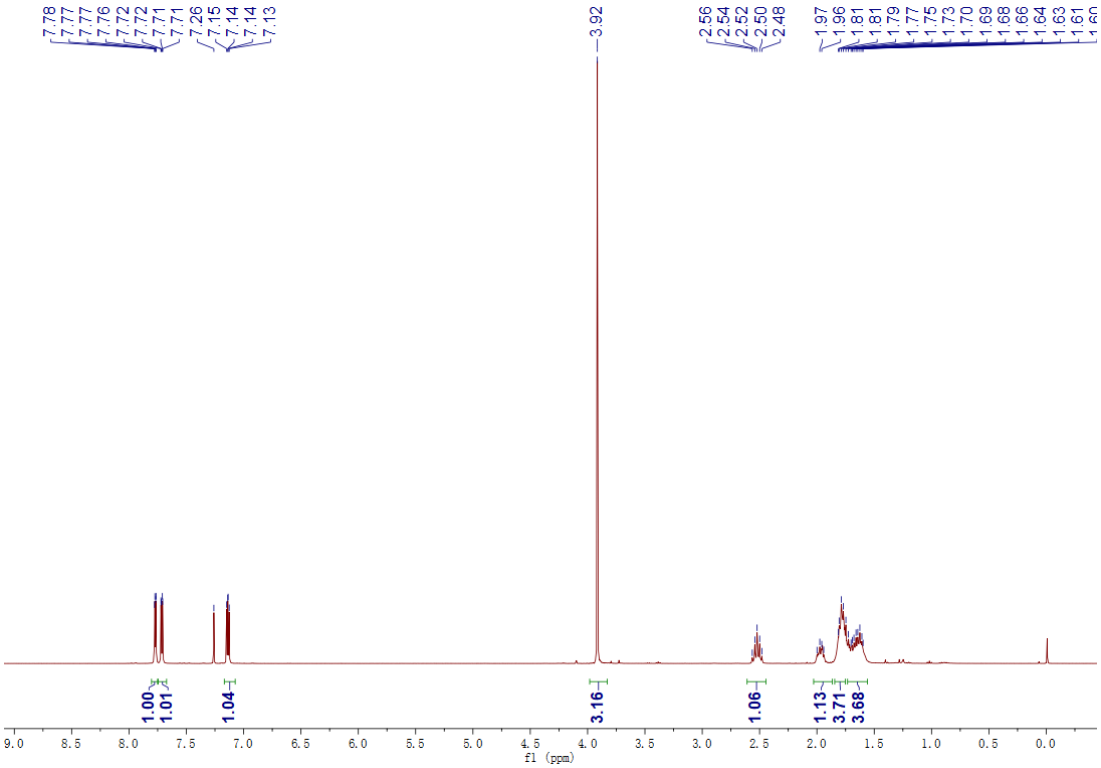
7.78
7.77
7.77
7.76
7.72
7.72
7.71
7.71
7.26
7.15
7.14
7.14
7.13
3.92
2.56
2.54
2.52
2.50
2.48
1.97
1.96
1.81
1.81
1.79
1.77
1.75
1.73
1.70
1.69
1.68
1.66
1.64
1.63
1.61
1.00
1.01
1.04
3.16
1.06
1.13
3.71
3.68
f1 (ppm)

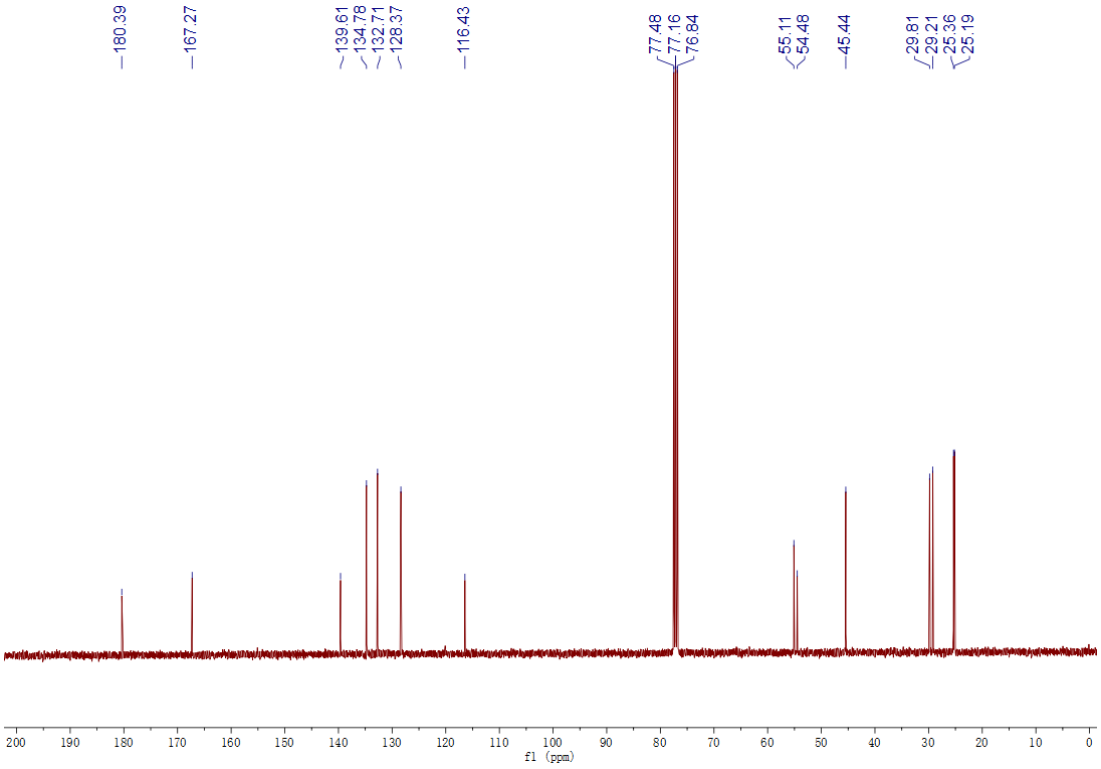
180.39
167.27
139.61
134.78
132.71
128.37
116.43
77.48
77.16
76.84
55.11
54.48
45.44
29.81
29.21
25.36
25.19
f1 (ppm)

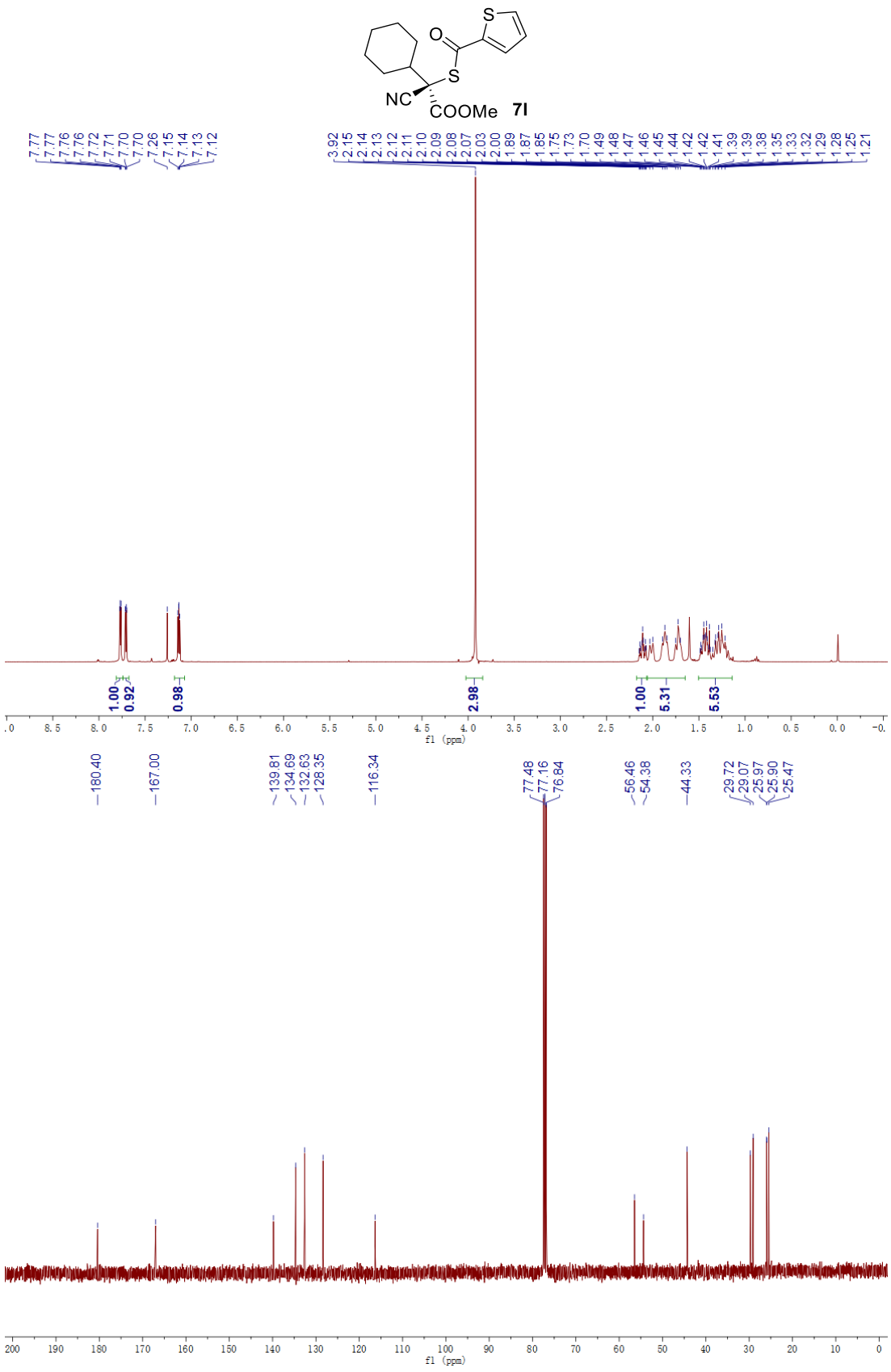
S
O
S
NC
COOMe
7l
7.77
7.77
7.76
7.76
7.72
7.71
7.70
7.70
7.26
7.15
7.14
7.13
7.12
3.92
2.15
2.14
2.13
2.12
2.11
2.10
2.09
2.08
2.07
2.03
2.00
1.89
1.87
1.85
1.75
1.73
1.70
1.49
1.48
1.47
1.46
1.45
1.44
1.42
1.42
1.41
1.39
1.39
1.38
1.35
1.33
1.32
1.29
1.28
1.25
1.21
1.00
0.92
0.98
2.98
1.00
5.31
5.53
f1 (ppm)
180.40
167.00
139.81
134.69
132.63
128.35
116.34
77.48
77.16
76.84
56.46
54.38
44.33
29.72
29.07
25.97
25.90
25.47
f1 (ppm)

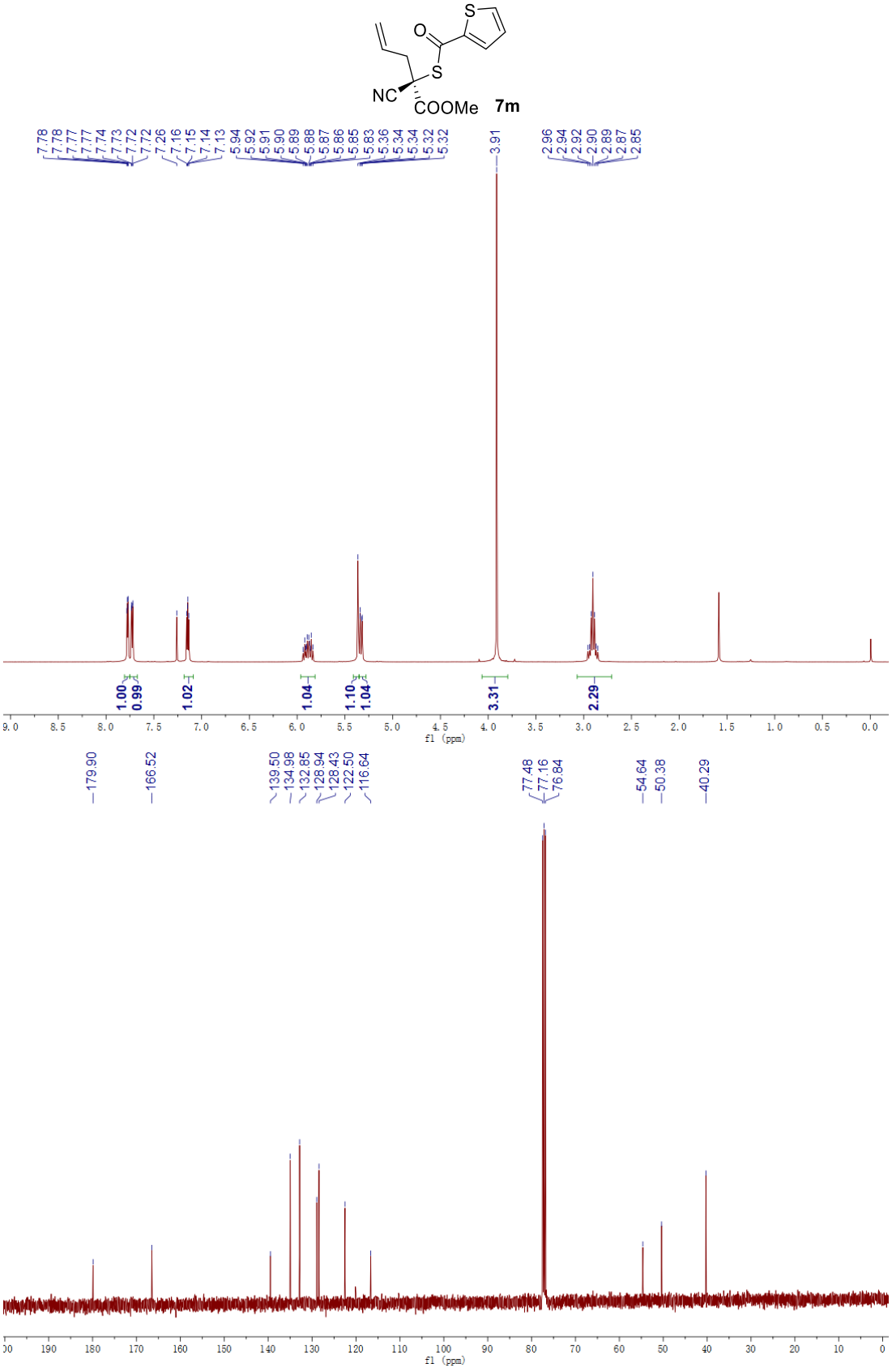
S
O
S
NC
COOMe
7m
7.78
7.78
7.77
7.77
7.74
7.73
7.72
7.72
7.26
7.16
7.15
7.14
7.13
5.94
5.92
5.91
5.90
5.89
5.88
5.87
5.86
5.85
5.83
5.36
5.34
5.34
5.32
5.32
3.91
2.96
2.94
2.92
2.90
2.89
2.87
2.85
1.00
0.99
1.02
1.04
1.10
1.04
3.31
2.29
f1 (ppm)
179.90
166.52
139.50
134.98
132.85
128.94
128.43
122.50
116.64
77.48
77.16
76.84
54.64
50.38
40.29
f1 (ppm)

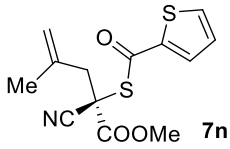
S
O
Me
S
NC
COOMe

7n

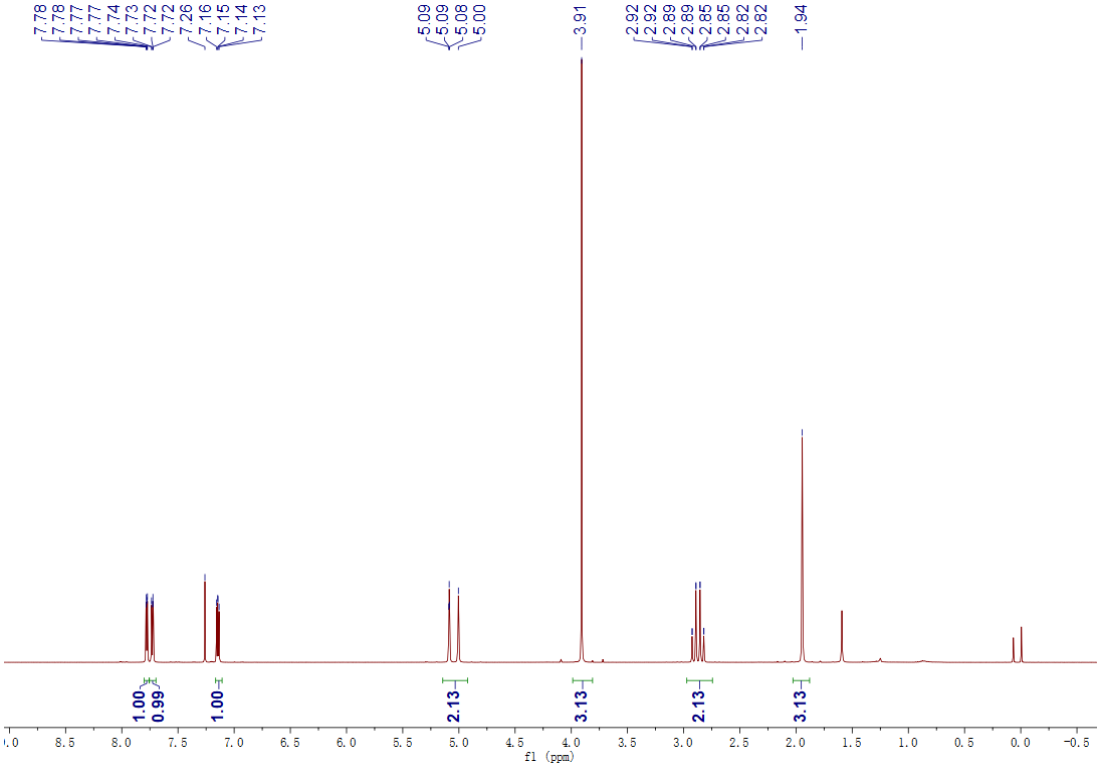
7.78
7.78
7.77
7.77
7.74
7.73
7.72
7.72
7.26
7.16
7.15
7.14
7.13
5.09
5.09
5.08
5.00
3.91
2.92
2.92
2.89
2.89
2.85
2.85
2.82
2.82
1.94
1.00
0.99
1.00
2.13
3.13
2.13
3.13
f1 (ppm)

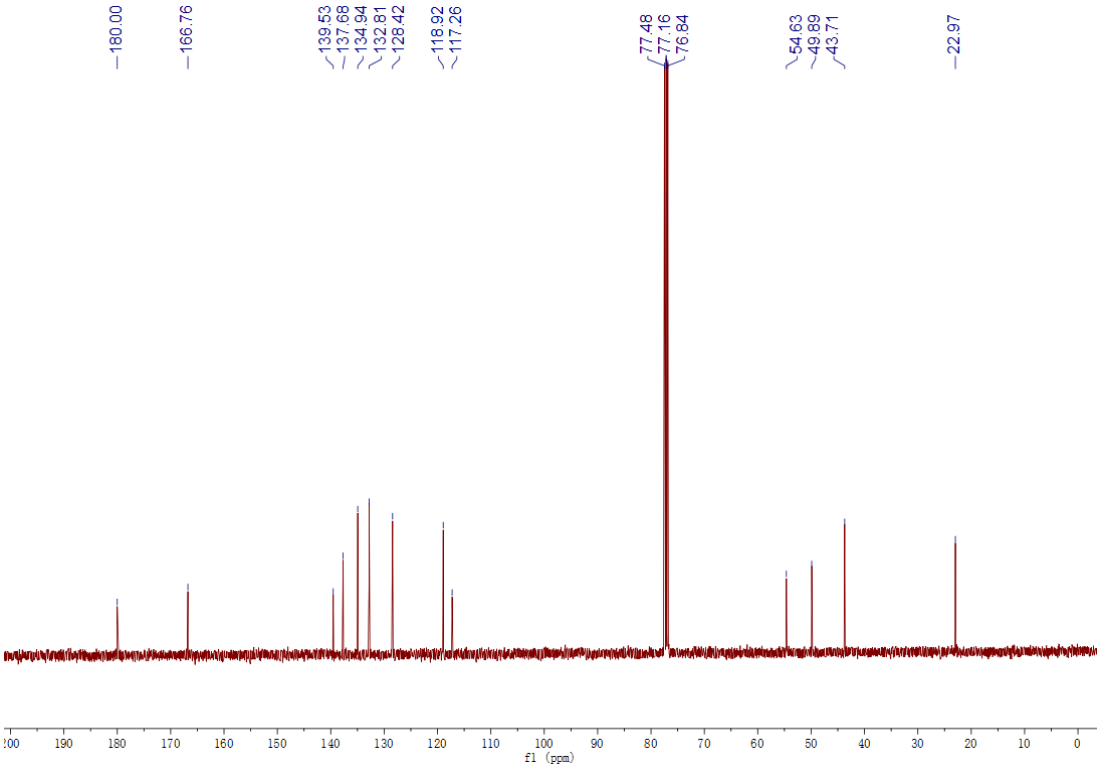
180.00
166.76
139.53
137.68
134.94
132.81
128.42
118.92
117.26
77.48
77.16
76.84
54.63
49.89
43.71
22.97
f1 (ppm)

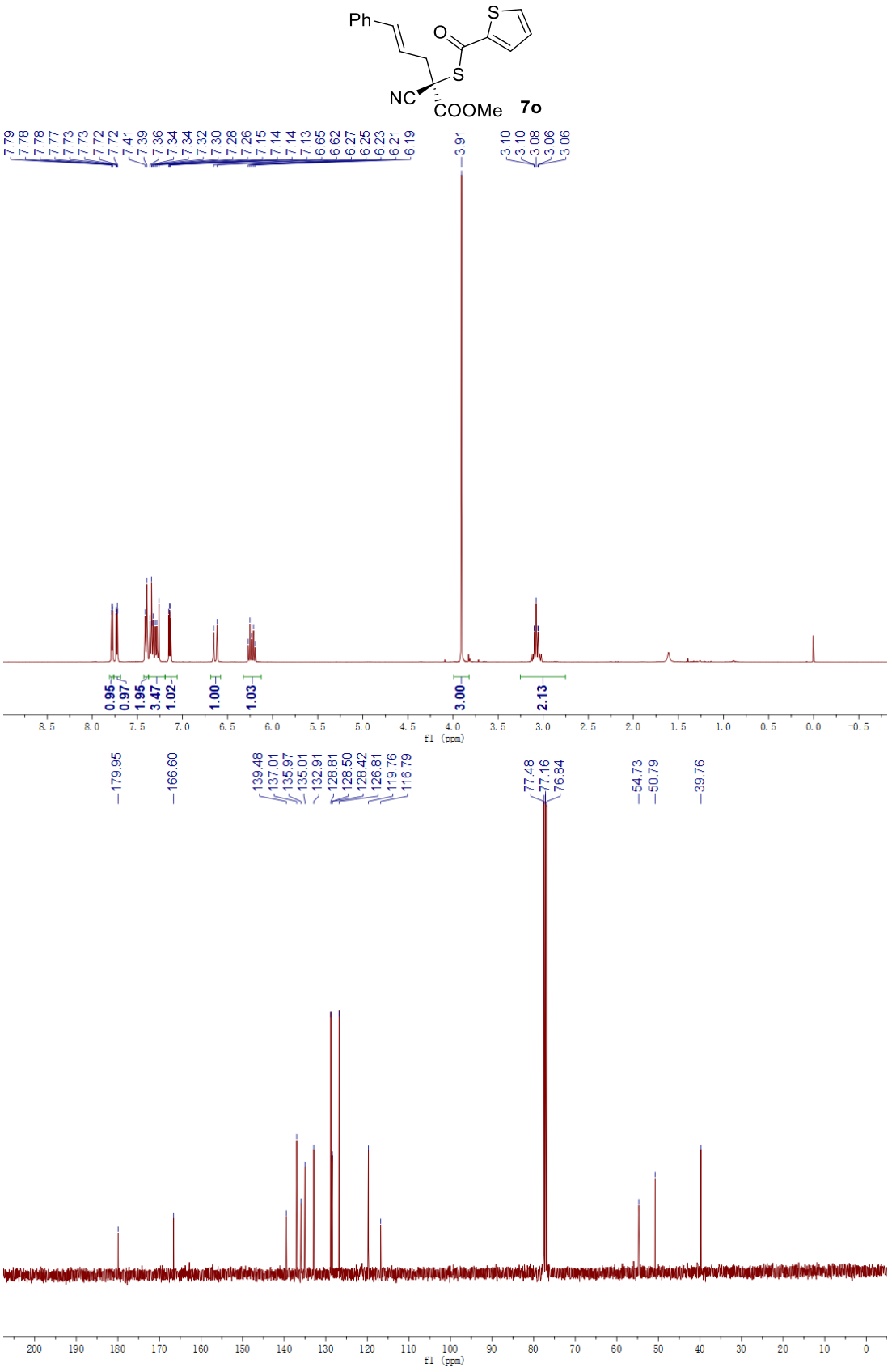
Ph
O
S
S
NC
COOMe
7o
7.79
7.78
7.78
7.77
7.73
7.73
7.72
7.72
7.41
7.39
7.36
7.34
7.34
7.32
7.30
7.28
7.26
7.15
7.14
7.14
7.13
6.65
6.62
6.27
6.25
6.23
6.21
6.19
3.91
3.10
3.10
3.08
3.06
3.06
0.95
0.97
1.95
3.47
1.02
1.00
1.03
3.00
2.13
f1 (ppm)
179.95
166.60
139.48
137.01
135.97
135.01
132.91
128.81
128.50
128.42
126.81
119.76
116.79
77.48
77.16
76.84
54.73
50.79
39.76
f1 (ppm)

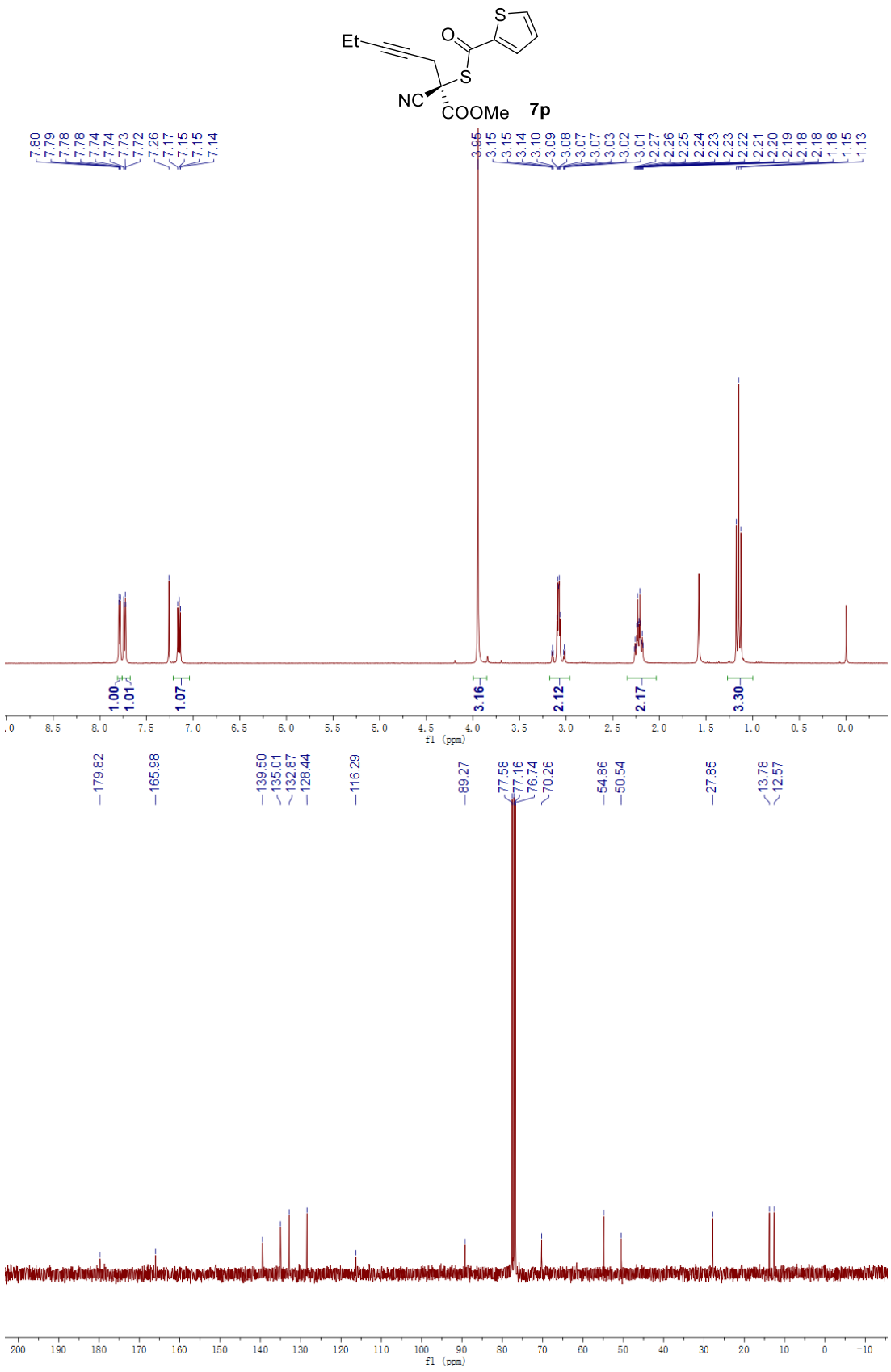
Et
O
S
S
NC
COOMe
7p
7.80
7.79
7.78
7.78
7.74
7.74
7.73
7.72
7.26
7.17
7.15
7.15
7.14
3.95
3.15
3.15
3.14
3.10
3.09
3.08
3.07
3.07
3.03
3.02
3.01
2.27
2.26
2.25
2.24
2.23
2.23
2.22
2.21
2.20
2.19
2.18
2.18
1.18
1.15
1.13
1.00
1.01
1.07
3.16
2.12
2.17
3.30
f1 (ppm)
179.82
165.98
139.50
135.01
132.87
128.44
116.29
89.27
77.58
77.16
76.74
70.26
54.86
50.54
27.85
13.78
12.57
f1 (ppm)

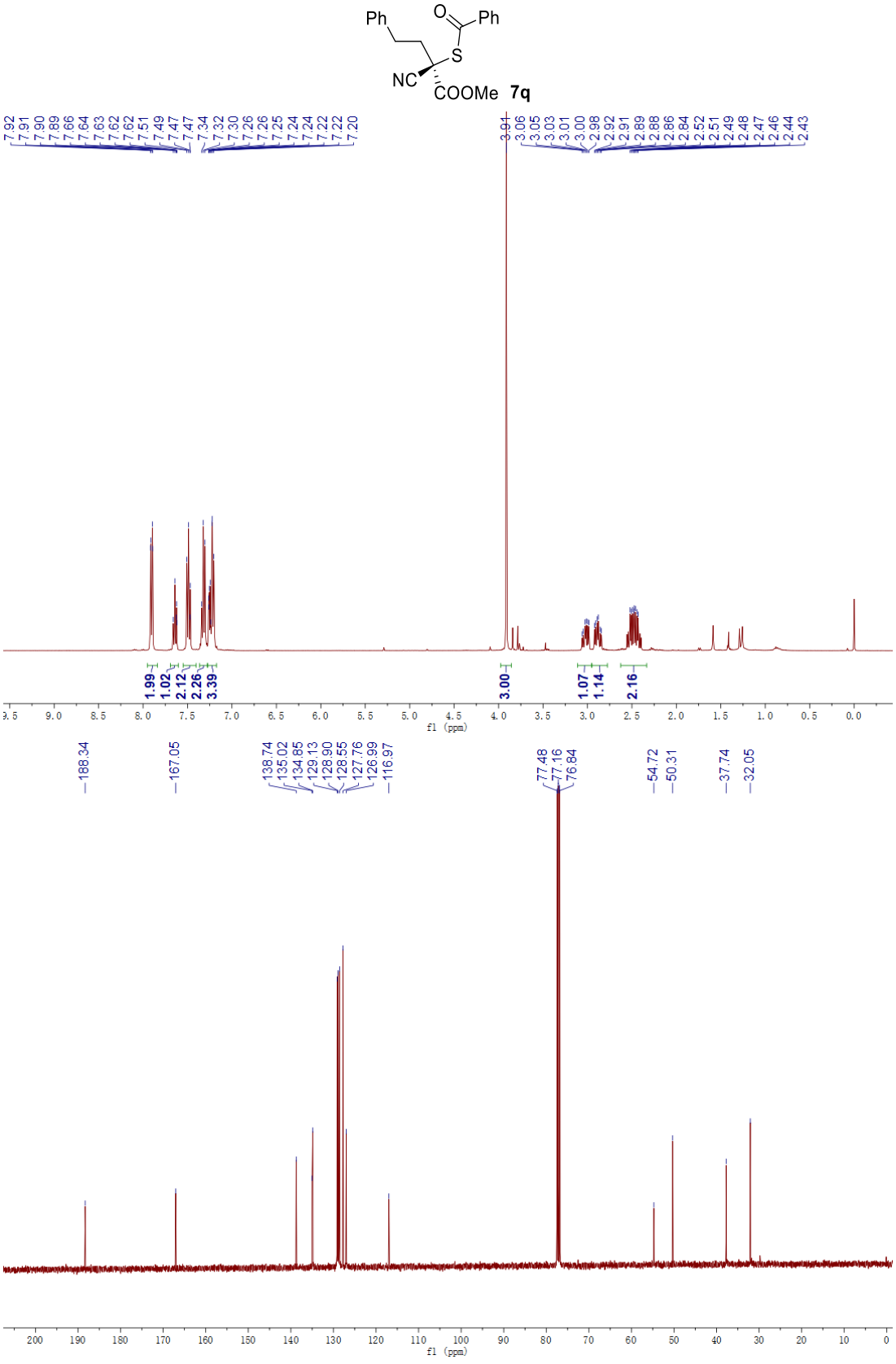
Ph
O
Ph
S
NC
COOMe
7q
7.92 7.91 7.90 7.89 7.66 7.64 7.63 7.62 7.62 7.51 7.49 7.47 7.47 7.34 7.32 7.30 7.26 7.26 7.25 7.24 7.24 7.22 7.22 7.20
3.01 3.06 3.05 3.03 3.01 3.00 2.98 2.92 2.91 2.89 2.88 2.86 2.84 2.52 2.51 2.49 2.48 2.47 2.46 2.44 2.43
1.99 1.02 2.12 2.26 3.39 3.00 1.07 1.14 2.16
f1 (ppm)
188.34 167.05 138.74 135.02 134.85 129.13 128.90 128.55 127.76 126.99 116.97 77.48 77.16 76.84 54.72 50.31 37.74 32.05
f1 (ppm)

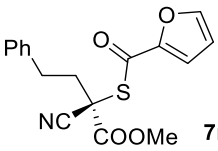
Ph
O
O
S
NC
COOMe

7r


7.65
7.65
7.65
7.65
7.36
7.36
7.34
7.33
7.32
7.30
7.30
7.29
7.29
7.28
7.28
7.27
7.24
7.24
7.22
6.64
6.63
6.63
6.63

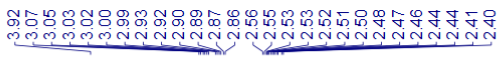
3.92
3.07
3.05
3.03
3.02
3.00
2.99
2.93
2.92
2.90
2.89
2.87
2.86
2.56
2.55
2.53
2.53
2.52
2.51
2.50
2.48
2.47
2.46
2.44
2.44
2.41
2.40

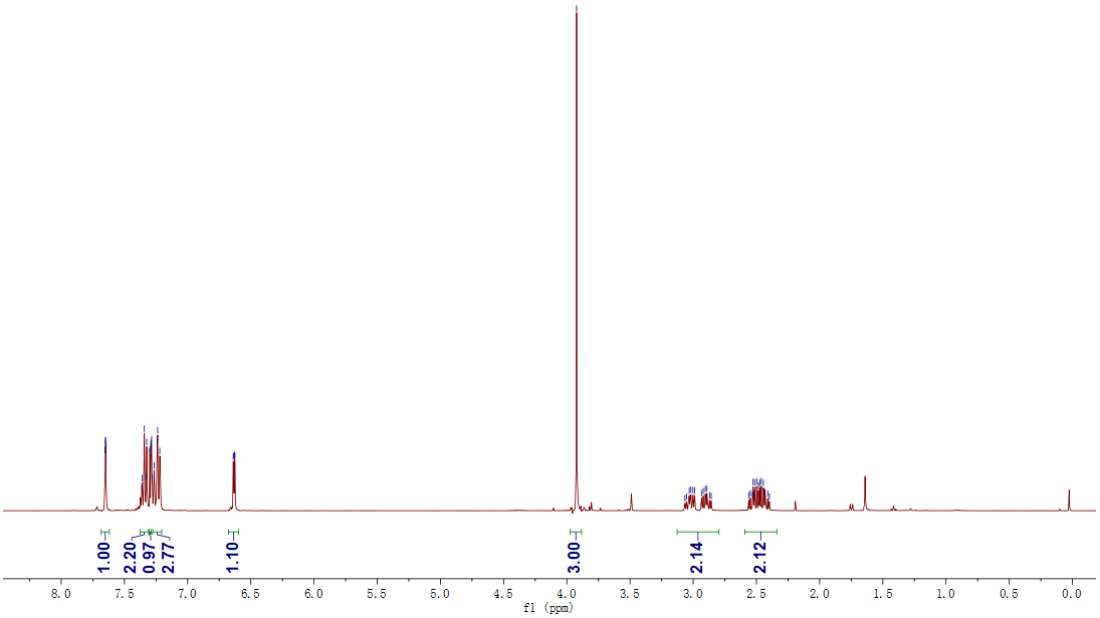
1.00
2.20
0.97
2.77
1.10
3.00
2.14
2.12
8.0
7.5
7.0
6.5
6.0
5.5
5.0
4.5
4.0
3.5
3.0
2.5
2.0
1.5
1.0
0.5
0.0
f1 (ppm)


176.54
166.88
149.11
147.53
138.66
128.88
128.53
126.99
117.69
116.80
113.15
77.48
77.16
76.84
54.71
49.75
37.71
31.96

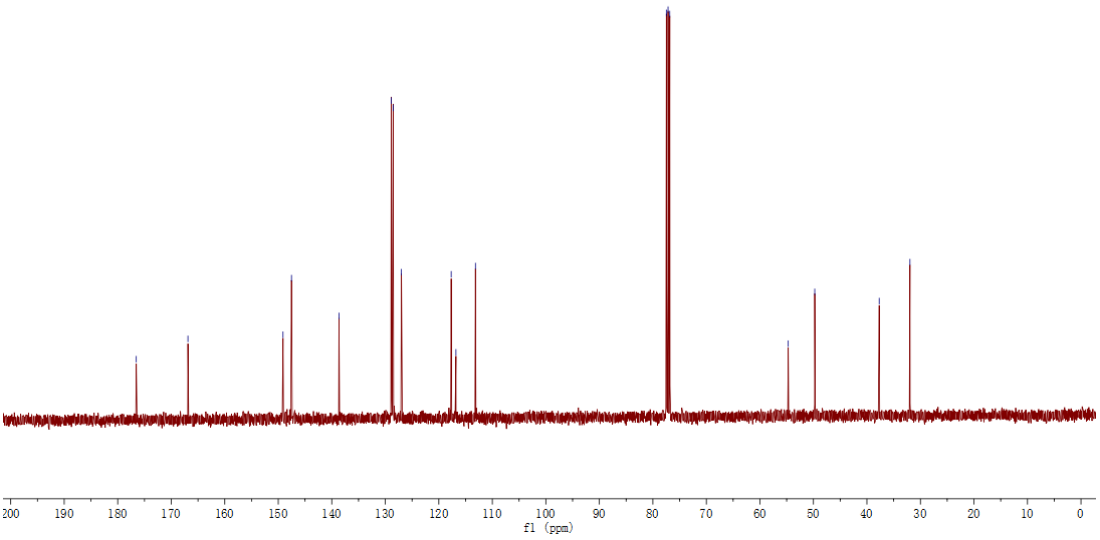
200
190
180
170
160
150
140
130
120
110
100
90
80
70
60
50
40
30
20
10
0
f1 (ppm)

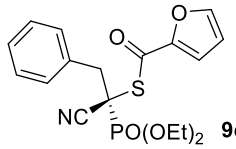
O
O
S
NC
PO(OEt)2

9c

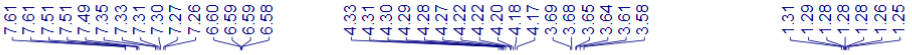
7.61
7.61
7.51
7.51
7.49
7.35
7.33
7.31
7.30
7.27
7.26
6.60
6.59
6.59
6.58
4.33
4.31
4.30
4.29
4.28
4.27
4.22
4.22
4.20
4.18
4.17
3.69
3.68
3.65
3.64
3.61
3.58
1.31
1.29
1.28
1.28
1.28
1.26
1.25

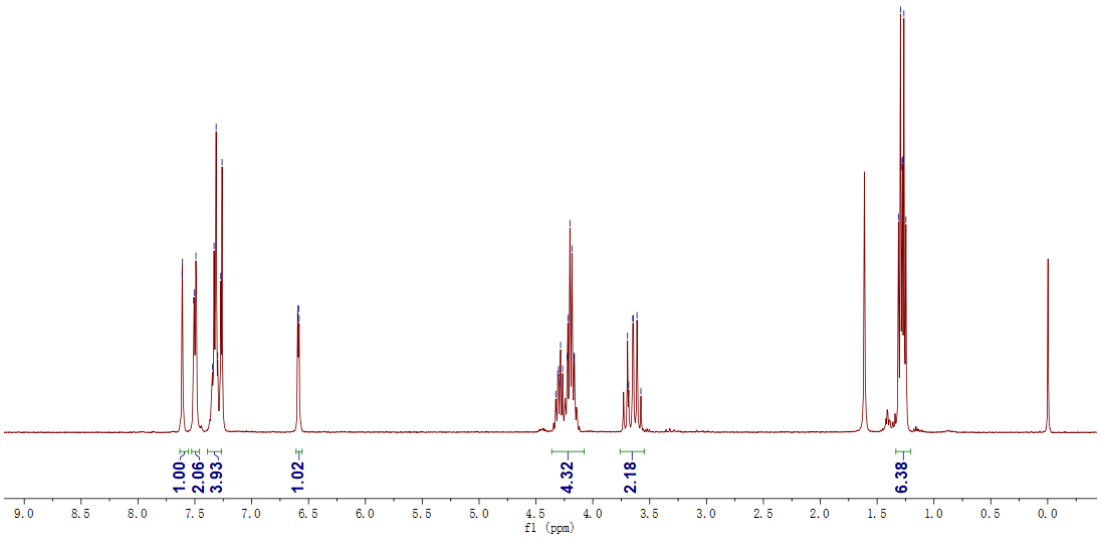
1.00
2.06
3.93
1.02
4.32
2.18
6.38
f1 (ppm)

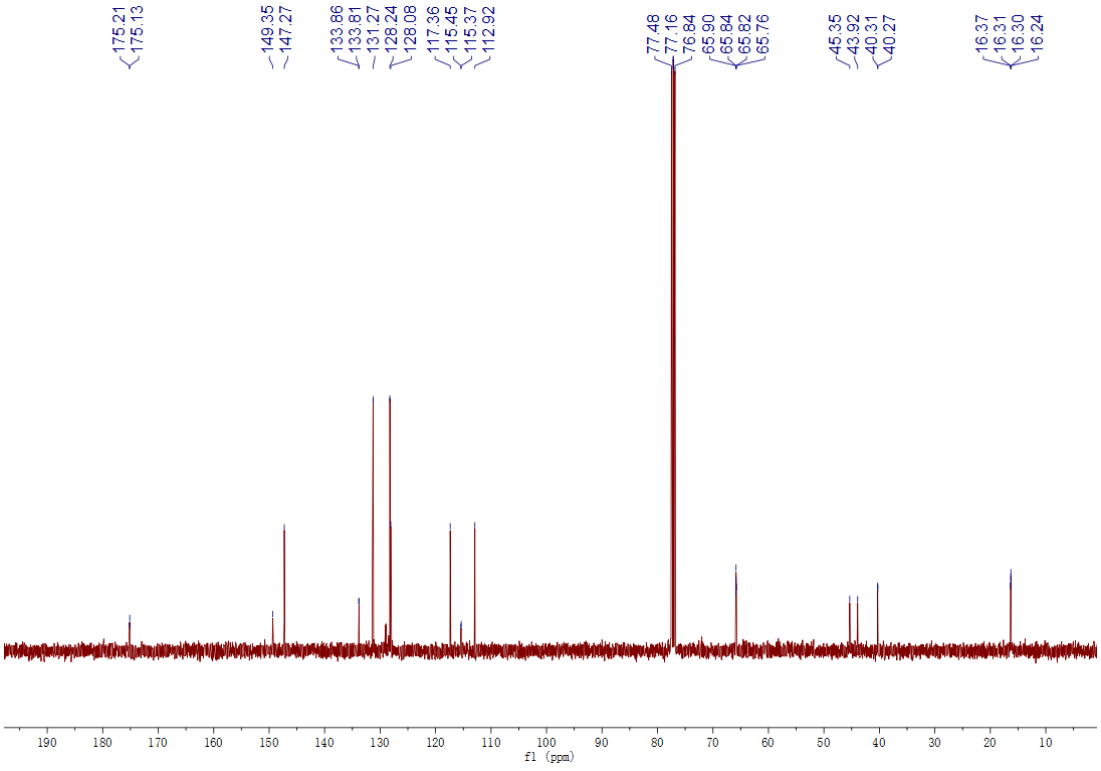
175.21
175.13
149.35
147.27
133.86
133.81
131.27
128.24
128.08
117.36
115.45
115.37
112.92
77.48
77.16
76.84
65.90
65.84
65.82
65.76
45.35
43.92
40.31
40.27
16.37
16.31
16.30
16.24
f1 (ppm)

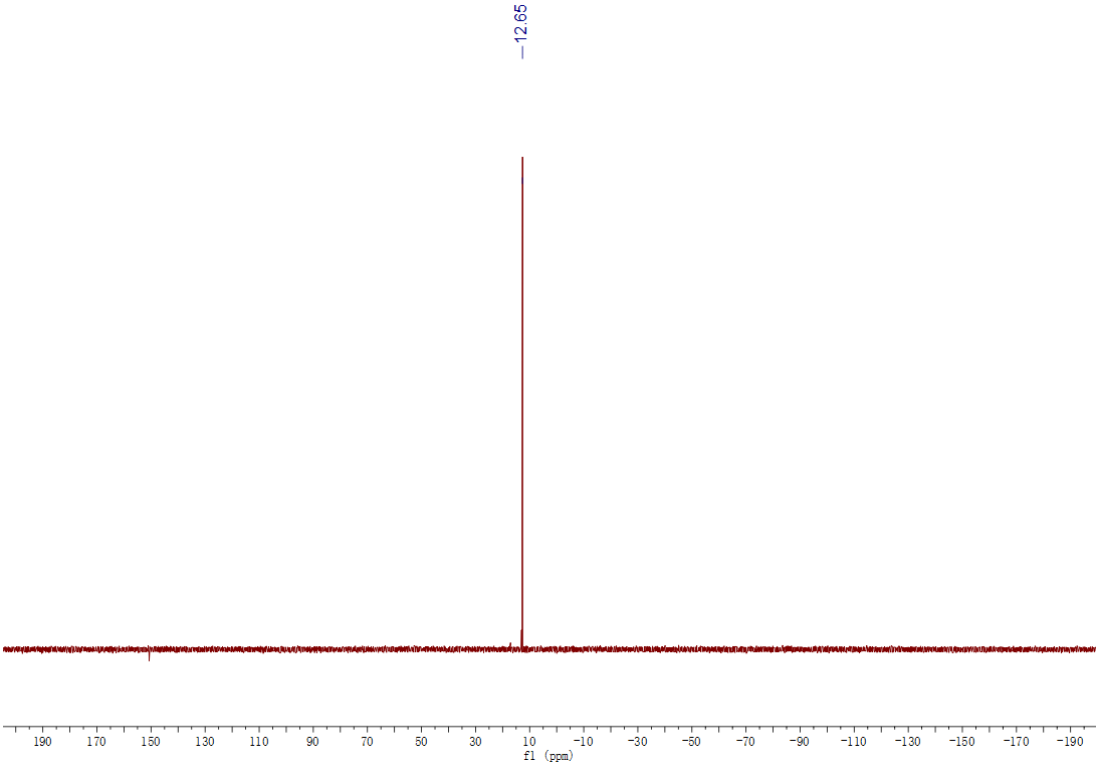
12.65
190 170 150 130 110 90 70 50 30 10 -10 -30 -50 -70 -90 -110 -130 -150 -170 -190
f1 (ppm)

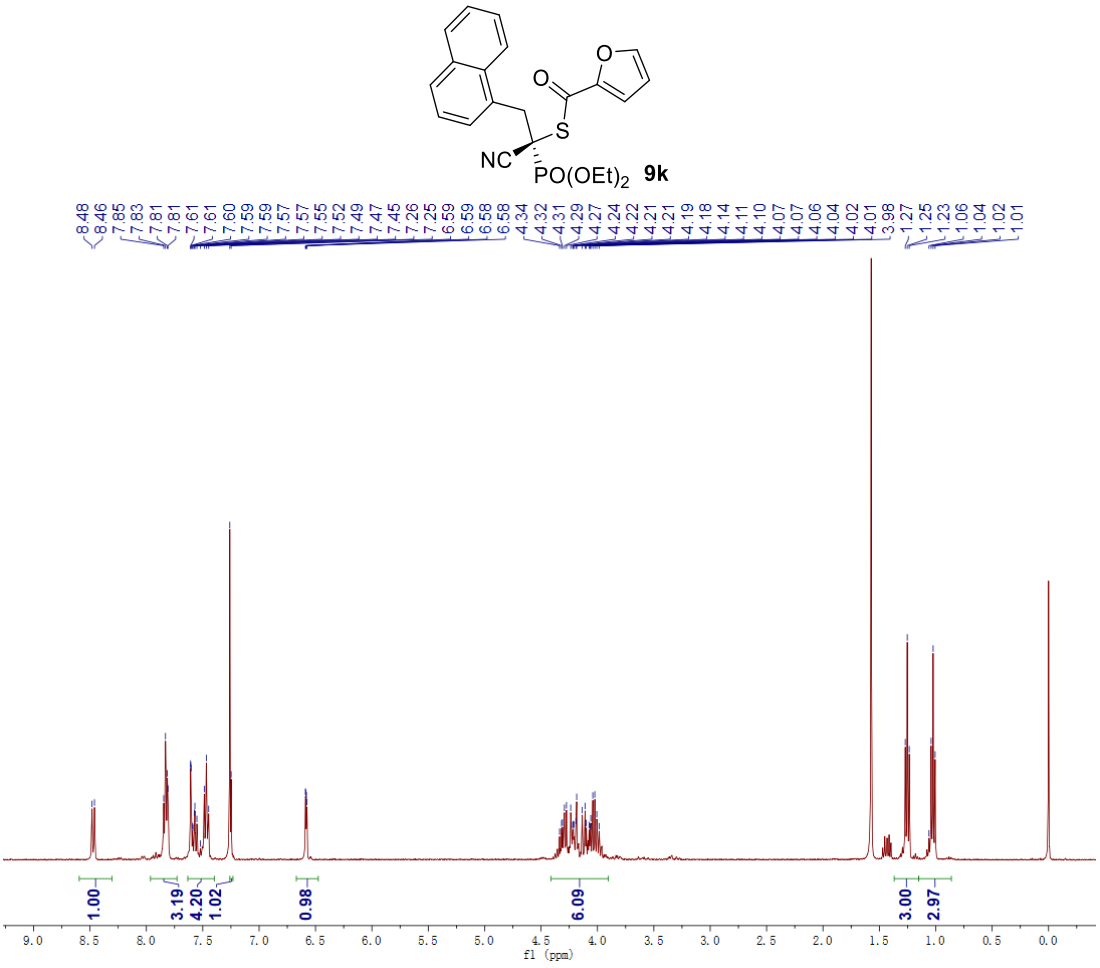
O
O
S
NC
PO(OEt)2
9k
8.48 8.46 7.85 7.83 7.81 7.81 7.61 7.61 7.60 7.59 7.59 7.57 7.57 7.55 7.52 7.49 7.47 7.45 7.26 7.25 6.59 6.59 6.58 6.58 4.34 4.32 4.31 4.29 4.27 4.24 4.22 4.21 4.21 4.19 4.18 4.14 4.11 4.10 4.07 4.07 4.06 4.04 4.02 4.01 3.98 1.27 1.25 1.23 1.06 1.04 1.02 1.01
1.00 3.19 4.20 1.02 0.98 6.09 3.00 2.97
9.0 8.5 8.0 7.5 7.0 6.5 6.0 5.5 5.0 4.5 4.0 3.5 3.0 2.5 2.0 1.5 1.0 0.5 0.0
f1 (ppm)

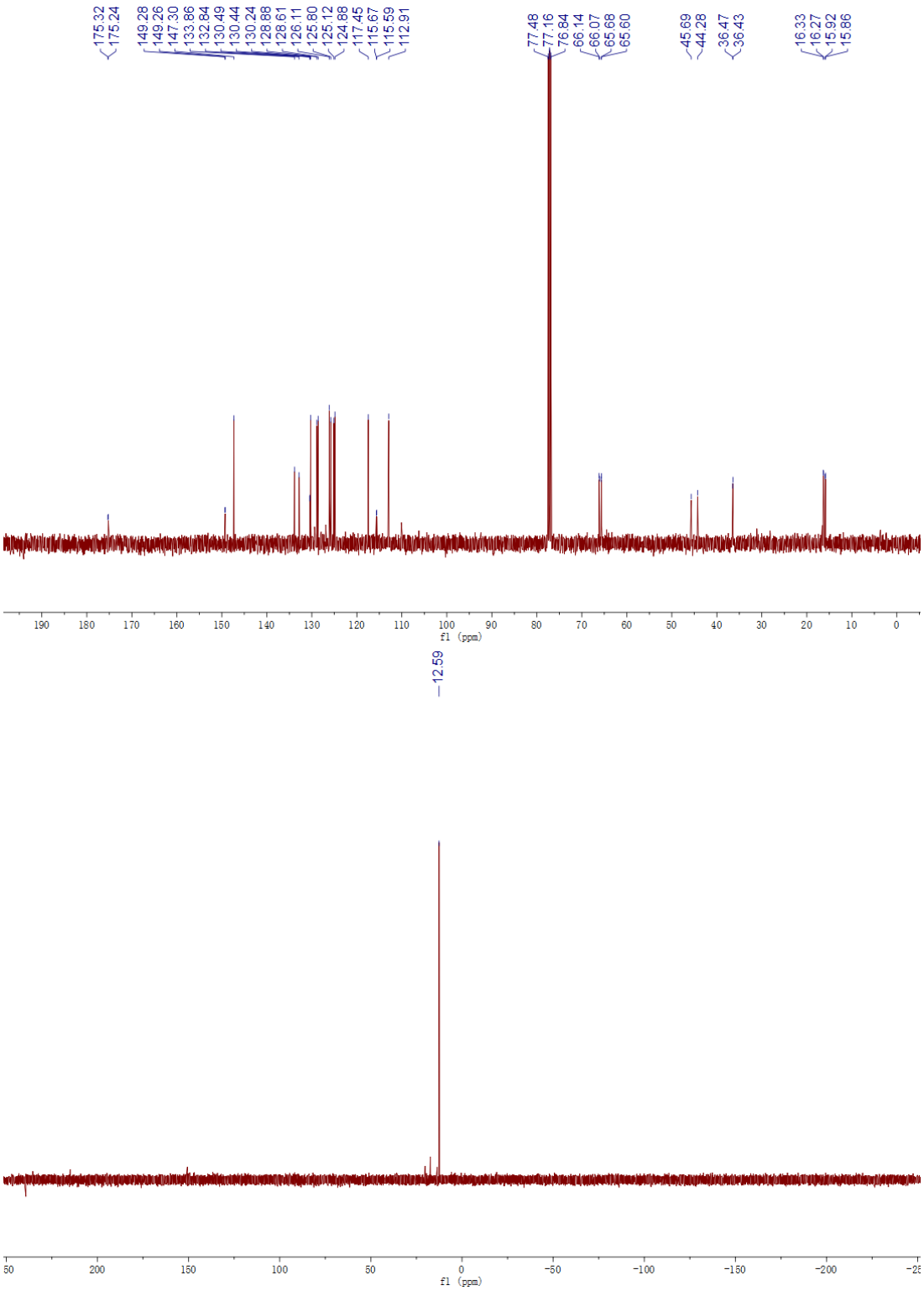
175.32
175.24
149.28
149.26
147.30
133.86
132.84
130.49
130.44
130.24
128.88
128.61
126.11
125.80
125.12
124.88
117.45
115.67
115.59
112.91
77.48
77.16
76.84
66.14
66.07
65.68
65.60
45.69
44.28
36.47
36.43
16.33
16.27
15.92
15.86
f1 (ppm)
12.59
f1 (ppm)

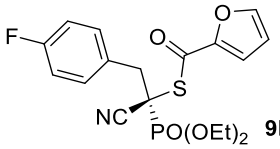
F
O
O
S
NC
PO(OEt)2

9l

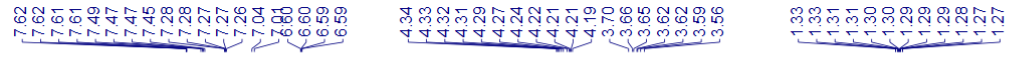
7.62
7.62
7.61
7.61
7.49
7.47
7.47
7.45
7.28
7.28
7.27
7.27
7.26
7.04
7.01
6.60
6.59
6.59
4.34
4.33
4.32
4.31
4.29
4.27
4.24
4.22
4.21
4.21
4.19
3.70
3.66
3.65
3.62
3.62
3.59
3.56
1.33
1.33
1.31
1.31
1.30
1.30
1.29
1.29
1.29
1.28
1.27
1.27

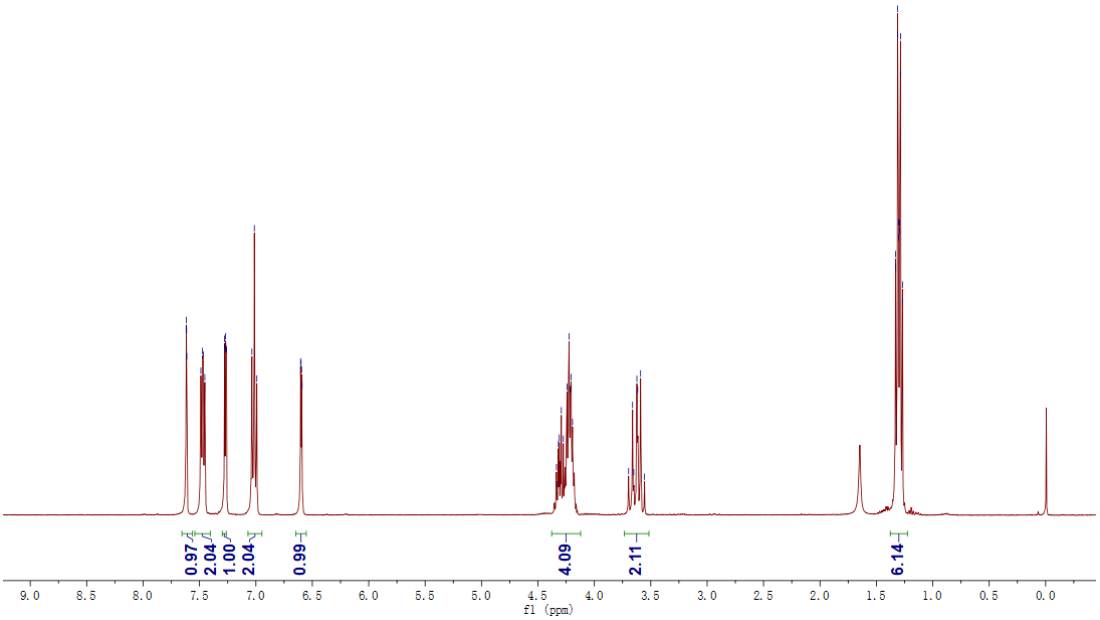
0.97
2.04
1.00
2.04
0.99
4.09
2.11
6.14
9.0
8.5
8.0
7.5
7.0
6.5
6.0
5.5
5.0
4.5
4.0
3.5
3.0
2.5
2.0
1.5
1.0
0.5
0.0
f1 (ppm)

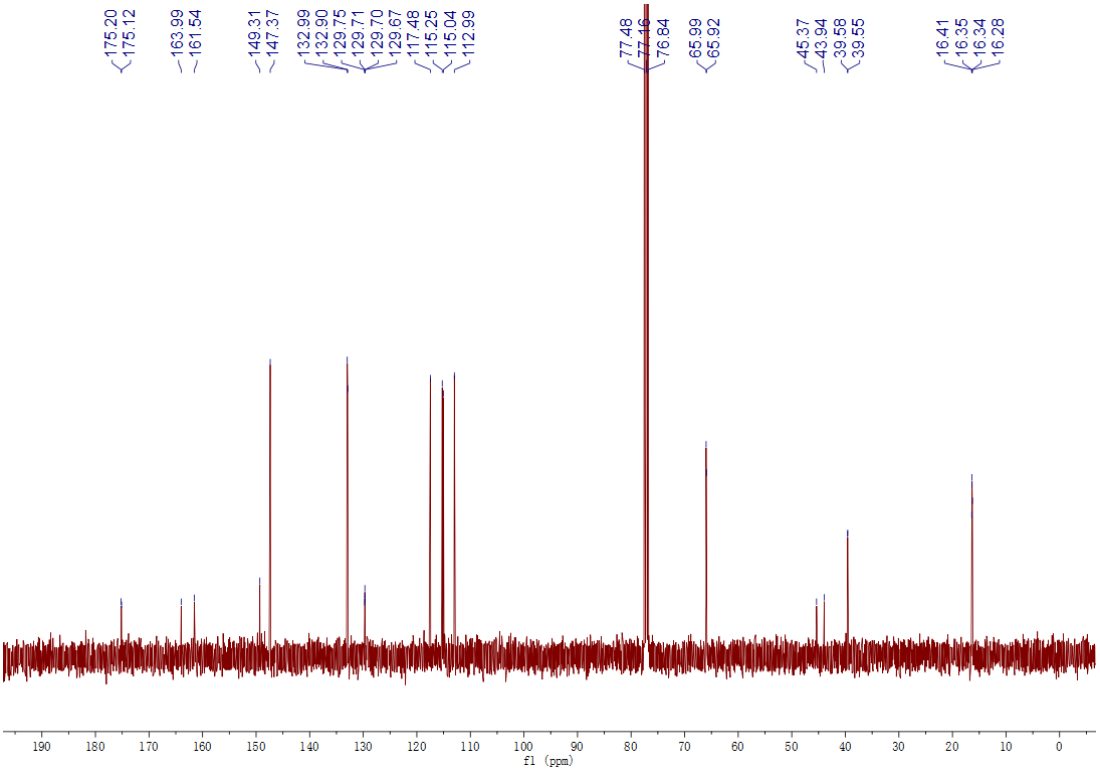
175.20
175.12
163.99
161.54
149.31
147.37
132.99
132.90
129.75
129.71
129.70
129.67
117.48
115.25
115.04
112.99
77.48
77.16
76.84
65.99
65.92
45.37
43.94
39.58
39.55
16.41
16.35
16.34
16.28
190
180
170
160
150
140
130
120
110
100
90
80
70
60
50
40
30
20
10
0
f1 (ppm)

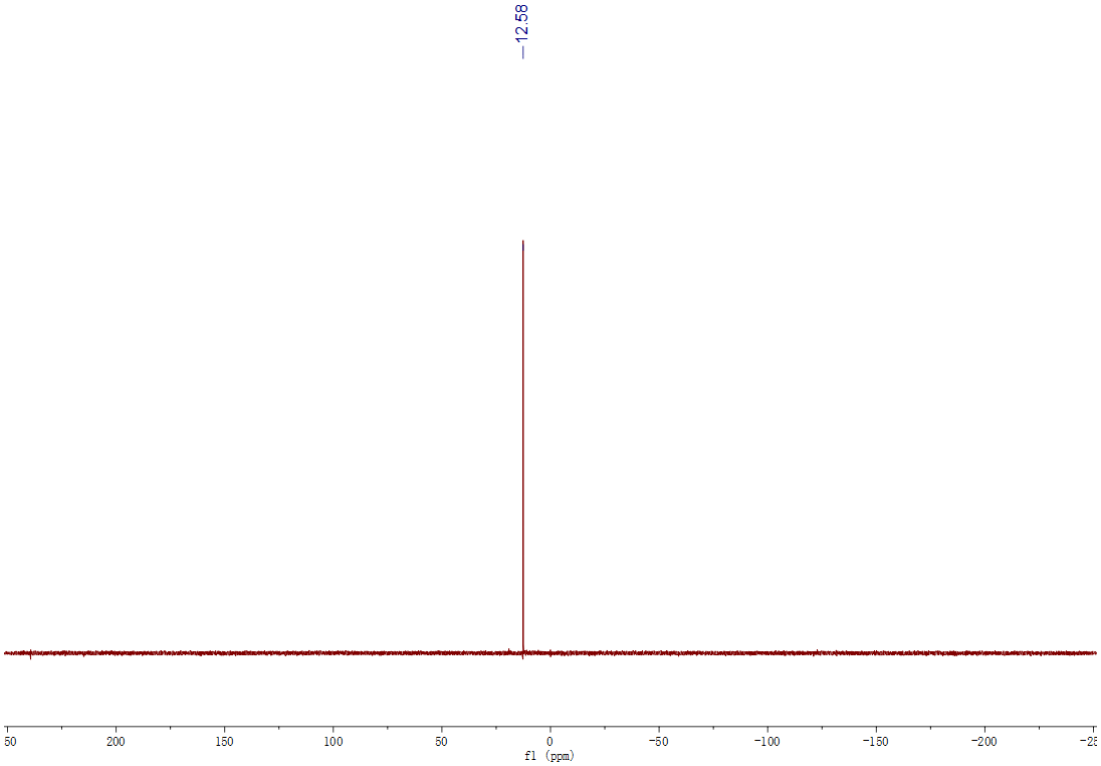

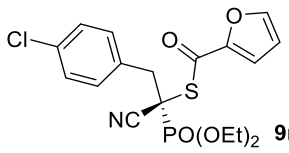

9m

7.64
7.47
7.45
7.33
7.31
7.30
7.29
7.28
6.63
6.62
6.62
6.62

4.27
4.26
4.25
4.24
4.23
4.22
3.68
3.64
3.60

1.35
1.33
1.32
1.31
1.31
1.29

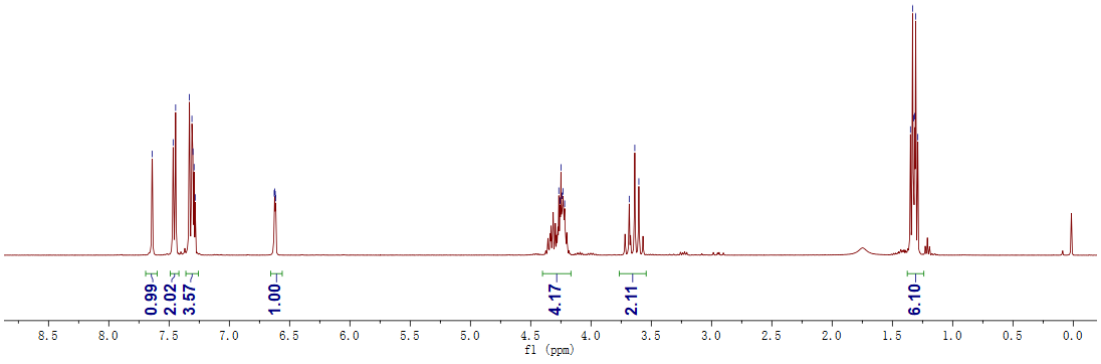

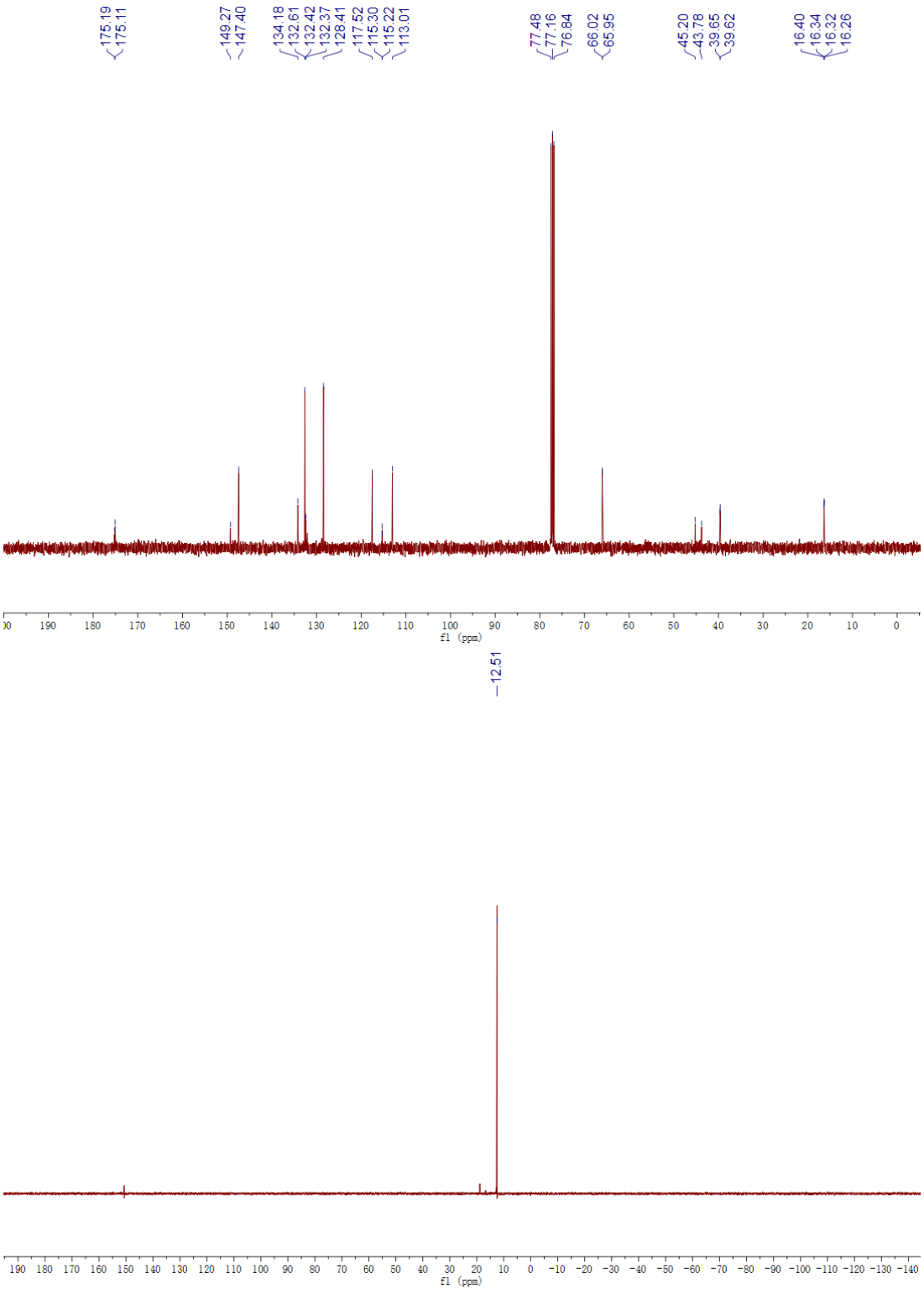
175.19
175.11
149.27
147.40
134.18
132.61
132.42
132.37
128.41
117.52
115.30
115.22
113.01
77.48
77.16
76.84
66.02
65.95
45.20
43.78
39.65
39.62
16.40
16.34
16.32
16.26
f1 (ppm)
12.51
f1 (ppm)

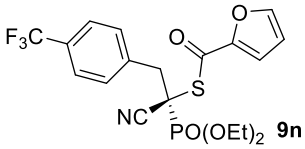
F3C
O
O
S
NC
PO(OEt)2

9n

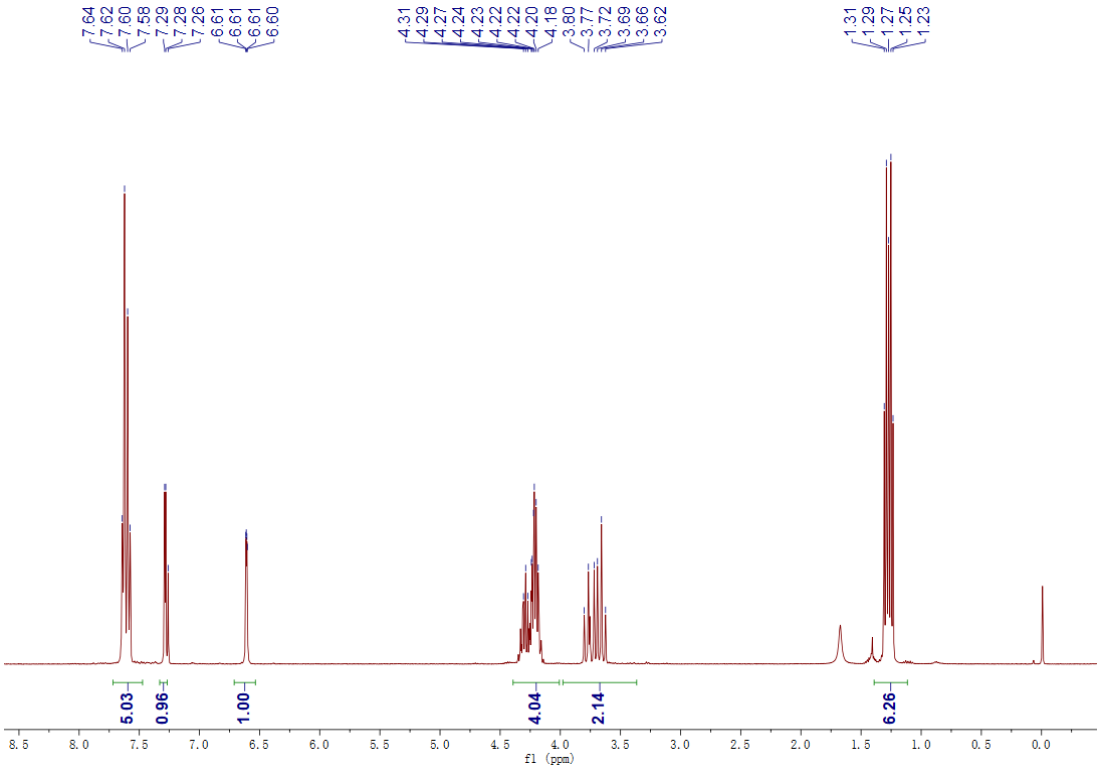
7.64
7.62
7.60
7.58
7.29
7.28
7.26
6.61
6.61
6.61
6.60
4.31
4.29
4.27
4.24
4.23
4.22
4.22
4.20
4.18
3.80
3.77
3.72
3.69
3.66
3.62
1.31
1.29
1.27
1.25
1.23
5.03
0.96
1.00
4.04
2.14
6.26
f1 (ppm)

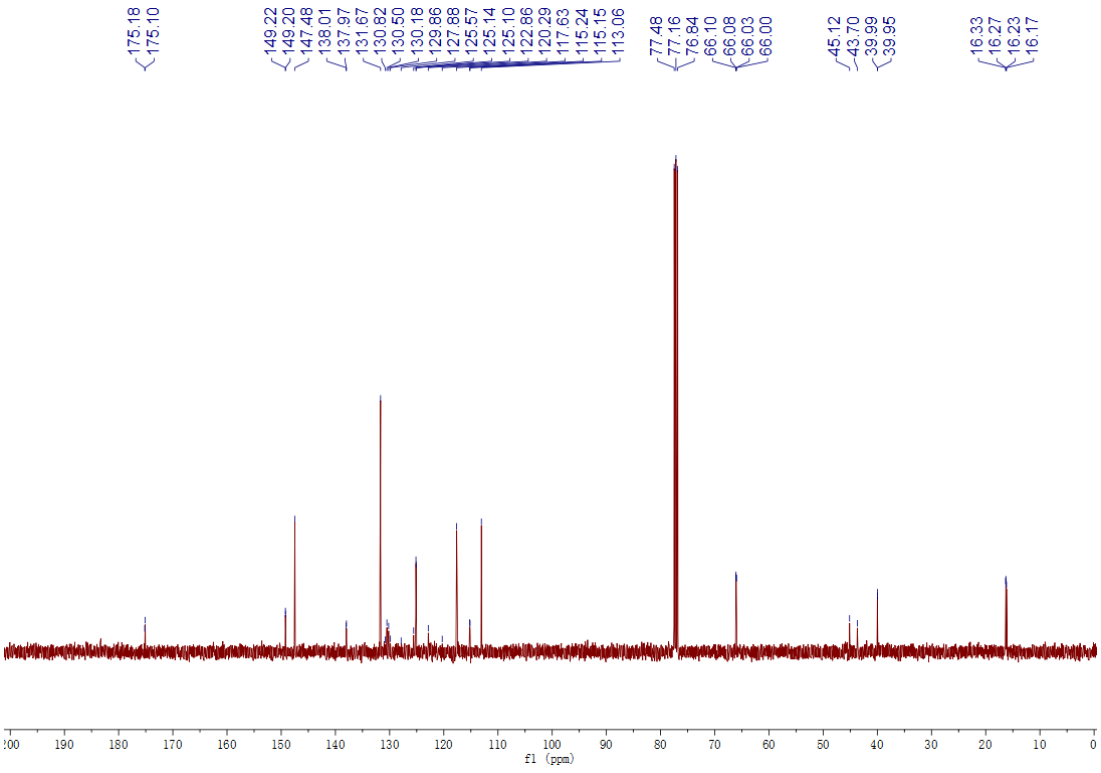
175.18
175.10
149.22
149.20
147.48
138.01
137.97
131.67
130.82
130.50
130.18
129.86
127.88
125.57
125.14
125.10
122.86
120.29
117.63
115.24
115.15
113.06
77.48
77.16
76.84
66.10
66.08
66.03
66.00
45.12
43.70
39.99
39.95
16.33
16.27
16.23
16.17
f1 (ppm)

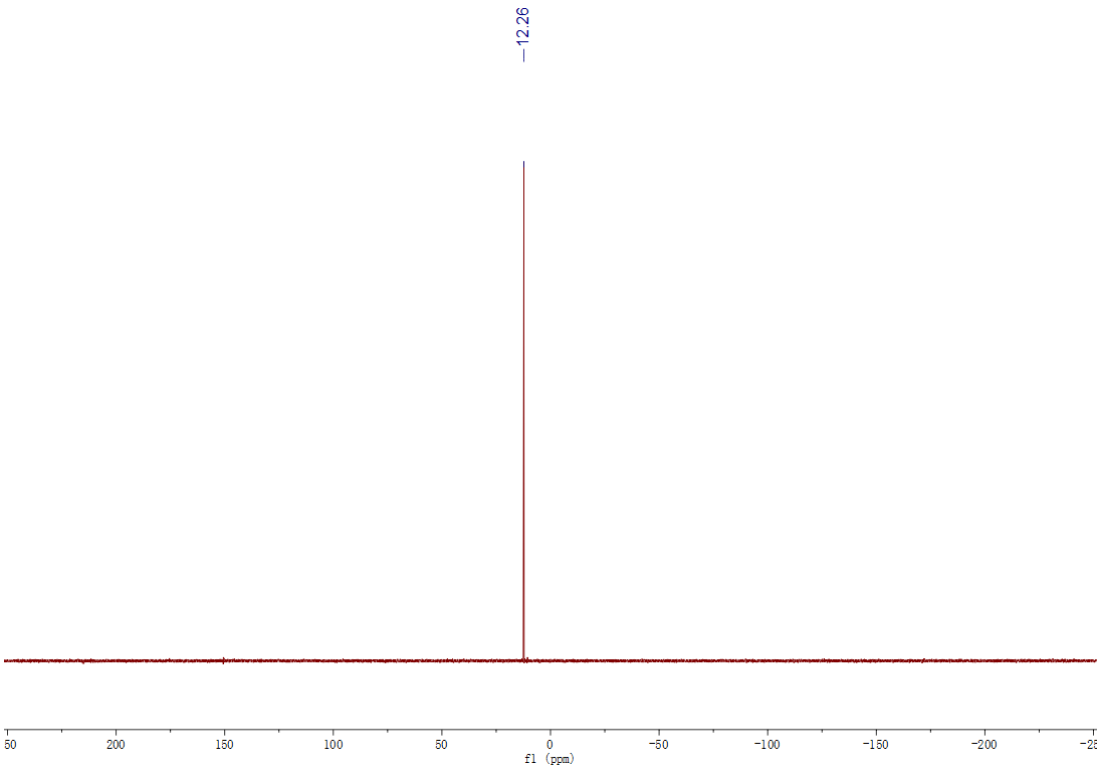
-12.26
250
200
150
100
50
0
-50
-100
-150
-200
f1 (ppm)

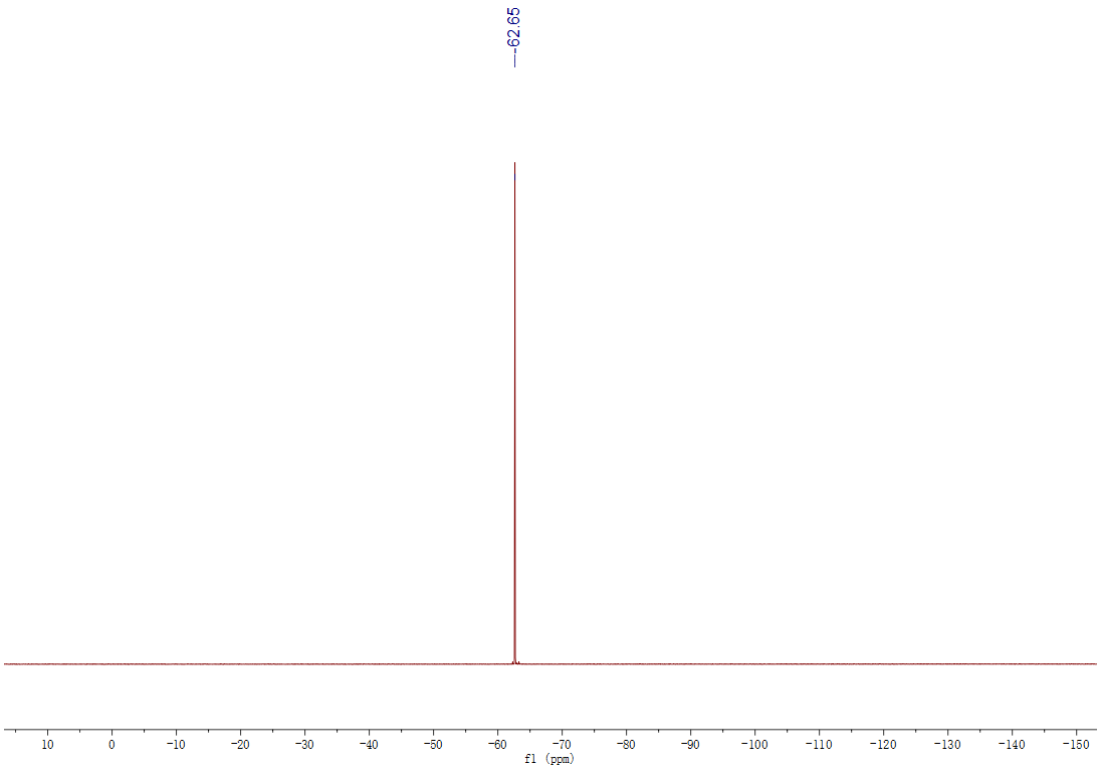
-62.65
10
0
-10
-20
-30
-40
-50
-60
-70
-80
-90
-100
-110
-120
-130
-140
-150
f1 (ppm)

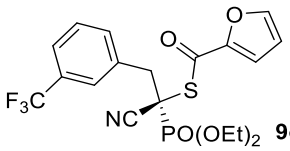
O
O
S
F3C
NC
PO(OEt)2

9o

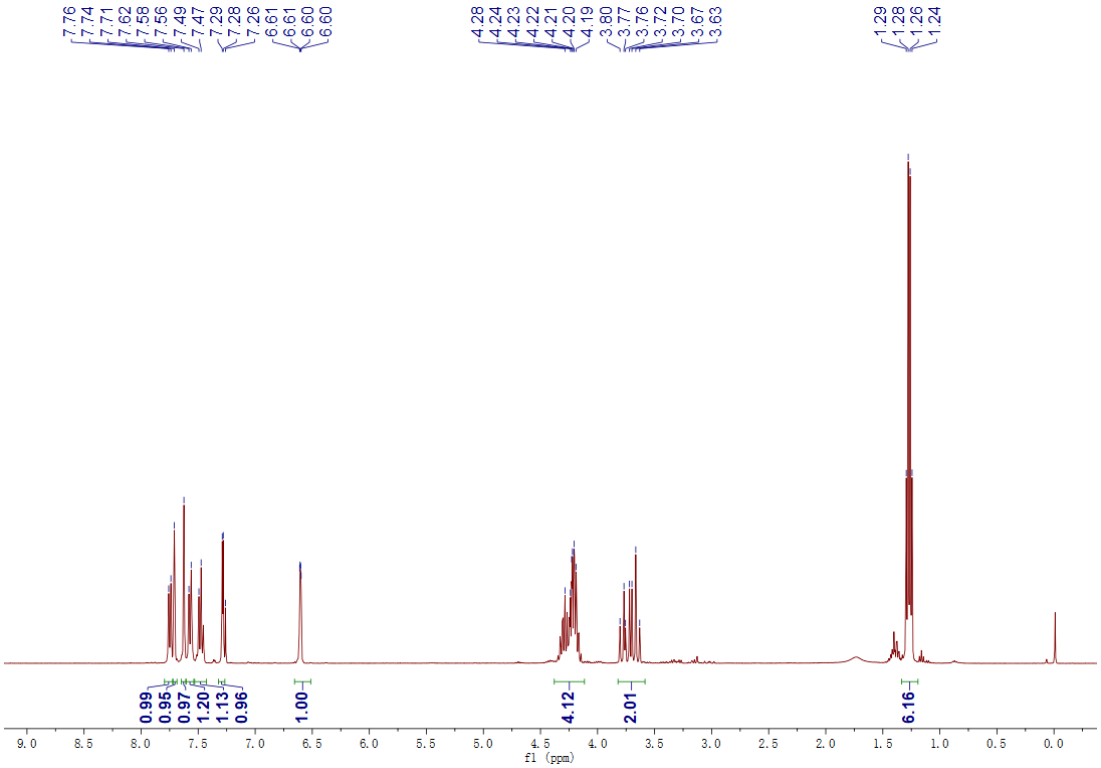
7.76
7.74
7.71
7.62
7.58
7.56
7.49
7.47
7.29
7.28
7.26
6.61
6.60
6.60
4.28
4.24
4.23
4.22
4.21
4.20
4.19
3.80
3.77
3.76
3.72
3.70
3.67
3.63
1.29
1.28
1.26
1.24
0.99
0.95
0.97
1.20
1.13
0.96
1.00
4.12
2.01
6.16
f1 (ppm)

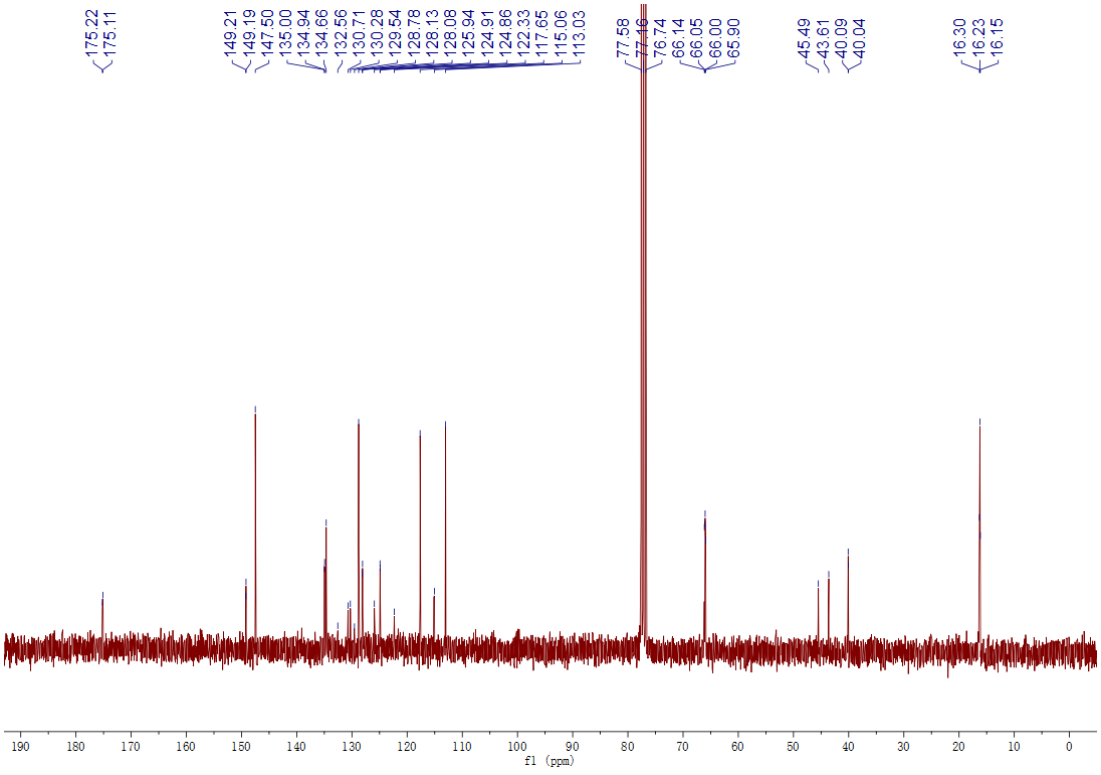
175.22
175.11
149.21
149.19
147.50
135.00
134.94
134.66
132.56
130.71
130.28
129.54
128.78
128.13
128.08
125.94
124.91
124.86
122.33
117.65
115.06
113.03
77.58
77.16
76.74
66.14
66.05
66.00
65.90
45.49
43.61
40.09
40.04
16.30
16.23
16.15
f1 (ppm)

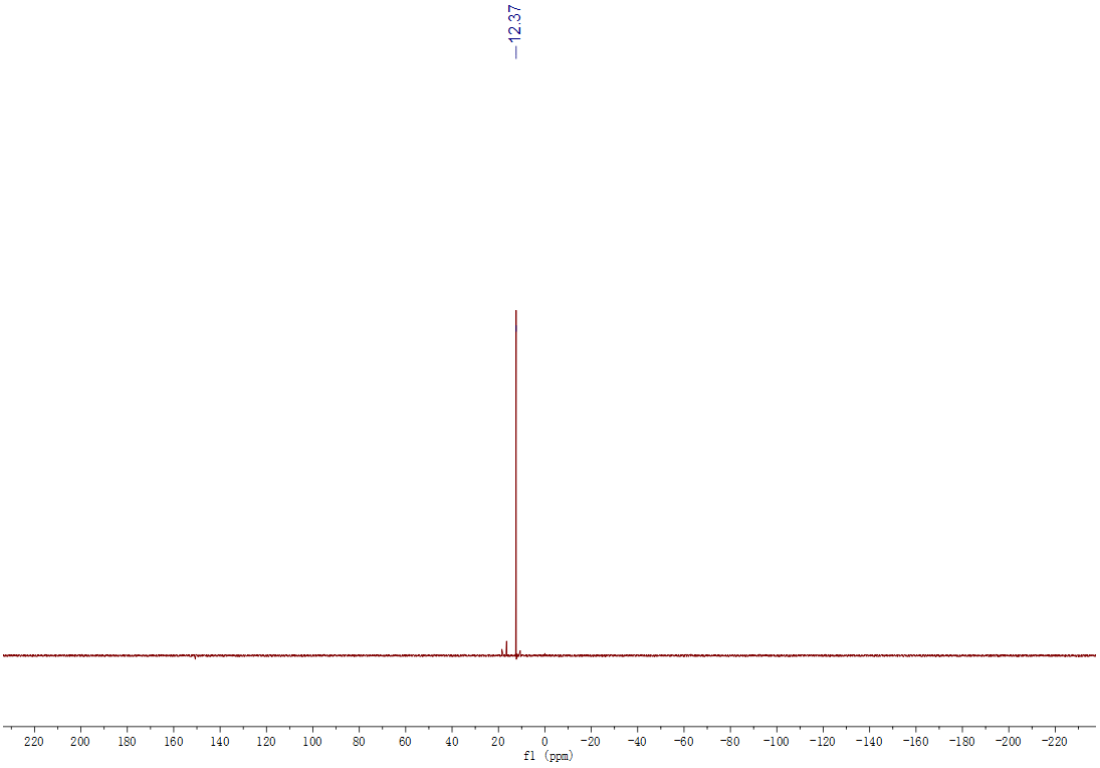
12.37
220 200 180 160 140 120 100 80 60 40 20 0 -20 -40 -60 -80 -100 -120 -140 -160 -180 -200 -220
f1 (ppm)

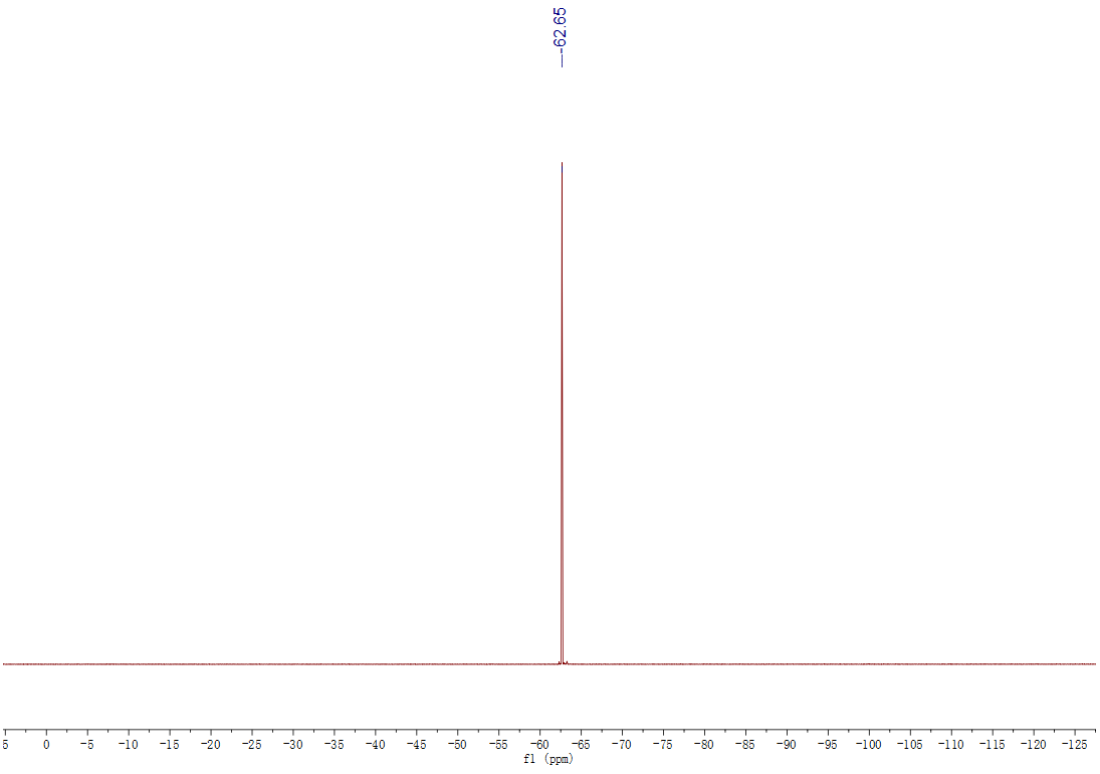
62.65
5 0 -5 -10 -15 -20 -25 -30 -35 -40 -45 -50 -55 -60 -65 -70 -75 -80 -85 -90 -95 -100 -105 -110 -115 -120 -125
f1 (ppm)

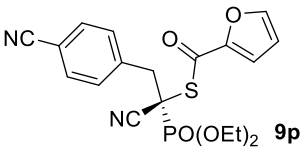
NC
O
O
S
NC
PO(OEt)2

9p

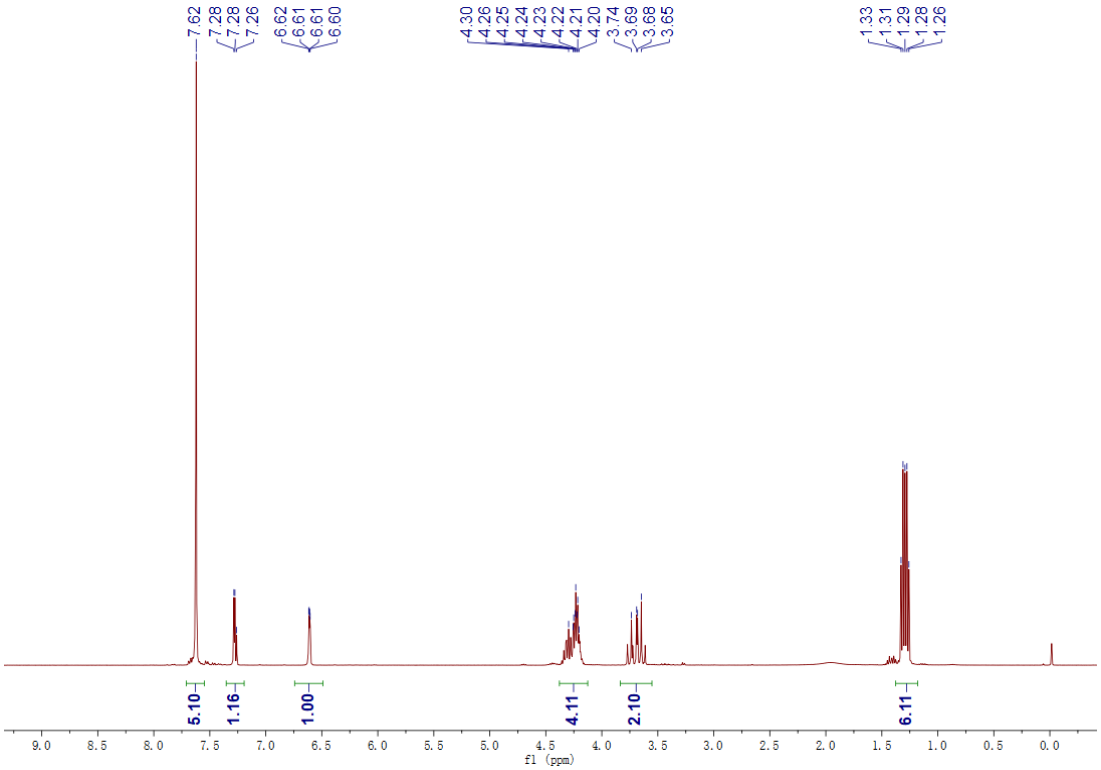
7.62
7.28
7.28
7.26
6.62
6.61
6.61
6.60
4.30
4.26
4.25
4.24
4.23
4.22
4.21
4.20
3.74
3.69
3.68
3.65
1.33
1.31
1.29
1.28
1.26
5.10
1.16
1.00
4.11
2.10
6.11
f1 (ppm)

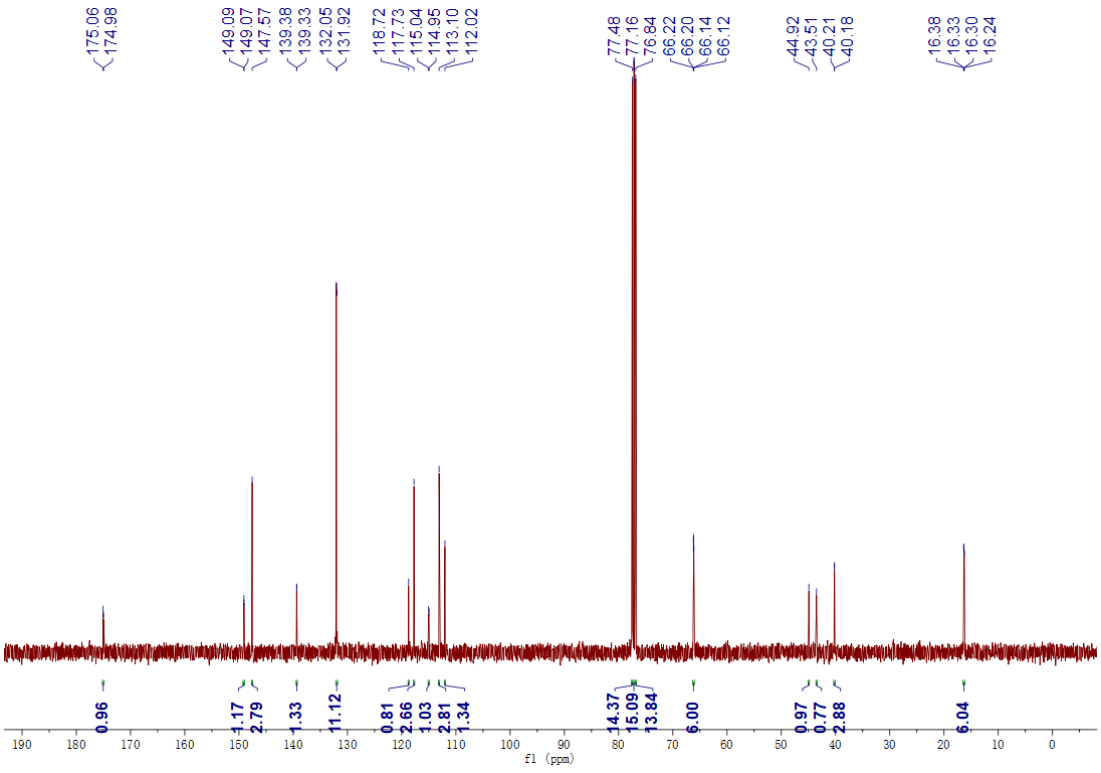
175.06
174.98
149.09
149.07
147.57
139.38
139.33
132.05
131.92
118.72
117.73
115.04
114.95
113.10
112.02
77.48
77.16
76.84
66.22
66.20
66.14
66.12
44.92
43.51
40.21
40.18
16.38
16.33
16.30
16.24
0.96
4.17
2.79
1.33
11.12
0.81
2.66
1.03
2.81
1.34
14.37
15.09
13.84
6.00
0.97
0.77
2.88
6.04
f1 (ppm)

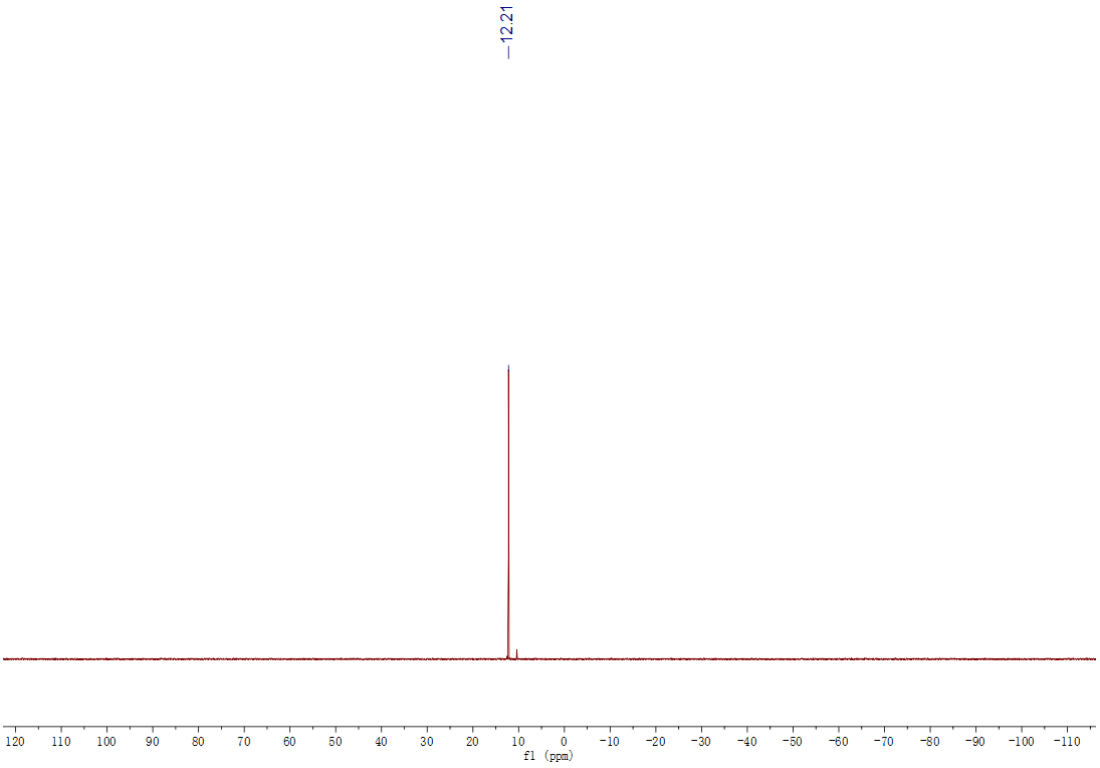
12.21
120 110 100 90 80 70 60 50 40 30 20 10 0 -10 -20 -30 -40 -50 -60 -70 -80 -90 -100 -110
f1 (ppm)

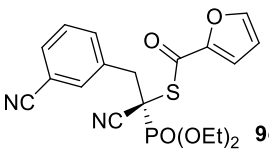
O
O
S
NC
NC
PO(OEt)2

9q

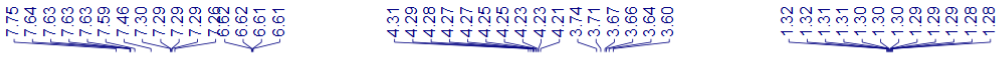
7.75 7.64 7.63 7.63 7.63 7.59 7.46 7.30 7.29 7.29 7.29 7.26 6.62 6.61 6.61
4.31 4.29 4.28 4.27 4.27 4.25 4.25 4.23 4.23 4.21 3.74 3.71 3.67 3.66 3.64 3.60
1.32 1.32 1.31 1.31 1.30 1.30 1.30 1.29 1.29 1.29 1.28 1.28

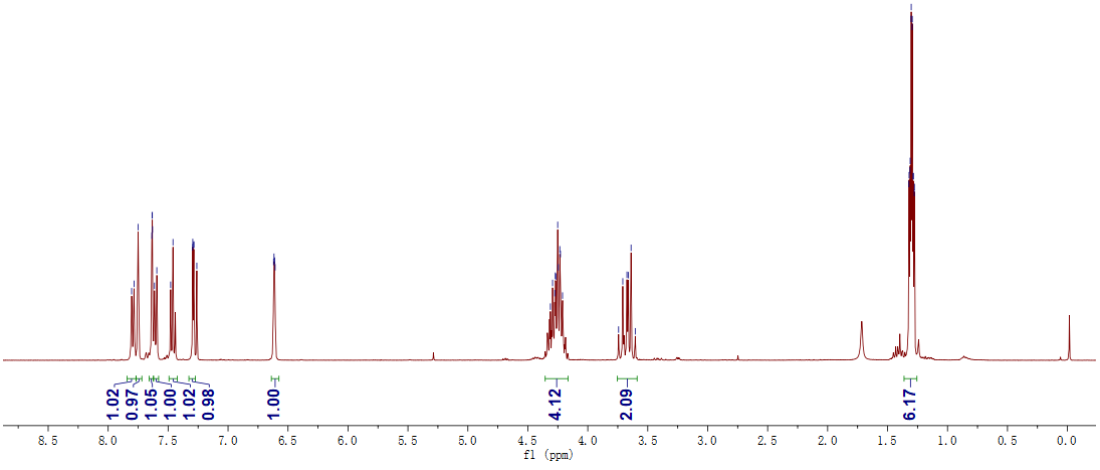
1.02 0.97 1.05 1.00 1.02 0.98 1.00 4.12 2.09 6.17
8.5 8.0 7.5 7.0 6.5 6.0 5.5 5.0 4.5 4.0 3.5 3.0 2.5 2.0 1.5 1.0 0.5 0.0
f1 (ppm)

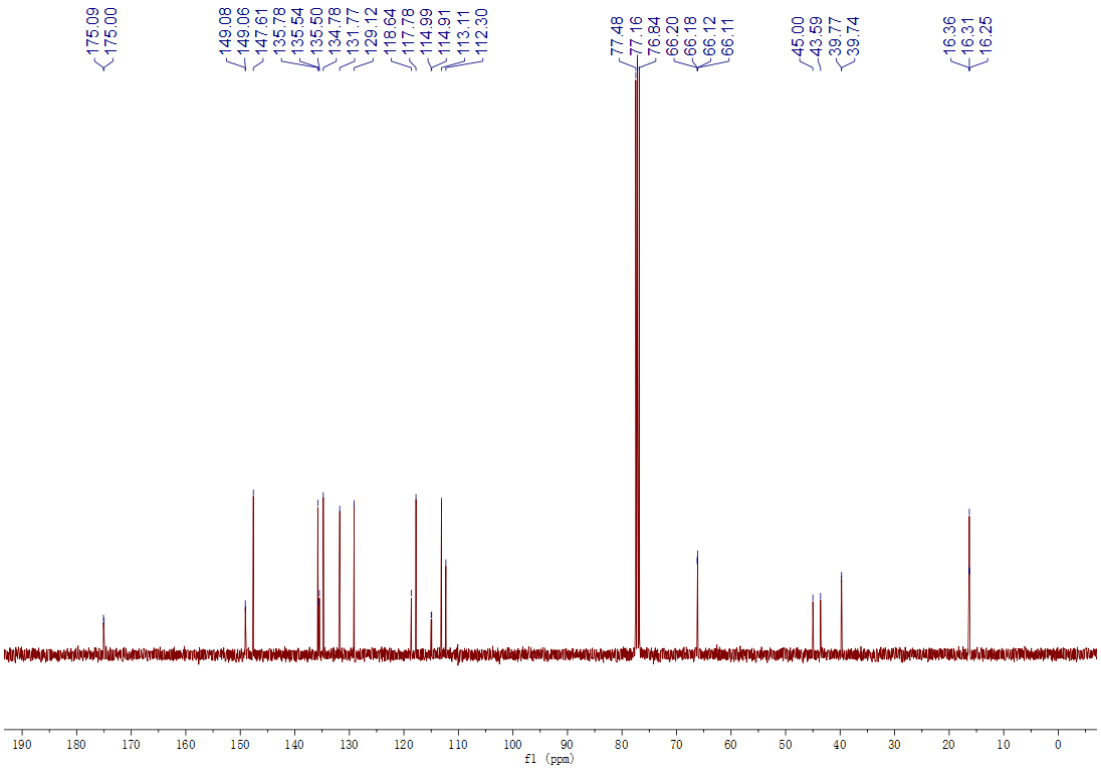
175.09
175.00
149.08
149.06
147.61
135.78
135.54
135.50
134.78
131.77
129.12
118.64
117.78
114.99
114.91
113.11
112.30
77.48
77.16
76.84
66.20
66.18
66.12
66.11
45.00
43.59
39.77
39.74
16.36
16.31
16.25
190 180 170 160 150 140 130 120 110 100 90 80 70 60 50 40 30 20 10 0
f1 (ppm)

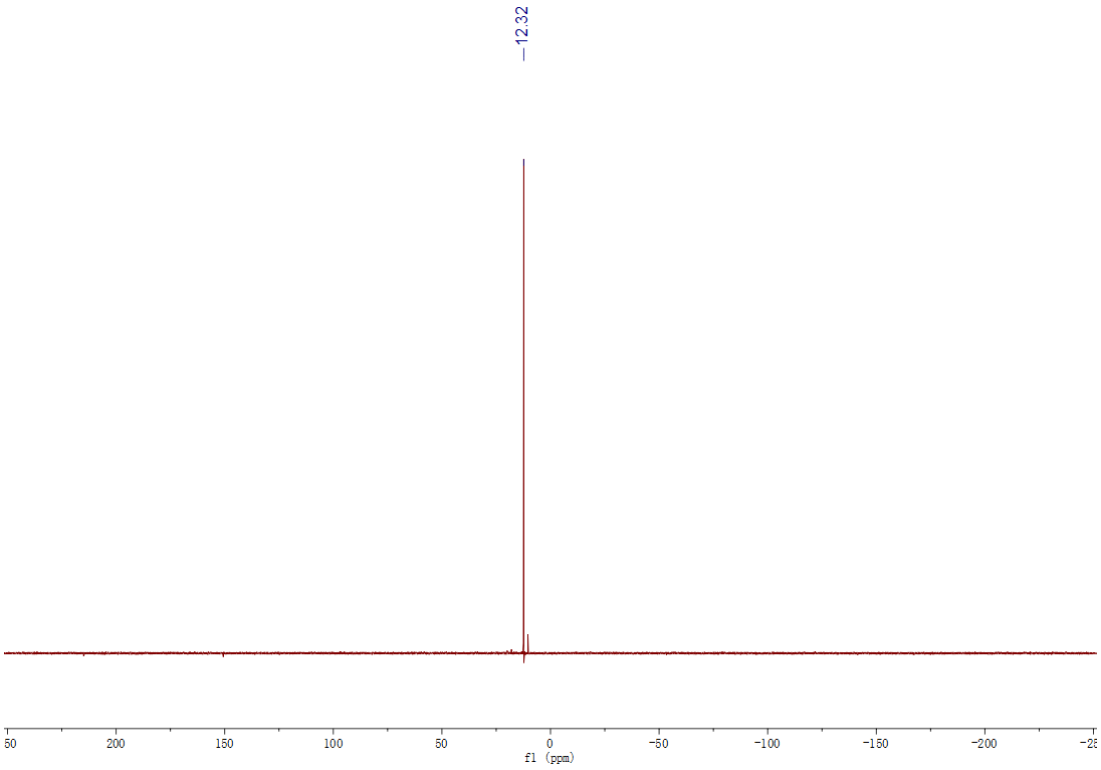
12.32
50 200 150 100 50 0 -50 -100 -150 -200
f1 (ppm)

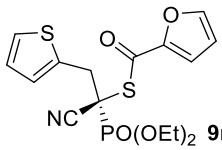
S
O
O
S
NC
PO(OEt)2

9r


7.61
7.61
7.28
7.27
7.26
7.25
7.25
7.24
7.24
7.18
6.98
6.97
6.97
6.96
6.60
6.59
6.59
6.58
4.31
4.30
4.29
4.28
4.27
4.26
4.26
4.26
4.24
4.22
3.92
3.89
1.35
1.34
1.32
1.32
1.31
1.29

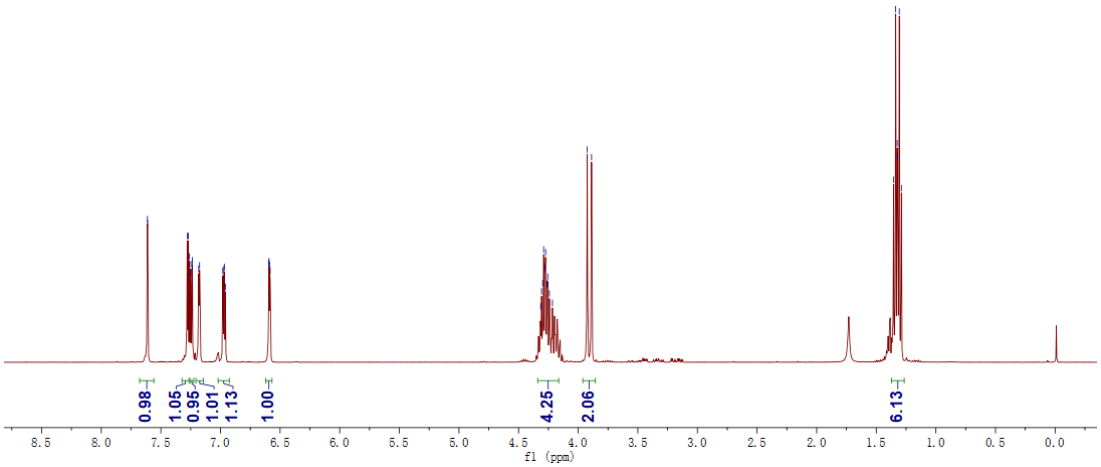
0.98
1.05
0.95
1.01
1.13
1.00
4.25
2.06
6.13
f1 (ppm)

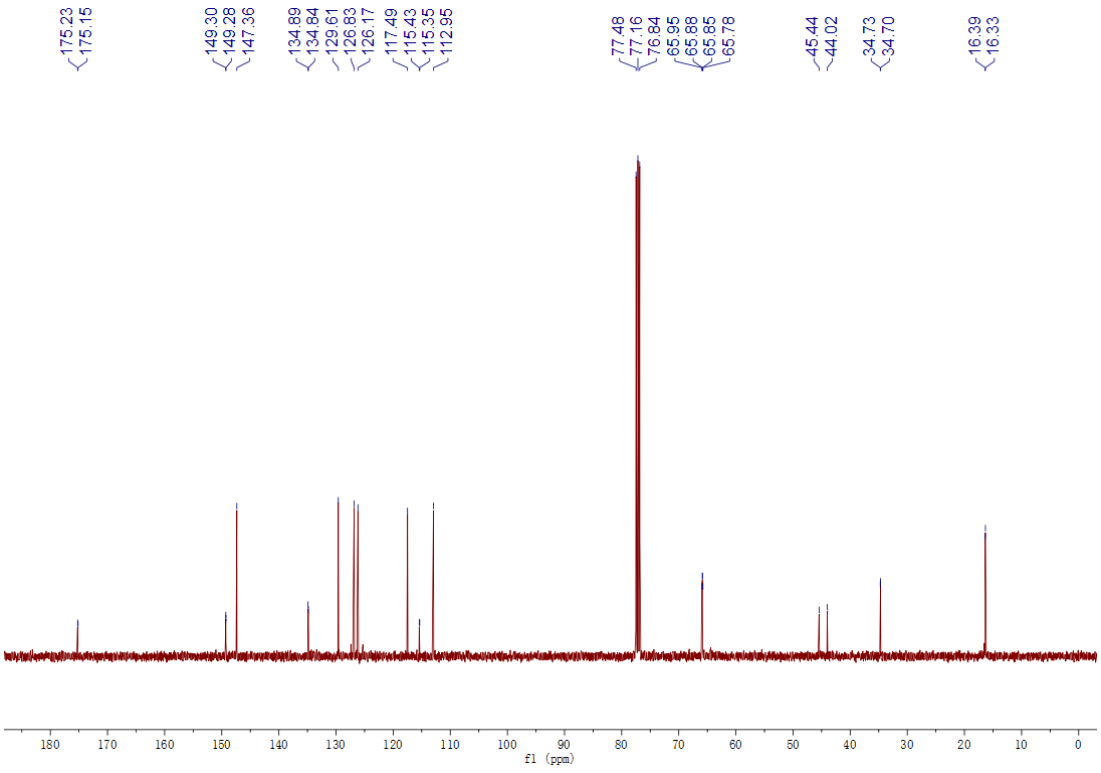
175.23
175.15
149.30
149.28
147.36
134.89
134.84
129.61
126.83
126.17
117.49
115.43
115.35
112.95
77.48
77.16
76.84
65.95
65.88
65.85
65.78
45.44
44.02
34.73
34.70
16.39
16.33
f1 (ppm)

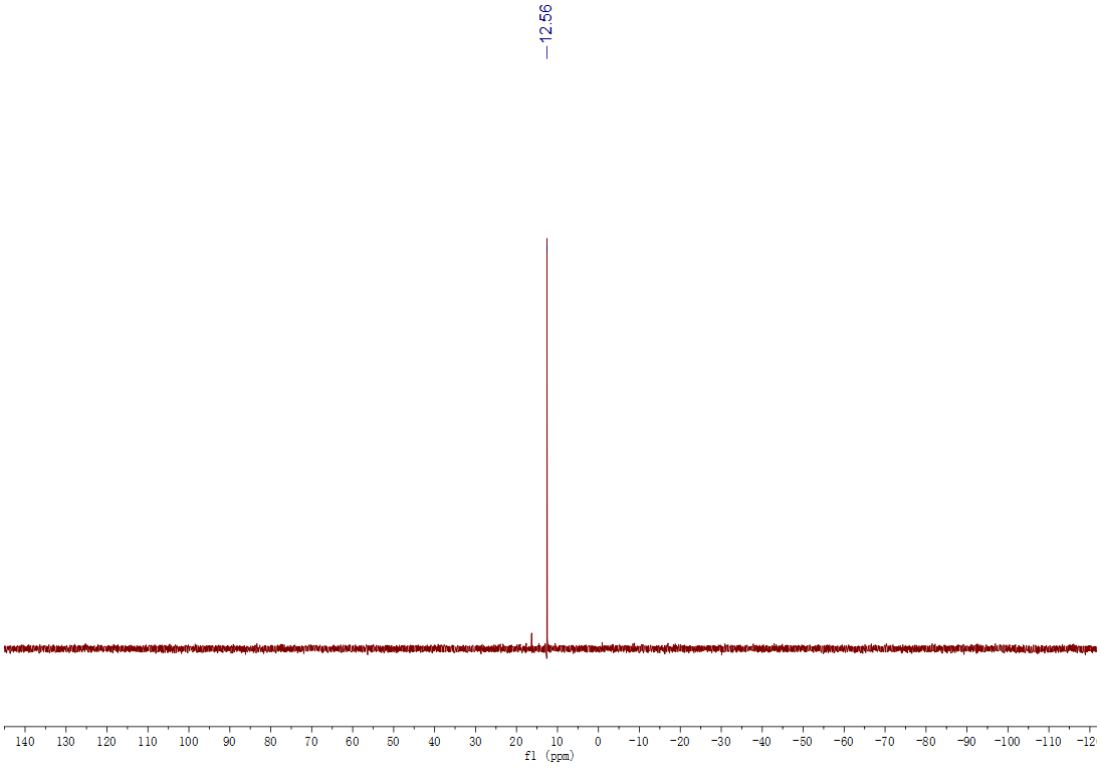
12.56
140 130 120 110 100 90 80 70 60 50 40 30 20 10 0 -10 -20 -30 -40 -50 -60 -70 -80 -90 -100 -110 -12
f1 (ppm)

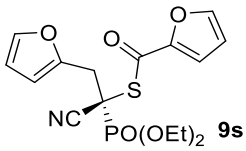
O
O
O
S
NC
PO(OEt)2

9s

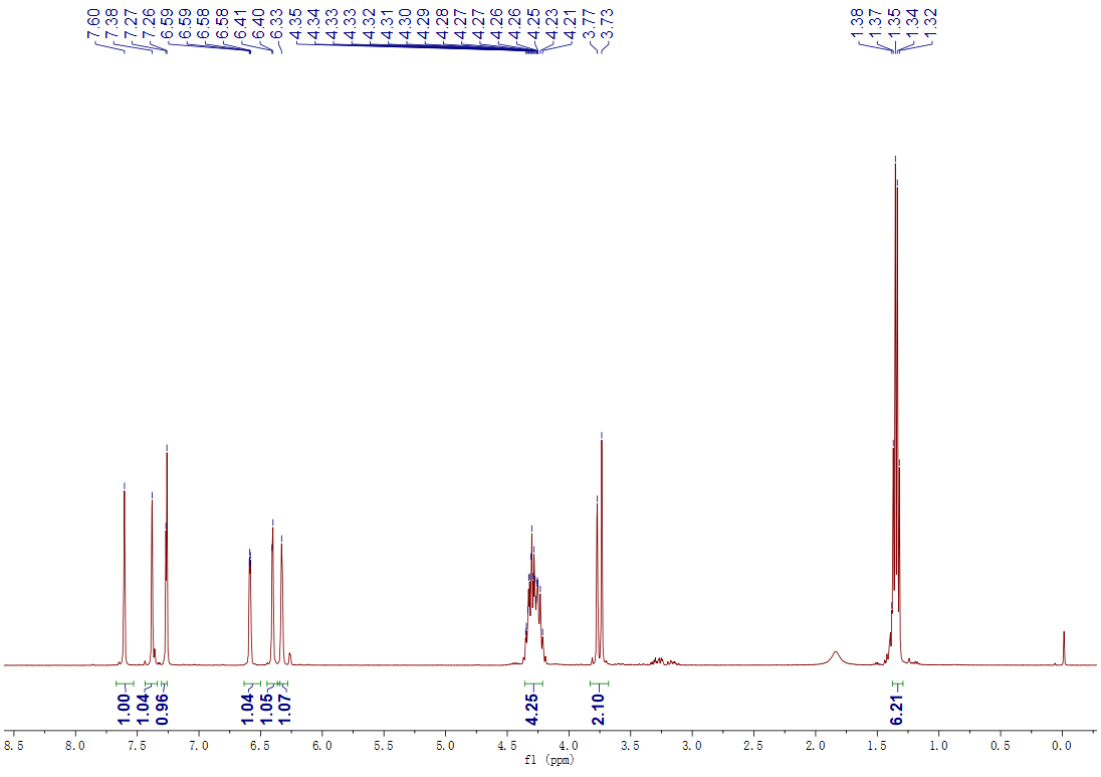
7.60
7.38
7.27
7.26
6.59
6.59
6.58
6.58
6.41
6.40
6.33
4.35
4.34
4.33
4.33
4.32
4.31
4.30
4.29
4.28
4.27
4.27
4.26
4.26
4.25
4.23
4.21
3.77
3.73
1.38
1.37
1.35
1.34
1.32
1.00
1.04
0.96
1.04
1.05
1.07
4.25
2.10
6.21
8.5 8.0 7.5 7.0 6.5 6.0 5.5 5.0 4.5 4.0 3.5 3.0 2.5 2.0 1.5 1.0 0.5 0.0
f1 (ppm)

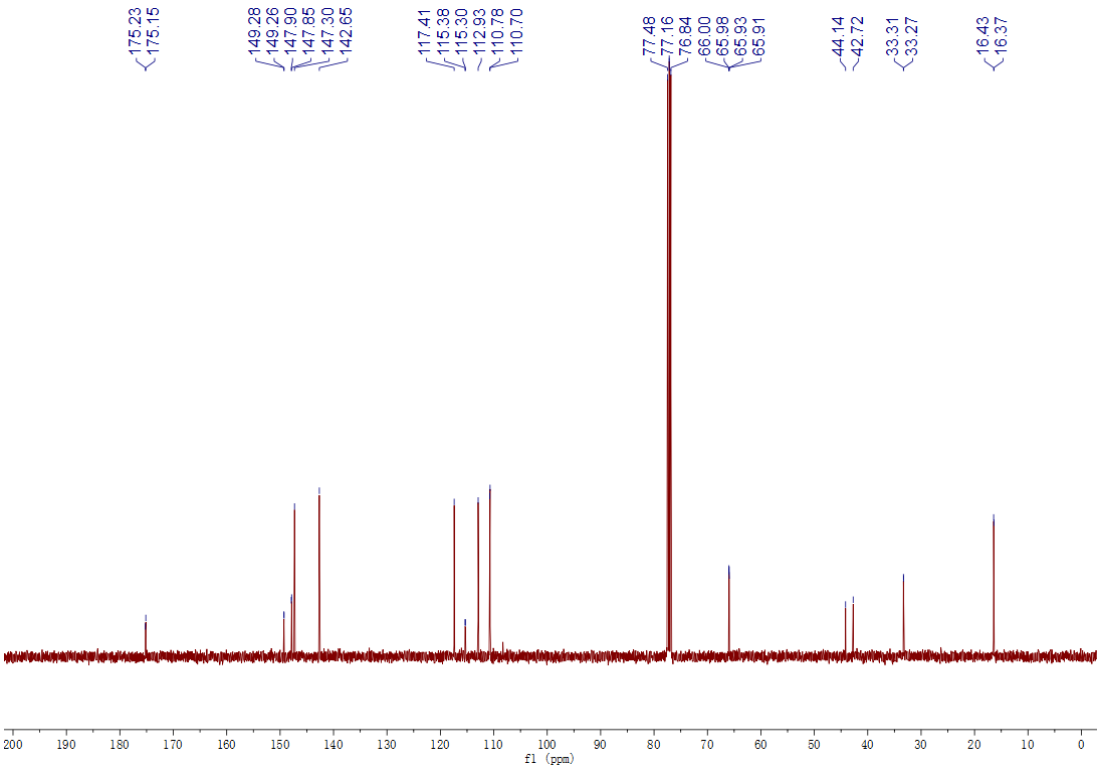
175.23
175.15
149.28
149.26
147.90
147.85
147.30
142.65
117.41
115.38
115.30
112.93
110.78
110.70
77.48
77.16
76.84
66.00
65.98
65.93
65.91
44.14
42.72
33.31
33.27
16.43
16.37
f1 (ppm)

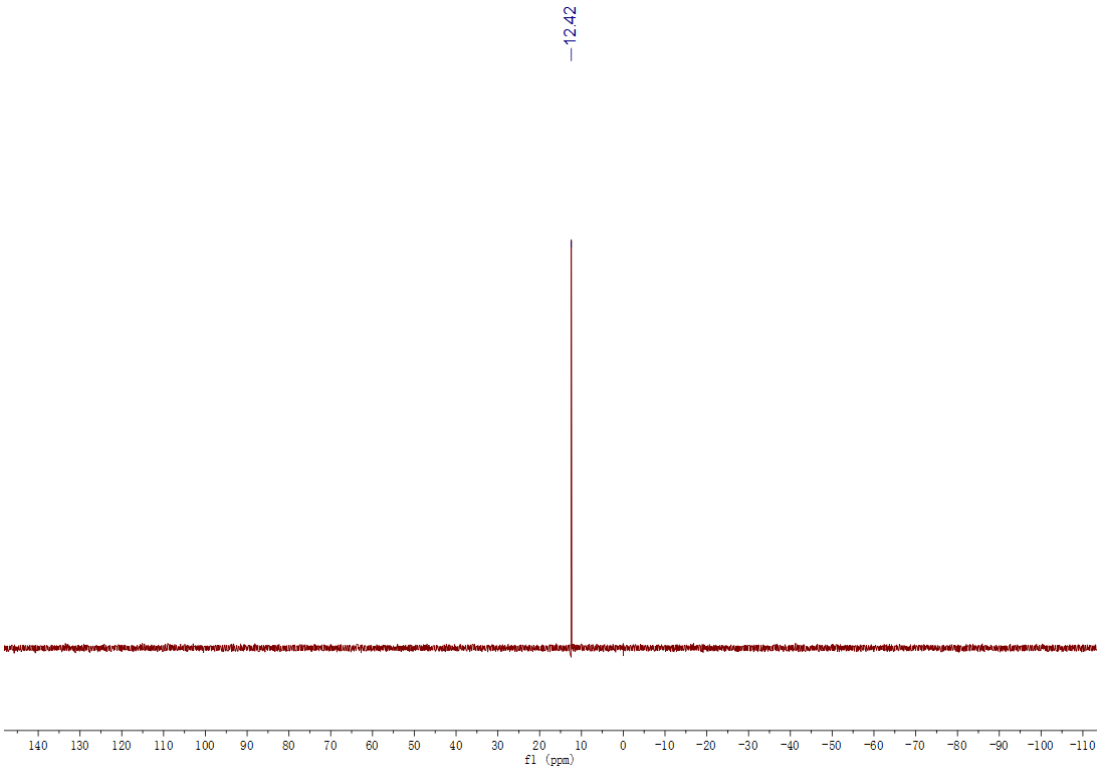
12.42
f1 (ppm)

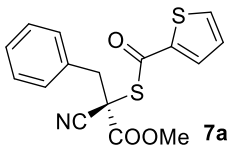

7a

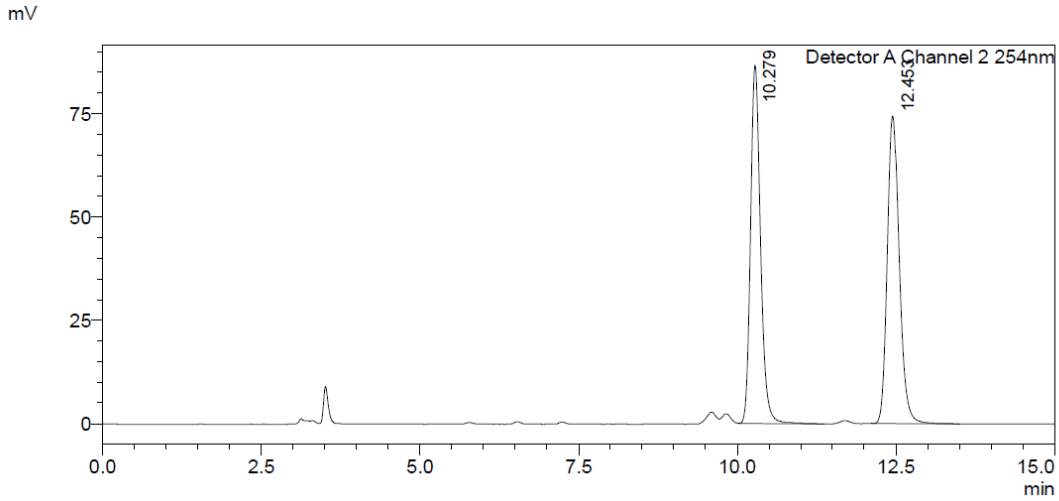

Detector A Channel 2 254nm

Peak#	Ret. Time	Area	Area%
1	10.279	950653	49.830
2	12.453	957130	50.170
Total		1907783	100.000

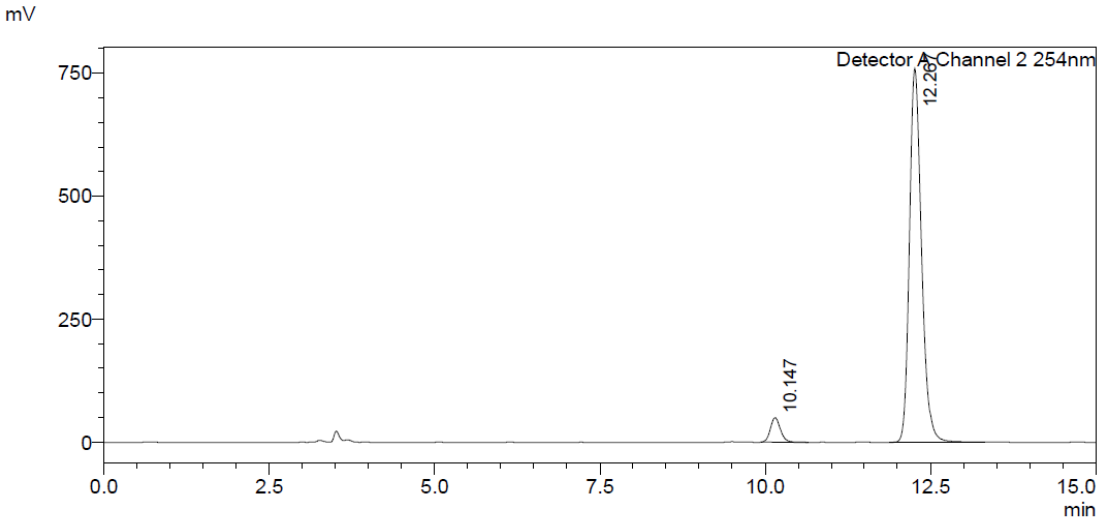

Detector A Channel 2 254nm

Peak#	Ret. Time	Area	Area%
1	10.147	526796	5.181
2	12.267	9640870	94.819
Total		10167666	100.000

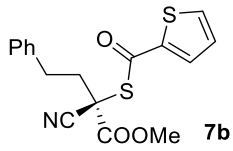

7b

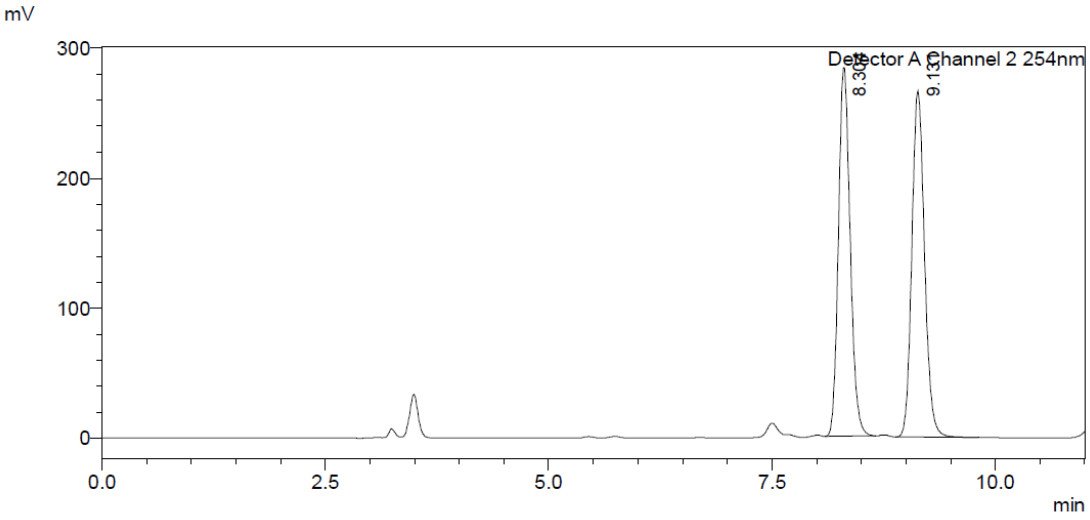

Detector A Channel 2 254nm

Peak#	Ret. Time	Area	Area%
1	8.304	2595468	49.649
2	9.131	2632160	50.351
Total		5227628	100.000

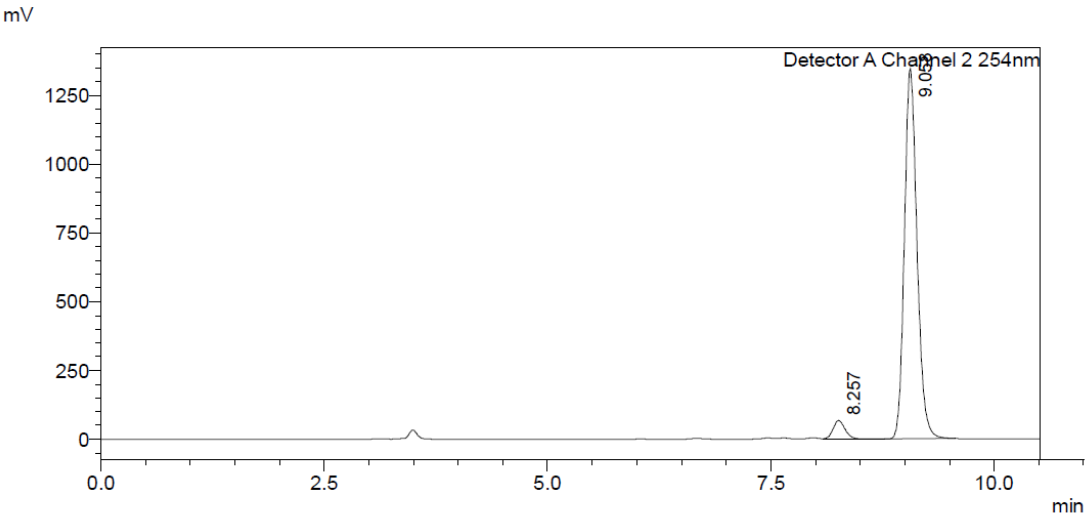

Detector A Channel 2 254nm

Peak#	Ret. Time	Area	Area%
1	8.257	607937	4.391
2	9.058	13238123	95.609
Total		13846060	100.000

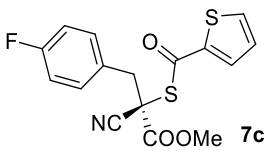

7c

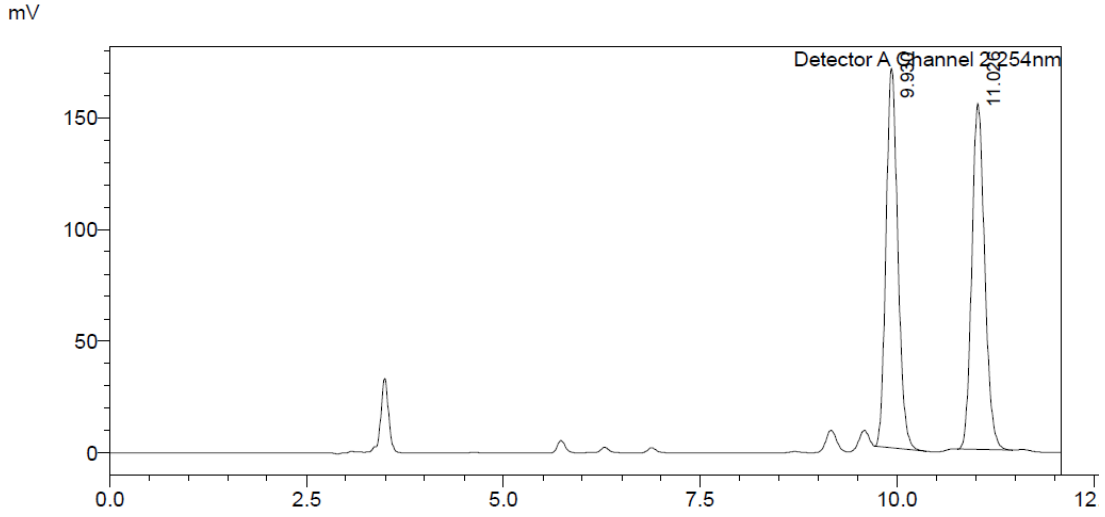

Detector A Channel 2 254nm

Peak#	Ret. Time	Area	Area%
1	9.930	1773290	50.043
2	11.026	1770264	49.957
Total		3543554	100.000

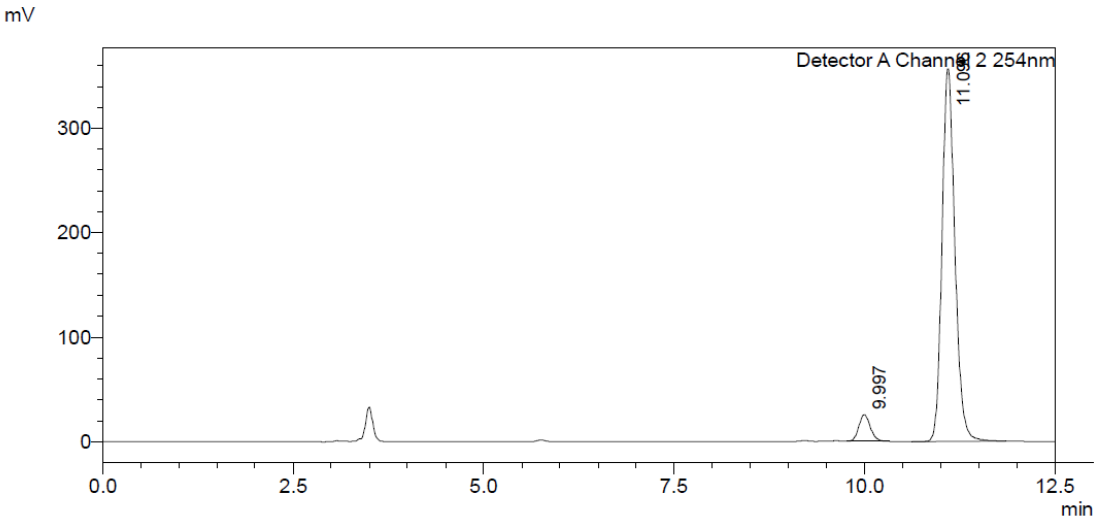

Detector A Channel 2 254nm

Peak#	Ret. Time	Area	Area%
1	9.997	269834	6.039
2	11.096	4198187	93.961
Total		4468021	100.000

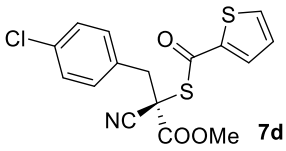

7d

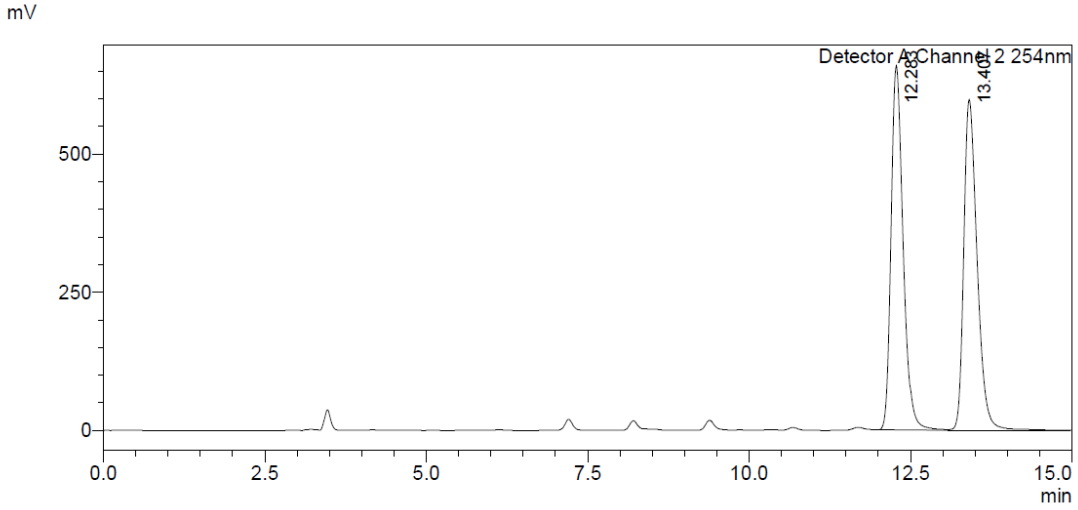

Detector A Channel 2 254nm

Peak#	Ret. Time	Area	Area%
1	12.283	8527365	49.741
2	13.407	8616199	50.259
Total		17143565	100.000

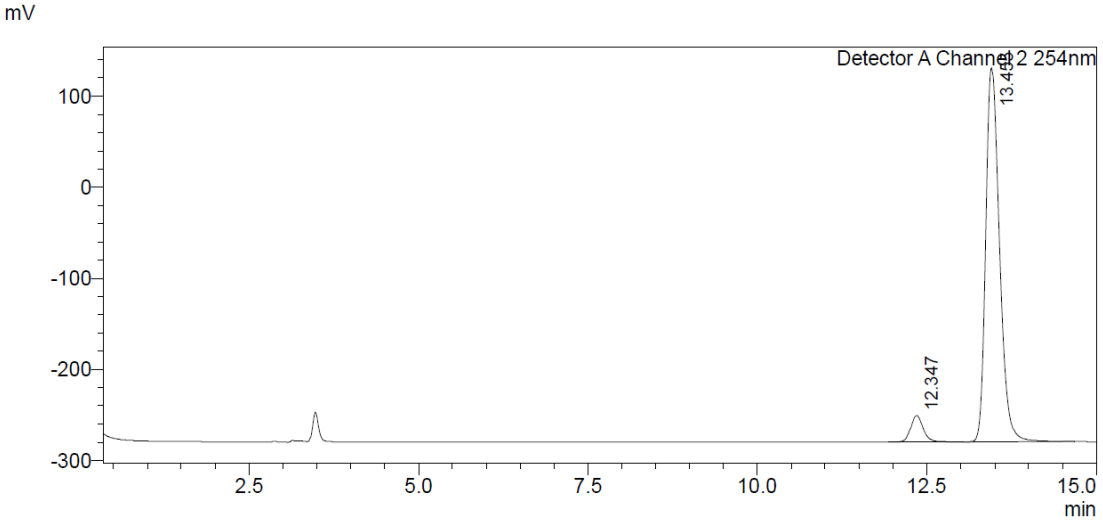

Detector A Channel 2 254nm

Peak#	Ret. Time	Area	Area%
1	12.347	372506	6.069
2	13.455	5765809	93.931
Total		6138316	100.000

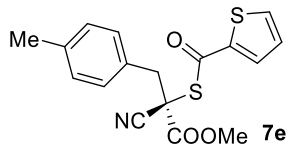

7e

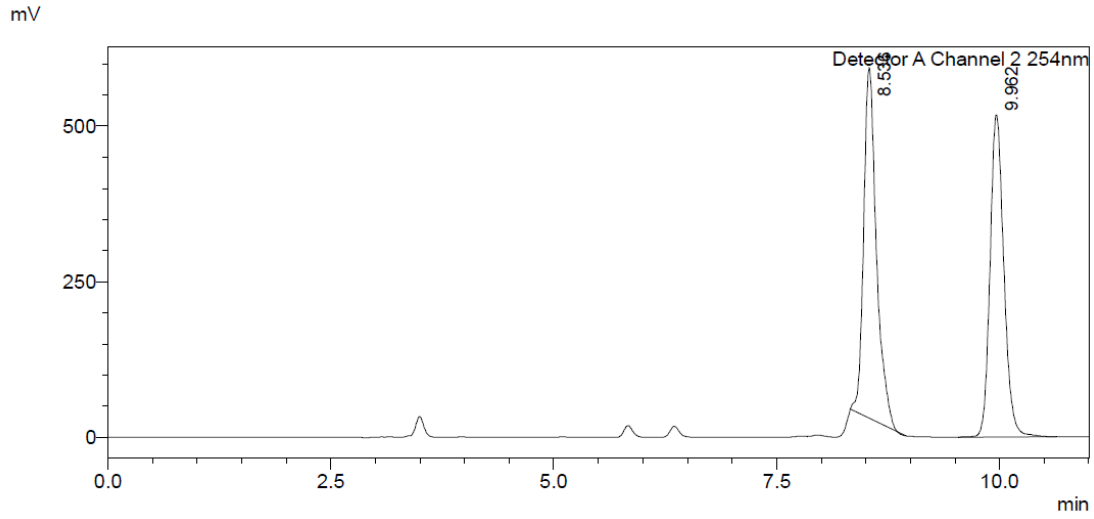

Detector A Channel 2 254nm

Peak#	Ret. Time	Area	Area%
1	8.536	5588173	50.108
2	9.962	5564138	49.892
Total		11152311	100.000

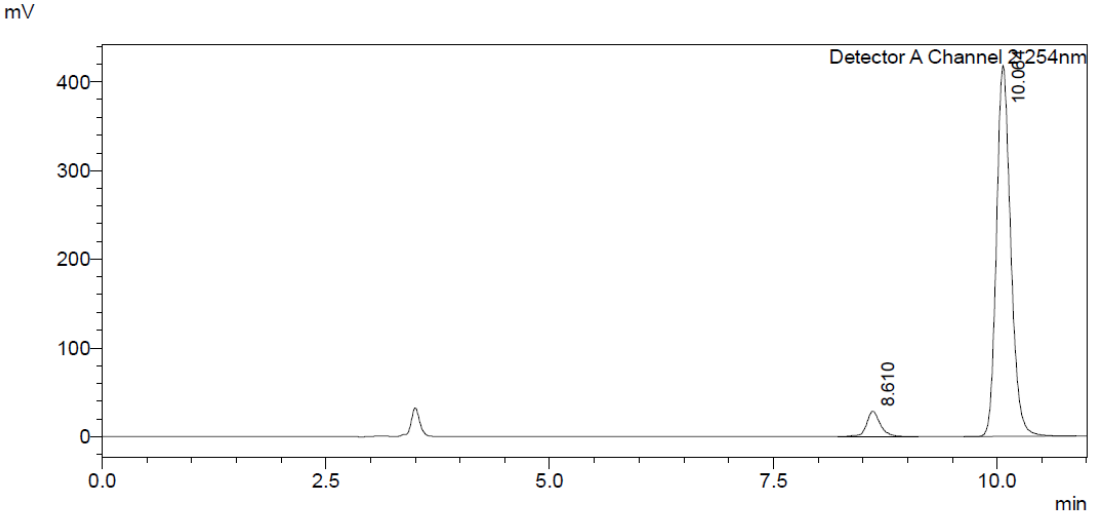

Detector A Channel 2 254nm

Peak#	Ret. Time	Area	Area%
1	8.610	304522	6.168
2	10.064	4632350	93.832
Total		4936872	100.000

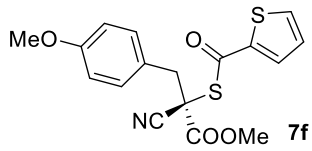

7f

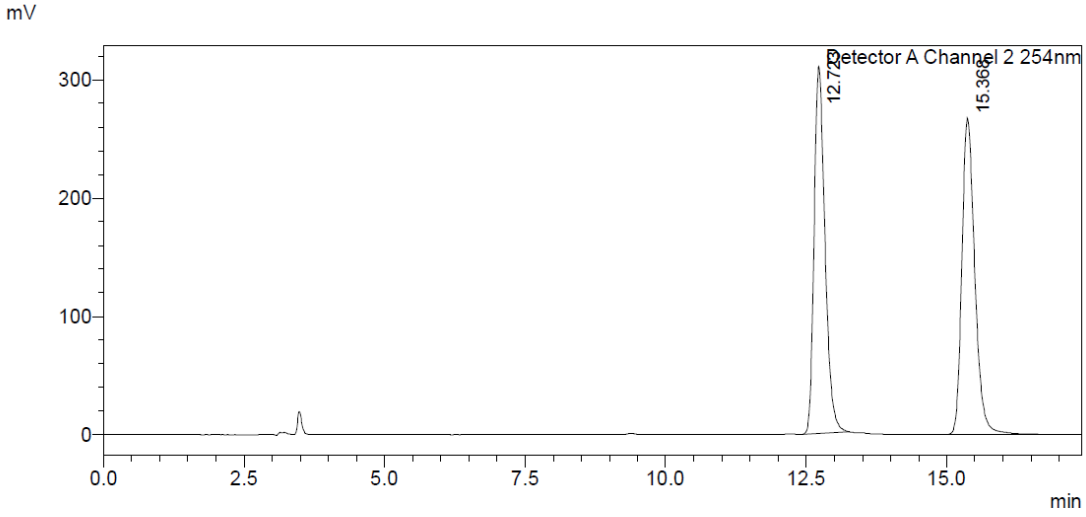

Detector A Channel 2 254nm

Peak#	Ret. Time	Area	Area%
1	12.723	4175616	49.412
2	15.368	4275049	50.588
Total		8450665	100.000

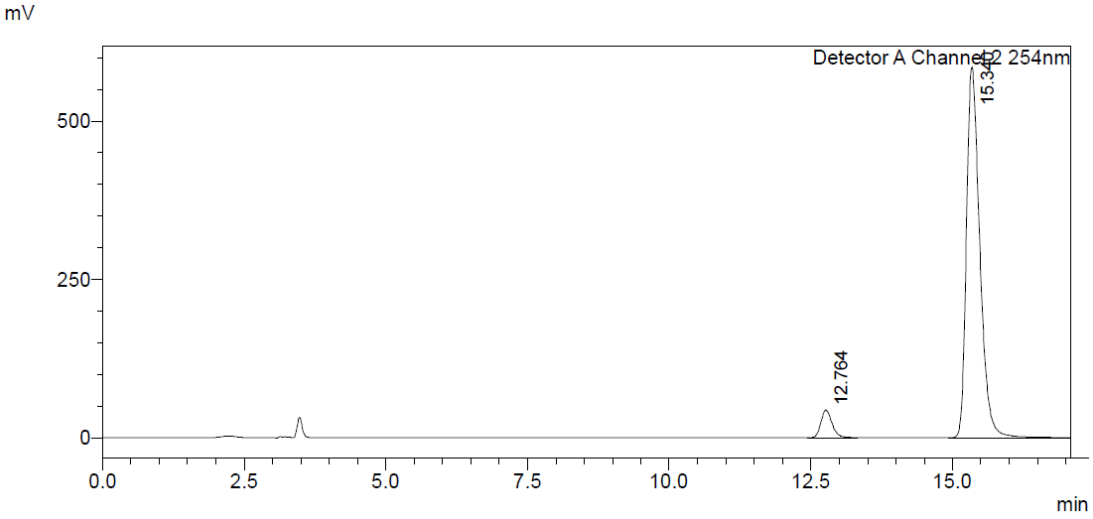

Detector A Channel 2 254nm

Peak#	Ret. Time	Area	Area%
1	12.764	595997	5.856
2	15.340	9582193	94.144
Total		10178190	100.000

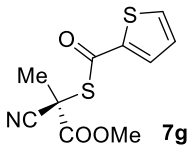

7g

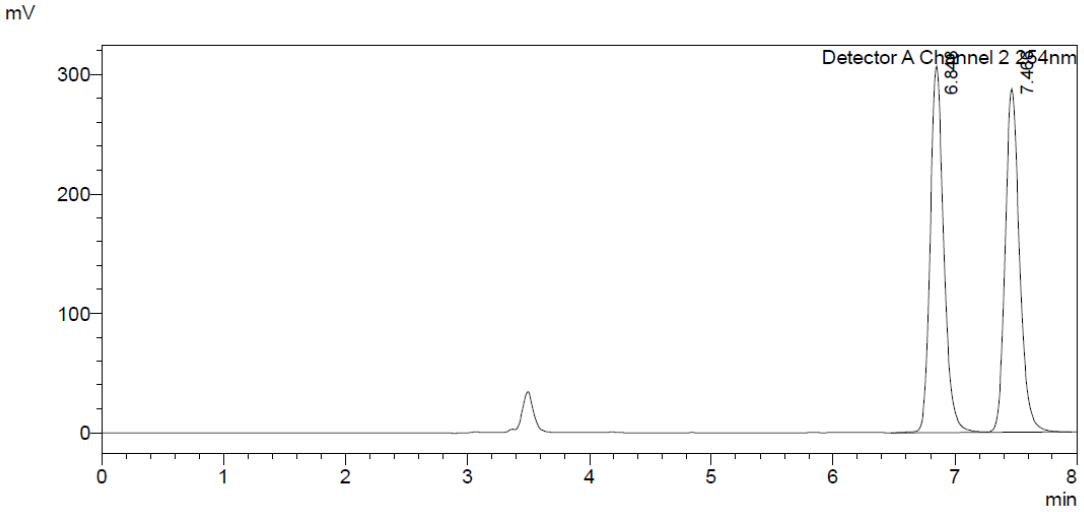

Detector A Channel 2 254nm

Peak#	Ret. Time	Area	Area%
1	6.848	2371515	50.166
2	7.466	2355801	49.834
Total		4727315	100.000

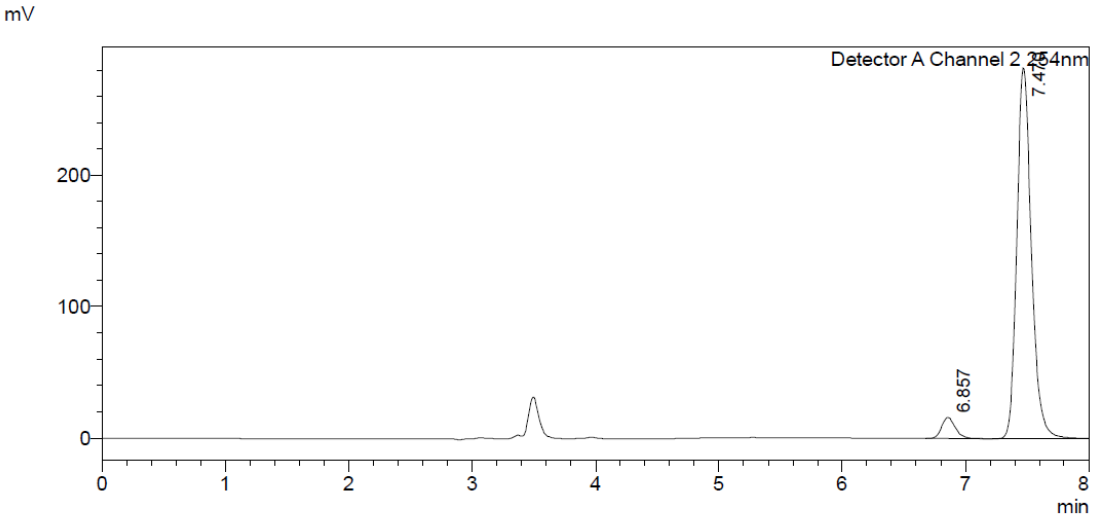

Detector A Channel 2 254nm

Peak#	Ret. Time	Area	Area%
1	6.857	123734	5.061
2	7.470	2321250	94.939
Total		2444984	100.000

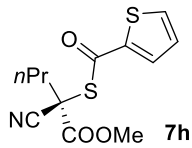

7h

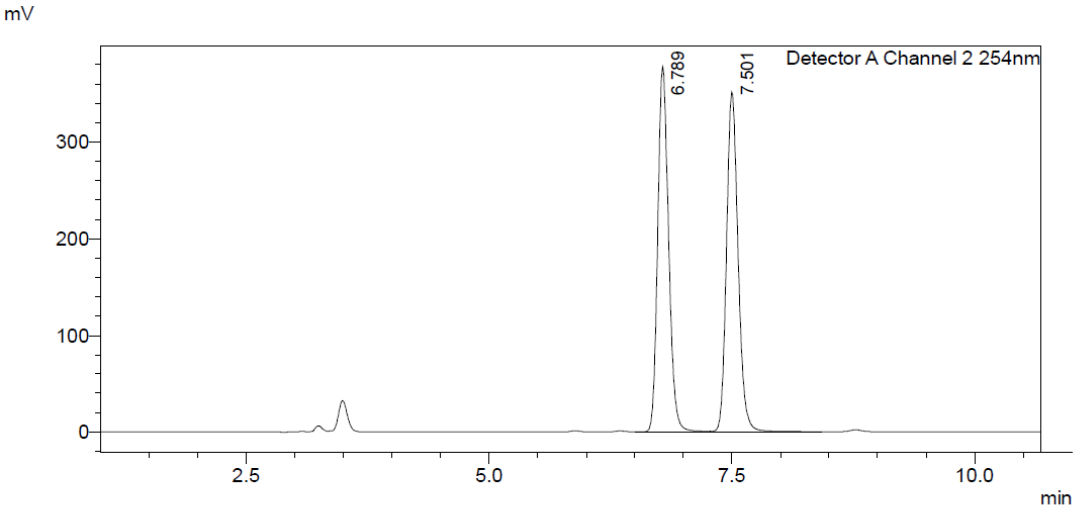

Detector A Channel 2 254nm

Peak#	Ret. Time	Area	Area%
1	6.789	2907329	49.884
2	7.501	2920818	50.116
Total		5828147	100.000

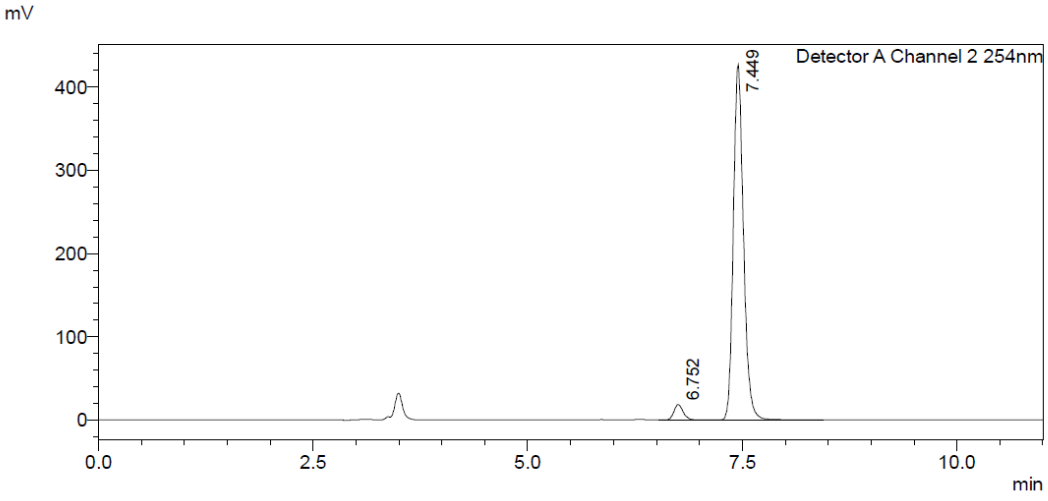

Detector A Channel 2 254nm

Peak#	Ret. Time	Area	Area%
1	6.752	143072	3.912
2	7.449	3513764	96.088
Total		3656837	100.000

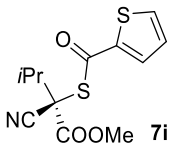

7i

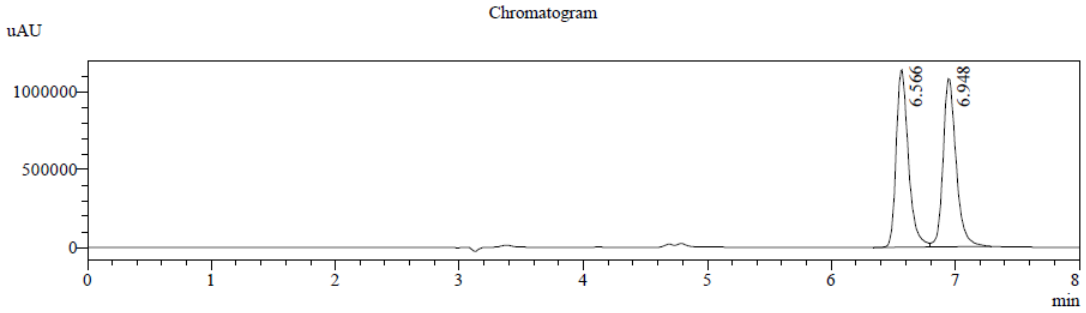

Peak Table

PDA Ch1 254nm

Peak#	Ret. Time	Height	Area	Area%
1	6.566	1138868	7821795	49.805
2	6.948	1079549	7882979	50.195
Total		2218416	15704774	100.000

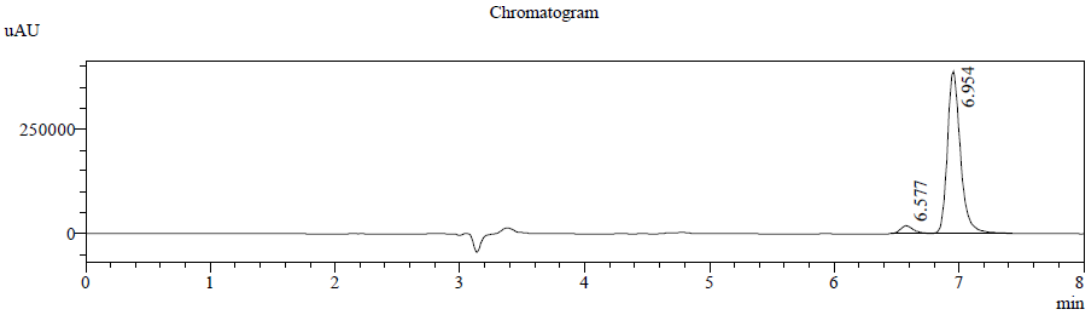

Peak Table

PDA Ch1 254nm

Peak#	Ret. Time	Height	Area	Area%
1	6.577	19050	134525	4.548
2	6.954	388525	2823077	95.452
Total		407575	2957602	100.000

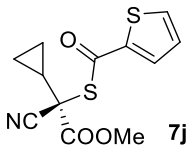

7j

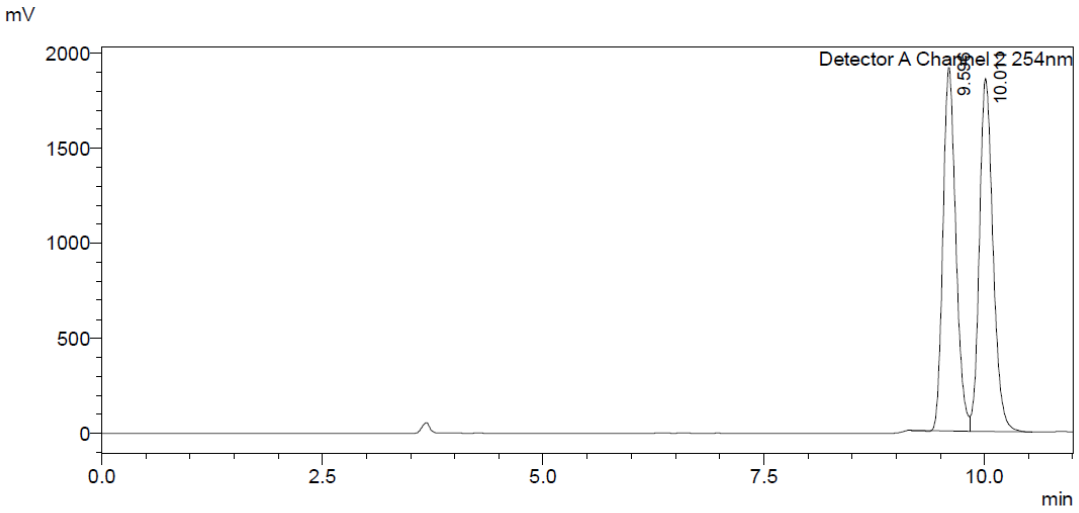

Detector A Channel 2 254nm

Peak#	Ret. Time	Area	Area%
1	9.596	19368155	49.399
2	10.011	19839210	50.601
Total		39207365	100.000

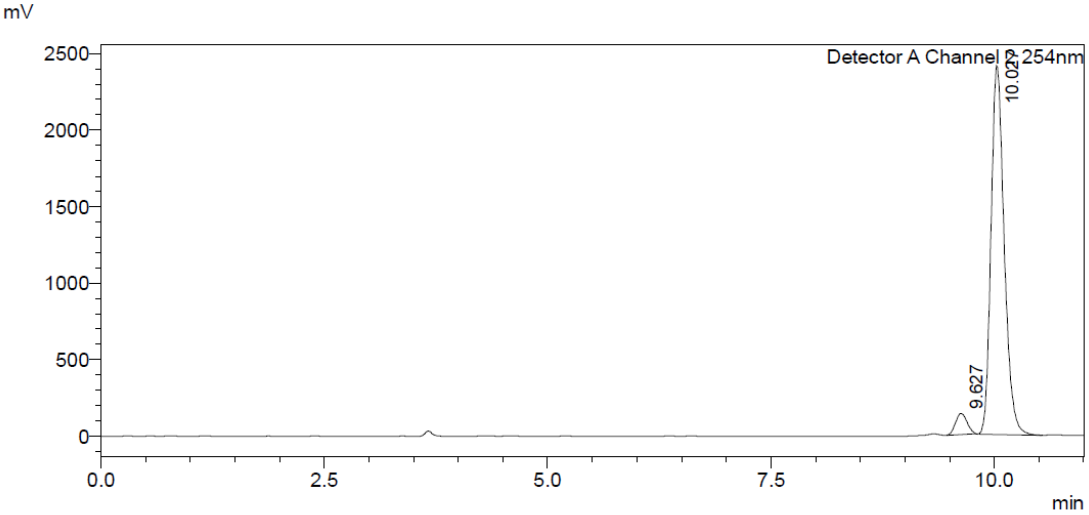

Detector A Channel 2 254nm

Peak#	Ret. Time	Area	Area%
1	9.627	1245853	4.803
2	10.027	24694512	95.197
Total		25940365	100.000

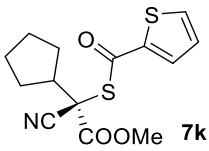

7k

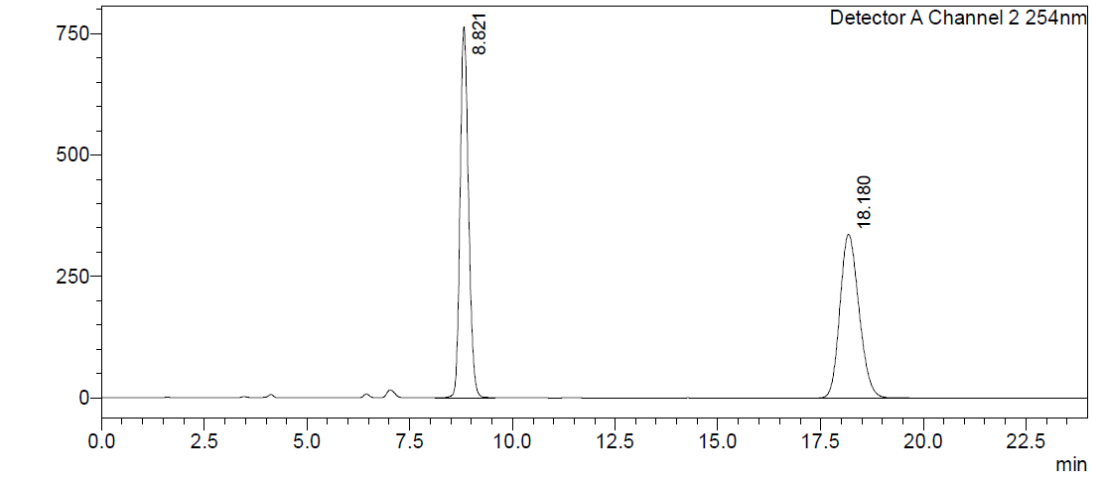

Detector A Channel 2 254nm

Peak#	Ret. Time	Area	Area%
1	8.821	10929766	50.068
2	18.180	10899875	49.932
Total		21829641	100.000

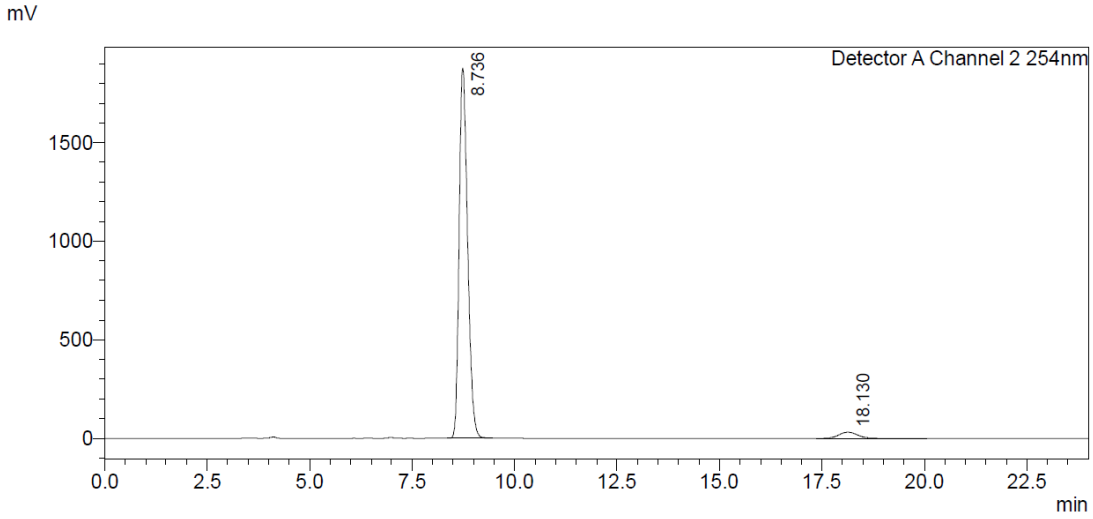

Detector A Channel 2 254nm

Peak#	Ret. Time	Area	Area%
1	8.736	27013800	96.439
2	18.130	997498	3.561
Total		28011298	100.000

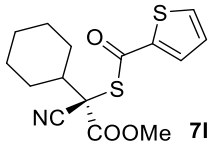

7l

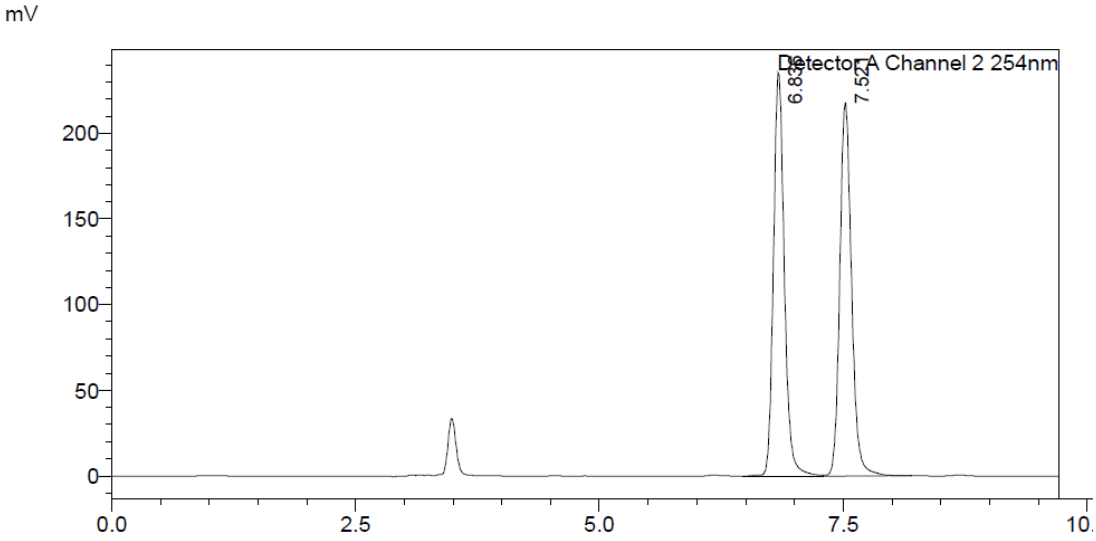

Detector A Channel 2 254nm

Peak#	Ret. Time	Area	Area%
1	6.836	1826781	50.040
2	7.521	1823846	49.960
Total		3650628	100.000

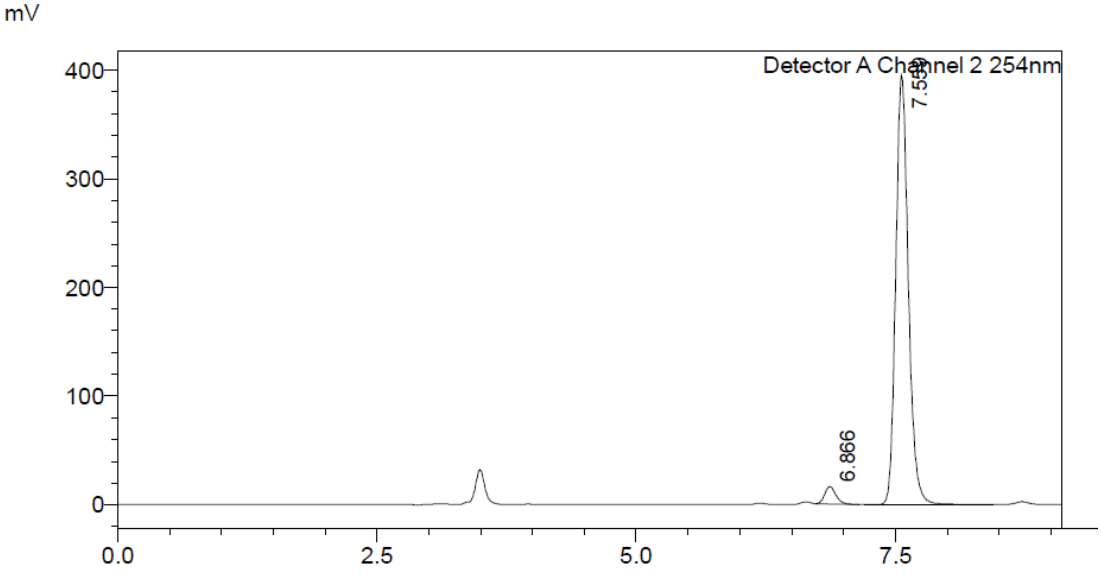

Detector A Channel 2 254nm

Peak#	Ret. Time	Area	Area%
1	6.866	120237	3.479
2	7.559	3335371	96.521
Total		3455608	100.000

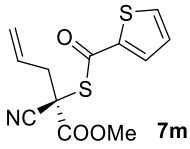

7m

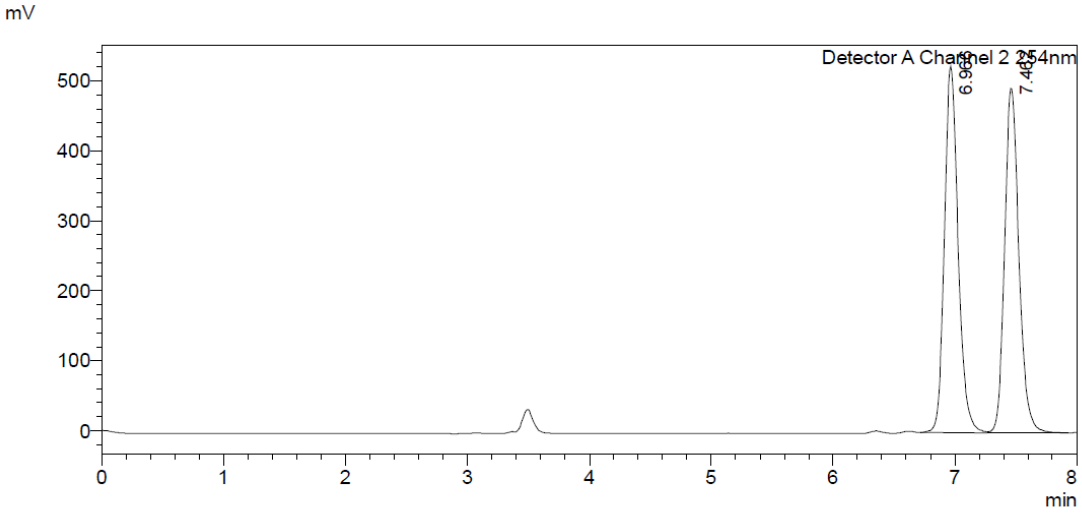

Detector A Channel 2 254nm

Peak#	Ret. Time	Area	Area%
1	6.966	4085673	50.482
2	7.462	4007686	49.518
Total		8093359	100.000

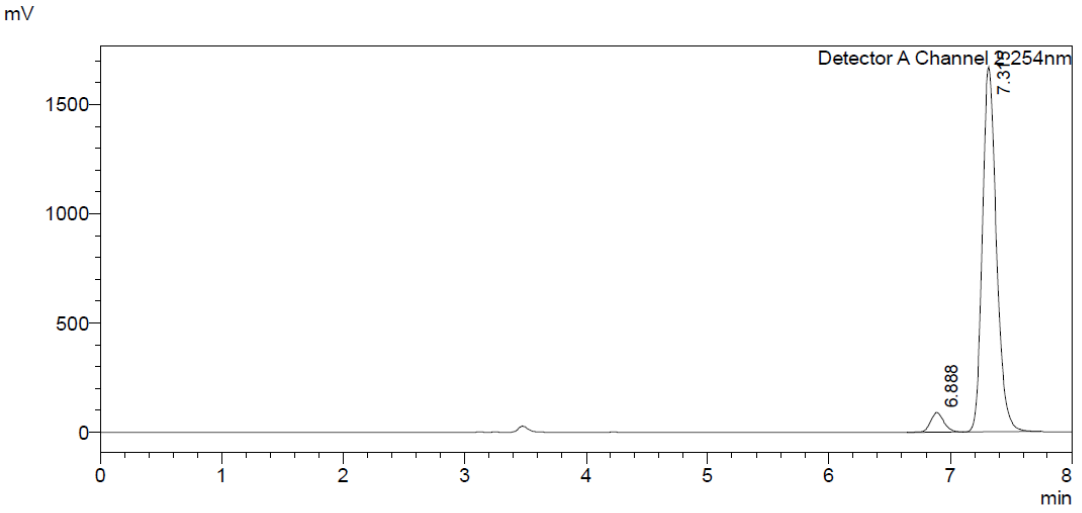

Detector A Channel 2 254nm

Peak#	Ret. Time	Area	Area%
1	6.888	674257	4.782
2	7.315	13426297	95.218
Total		14100554	100.000

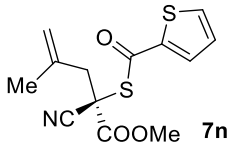

7n

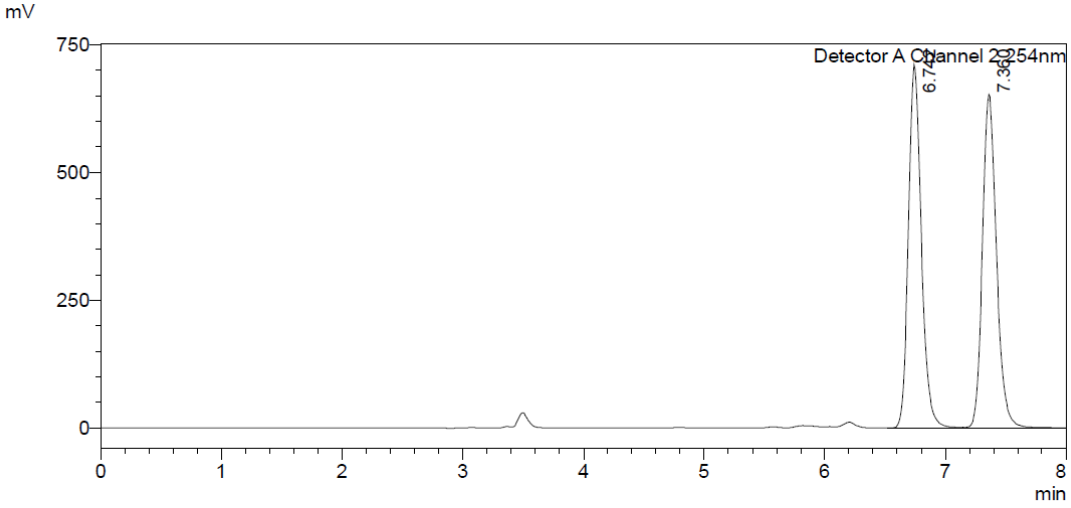

Detector A Channel 2 254nm

Peak#	Ret. Time	Area	Area%
1	6.742	5320920	50.204
2	7.360	5277615	49.796
Total		10598535	100.000

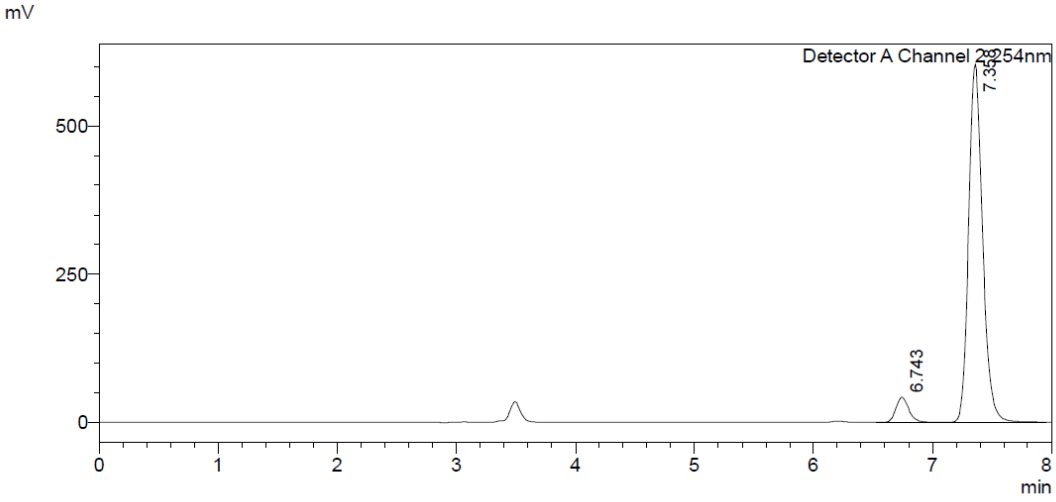

Detector A Channel 2 254nm

Peak#	Ret. Time	Area	Area%
1	6.743	321104	6.137
2	7.358	4911196	93.863
Total		5232300	100.000

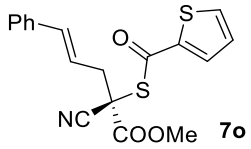

7o

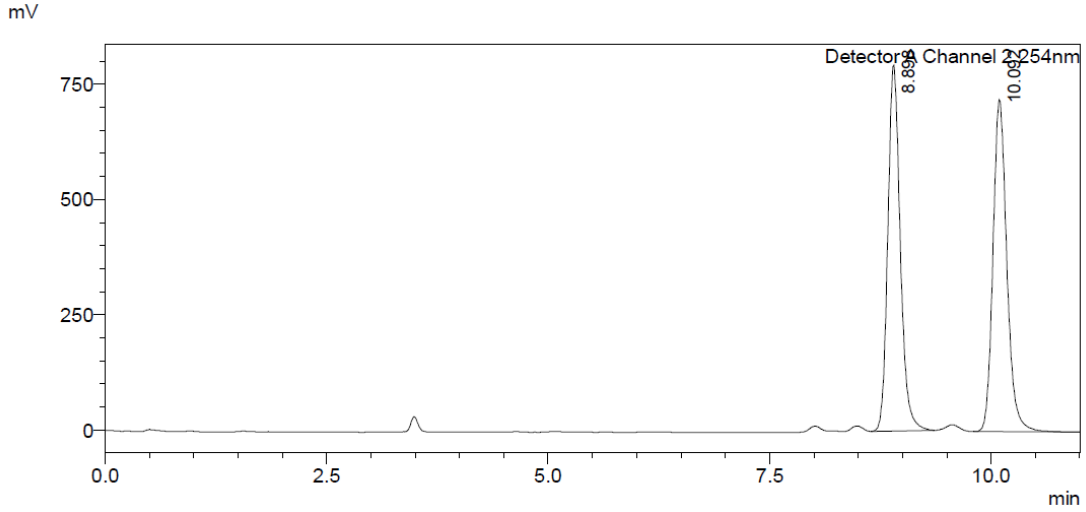

Detector A Channel 2 254nm

Peak#	Ret. Time	Area	Area%
1	8.898	7742109	49.671
2	10.092	7844677	50.329
Total		15586786	100.000

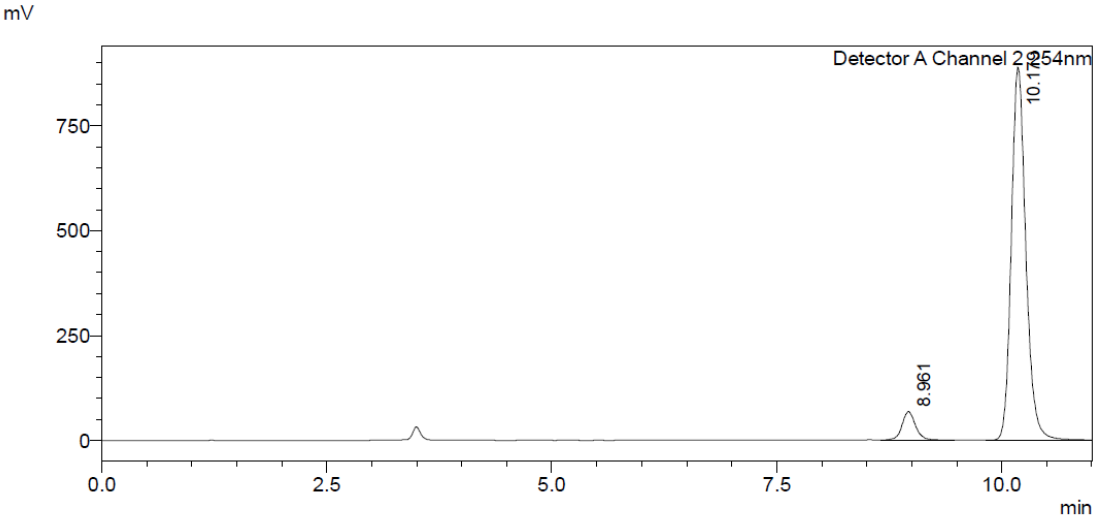

Detector A Channel 2 254nm

Peak#	Ret. Time	Area	Area%
1	8.961	712801	6.647
2	10.179	10010057	93.353
Total		10722858	100.000

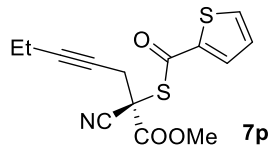

7p

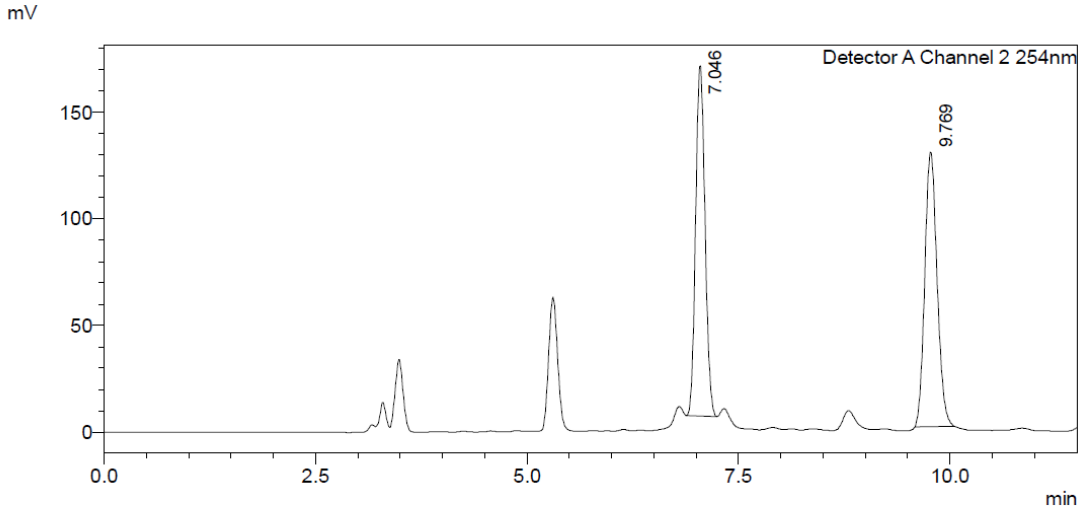

Detector A Channel 2 254nm

Peak#	Ret. Time	Area	Area%
1	7.046	1261813	49.306
2	9.769	1297339	50.694
Total		2559152	100.000

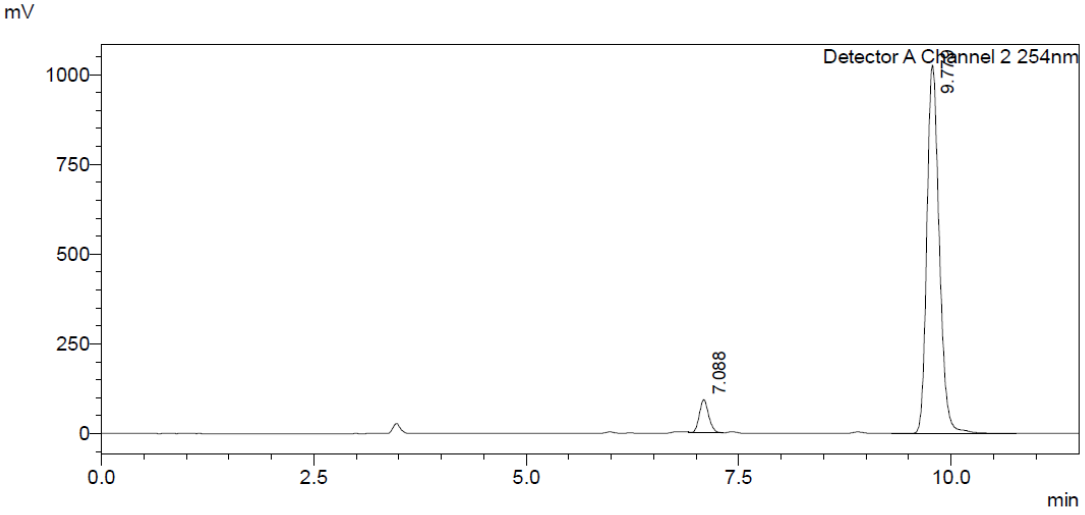

Detector A Channel 2 254nm

Peak#	Ret. Time	Area	Area%
1	7.088	709538	6.368
2	9.779	10433220	93.632
Total		11142758	100.000

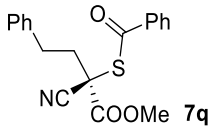

7q

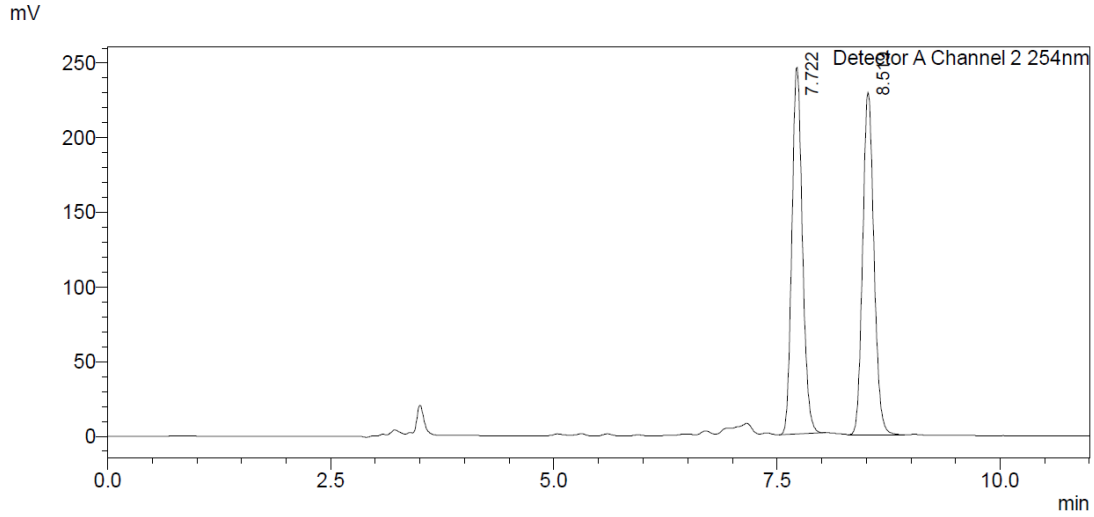

Detector A Channel 2 254nm

Peak#	Ret. Time	Area	Area%
1	7.722	2013632	49.981
2	8.519	2015128	50.019
Total		4028761	100.000

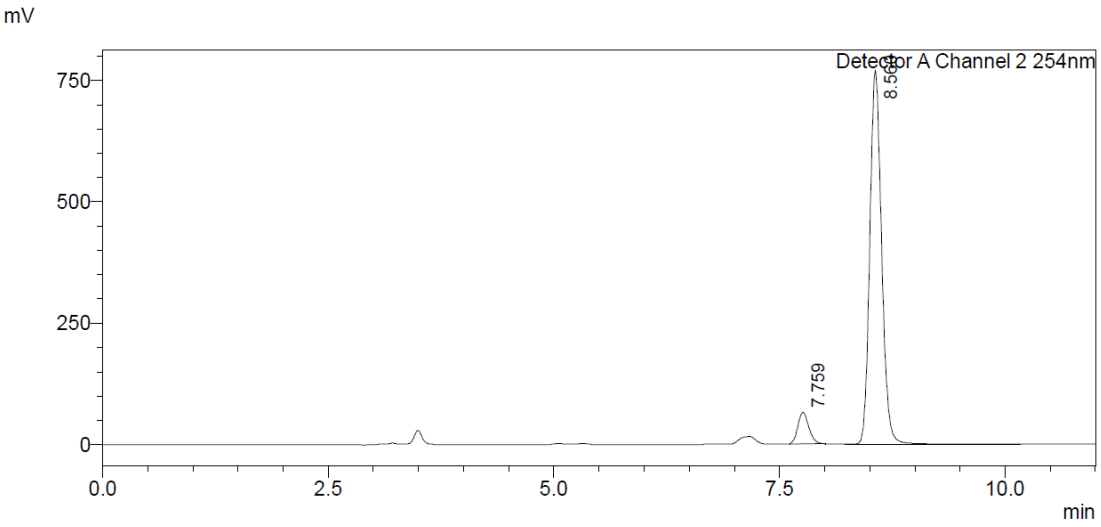

Detector A Channel 2 254nm

Peak#	Ret. Time	Area	Area%
1	7.759	548835	7.279
2	8.560	6991207	92.721
Total		7540042	100.000

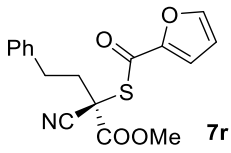

7r

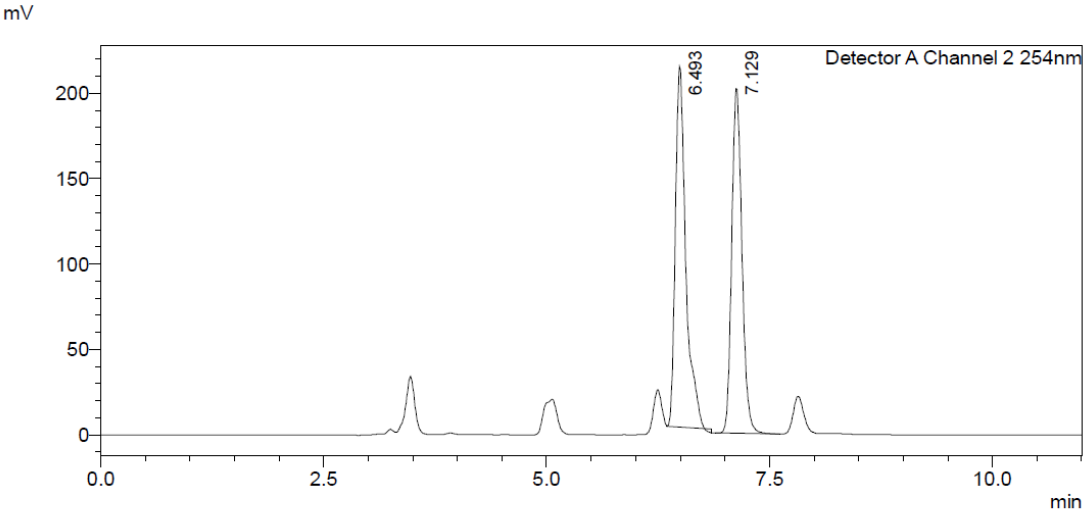

Detector A Channel 2 254nm

Peak#	Ret. Time	Area	Area%
1	6.493	1708930	51.528
2	7.129	1607586	48.472
Total		3316516	100.000

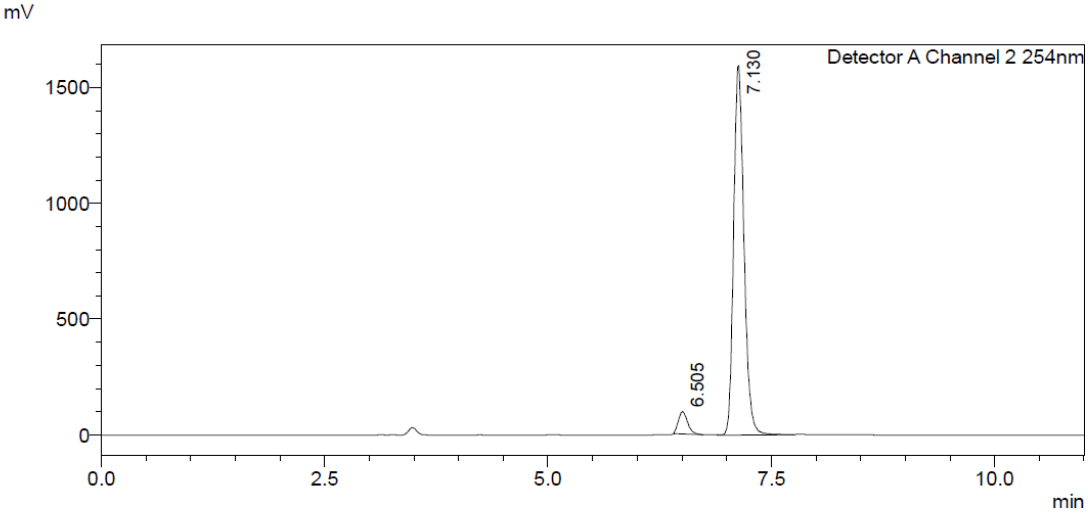

Detector A Channel 2 254nm

Peak#	Ret. Time	Area	Area%
1	6.505	698877	5.184
2	7.130	12781708	94.816
Total		13480586	100.000

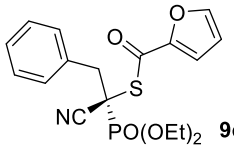

9c

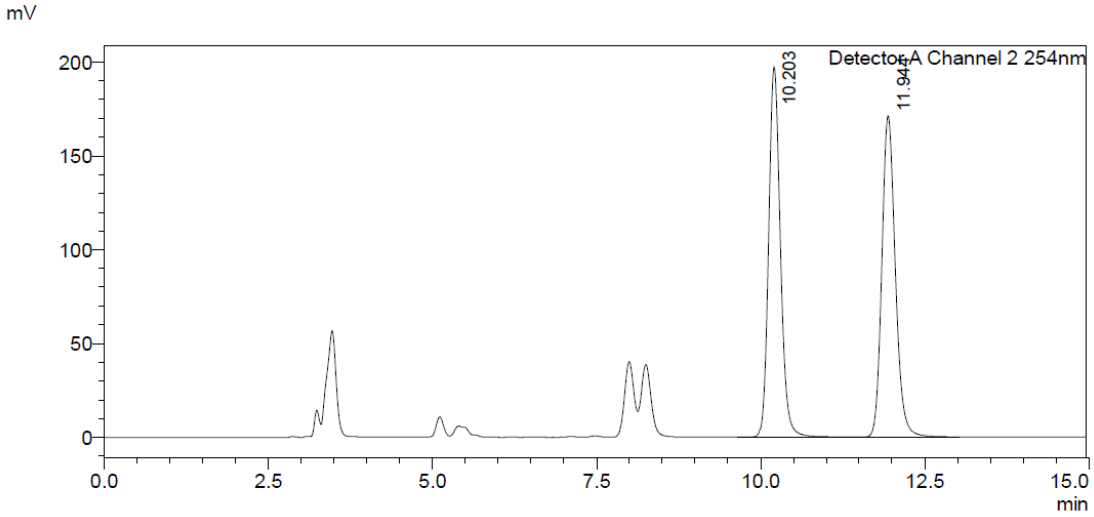

Detector A Channel 2 254nm

Peak#	Ret. Time	Area	Area%
1	10.203	2465808	50.090
2	11.944	2456933	49.910
Total		4922742	100.000

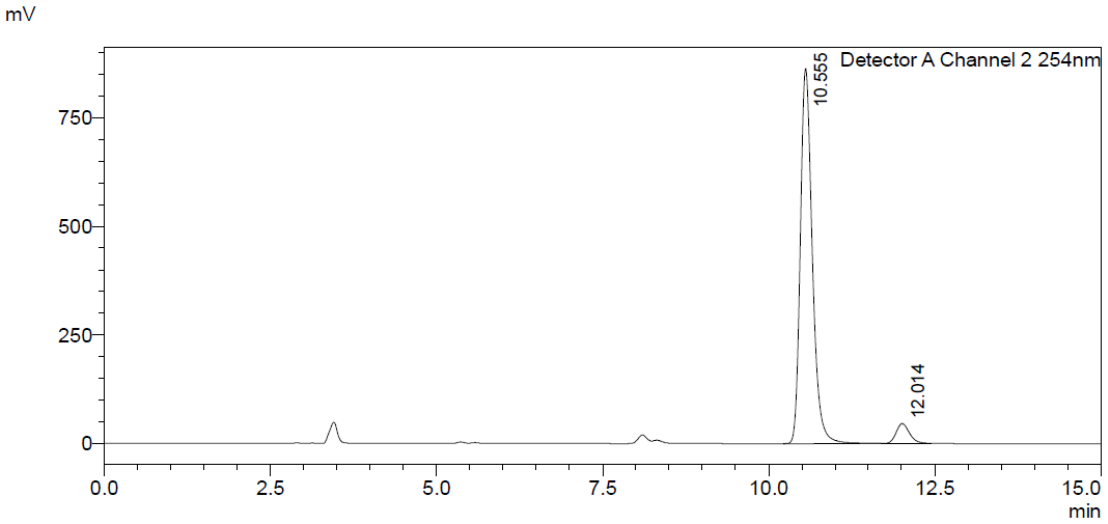

Detector A Channel 2 254nm

Peak#	Ret. Time	Area	Area%
1	10.555	10831793	94.490
2	12.014	631601	5.510
Total		11463394	100.000

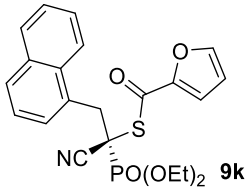

9k

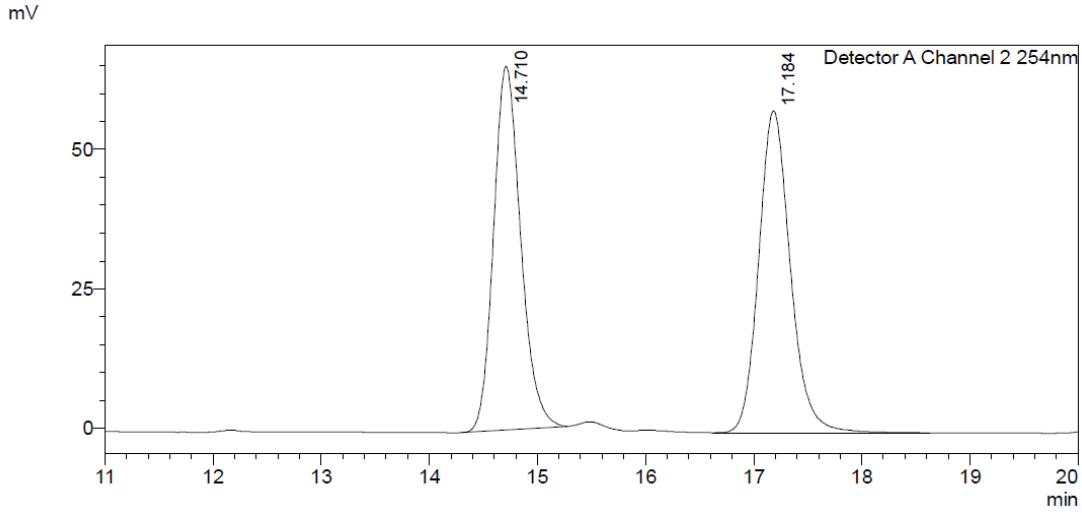

Detector A Channel 2 254nm

Peak#	Ret. Time	Area	Area%
1	14.710	1136578	49.115
2	17.184	1177560	50.885
Total		2314137	100.000

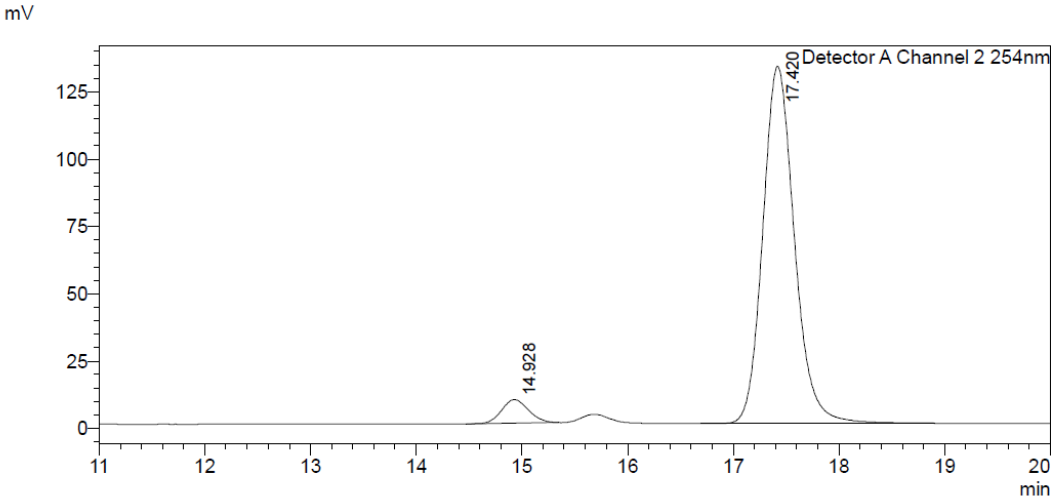

Detector A Channel 2 254nm

Peak#	Ret. Time	Area	Area%
1	14.928	154098	5.300
2	17.420	2753298	94.700
Total		2907396	100.000

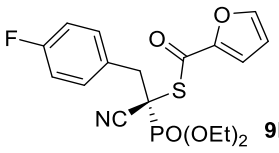

9l

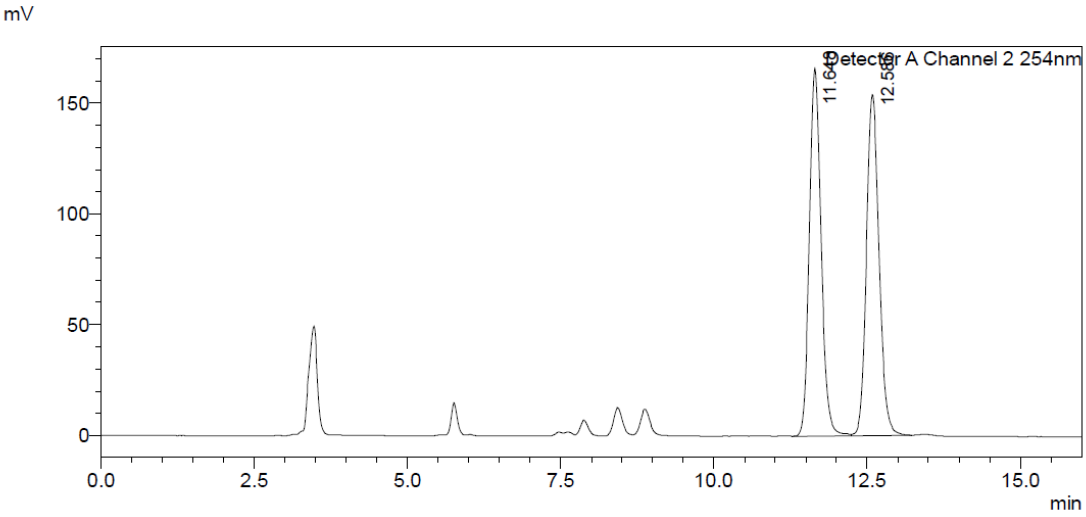

Detector A Channel 2 254nm

Peak#	Ret. Time	Area	Area%
1	11.648	2223726	50.248
2	12.586	2201742	49.752
Total		4425468	100.000

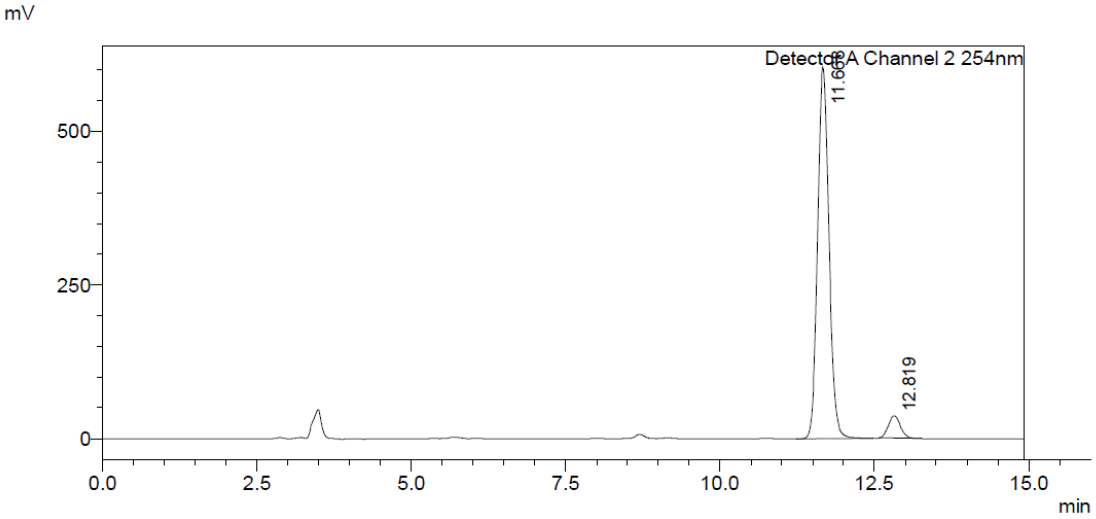

Detector A Channel 2 254nm

Peak#	Ret. Time	Area	Area%
1	11.668	7751975	93.964
2	12.819	498007	6.036
Total		8249983	100.000

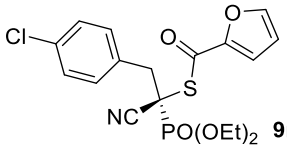

9m

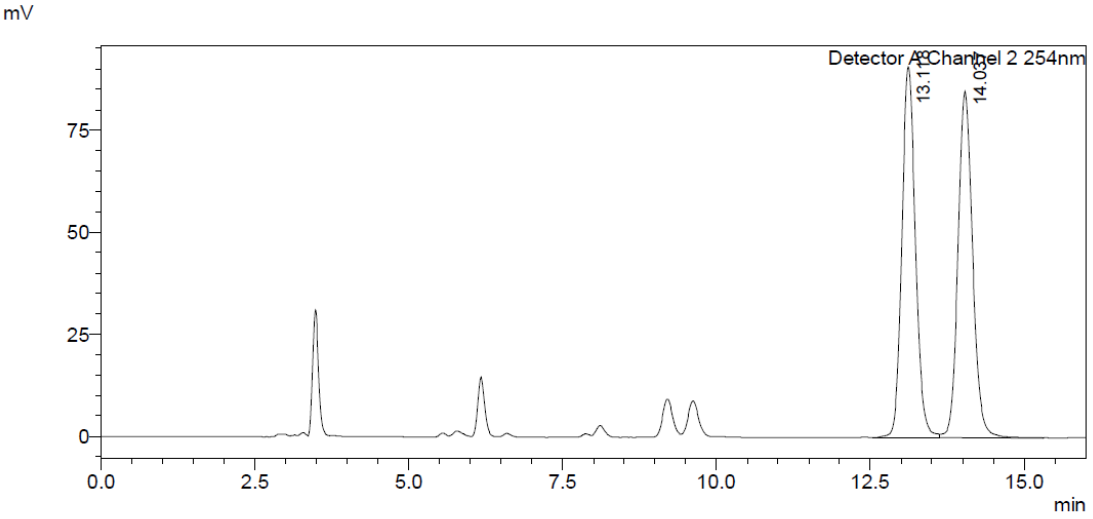

Detector A Channel 2 254nm

Peak#	Ret. Time	Area	Area%
1	13.118	1394963	49.819
2	14.037	1405098	50.181
Total		2800061	100.000

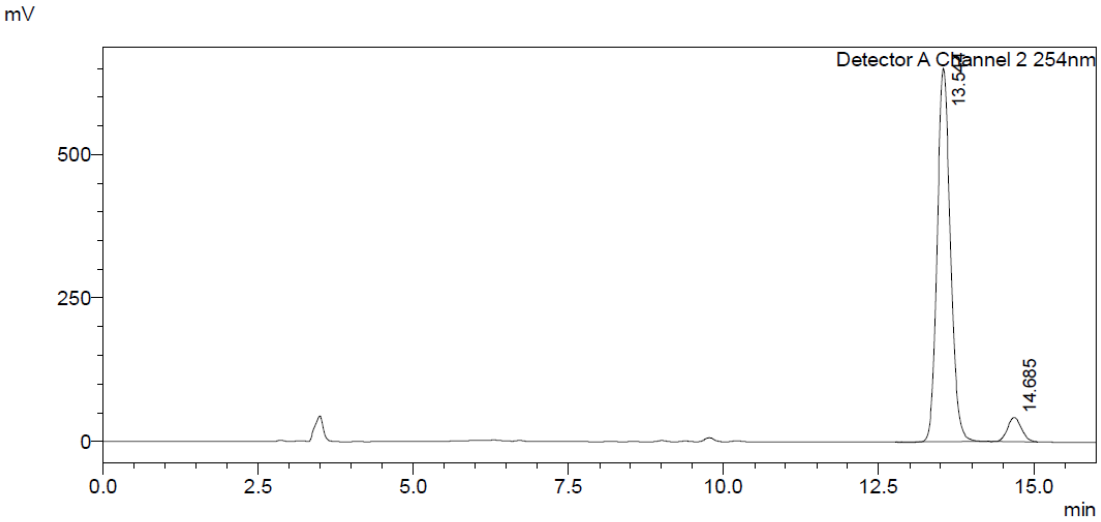

Detector A Channel 2 254nm

Peak#	Ret. Time	Area	Area%
1	13.544	9658236	93.604
2	14.685	659939	6.396
Total		10318176	100.000

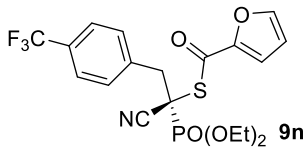

9n

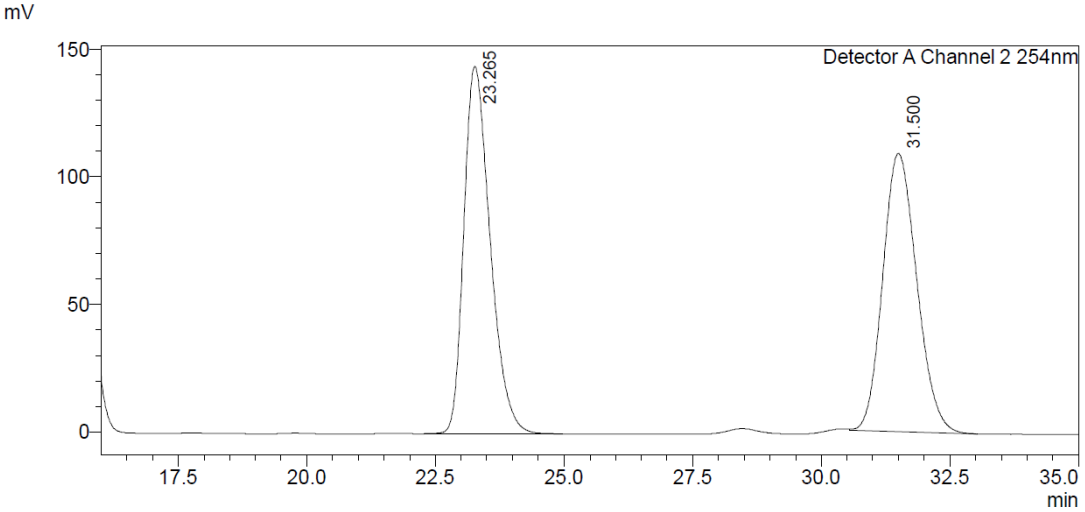

Detector A Channel 2 254nm

Peak#	Ret. Time	Area	Area%
1	23.265	5131001	50.549
2	31.500	5019461	49.451
Total		10150462	100.000

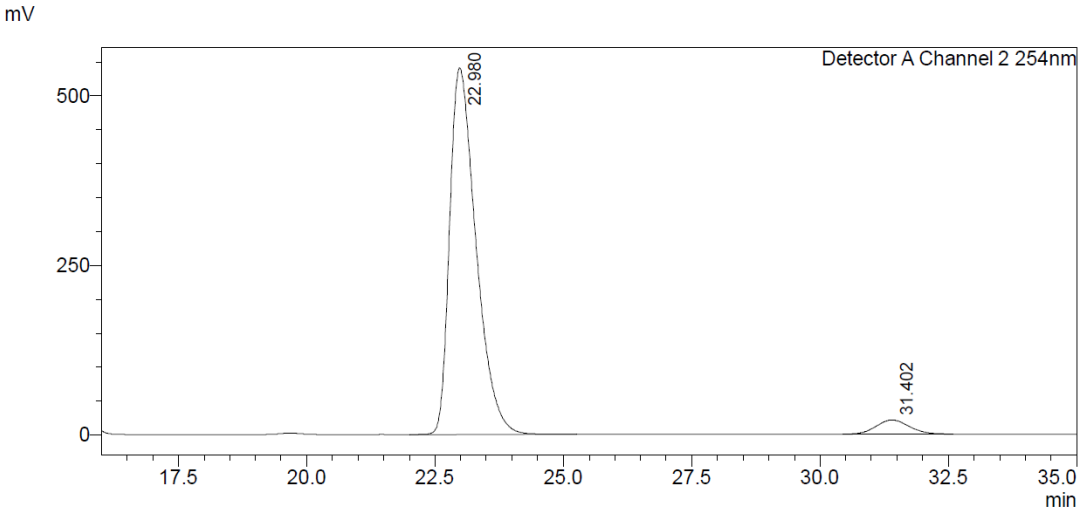

Detector A Channel 2 254nm

Peak#	Ret. Time	Area	Area%
1	22.980	19329122	95.361
2	31.402	940371	4.639
Total		20269493	100.000

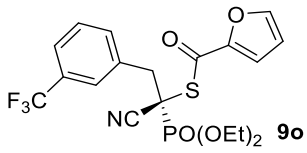

9o

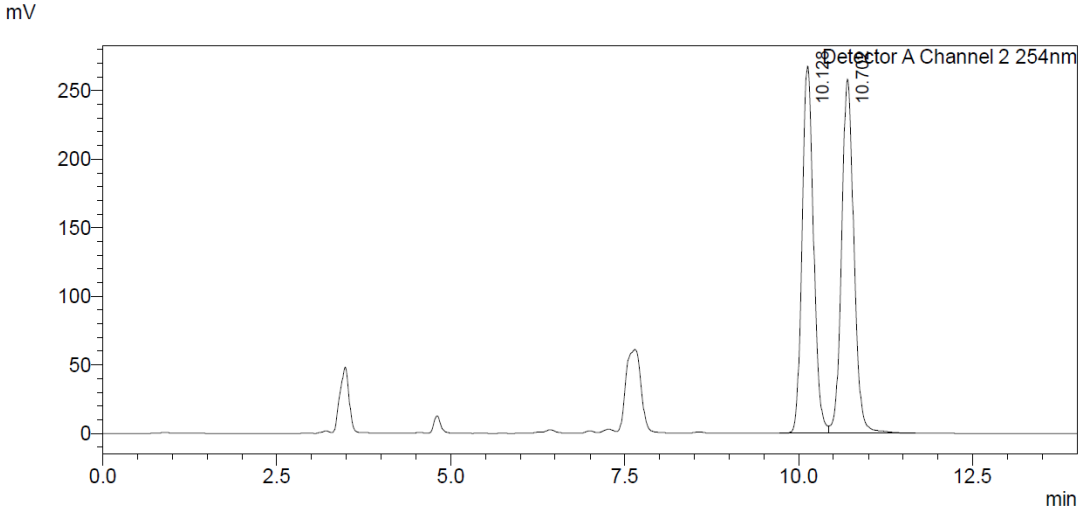

Detector A Channel 2 254nm

Peak#	Ret. Time	Area	Area%
1	10.128	3065371	48.973
2	10.702	3193909	51.027
Total		6259280	100.000

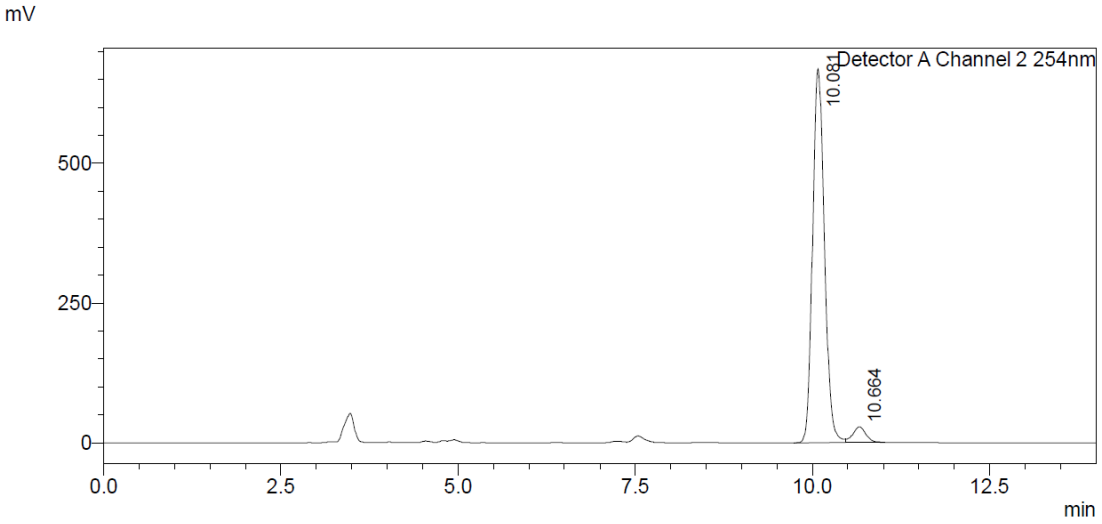

Detector A Channel 2 254nm

Peak#	Ret. Time	Area	Area%
1	10.081	7781805	95.618
2	10.664	356660	4.382
Total		8138465	100.000

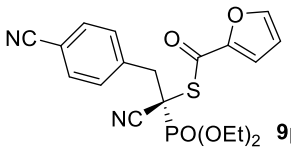

9p

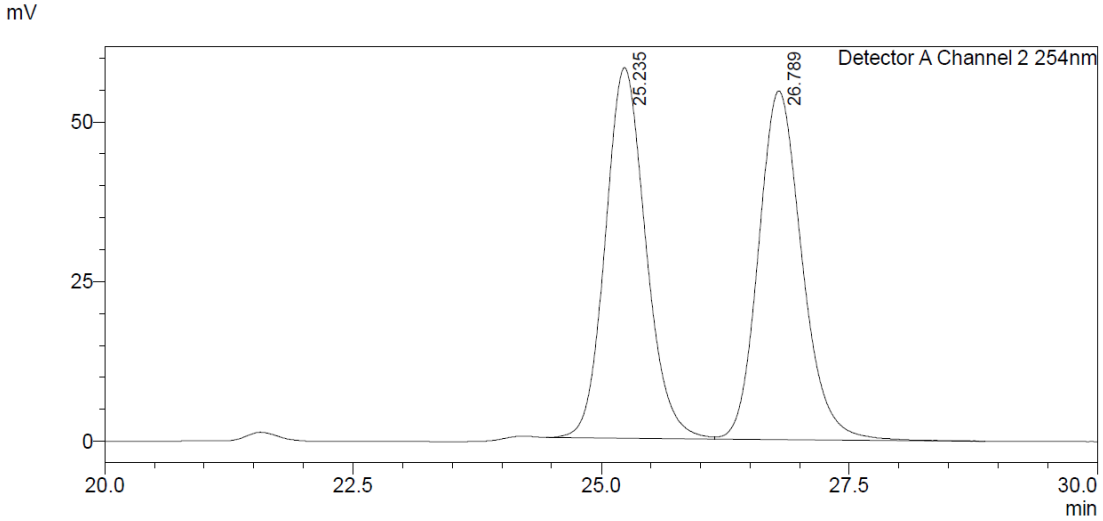

Detector A Channel 2 254nm

Peak#	Ret. Time	Area	Area%
1	25.235	1648223	49.825
2	26.789	1659819	50.175
Total		3308043	100.000

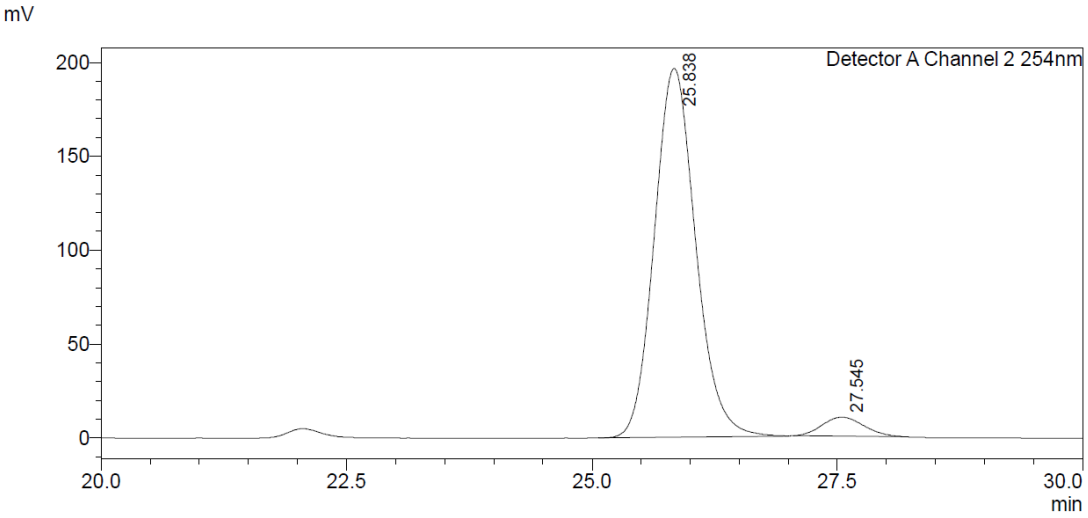

Detector A Channel 2 254nm

Peak#	Ret. Time	Area	Area%
1	25.838	5741659	95.002
2	27.545	302054	4.998
Total		6043713	100.000

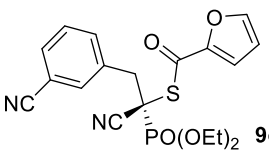

9q

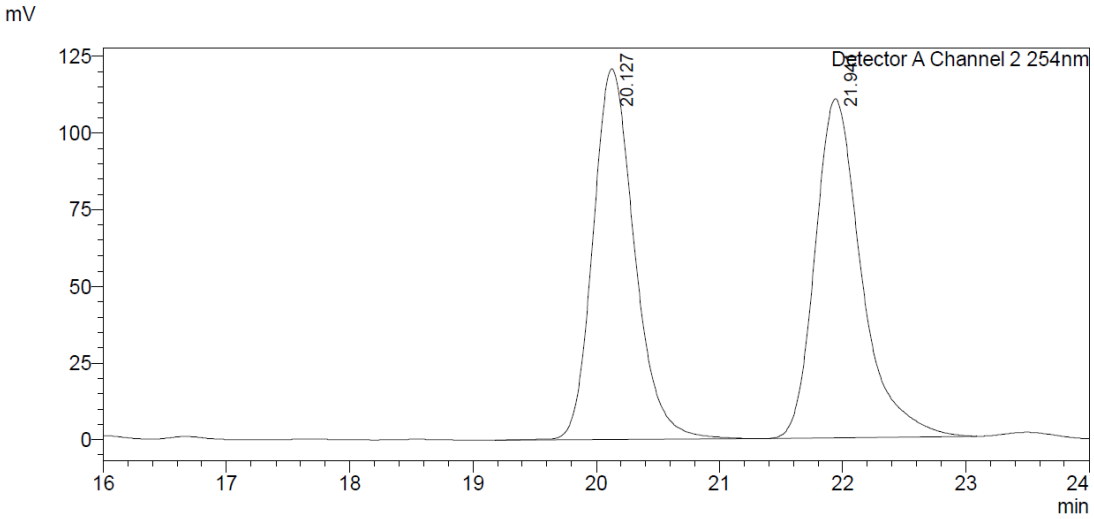

Detector A Channel 2 254nm

Peak#	Ret. Time	Area	Area%
1	20.127	2826017	49.403
2	21.941	2894330	50.597
Total		5720347	100.000

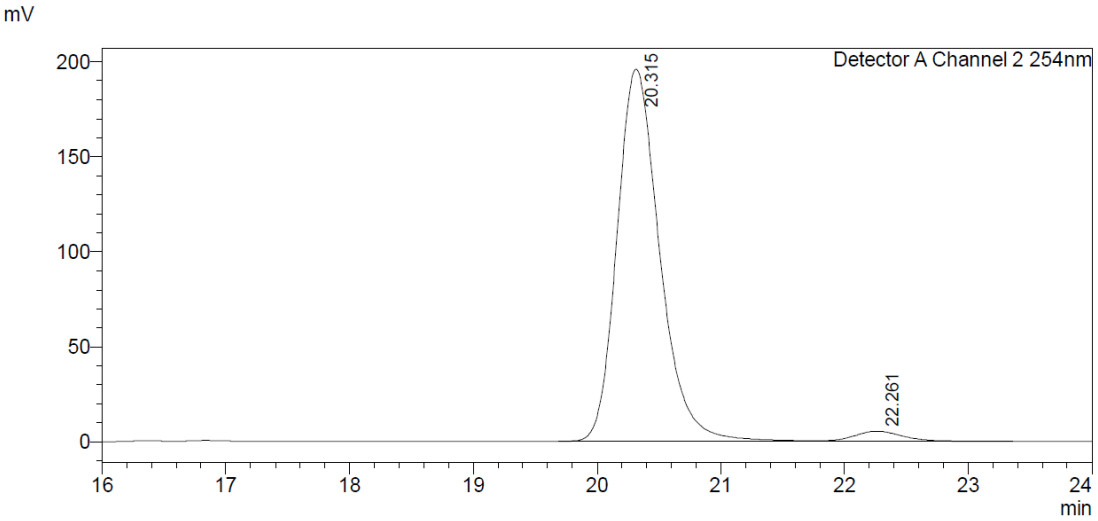

Detector A Channel 2 254nm

Peak#	Ret. Time	Area	Area%
1	20.315	4702969	96.923
2	22.261	149299	3.077
Total		4852268	100.000

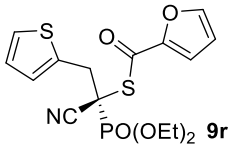

9r

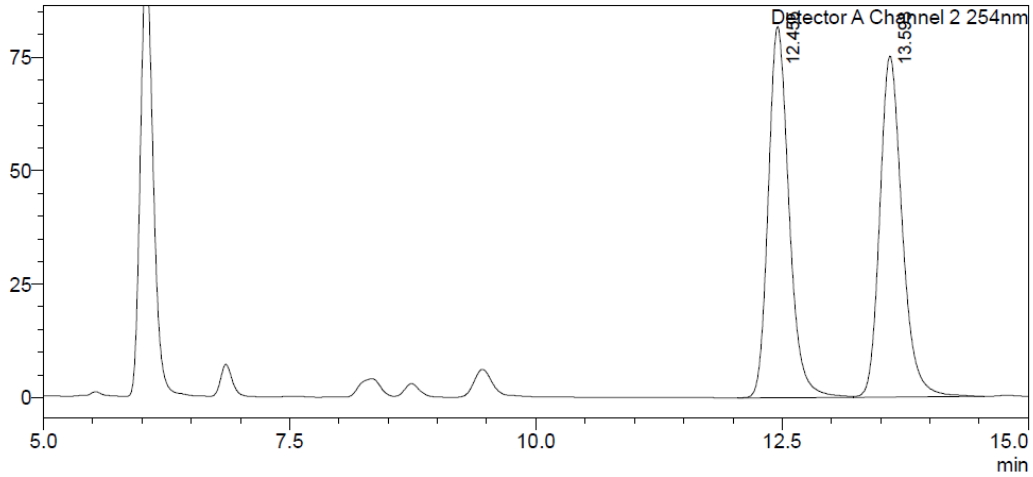

Detector A Channel 2 254nm

Peak#	Ret. Time	Area	Area%
1	12.455	1190875	49.940
2	13.593	1193715	50.060
Total		2384591	100.000

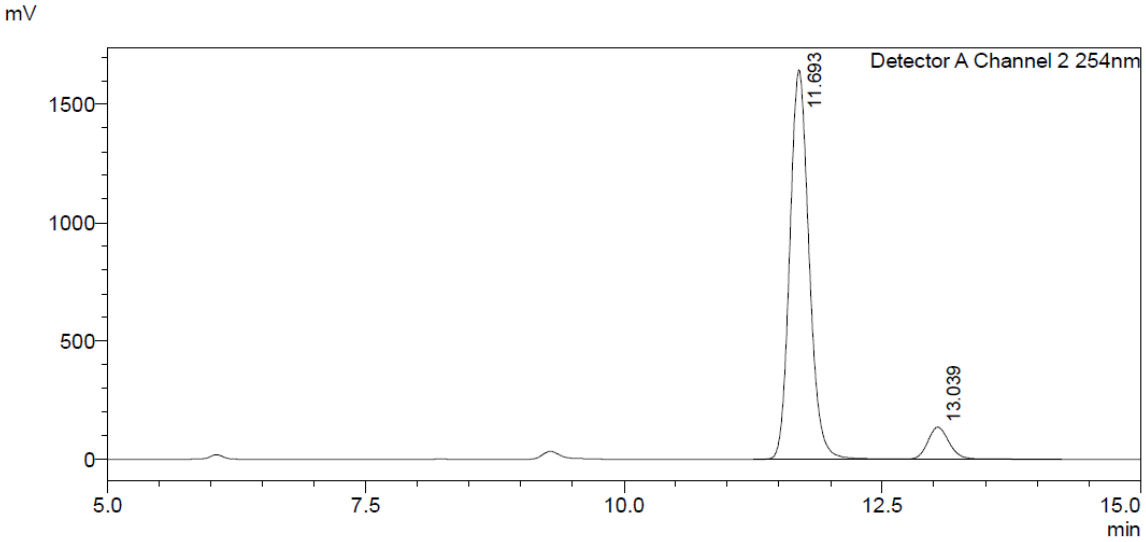

Detector A Channel 2 254nm

Peak#	Ret. Time	Area	Area%
1	11.693	21223277	91.435
2	13.039	1987959	8.565
Total		23211236	100.000

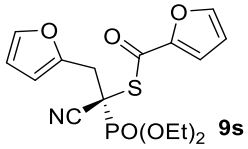

9s

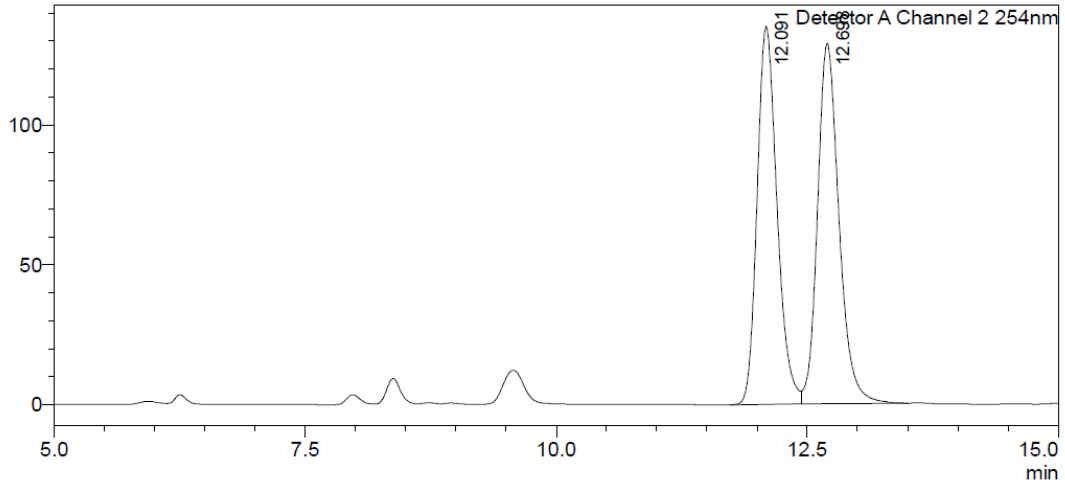

Detector A Channel 2 254nm

Peak#	Ret. Time	Area	Area%
1	12.091	1873411	49.359
2	12.698	1922038	50.641
Total		3795448	100.000

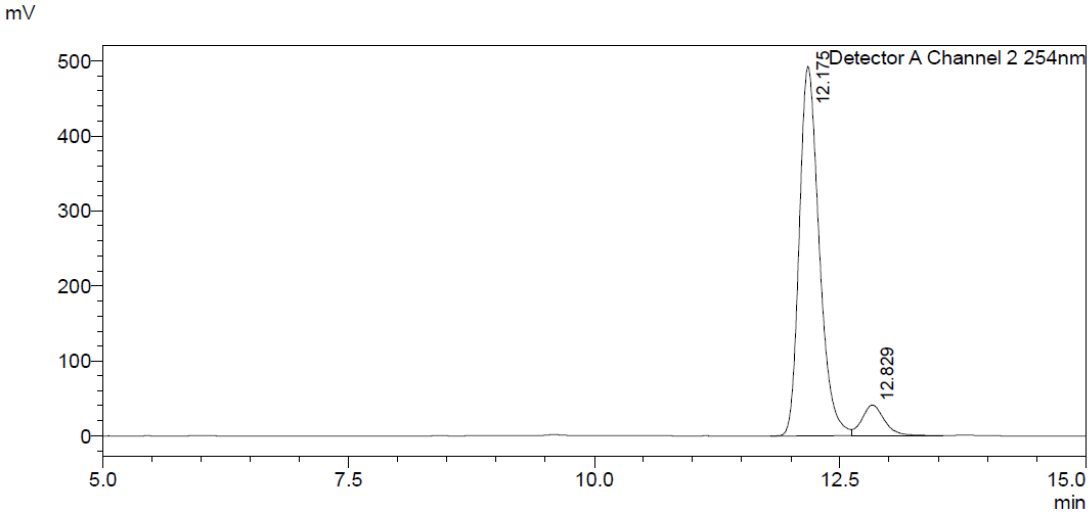

Detector A Channel 2 254nm

Peak#	Ret. Time	Area	Area%
1	12.175	6963681	91.399
2	12.829	655350	8.601
Total		7619032	100.000

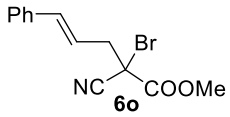

6o

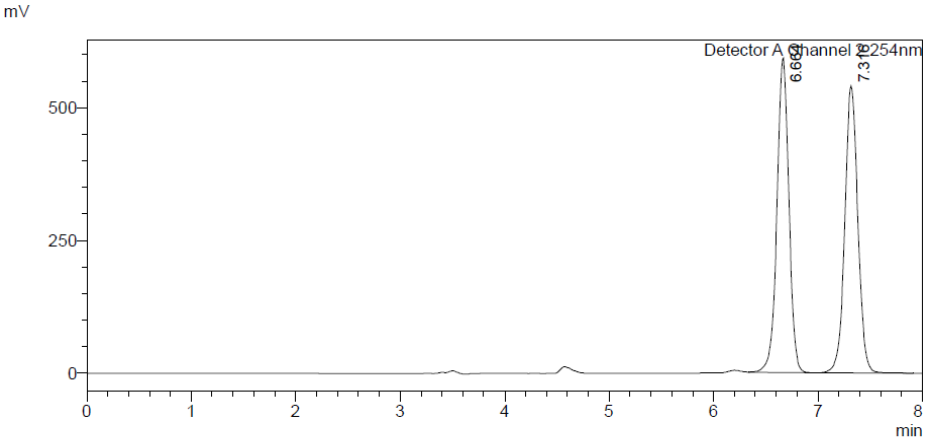

Detector A Channel 2 254nm

Peak#	Ret. Time	Area	Area%
1	6.664	4701899	50.099
2	7.316	4683345	49.901
Total		9385244	100.000

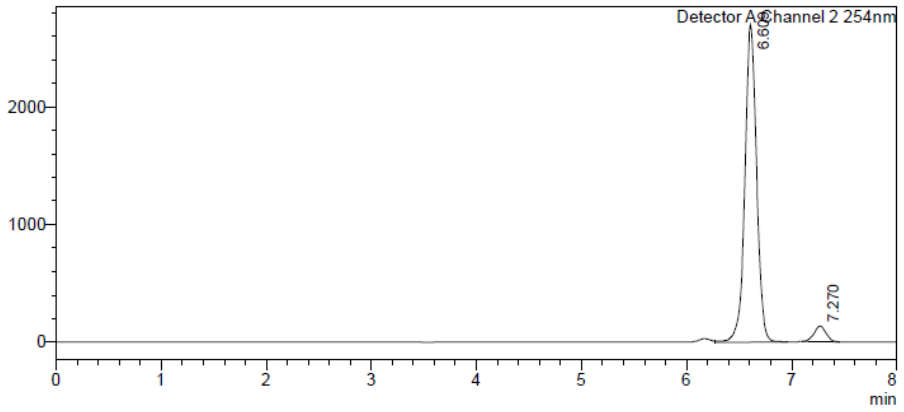

Detector A Channel 2 254nm

Peak#	Ret. Time	Area	Area%
1	6.609	20922456	95.243
2	7.270	1045003	4.757
Total		21967459	100.000

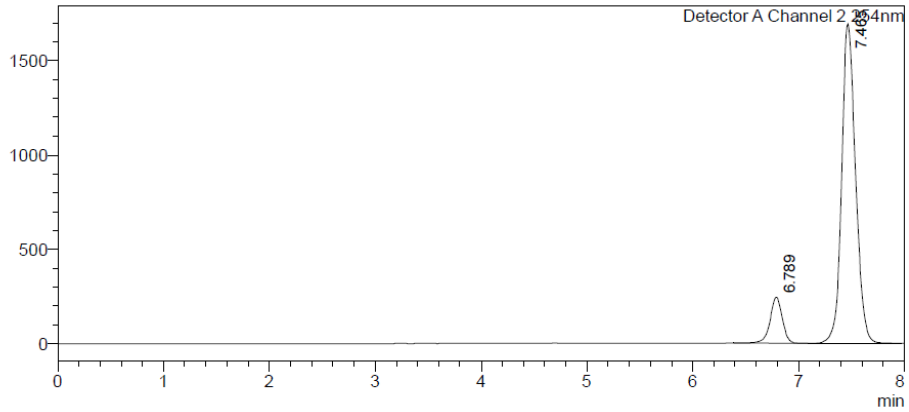

Detector A Channel 2 254nm

Peak#	Ret. Time	Area	Area%
1	6.789	1975600	11.344
2	7.465	15440231	88.656
Total		17415830	100.000